Università degli Studi di Ferrara

DOCTORAL COURSE IN
"CHEMICAL SCIENCES"

CYCLE XXXV

DIRECTOR
Prof. Cavazzini Alberto

Study and development of green water-based methodologies to process biobased and biodegradable polymers for coatings and electronics applications

Scientific/Disciplinary Sector (SDS) CHIM/04

Candidate
Dott. Belletti Giada

Supervisor
Prof. Bertoldo Monica

Years 2019/2022

List of abbreviations and acronyms

AgNW: Silver nanowire

AD: Acetylation degree

AFM: Atomic force microscopy

ATR: Attenuated total reflectance

BCPO: Bis-4-(Ncarbazolyl)phenyl)phenylphosphine oxide

Conc: Concentration

CMC: Carboxymethyl cellulose

CNC: Cellulose nanocrystal

CW: Coating weight

EtOAc: Ethyl acetate

DCM: Dichloromethane

DIC: Digital image correlation

DLS: Dynamic light scattering

DSC: Differential scanning calorimetry

EC: Ethyl cellulose

EL: Electroluminescence

EQE: External quantum efficiency

EtOAc: Ethyl acetate

EVOH: Ethyl vinyl alcohol

FF: Fill factor

FT-IR: Fourier transform infrared spectroscopy

GC-MS: Gas chromatography-mass spectroscopy

GP: Grease permeability

HASE: Hydrophobically modified alkali-swellable emulsion

HEC: Hydroxyethyl cellulose

HEUR: Hydrophobically modified ethoxylated urethane

HLB: Hydrophilic-lipophilic balance

HMC: Hydrophobically modified cellulosic

HMPAM: Hydrophobically modified polyacrylamide

HPC: Hydroxypropyl cellulose

ICP-OES: Inductively coupled plasma–optical emission spectrometry

ICP-MS: Inductively coupled plasma-mass spectrometry

Irppy2(acac):(3Z)-4-(Hydroxy-κO)-3-penten2-onato]{bis[2-(2-pyridinyl)phenyl]}iridium

IPD: Polydispersity index

ITO: Indium tin oxide

J_{SC}: Solar cell short-circuit density

LCD: Liquid Crystal Display

LLDPE: Linear low-density polyethylene

LVR: Linear viscoelastic region

LWP: Liquid water permeability

MC: Methyl cellulose

MFC: Microfibrillated cellulose

MFTT: Minimum film formation temperature

MMT: Montmorillonite

NCF: Nano-cellulose fibers

NMR: Nuclear magnetic resonance

NRL: Natural rubber latex

OLED: Organic light-emitting diode

OSC: Organic solar cell

PAL: Poly(aspartic acid-*co*-lactide)

PALS: Phase Analysis Light Scattering

PBAT: Polybutylene adipate terephthalate

PBS: Poly(butylene succinate)

PBSA: Poly(butylene succinate-*co*-butylene adipate)

PCE: Power conversion efficiency

PCL: Poly(caprolactone)

PDLLA: Poly-D,L-lactide

PEG: Poly(ethylene glycol)

PGA: Poly(glycolide)

PHAs: Poly(hydroxyalkanoates)

PHB Poly(3-hydroxybutyrate)

PLA: Poly(lactic acid)

PDLA: Poly(D-lactide)

PLLA: Poly(L-lactide)

PS: Polystyrene

PVA: Poly(vinyl alcohol)

PVAc: Poly(vinyl acetate)

PEO: Poly(ethylene oxide)

PES: Polyethersulfone

PET: Polyethylene terephthalate

PIT: Phase inversion temperature

PPO: Poly(propylene oxide)

PTFE: Polytetrafluoroethylene

PUEP: Polyurethane elastomer prepolymer

RCF: Regenerated cellulose film

RMS: Root-mean-square

SA: Sodium alginate

SC: Solar cell

SDS: Sodium dodecyl sulfate

SEC: Size-exclusion chromatography

SEM: Scanning electron microscopy

SYN: Synperonic PE/F68

TCTA: 4,4',4''-tris(Ncarbazolyl)triphenylamine

Tg: Glass transition temperature

TGA: Thermogravimetric analysis

Tm: Melting temperature

TPBi: 1,3,5-tris(N-phenylbenzimidazole-2-yl)benzene

TPU: Thermoplastic polyurethane

$V_{OC:}$ Open-circuit voltage

XG: Xanthan gum

WVTR: Water vapor transmission rate

Table of contents

CHAPTER 1

General introduction

1.1. Biodegradable and bio-based polymers

Nowadays, due to their durability and great versatility, plastics are employed in several application sectors that make modern life possible, such as packaging, building and biomedical materials as well as hygiene products. The expansion and development of modern plastics can be placed in the first 50 years of the twentieth century, when at least 15 new classes of polymers were synthesised [1]. Currently, most of the plastic products in use are derived from fossil fuels; a non-renewable resource, which is being consumed at an alarming rate. Besides, the majority of single-use plastic products are not biodegradable and their increasing accumulation in the environment represents a threat to the planet. Consequently, for all the applications where recycling and recovery of the plastic item is not possible, it is of utmost importance the replacement of traditional plastics with biodegradable and bio-based polymers [2].

Biodegradation is defined as the process by which organic substances are decomposed by microorganisms (mainly aerobic bacteria) into simpler compounds such as carbon dioxide, water and ammonia. Materials that can be disposed of in organic (or wet) waste due to their ability to convert themselves into compost together with wet waste under the controlled conditions of industrial composting are named compostable plastics. The compost produced must meet requirements that make it suitable for use as a fertilizer. Indeed, the difference between a biodegradable and a compostable plastic relies on the fact that a compostable material, under particular operative conditions, fully decomposes within 3 months, while a biodegradable one degrades to at least 90% in 6 months [3].

In recent years, in an effort to produce more eco-friendly products, renewable and biodegradable polymers have been investigated as emerging materials [4]. For instance, recent market research predicts a doubling, for 2024 in Europe alone, of the biodegradable plastic market compared to 2019, considering only the segment for use in extrusion coating processes [Europe Biodegradable Polymers Market, Published Date: Jan 2020 | Report Code: CH 7505] (as depicted in Fig.1.1).

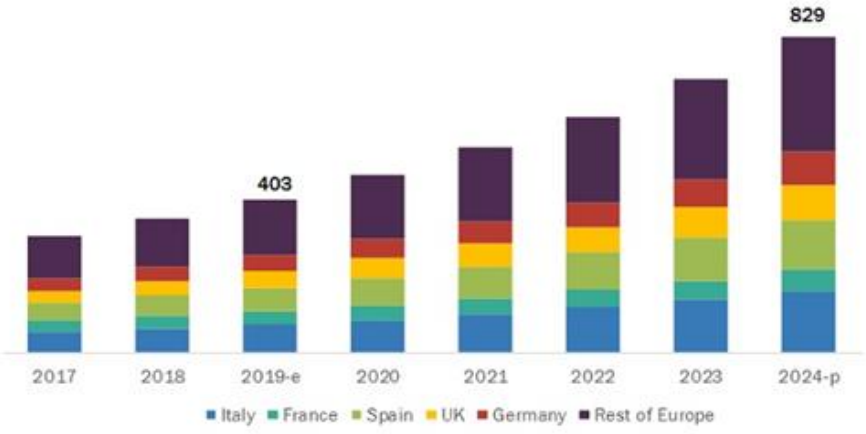

Figure 1.1: European biodegradable polymer's market for extrusion coating, by country (USD million).

Biodegradable and biobased polymer that can be found in nature, such as plant gum, cellulose and starch, have been known and used for thousands of years [5], however, it was only in 1862 that the first man-made plastic cellulose based, namely Parkesine (or celluloid), was created. As regards the modern bioplastics sector, during the 1980's there was a wide expansion of the bioplastic use and production, due to the fact that detrimental effects of the common plastics on the environment became evident. In these years, starch blended with synthetic polymers was employed to produce manufacts partly made from natural feedstock with improved mechanical properties [6]. Nowadays, many biodegradable polymers are known and overall they can be divided in four main categories (Figure 1.2) [7]. The first one is constituted by macromolecules that can be obtained from biomass, such as polysaccharides and proteins. These polymers are very often water-soluble and therefore they can be processed in water. The second category is represented by polymers that are synthesised by microorganisms and obtained by extraction, namely polyhydroxyalkanoates (PHAs). The third class includes polymers synthesised from monomers obtained from biotransformation or biomass. Polyesters such as polylactic acid (PLA) and polybutylene succinate (PBS) are included in the latter category. The last class comprises biodegradable polymers, which are made from fossil non-renewable sources, like polycaprolactone (PCL). Notice that the last two classes are not perfectly distinct since new processes are under development and others are already operative to produce from biomass monomers that were traditionally produced from fossil-oil. The last three mentioned

classes of polymers are mainly constituted by molecules which are insoluble in water; therefore, these polymers, unlike the ones produced from biomass, cannot be easily processed in water.

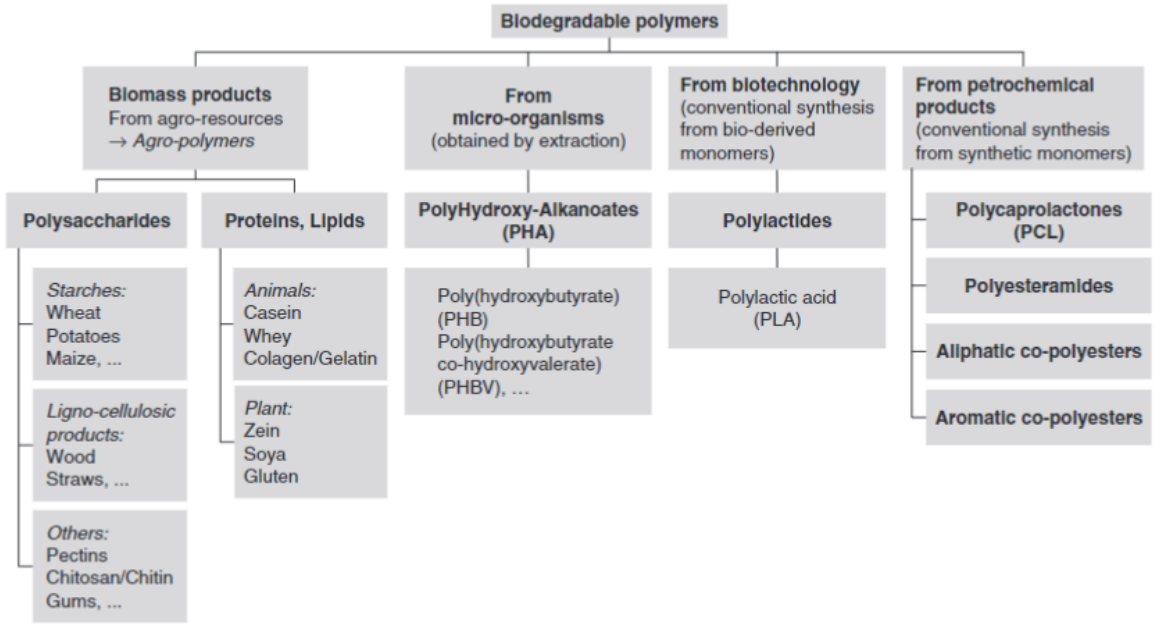

Figure 1.2: Biodegradable polymers' classification [7].

1.1.1. Poly (vinyl alcohol) (PVA)

Poly (vinyl alcohol) (PVA) is a semicrystalline water-soluble synthetic polymer which is biodegradable under both aerobic and anaerobic conditions and belongs to the last class of polymer mentioned in the previous paragraph. It possesses a glass transition temperature of nearly 80 °C and a melt temperature of almost 230 °C. It was first synthesized through saponification of poly(vinyl ester) with sodium hydroxide by Hermann and Haehnel in 1924 [8]. PVA cannot be synthesized through polymerization of its correspondent monomer (vinyl alcohol), due to the unstable nature of the latter. For this reason, it is synthesised by polymerization of vinyl acetate followed by subsequent controlled partial alkaline hydrolysis with sodium hydroxide. The saponification reaction time determines the degree of hydrolysis of PVA [9] (Fig. 1.3). In particular, the physicochemical properties of PVA highly depend on the hydrolysis and crystallinity degree as well as moisture content and molecular weight [10]. Indeed, there are several PVA grades with different

hydrolysis degrees and molecular weights available on the market displaying diverse melting point, viscosity, pH and refractive index.

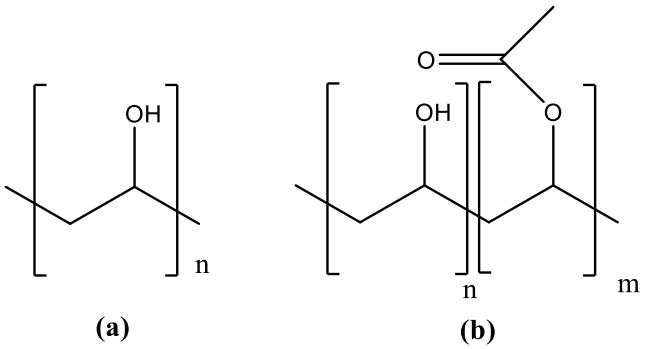

Figure 1.3: Chemical structure of PVA (A) fully hydrolysed and (B) partially hydrolysed.

Due to its versatile characteristics PVA is used in a wide range of industries especially in fabric and paper sizing, fiber coating, adhesives and films for packing and farming [11]. It is also largely employed as a thickener and emulsion stabilizer in poly(vinyl acetate) (PVAc) adhesive formulations and in 3D printing [12][13]. Its success in the packaging sector is ascribed to the combination of excellent oxygen/aroma barrier properties with strength, flexibility and transparency. Its non-toxicity, biocompatibility and ability to form hydrogels allowed the use in the biomedical field for cartilage replacement and production of content lenses as well as vascular strength and drug delivery systems [14].

1.2. Biodegradable polyesters

Most of the commonly studied and employed biodegradable polymers are the aliphatic polyesters, such as PLA and PCL. These polymers contain an ester group $(COOR)_x$ in which the nature of R groups greatly influences the final properties of the material. Biodegradable polyesters can belong to any of the last three classes mentioned in the previous paragraph: they can be obtained either by extraction from microorganisms, such as PHAs, or by conventional synthesis from bio-based or synthetic monomers, like PLA and PCL [15].

Most biodegradable polyesters are thermoplastic; therefore, the main conversion methods for the production of biodegradable polyester items are based on melt processing, such as cast extrusion, extrusion coating, injection molding and blown extrusion [16][17]. These processes consist in heating the thermoplastic polymer material above its melting temperature to shape the molten polymer into desired item. However, most biodegradable polyesters are hygroscopic materials that undergo hydrolytic degradation when they are processed at high temperatures in the presence of moisture. For this reason, before processing these polymers by melting it is necessary to dry them to reduce the water content and prevent the hydrolysis of the main chain.

The macromolecular structure, the relevant properties and the main actual applications of the biodegradable polyesters relevant for this thesis work are presented below.

1.2.1. Polylactic acid (PLA)

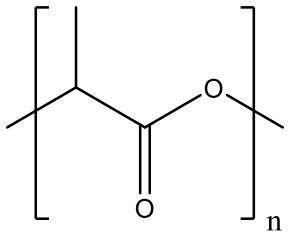

Figure 1.4: Chemical structure of PLA.

PLA has emerged as one of the most promising alternatives to non-renewable fossil-based plastics (Fig. 1.4). It was first synthesised by DuPont scientist Wallace Carothers in 1931 through heating of lactic acid under vacuum [18]. Due to its biodegradability and biocompatibility its applications ranges from the packaging industry (food and beverage containers, cups, overwrap, blister packages, as well as coating on paper and board) [19][20][21] to the biomedical sector (such as implants, sutures, drug encapsulation, etc) [22]. Furthermore, PLA is produced on an industrial scale at relatively low cost. Indeed, its production on a worldwide scale has constantly increased during the last decade, as it is possible to observe from Fig. 1.5.

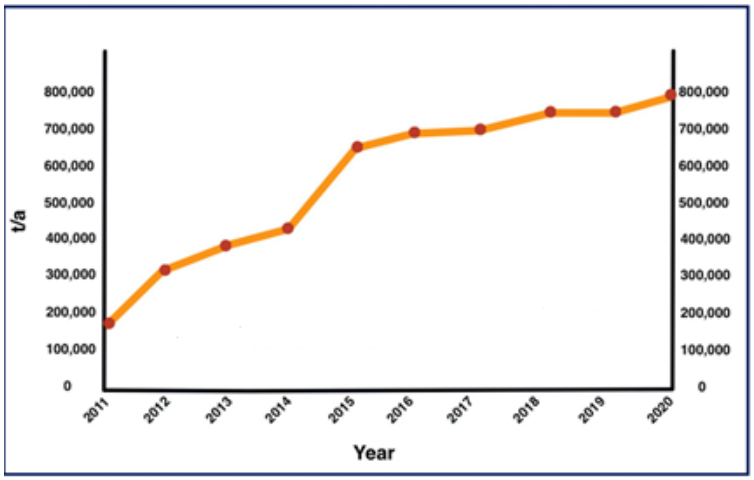

Figure 1.5: Evolution of PLA production capacities (t/a) worldwide between 2011 and 2020.

The precursor for the synthesis of PLA is lactic acid. Lactic acid can be either obtained by carbohydrate fermentation or by common chemical synthesis; consequently PLA can be also produced from renewable biomass, like starch or fossil based sources [23]. Due to the presence of an asymmetric carbon atom, two different optically active configurations of lactic acid are available, respectively the L and D isomer. Both isomers can be produced in bacterial systems, whilst mammalian organisms only produce the L isomer.

Overall, there are three different synthetic routes to produce PLA (Scheme 1) [17]. The first one is direct condensation polymerization, which is the cheapest route. However, this method allows to obtain just low molecular weight PLA. In order to extend the chain length, it is necessary to add a second step that employs chain coupling agents (multi-step process). The second route is the azeotropic dehydrative condensation. This procedure avoids the insertion of chain coupling agents in the reaction mixture since the monomer and the catalyst are azeotropically dehydrated in a high boiling aprotic solvent under reflux and under reduced pressure. The water produced by condensation of lactic acid is rapidly removed from the reaction mixture, hence allowing to obtain high molecular weight PLA. The third and last synthetic route involves the polymerization through lactide formation and this is the most common strategy exploited to prepare high molecular weight PLA (Mw > 100 000 g/mol). The route proceeds by ring opening polymerization of the lactide, which is the cyclic dimer of lactic acid. This monomer is usually obtained by

the depolymerization of low molecular weight PLA under reduced pressure (Scheme 1.1).

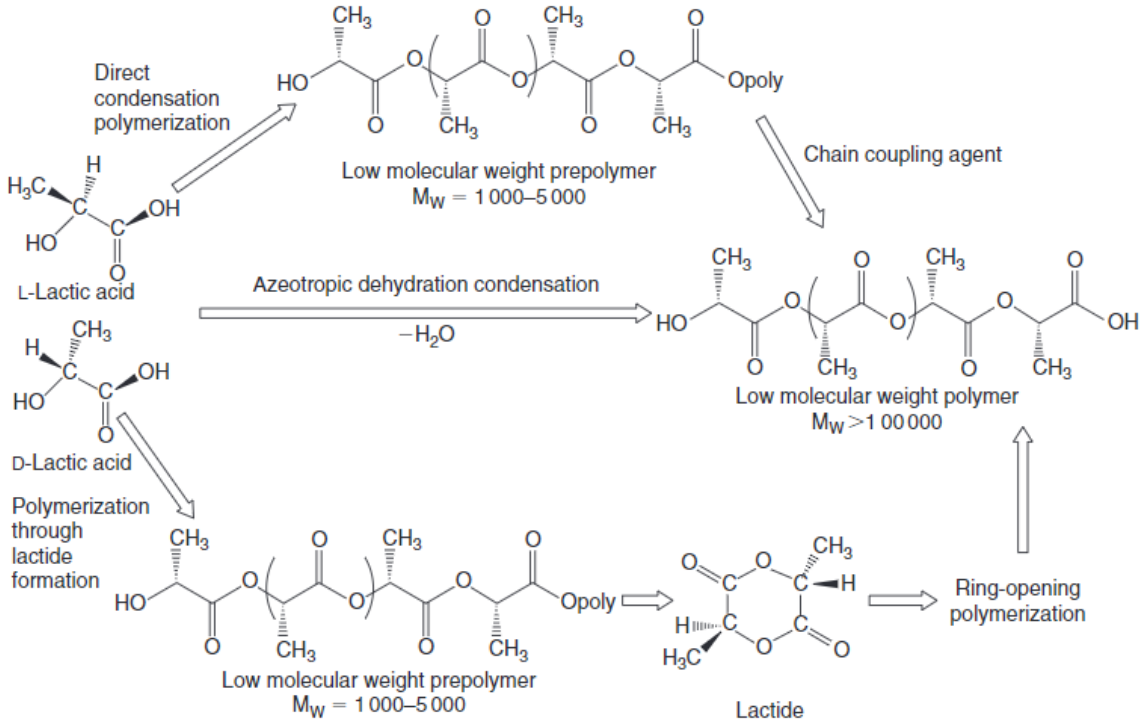

Scheme 1.1: Synthetic routes to obtain PLA [23].

From a formal point of view, lactide is obtained by the combination of two lactic acid molecules, which are chiral species (Scheme 1). Then, based on the configuration of the two condensed acids, two optically active enantiomers can be obtained: (3S,6S)-3,6-dimethyl-1,4-dioxane-2,5-dione and (3S,6S)-3,6-dimethyl-1,4-dioxane-2,5-dione. The two cycles are commonly named L-lactide and D-lactide, respectively. If two lactic acids with opposite configuration condense, the optically inactive meso-lactide is obtained ((3R,6S)-3,6-Dimethyl-1,4-dioxane-2,5-dione). A mixture of the optically active L- and D- lactides is a racemic lactide (rac-lactide). An important step in the preparation of the lactide consists in the separation by vacuum distillation of the different stereoisomers in order to reach stereoisomeric control of the final PLA [24]. Indeed, the structural, thermal, barrier and mechanical properties of the material are strongly influenced by the stereochemistry of the final polymer [25]. For instance, poly(L-lactide) (PLLA) and poly-D-lactide (PDLA) are semicrystalline, while poly-D,L-lactide (PDLLA) is amorphous. When mechanical strength is required, semicrystalline PLA is preferred, indeed the latter has an

approximate tensile modulus of 3 GPa, tensile strength of 50–70 MPa, flexural modulus of 5 GPa, flexural strength of 100MPa and an elongation at break of around 4% [26]. In particular, PLLA is more employed due to the major availability of the latter stereoisomer [27]. However, semicrystalline PLA biodegrades slowly in comparison to the amorphous PLA [28]. Usually, PLA with L-ratio higher than 90% is able to crystallize, while lower rations lead to amorphous polymer. Besides, the melting temperature (T_m) and glass transition temperature (T_g) of PLA decrease with the increment of D-isomer content [26], as shown in Table 1.1.

PLLA possesses a melting point close to the one of polypropylene (125-180 °C depending on the specific structure of the main chain) and a glass transition temperature higher than room temperature (between 53 and 63 °C).

Table 1.1: Glass transition temperature (T_g) and melting temperature (T_m) of different PLA stereoisomers [29].

Copolymer ratio (L/D,L)-PLA	**T_g (°C)**	**T_m (°C)**
100/0	63	178
95/5	59	164
90/10	56	150
85/15	56	140
80/20	56	125

1.2.2. Polybutylene succinate (PBS) and Polybutylene succinate-co-butylene adipate (PBSA)

Polybutylene succinate (PBS) is a semicrystalline polymer actually synthesised through polycondensation between succinic acid and 1,4-butanediol (Scheme 1.2). This polymer, whose crystallinity can reach values up to 35-45%, possess a glass transition temperature of -32 °C and a melting point around 115 °C [30]. It was studied in the 30's as a possible synthetic fiber alternative to natural silk [31]. However, due to the invention of Nylon 6,6 and the poor properties of PBS as a fiber, the latter was abandoned. After being forgotten, in the early 90s of the last

century, this polymer received renewed interest due to the growing demand for biodegradable polymers.

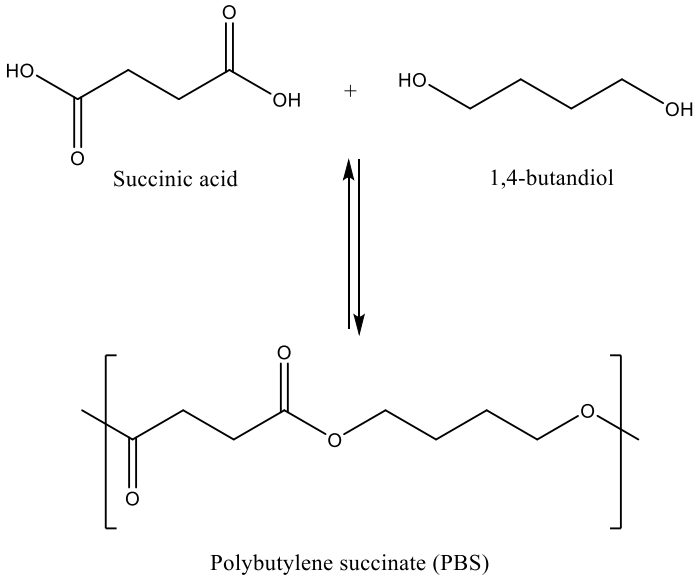

Scheme 1.2: Synthetic route to obtain PBS.

PBS, in comparison to the common non-biodegradable plastics, shows great biodegradability, balanced performances in thermal and mechanical properties as well as thermoplastic processability [32]. Furthermore, PBS is usually copolymerized in order to extend its properties in a wide range [33]. For instance, since PBS has a low elongation at break compared to polyolefins, which are actually used to obtain films, polybutylene succinate-co-butylene adipate (PBSA) was also developed. The latter is obtained by inserting in the polymerization adipic acid in addition to succinic acid, as depicted in Scheme 1.3. This material shows various advantages in film production even though it has a lower melting point in comparison to PBS, namely 84 °C. PBSA exhibits a higher degradation rate than PBS and besides it shows very similar properties to linear low-density polyethylene (LLDPE), thus making it suitable for instance for kitchen waste compostable bags [34]. PBS copolymers also found applications in food packaging and bottles, flushable hygiene products and supermarket bags as well as additives for polyurethane elastomers [35].

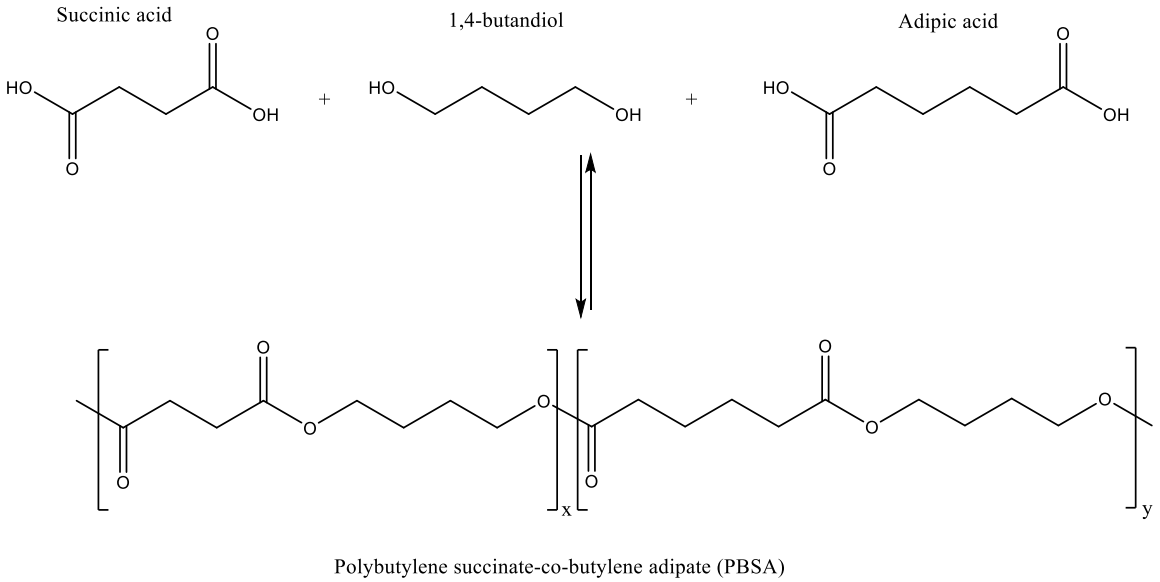

Scheme 1.3: Synthetic route to obtain PBSA.

1.2.3. Other biodegradable polyesters

Among the other biodegradable polyesters, it is worth mentioning Polycaprolactone (PCL) and Polyhydroxyalkanoates (PHAs).
PCL is a semicrystalline biodegradable aliphatic polyester constituted by hexanoate repeat units.

It possesses a low melting temperature (57 °C) and a glass transition temperature lower than room temperature (-60 °C) [36]. As illustrated in Scheme 1.4, PCL is usually synthesised through ring opening polymerization of the ε-caprolactone (at present a fossil-based substrate) in the presence of a catalyst (such as stannous octoate) under heating. In this way high molecular weight polymers can be achieved.

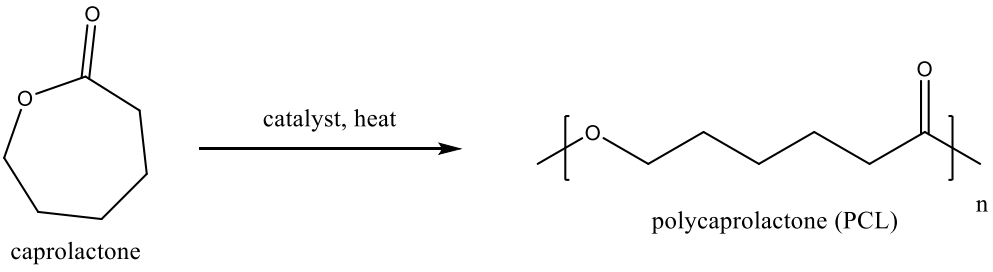

Scheme 1.4: Synthetic route to obtain PLA.

The physical and mechanical properties of PCL depend mainly on the degree of crystallinity, which can reach values up to 70%. Generally, PCL can be considered as a semi-rigid material at room temperature: it has a flexural modulus of about 300 MPa, low tensile strength and high elongation at break (around 1000%) [37].
Since it is easily biodegradable, it was initially employed for the production of films for applications like take-out bags [38]. Nevertheless, its use was soon abandoned due to its low melting point. To partially overcome this issue, PCL, which is able to provide the final product with high elongation at break, is often used in a mixture with other biodegradable and bio-based polymers such as PLA, polyglycolide (PGA), starch, etc [39][12][40][41]. PCL, as PLA, undergoes hydrolysis of its ester bonds under physiological conditions (for instance in the human body) and has therefore been employed in the biomedical fields for implantable biomaterials, drug releasing systems, suture and adhesion elements [42]. In particular, compared with PLA, PCL is more suitable for the construction of long-lasting implants due to its slower degradation rate [43]. Moreover, PCL is used as a polymeric plasticizer for PVC and other polymers and as additive for polyurethanes [44][45]. Indeed, it imparts good solvent and water resistance to the final polyurethane products.

Polyhydroxyalkanoates (PHAs) are biogenic polyesters that can be naturally accumulated in microbial culture. Indeed, they can be synthesised by different types of bacteria (Bacillus, Rhodococcus, Pseudomonas, etc.) through fermentation of lipids and sugars. Since PHAs are a carbonaceous reserve for bacteria, the latter are able to produce them in high concentrations under particular cultivation conditions. These polymers are accumulated in granules within the bacterium, until values up to 90% of the dry weight of the bacterial mass are reached (Fig. 1.6) [46]. PHAs possess high process versatility and high biodegradability in different environments, including in sea water. However, the difficulties of industrial scale production, by means of batch bio-fermentation, have limited its commercial potential [47]. Considering the great variability of the side chains (-R) and of the length of the main chain, PHAs may possess very different physical and chemical properties. Indeed, these properties range from those typical of thermoplastic polymers to those typical of elastomers with melting points between 40 and 180 ° C and glass transition temperature between 2 and 8 °C [48].

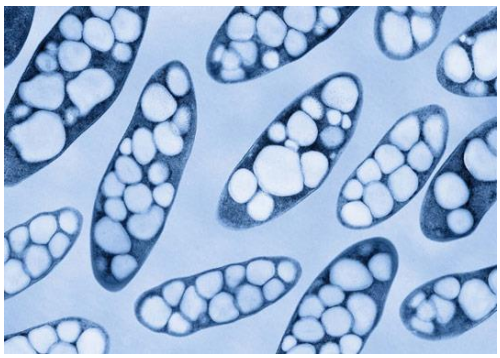

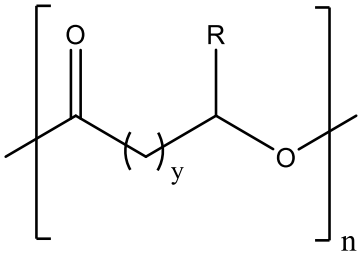

Figure 1.6: Electron microscope photograph of a bacterial cell showing the intracellular granules of PHAs at the left and generic structure of PHAs at the right.

One of the most studied and characterised members of the polyhydroxy-alkanoates family is the poly(3-hydroxybutyrate) (PHB) [49]. PHB is a linear polyester of D (-)-3-hydroxybutyric acid with a molecular weight that differs depending on the organism, conditions of growth and method of extraction. Some grades of additive PHB are similar in their material properties to polypropylene (PP), and they offer good resistance to moisture and aroma barrier properties [50].

1.3. Polysaccharides of industrial interest

Polysaccharides are an important class of biological polymers composed of saccharide units linked together by glycosidic bonds. Their structure, which is often heterogeneous, can be linear or branched and usually slight modification of the repeating units are present. The main functions of polysaccharides in living organisms are structural support (e.g., starch, glycogen and galactogen) and energy storage (e.g., cellulose and chitin) [51]. The industrial relevance of polysaccharides is due to their capacity to alter the basic properties of water (e.g., thickening and gelling). Moreover, polysaccharides display related secondary functions, such as emulsification, suspension, stabilization, encapsulation, flocculation, film forming, binding and coating [52]. Furthermore, they are largely employed in the food industry for the control of the food texture and flavour, as well as appearance and colour [53]. Many kinds of polysaccharides with different functions, structures and chemical properties exist in nature. The structure, properties and application of the polysaccharides relevant for this work are presented below.

1.3.1. Starch

Starch is one of the most widespread polysaccharides, indeed it is produced by most green plants for its energy storage functions. Nowadays starch is extracted from more than 50 types of plants (including corn, wheat, rice, potato and much more) by grinding seeds, roots and tubers [54]. Starches are usually composed by two different D-glucopyranose polymers, namely amylose and amylopectin (Figure 1.7). Amylose is essentially a linear polymer consisting of (1,4)-linked α-D-glucopyranosyl units, whilst amylopectin is a branched polymer of α-D-glucopyranosyl units primarily linked by (1,4) bonds with branches resulting from (1,6) linkages [55]. Generally, amylopectin is the major constituent of starch (65–85 %), although in some genetically modified plants, the amylopectin content can even reach 100 % (with a resultant sample known as “waxy starch”). In nature, starch molecules are found arranged in the form of semi-crystalline granules and each type of plant possesses a different starch granular size. The granular architecture is complex and it is generally constituted by an amorphous core surrounded by concentric semicrystalline rings alternating with amorphous ones [56].

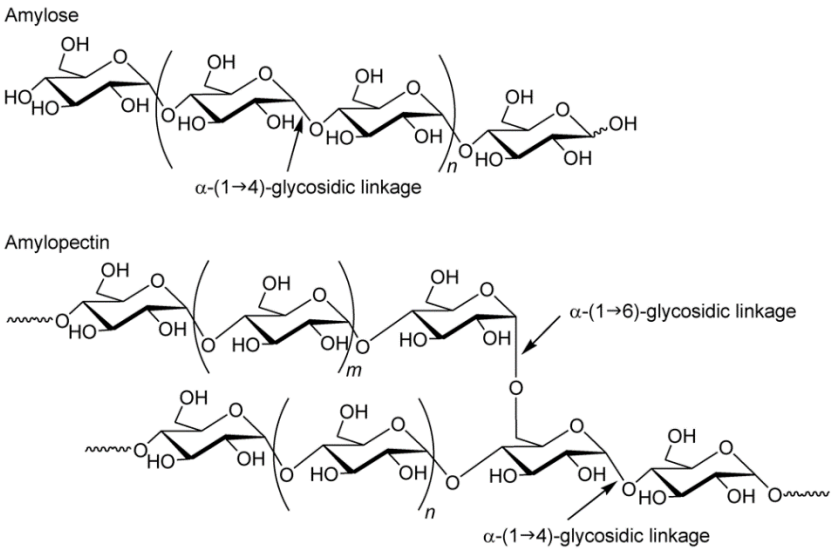

Figure 1.7: Structure of the amylose and amylopectin molecules.

The granule is composed mainly by amylose and amylopectin even if small amounts of proteins, fatty acids and minerals are also present. The size of the amorphous core depends on the amylose content of the starch; with greater amylose content

that corresponds to larger cores [57]. If the starch granules are heated in water, they undergo hydration and swelling with a consequent transformation into a paste. With heat, the granule architecture collapses due to melting of crystalline domains, losing its characteristic features. This process is known as gelatinization of starch and is fundamental in many industrial applications where gelling and thickening properties are required, such as the food sector [58]. Only if the native starch undergoes a pre-cook process is it able to gelatinize in cold water. Additionally, starches can be modified in order to improve their performance in different applications [59]. The most common modification procedures of starch include acid modification and oxidation. In both treatments, starch molecules are broken down thus decreasing the final chain length and the viscosity of the resulting solutions.

Starch is of utmost importance for the production of sugars used in processed food and also for the production of ethanol through fermentation [60]. Besides, it finds application in several industrial sectors. For instance, it is largely employed in the food industry as thickening and gelling agents for puddings, salad dressings, pie filling and candies [61]. Acid-modified starches are used in gum candies due to their ability to form strong gels after a heating and cooling step [62]. Moreover, they are used as binders to carry flavours and colours. Regarding the non-food application native starch is principally used in mining [63], adhesives [64] and paper industries [65]. Pregelatinized starches are widely present in papermaking as an internal fiber adhesive, while acid-modified ones find applications in the textile industry due to their ability to increase yarn strength and abrasion resistance [62]. Oxidized starches, usually prepared by hypochlorite oxidation, are used in paper coatings and adhesives to improve surface characteristics for printing or writing [66]. Starch found applications also in the pharmaceutical industry, where it is used as an excipient, disintegrant, and binder [67].

Moreover, starch is an important natural polymer for the production of biodegradable and biobased plastics. Indeed, starch can be converted into "thermoplastic starch" by addition of water and plasticizer using conventional polymer processing techniques, e.g., extrusion, injection moulding and compression moulding [68]. Due to the low mechanical properties and stability of starch the latter can be combined with other biodegradable polymers such as PCL in order to obtain performing bioplastic, like Mater-Bi® which is currently available on market [69].

1.3.2. Xanthan gum

Xanthan gum is a high molecular weight branched polysaccharide, produced by fermentation of the bacteria Xanthomonas Campestris [70]. This biopolymer consists of a cellulosic backbone with negatively charged trisaccharide sidechains. The latter are linked with α-1,3 bonds to the glucose residues of the main chain and are constituted of a β-D-glucuronic acid residue between two D-mannose units. Approximately one-half of the D-mannose side chain terminals contain a pyruvic acid residue linked via keto group to the 4 and 6 positions, with an unknown distribution, while the inner D-mannose unit carries an O-6-acetyl group [71] (Fig. 1.8). Xanthan gum is a polysaccharide with many industrial applications, especially as a food additive. It is an effective thickening agent, emulsifier and stabilizer, which avoids ingredient separation. Its excellent properties as thickener are due to the fact that xanthan chains are able to build up a network in solution, even at low concentrations, providing the media with high viscosity [72].

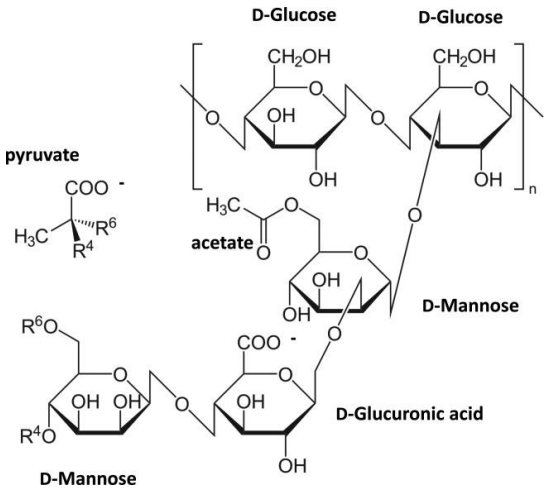

Figure 1.8: Structure of xanthan gum.

Indeed, xanthan gum is commonly used as rheological modifier in food [73], cosmetic, agricultural, pharmaceutical [74] and petroleum industry applications [75], as well as in home and personal care product formulations [76]. For instance, in the bakery sector the addition of xanthan gum improves the cohesion of starch granules and by binding moisture it increases shelf-life of the final product [77]. Thanks to its ability to absorb water, this biopolymer is also able to increase the stability of frozen products. Additionally, in beverages, xanthan gum is an efficient additive for the

suspension of fruit pulps for a long period of time, furnishing to the drink an enhanced taste and good flavour release [78].

1.3.3. Sodium alginate

Sodium alginate is the salt of alginic acid that is naturally found in brown algae. Indeed, it is a cell wall component of algae and contains approximately 30 to 60% alginic acid. Sodium alginate is a linear polysaccharide composed of blocks of (1,4)-linked β-D-mannuronate (M) and α-L-guluronate (G) residues, respectively in different proportions. The block of G and M residues can be either consecutive or alternating (Fig. 1.9) [79].

This polysaccharide is extremely hydrophilic and when it is hydrated it forms a viscous solution [80]. Additionally, it also possesses gelling, chelating and film forming abilities.

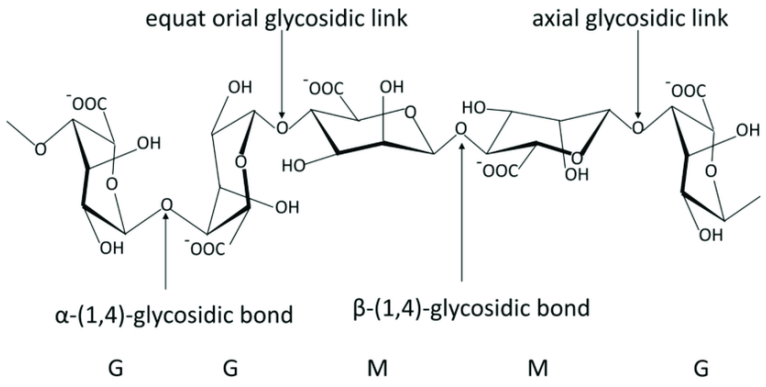

Figure 1.9: Structure of the sodium alginate.

Due to its outstanding properties, sodium alginate is used in many industries including food, pharmaceutical [81] and textile sectors [82]. It is also employed in orthodontics for the creation of gels for dental impression [83]. In the food industry it is used as an additive for its dehydration properties. Besides, it is a good thickening agent for drinks and ice-creams and a gelling agent for candies and jellies. Its use as a thickener expands also in the reactive dye printing technology [84]. In the biomedical field, sodium alginate has potential as drug and gene delivery systems, tissue engineering, and wound dressing [85]. Particularly, drug delivery systems that contain sodium alginate hydrogels are employed for its slow drug release. These

hydrogels are indeed employed to encapsulate anticancer, antiviral and pain-killer agents [86]. Moreover, sodium alginate hydrogels are common biomaterials for the production of scaffolds for tissue and bone regeneration, due to the fact that it improves porosity, cell proliferation and mechanical strength of the manufact [87].

1.4. Polymer dispersions and emulsions

Water polymer emulsions and dispersions are largely employed in many application fields such as paints [88], adhesives [89], inks [90][91] and the packaging sector [92][93]. Emulsions and dispersions have similar characteristics; however, an emulsion is a uniform mixture of two or more immiscible liquids (for instance oil and water), whilst a dispersion is formed when particles are mixed in a liquid which do not solubilize them. The dimension of the dispersed phase can range from 20 nm to 1 μm, on the contrary, when the dimensions exceed the micrometer the system can be ascribed as a suspension. Generally, the term “polymer emulsion or dispersion” is used to describe a colloidal dispersion of discrete polymer particles with a typical particle diameter of 0.01–1.0 microns in a medium such as water [94]. Usually, polymer emulsions are prepared by dispersing in a water-phase an organic solvent immiscible with water in which the polymer is dissolved. If the organic solvent of the dispersed phase is allowed to evaporate, a dispersion consisting of polymeric particles in water is obtained. Alternatively, polymer dispersions can be prepared through emulsion polymerization [95]. These two methodologies are deeply discussed in Paragraph 2.1.1 of Chapter 2.

1.4.1. Destabilisation process

In order to ensure the final application, emulsions and dispersions must maintain their characteristic features unchanged over time. This ability to resist changes in properties is referred to as stability. Overall, there are five types of instability in emulsions: creaming/sedimentation, flocculation, Ostwald ripening, coalescence and phase inversion (Fig. 1.10) [96].

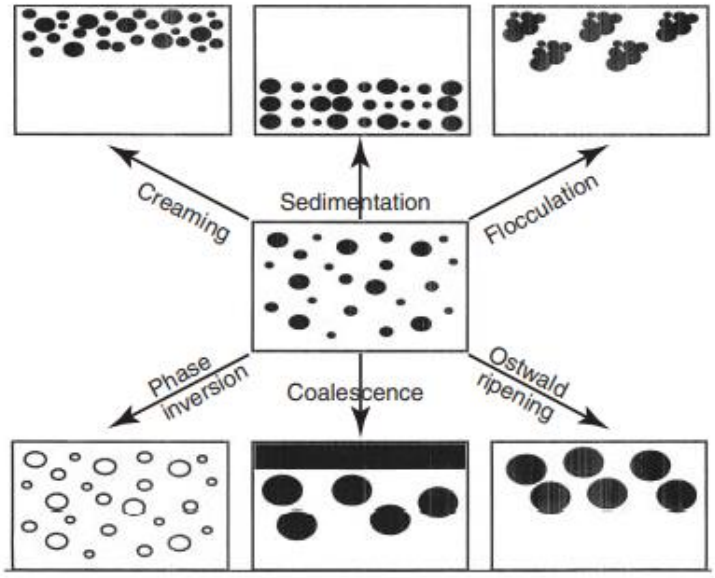

Figure 1.10: Types of instabilities in emulsions.

Both creaming and sedimentation are phenomena caused by external forces, such as gravitational and centrifugal ones. If these forces overcome the thermal movement of the droplets, a concentration gradient in the system builds up. As a consequence, if the dispersed phase is less dense than the continuous one the droplets tend to rise on the top of the emulsion (creaming). On the other hand, when the dispersed phase is denser than the medium one, the gravitational forces pull the droplets to the bottom (sedimentation) [97]. Usually, thickeners are added with the purpose of preventing creaming and sedimentation through alteration of the continuous phase's rheology. Particularly, the effect of the addition of a thickener like xanthan gum on the stability against creaming of sterically stabilized oil-in-water (O/W) emulsions was an object of study [98]. It was disclosed that at a concentration of xanthan gum higher than 0.5 % the resulting preparation was stable at least for 6 months. Additionally, it should be considered that by reducing the droplet size creaming and sedimentation can be prevented. This is due to the fact that, below certain sizes, the Brownian diffusion may overcome the gravity force. Indeed, nanoemulsions (diameters between 50 and 550 nm) are less subjected to destabilization phenomena than microemulsions [99].

Besides, emulsions and dispersions undergo flocculation when the droplets aggregate while keeping their diameter unchanged. In these cases, the repulsion forces are not able to overcome the Van der Waals attraction forces that are present

in all dispersed systems. In particular, studies regarding the flocculation of sterically stabilized polymer dispersions were conducted, revealing that flocculation can be induced by decreasing the solubility of the polymeric stabilizer chains into the continuous media [100]. Moreover, it was disclosed that, in this case, in order to ensure stability, the polymeric moieties must assume an ideal random coil conformation in the continuous phase, by choosing a suitable solvent. Another type of flocculation is the depletion flocculation that is generated by addition of a non-adsorbing polymer in the continuous phase (Fig. 1.11).

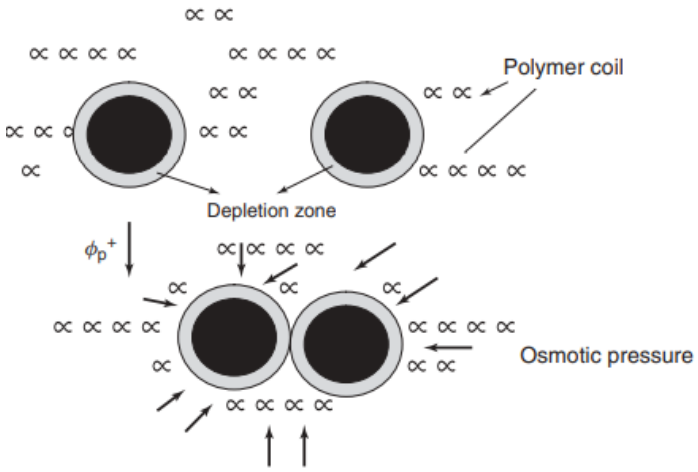

Figure 1.11: Depletion flocculation mechanism.

This phenomena was firstly reported in studies that investigated the creaming of natural rubber in the presence of water soluble polymers [101]. Subsequently, further works were focused on presenting a first quantitative analysis of this mechanism [102]. At critical concentration of non-absorbing polymers a “depletion zone”, in which the polymer concentration is lower than the bulk solution, is formed [103]. This depletion zone originates by conformational entropy restrictions of the non-adsorbing polymer coils. Hence, when the separation between particles is lower than the free polymer coil diameter, the polymer coils are excluded from the particle’s interstices, leading to the formation of a region of pure solvent. An osmotic pressure is thus generated, causing the solvent movement from less to a high polymer concentrated region. The pressure in the interstitial zone decreases leading to an increment of the attraction forces between particles that aggregate.

In general, intermediate non-adsorbing polymer concentrations cause destabilization through the promotion of creaming. Indeed, under these conditions,

droplet flocculation occurs and the increase in the particle size leads to creaming since the viscosity of the media is not enough to counteract this phenomenon. On the other hand, non-adsorbing polymers can be used at high concentrations to promote stability. In these cases even if the droplets flocculate, the high viscosity of the media makes them incapable of moving, hence avoiding creaming [104]. In general, with the purpose of avoiding flocculation, it is essential to employ a sufficient amount of emulsifier to fully saturate the interface during the emulsification process [105].

Another type of destabilization mechanism is coalescence. It occurs when droplets combine and merge to form a larger droplet, with a total increase of the average droplet size. The surface fluctuation can result in a closer contact among the particles, where the Van der Waals forces are so significant that the merging of the droplets cannot be avoided. In particular, it was demonstrated that continuous phase rheology has an effect on emulsion stability. From the studies it emerged that, especially for small droplets, the elasticity in the continuous phase causes a significant decrease of creaming [106]. As for flocculation, also in this case the choice of the right surfactant is of fundamental importance to provide a sufficiently high energy barrier against coalescence. Therefore, the relative rates of the surfactant adsorption and desorption are relevant [107]. Furthermore, it was also demonstrated that a mix of surfactants is efficient in the formation of multilayer structures that envelop the droplets, thus reducing the Van der Waals attraction forces between particles [108].

Ostwald ripening (or disproportionation) is a destabilization mechanism driven by the difference in thermodynamic stability between large and small particles [109]. Small particles possess a higher surface to volume ratio than large one and this results in a higher surface tension and a major thermodynamic instability. Accordingly, the molecules at the surface of the smaller droplets will have larger solubility when compared with the larger ones, with a consequent solubilization of small particles and increment of the concentration of free molecules in solution. Overall, all the smaller droplets will tend to disintegrate in favor of the growth of the larger ones. Several strategies can be exploited for the reduction of Ostwald ripening; one of them involves the addition of a second less soluble component in the dispersed phase, usually squalene [110]. Consequently, partitioning of squalene between droplets with different sizes occurs, with a major concentration in the smaller droplets. The Ostwald ripening rate is hence reduced due to the fact that the

difference in chemical potential among distinct droplets size is balanced by the difference in chemical potential resulting from partitioning of the two dispersed components. Besides, it has been shown that the use of block copolymeric surfactants that are strongly absorbed at the interface without desorbing during ripening significantly reduce the rate of this phenomena [111][112]. For example, amphiphilic styrene-b-acrylic acid macro-RAFT diblock copolymers were revealed to be efficient emulsifiers against Ostwald ripening in polystyrene waterborne dispersions [111].

When phase inversion takes place there is an exchange between the dispersed phase and the medium. This phenomenon might be caused by a variation of the temperature. Since it was found that many emulsions stabilized with non-ionic surfactants at a critical temperature are subjected to a phase inversion, this phenomenon is exploited to prepare emulsions with the use of low energy. One of the most diffused methods belonging to this class is the phase inversion temperature (PIT) [113,114]. It exploits the affinity changes of non-ionic poly(ethylene oxide) (PEO)-type surfactants for both aqueous and oil phases in response to a temperature change.

1.4.2. Methodologies to determine the stability

Over the years, different techniques were developed to assess the stability of emulsions. For instance, one the simplest and cheapest method to determine if creaming or sedimentation occurs is the visual observation, even though mathematical models that apply Stoke's Law are also applicable. In the visual observation, the sample is placed in a transparent tube and the height of the different layers eventually formed over time is measured. With the purpose of making visual observation more objective, video imaging instruments were recently developed [115][116]. Most of the methodologies for measuring the stability of emulsions involve controlling the size and the concentration of the droplets. For example, by physically sectioning an emulsion it is possible to assess the variation in droplet concentration with time and height [117]. In this case, the sample is rapidly frozen after storage in a tube for a certain amount of time. The emulsion is then cut into vertical sections and the particles concentration in each section is measured exploiting different methodologies like evaporation, solvent extraction, density, spectroscopy or turbidity measurements. However, instrumental methods are

commonly used to determine the variation of droplet size and concentration as a function of storage time and height. Usually, dynamic or multiple light scattering are used to assess the variation of the particle's size during time or the variation of the dimension as a function of the sample height, respectively [118][119][120]. In these cases, the sample is irradiated with a monochromatic beam of a near infrared light in one or multiple points. The detector measures the percentage of transmitted and/or back scattered light, which is correlated to the dimension of the droplets. The limitation of these methods consists in the fact that the sample must be diluted in order to be analysed by the instrument and, in this way, information about the real physical state of the preparation is not available. For instance, a new technology, namely Turbiscan, based on multiple light scattering has been developed to characterize even fairly concentrated dispersions without diluting them [121].

Besides, there are methodologies that can predict the long-term stability of the formulation in relatively short time, avoiding time-consuming tests. For example, the creaming instability of a preparation can often be accelerated by centrifuging an emulsion at a fixed speed for a certain length of time [122]. After centrifugation the stability can be determined by using one of the methods described above (optical inspection, physical sectioning or droplet concentration profiling). For example, LUMiSizer®, an analytical centrifugation technique was efficiently employed to study the stability and the sedimentation behaviour of sterically stabilized polystyrene colloidal particles [123]. In particular, LUMiSizer® is an analytical centrifugation instrument able to measure the transmitted light intensity as a function of time and position over the dispersion sample length. Even if these methodologies efficiently reduce the time of testing, it must be taken into account that the factors that govern the droplet movement in a gravitational field might differ from the ones of the centrifugal field. Furthermore, several non-destructive methods have been developed to provide information on droplets concentration profiles in emulsions and dispersions without requiring dilution/or modification of the sample. Specifically, electrical conductivity[124], ultrasound [125] and nuclear magnetic imaging and resonance [126] have been widely exploited for this purpose.

However, all the techniques previously described are not optimal to determine if flocculation takes place, considering that in this case the particle dimension does not vary. Usually, microscopy is the most simple and direct method to provide information on the droplet flocculation [96]. For instance, an interesting study efficiently used confocal laser scanning microscopy to investigate the flocculation

and phase separation of caseinate-stabilised emulsion containing xanthan gum [127]. Usually, techniques to establish the particle's size distribution can provide information on particle's aggregations more rapidly than microscopy methodologies. Nevertheless, they are not able to distinguish between the different types of aggregation (flocculation, coalescence or Ostwald ripening). Besides, it has been demonstrated that changes of viscosity in colloidal suspension can provide indications on the formation of the flocs [128].

Regarding coalescence, one of the most useful methods to observe this phenomena is optical microscopy [129]. For example, an alternative approach based on optical microscopy observation to observe the coalescence of an emulsion droplet with a planar oil-water interface was disclosed [130]. In this technique the time it takes a single oil droplet released from a capillary tube to merge with a planar interface due to gravity is measured through an optical microscope. However, in this way only droplets size higher than 1 μm can be observed and besides when coalescence occurs slowly the measurement is time consuming. A similar methodology proposed to measure coalescence is the film trapping technique, which involves the observation of single oil droplets compressed against an oil-water interface [131]. Usually, an extensive coalescence leads to the formation of an oil layer on the top of oil-in-water emulsions. The amount of oil phase that formed this layer can be exploited to assess the degree of coalescence. Furthermore, as for the instability to creaming, also the coagulation phenomena can be accelerated by centrifugation in order to study the long term behaviour of the formulation [132]. The majority of the techniques used for monitoring coalescence, can also be exploited to determine Ostwald ripening, such as optimal microscopy [133] and techniques that measure the distribution of the droplets size over time [134] even if it is always challenging to distinguish between the two phenomena.

When an emulsion is subjected by phase inversion the nature of the continuous phases changes and consequently its characteristics are modified. As a consequence, every analytical method that is able to detect a variation in the continuous phase characteristic can be used for monitoring this phenomenon. Usually, after phase inversion there is a significant change in viscosity, indeed the measurement of the latter has been studied to follow this destabilization mechanism in emulsions [135]. Besides, when water constitutes the continuous phase, the conductivity is high and when the oil-phase becomes the continuous one there is a significant decrease of this parameter. For this reason, electrical conductivity

measurements are largely employed to monitor phase inversion [136]. Also dynamic light scattering (DLS) has been used to assess this destabilization mechanism, since there is an evident change in the droplet size around the inversion point [134].

1.5. Film formation from aqueous-based polymeric dispersions

Considering the industrial importance of polymer latexes, their film formation processes have been an object of many studies, especially for coating purposes. It must be noted that, in the last decades, the preparations employed to prepare films have shifted from organic-based polymer solutions to aqueous-based dispersion due to environmental and safety reasons [137]. Besides, aqueous-based dispersions present a processing advantage over the organic-based polymer solutions due to the fact that for the former preparation the viscosity of the system is not influenced by the polymer concentration or its molecular weight, consequently higher polymer concentrations can be applied in coating processes [138].

When water polymer dispersions are used to prepare coatings, the preparation is casted onto the chosen substrate and, as water evaporates, the polymer particles merge and form a homogenous film on the coated surface (Fig. 1.12). In this case, the most commonly accepted film formation mechanism is composed of three stages: drying, deformation and coalescence [139]. During the first step (drying), after application to the substrate, as the water evaporates at a constant rate, the polymer particles become closely packed together [140]. Generally, at the end of the drying stage the polymer reaches 60-70% of the volume fraction. In the second step (deformation), as the medium evaporation rate slows down, the polymer spheres undergo deformation in order to fill in the void left by the evaporating water. Even though these steps are generally recognized as part of the film forming process, the mechanisms involved in the particles deformation and coalescence are subject of conflict in literature. At first, the driving force for the particle's deformation has been ascribed to the viscous flow of the polymer resulting from shearing stresses caused by polymer-air surface tension [141].

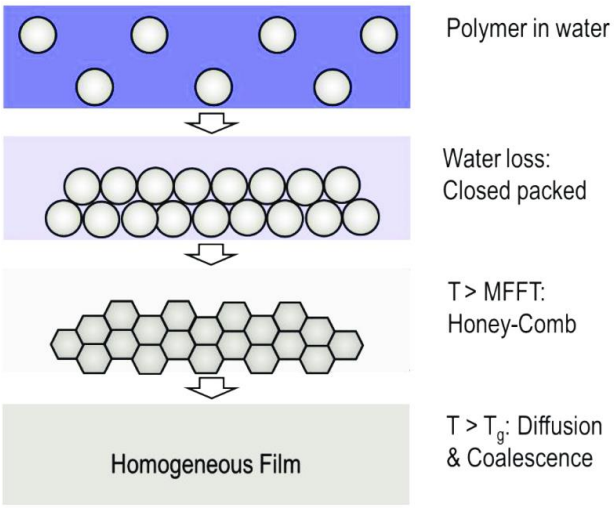

Figure 1.12: Different stages in the film formation from aqueous base polymeric dispersions.

In particular, in this approach the contact angle of a polymer dispersed sphere (θ^2) is correlated to the surface tension between air and polymer (σ), the radius of the polymer sphere (r), and the viscosity of the sphere (η), as depicted in equation 1.1.

$$\theta^2 = \frac{3\sigma t}{2\pi\eta r} \qquad (1.1)$$

At the beginning of the film forming process the contact angle is zero and it increases when two particles merge together. The equation demonstrates that a small particle size requires less forces to coalesce in comparison to the large polymer spheres. Subsequently, in contrast to this theory, the driving force for the particle's deformation has been ascribed to the capillary pressure of the interstitial water [142]. Indeed, it was demonstrated that the capillary pressure (Pc) between three adjacent polymer spheres is dependent from the interfacial tension between water and air (γ_w) and the radius of the latex particles (r), as shown in equation 1.2.

$$P_c = \frac{12{,}9\gamma_w}{r} \qquad (1.2)$$

As in the previous case, a decrease of the polymer size results in an increase in the capillary pressure, with a consequent increase of the coalescence phenomena. In

particular, it has been shown that rapid evaporation rates can result in inhibition of coalescence due failure to achieve adequate capillary pressure [143]. Besides, it was found that high humidity favours coalescence by providing an adequate capillary pressure and by increasing polymer chain interdiffusion [144]. Moreover, water can plasticize the polymer spheres hence promoting polymer chain interpenetration.

Another parameter which plays an essential role in the film formation is the drying temperature. Indeed, the formation of a continuous film that is transparent and crack-free is then dependent on the minimum film formation temperature (MFFT) of the polymer. When the drying temperature is above the MFFT the particles undergo deformation and cohesion, hence creating a homogeneous film. Contrastingly, if the drying temperature is below the MFFT, a brittle discontinuous film or a compact powder may be obtained [138]. Typically, the MFFT tends to be close to the glass transition temperature (T_g) of the polymer or above it; indeed above the glass transition temperature the molecular mobility is increased, therefore allowing chain-interdiffusion between the polymer particles. The MFFT concept was firstly described by Protzman and Brown in 1960, developing a standard test for defining MFTT as the lowest possible temperature at which film formation can occur as determined by visual observation of cracking or whitening [145].

The MFFT is influenced by the type of polymer, the particle size [146] and the presence of additives. For instance, in some cases plasticisers or coalescing aids might be added into the formulation with the purpose of facilitating the film formation. Indeed, plasticizers soften the polymers particles, thus lowering the T_g of the polymer and allowing the coalescence at lower temperatures [138]. Additionally, plasticizers can be exploited to modulate the permeability properties of the polymeric films. For instance, the use of glycerol triacetate or glycerol tributyrate as plasticizers for acrylates films was reported, discovering that an increase of the hydrophilicity of the plasticizers mix resulted in an increment of the urea permeability [147].

Regarding coalescing aids, organic solvents are typically used as additives in order to promote polymer diffusion across particle boundaries. Particularly, their addition causes a temporary plasticization that increases polymer chain motion. Subsequently, the organic solvents evaporate leaving the film properties unchanged [148].

The use of an emulsifier is necessary for the formation and stabilization of the polymer latexes; however, the nature and the distribution of the surfactant in the resulting polymeric film can significantly influence the final properties of the latter. For example, during film formation, the surfactants can be dissolved into the polymer if there is compatibility between them. The emulsifier compatibility depends not only on the nature of the polymer but also on its HLB value. As a matter of fact, studies revealed that higher HLB non-ionic surfactants are more compatible with vinylic-acrylic latexes, thus facilitating the film coalescence [149].

If there is incompatibility between surfactant and polymer, during film formation the emulsifier can migrate towards the interfaces of the film (exudation) or it can concentrate in various islets. This phenomenon was firstly observed in poly(styrene-butadiene) waterborne dispersions containing nonylphenol-polyoxyethylene as surfactants [150]. It was demonstrated that emulsifiers with long polyoxyethylene moieties exuded to the surface, whilst the ones with short chains were compatible with the polymer. It was hypothesised that as the polymer particles merge and the film becomes more homogeneous, incompatible substances are exuded to the surface. Moreover, cellulose latexes containing SDS as emulsifier were reported to undergo phase separation during film formation [151]. It was observed that SDS was present in islets whose size was influenced by the surfactant concentration, the preparation and drying methodology, and the amount and nature of the incorporated plasticizer.

In case of incompatibility between the polymer and the emulsifier, the latter can also remain at the interfaces between particles during film formation. Particularly, if it remains totally adsorbed in a monolayer coverage, it forms a continuous network of surfactant which embed the polymer particles. For instance, in poly(butyl methacrylate) dispersions with SDS as surfactants [152] a monolayer coverage corresponded to improved water barrier properties. It has been hypothesized that a better packing order of the particles occurs due to the increased stabilization of the charge. On the other hand, below monolayer coverage the barrier properties increment with an increase in the SDS concentration.

1.6. Waterborne dispersions and emulsions of biodegradable polyesters

In literature, the preparation of emulsions and dispersions of biodegradable polyesters has been reported almost exclusively for applications in the biomedical field, especially for the obtainment of biodegradable polyesters nano and micro particles for drug delivery. The most widespread polyester employed for this purpose is PLA, due to its commercial availability. Very diluted dispersions of PLA particles have been obtained by nanoprecipitation [153][154][155][156], salting-out [157][158][159] and emulsification-diffusion methods [153][160][161]. Nevertheless, these works aim at the isolation through centrifugation or lyophilization of the PLA nanoparticles. As a consequence, the dispersion stability over time is usually not investigated and besides the final PLA content is usually lower than 5 wt. %. On the other hand, PLA dispersions with a higher polymer content (maximum 20 wt. %) are accessible with the use of chlorinated solvents by means of emulsification-evaporation methods [92][162][163][164]. Also PCL received considerable attention for the preparation of nano and microparticles, due to its slow ester bond hydrolysis at neutral pH [165]. For example, the preparation of α-tocopherol loaded PCL nanoparticles with the emulsification-evaporation method was reported [166]. However, for biomedical application, PCL has often been reported copolymerized with other biodegradable polyesters, mainly PLA and PEG [39] with the purpose of tuning the final properties, such as the biodegradation and release rate, of the polyester particles. Additionally, the emulsification-evaporation method has been exploited to obtain PHB drug-loaded nanoparticles which were subsequently functionalized with a tumour-specific ligand [167]. The latter technique was also used to prepare blends of PLA, PCL and PBSA with hydrophilic polymers such as chitosan [168][169], lignin [170] and nanocellulose [171][172] and gelatin [173]. Nevertheless, in the latter cases, the studies focus on the preparation of thermoplastic composites and consequently, the stability of the dispersion was not an issue and thus not reported. Besides, in the emulsion-evaporation methods, the toxicity associated with the chlorinated solvent used in these processes limits the biocompatibility and the use of the prepared dispersion for food contact applications. Another methodology used for the preparation of biodegradable micro-and nanospheres is the double emulsion-solvent evaporation method. This is a

technique widely employed for the encapsulation of highly hydrophilic drugs that in oil-in-water emulsion are rapidly partitioned from the polymer solution into the external water media. The preparation of a water-in-oil-in-water emulsion requires firstly the formation of a water-in-oil emulsion, which is then emulsified in another water phase. In this way an organic layer protects the hydrophilic drug from portioning. This methodology was indeed exploited for preparation of hydrophobic drug-loaded particles of PLA [174], PHA [175][176] and PCL [177][178]. Nevertheless, in all the papers cited above, the main goal consists in the isolation and characterization of the drug loaded polyester particles; therefore, the dispersion stability over time is not subject of study and the final polyester content is irrelevant for the final application. In general, in literature, only few examples exist regarding the use of polyester emulsion and dispersion for coating applications. For instance, the preparation of water-in-oil emulsion of PHAs used to coat metallic biomedical implants was reported [179][180]. The PHAs in this case acted as a matrix for carrying an antimicrobial and antibiotic agent and the polyester layer was formed through a dip-coating process.

On the other hand, the preparation of waterborne polyester dispersion for coating applications has been the subject of some recent patents. In some cases, PLA [181][182], and PHAs [183] formulations with high final content (25-70 wt. %) are obtained, in the absence of organic solvents, by continuously and simultaneously introducing melted polyester and aqueous phase into a blender of an emulsifying unit. Nevertheless, with these techniques the polymer is always processed at high temperatures and usually, high amounts of viscosity reducing agents, plasticizers or additives are needed. Furthermore, the polymer particles thus obtained are in the micrometric size range. Another patent reports the preparation of an aqueous dispersion of PHAs by directly dispersing the polyester's powders in the water phase in the presence of surfactants [184]. Even though the methodology is fully eco-sustainable due the fact that organic solvents are not employed, the stability of the preparation over time is limited (between 1 week and 2 months). Additionally, the preparation of poly-D and poly L-lactides dispersions through emulsion-evaporation method has been patented [185]. In this case the polymer is solubilized in a proper organic solvent and the solution thus formed is mixed with the use of ultrasound into a water phase containing surfactants. The poly-D and poly-L-lactide dispersions prepared were then eventually mixed together in different proportions and applied

onto the chosen substrates (e.g., glass plates, metal and resin plates). After drying a biodegradable polymer layer with thickness between 10 to 100 micron is obtained. In this patent the dispersion possesses a final polymer content around 10 wt. %, whilst the particles in the water media are in the micrometric range size. Besides, the properties provided by the polyester coating were not studied and analysed.

1.7. Aim of the thesis

Aim of the present work was the development of green water-based methodologies for the process of biodegradable and bio-based polymers. Another objective of this thesis was the study and application of aqueous biodegradable and bio-based polymer formulations as barrier layers for packaging purposes and as substrates for recyclable electronic devices. In this context, polylactic acid (PLA) was selected for the preparation of aqueous formulations for coating purposes, whilst sodium alginate (SA) was chosen for the production of transparent, flexible, freestanding substrates for electronic apparatuses.

PLA was primarily selected for the formation of aqueous polymer dispersions due to its promising properties such as biodegradability, biocompatibility and production on an industrial scale at relatively low cost [186][26][187]. One goal of this work is the development of a green and water-based methodology to prepare PLA aqueous dispersions for coating purposes. To this aim, various operating parameters will be studied and optimized. In order to render the formulation applicable also for food contact purposes, only chemicals and solvents approved for this application will be employed for the preparation. For this purpose, an amorphous grade PLA soluble in a non-chlorinated solvent, like ethyl acetate, was selected. Once a water-based PLA dispersion will be devised, the extensibility of the preparation to other biodegradable polyesters, like poly(butylene succinate-co-butylene adipate), PBSA, will be investigated.

Another objective of this part of the work consists in studying the limits and advantages of the aqueous formulations developed as well as their application potential. At first, the stability and filmability of the formulation will be examined. After that, the polyester dispersions will be applied as coating on paper substrates in order to provide to the latter resistance to external agents such as water and grease.

Different paper substrates as well as distinct coating methodologies will be tested. With the aim of determining the effectiveness of the deposited polymer layers, the barrier properties to liquid water and grease of the coated papers will be examined and correlated with the weights and morphology of the coatings. Moreover, an objective of the work is to study the application potential of the PLA dispersion for the preparation of biodegradable polymer blends. Particularly, PVA will be initially chosen as the other component of the blend for its biocompatibility, high flexibility and possibility of forming hydrogen bonds with the oxygen atom of the PLA ester groups. Solution in water of different PVA types will be added to the PLA formulations and, after that, the filmability of the formed PLA/PVA latexes will be examined. The thermal stability, the morphological structure, and the mechanical properties of the PLA/PVA blends will be deeply investigated in order to determine if these characteristics will be improved with the introduction of PVA.

The aim of the second part of the research project is the study of a potential green water process for the preparation of substrates for flexible electronic devices. To this aim, sodium alginate (SA), a natural biodegradable polymer, soluble in water and easy to handle, was selected. In particular, the solubility of SA in water will be exploited to produce SA alginate foils through casting of a water solution of the latter. The film morphology will be properly characterized to verify the applicability of the polymer foils in the electronics sector. After that, organic light-emitting diodes (OLEDs) and organic solar cells (OCSs) will be built on the SA substrates through a bottom-up approach. Considering the different skills and expertise required, the research work will be conducted in collaboration with three different institutes of the CNR (Italian National Research Council), namely ISOF (Institute for Organic Synthesis and Photoreactivity), IMM (Institute for Microelectronics and Microsystems), and INO (National Institute of Optics), and the engineering department of the University of Modena (UNIMORE). After the preparation of SA based electronic devices, the performances of the latter will be measured in order to verify if with the use of SA as substrate good results will be achieved. Another part of this project aims at the development of a green procedure to disassemble and recycle the SA-based electronic devices produced through environmentally safe water processes. In this way, all the valuable components will be recovered and the generation of the electronic waste will be avoided or reduced. Different solvents capable of selectively solubilizing the component of the manufacts will be

employed. As much as possible the use of toxic and hazardous solvents as well as the use of chemicals produced from fossil sources will be avoided. Furthermore, the possibility of enzymatically degrading, in a water environment, the sodium alginate substrate will be examined. As an enzymatic catalyst, alginate lyase will be tested due to its ability to cleave particular activated glycosidic bonds that can be found in acidic polysaccharides.

CHAPTER 2

Water dispersions of biodegradable polyesters: preparation

Most of the work described in this Chapter is based on the following open access publication: Belletti, G.; Buoso, S.; Ricci, L.; Guillem-Ortiz, A.; Aragón Gutiérrez, A.; Bortolini, O.; Bertoldo, M.; “Preparations of Poly(lactic acid) Dispersions in Water for Coating Applications” *Polymers,* 2021, *13*(16), 2767.

2.1. INTRODUCTION

2.1.1. Mechanism and methods of emulsification

Emulsion formation is a non-spontaneous process; therefore, energy is required to produce dispersed droplets. Generally emulsions can be formed using static mixers and common stirrers [188], rotor-stator devices, high-pressure systems, membrane systems and ultrasonic generators [189]. For the formation of micrometric range size droplets magnetically stirring or high speed-stirrer, such as Ultraturrax, are sufficient to produce the emulsion. Ultraturrax is one of the most typical rotor-stator devices in which the oil and water phase are mixed at high rotation speeds in a narrow gap between a static disk (stator) and a rotating disk (rotor) (Fig. 2.1). In this way the droplets break-up by mechanical impingement against the wall due to the high liquid acceleration and shear stress in the turbulent flow between rotor and stator. Furthermore, rotor-stator devices for continuous operations, such as colloid mills and gear-rim dispersion machines exist [190].

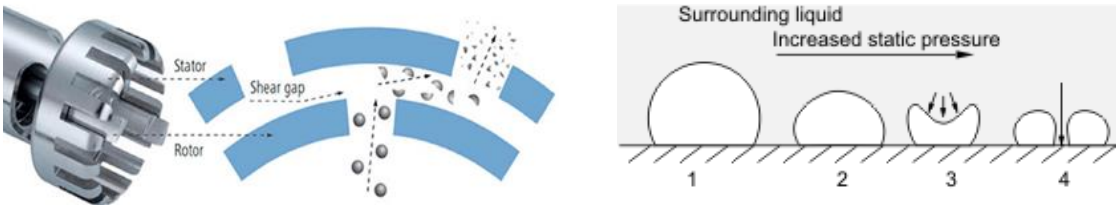

Figure 2.1: Ultraturrax emulsification mechanism at the left and implosion of a cavitation bubble generated by Ultrasound treatment at the right.

On the other hand, for the formation of submicrometric dispersed particles large amounts of emulsifiers and/or high energy are required. In this case, the use of an Ultrasound generator to provide the energy can be considered an appropriate choice (Fig. 2.1) [191]. The latter applies ultrasonic frequencies (>20 KHz) to the system, thus generating liquid acoustic cavitation. The rapid change of pressure in the liquid causes the formation of vapour cavities that, when subjected to high pressure, collapse and generate an intense shock wave. In contrast, emulsification with microporous glass or ceramic membranes is a relatively new continuous emulsification process. In this methodology the dispersed phase is pressed through the pores of a microporous membrane, whilst the continuous phase flows along the membrane surface [192]. The process parameters that are essential for controlling the droplet size are the membrane pore diameter and the flux of the continuous phase. With this technique, nanometric particles and very narrow droplet's size distribution can be obtained. On the other hand, in high pressure homogenizers pumps the fluid through a narrow gap valve using high pressure intensifiers, which greatly increases fluid speed creating depressurization with consequent cavitation and high shear stress [193].

As previously anticipated in Paragraph 1.4 of Chapter 1, two different approaches can be employed for the preparation of polymer emulsions and dispersions: emulsion polymerization and emulsification of pre-formed polymers. Emulsion polymerization is widely employed for the production of acrylate dispersions and methacrylate polymers as well as the production of several other commercially relevant polymers [194]. This technique requires the formation of an oil-in water emulsion in which droplets of monomer are dispersed in a continuous water phase with the use of a suitable emulsifier (Fig. 2.2).

In this way large drops of monomer are produced, whilst the surfactant in excess forms micelles in water where the polar heads of the emulsifier are turned towards the outside and the apolar tails are turned inwards. In any case, small amounts of monomer will be present also in the water media due to diffusion. Subsequently, a water-soluble free-radical initiator, which forms a radical species, is added. The radical forms an oligomeric species with the monomer present in the aqueous phase, which rapidly becomes incompatible with the aqueous medium and spreads towards the dispersed phases present in the system (micelles or monomer drops). Since the total surface area of the micelles (which act as reactors) is higher than the

area of the few larger drops of monomer (which act as reagent "reservoirs"), the oligomer will diffuse mainly inside the micelles. As the polymeric chain grows in the micelles, more monomer diffuses from the droplets to the growing particles until the reagent reservoirs disappear with consequent termination of the polymeric reaction. The final product of the processes is a dispersion of polymer particles in water also known as latex. For applications such as adhesive, paints, paper and textile coatings, where the final product is the dispersion itself, no further separation operations are required. If the desired product is the solid polymer, it is necessary to provide heat in order to remove the water from the formulation.

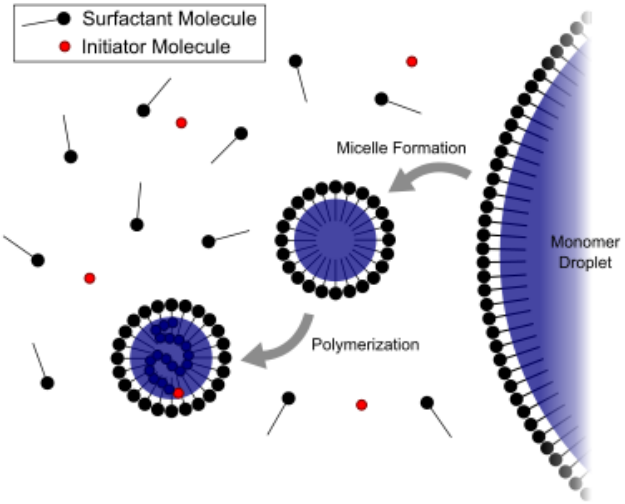

Figure 2.2: Emulsion polymerization mechanism.

Emulsion polymerization presents many advantages including the obtainment of high molecular weight chains, eliminating the use of organic solvents and efficient heat removal from the aqueous medium [195]. Due to the intrinsic eco-sustainability of the process, the latter methodology has been widely exploited for the polymerization of bio-based monomers to obtain renewable materials. Indeed, the polymerization in aqueous dispersed media of a vast range of fully or partially bio-based monomers such as terpenes, carbohydrates, lignin derivatives, proteins, vegetable oils and lipids has been reported [196]. Monomers usually derived from fossil fuels, such as acrylic acid, ethylene and styrene, can be synthesized from renewable sources and used as a starting material for the emulsion polymerization process [197][198]. Nevertheless, emulsion polymerization is a technique applicable

only to free radical polymerizable monomers and therefore many biodegradable polyesters cannot be prepared with this process. In these cases, the production of polymer dispersions and emulsions is achieved by dispersing the pre-formed polymer [199]. Generally, the pre-formed polymer is solubilized in a proper organic solvent and this solution is then dispersed in the water phase. In this case, even though harmful organic solvents are often employed to solubilize the pre-polymer, it is easier to control the molecular weight and the features of the chosen polymer. For instance, in the acetone process, often employed for the preparation of polyurethane-polyurea dispersions, the pre-polymer is firstly chain extended in acetone to give the desired molecular weight and then the organic phase is emulsified in the aqueous one [200][201]. Besides, in comparison with emulsion polymerization, the preparation of polymer dispersion and emulsion presents some advantages including the absence of toxic monomers, oligomers, and catalysts residua.

In general, the salting-out, emulsification-diffusion, and nanoprecipitation are amongst the most common methodologies that exploit the emulsification of the preformed polymer (Fig. 2.3) [202]. Nanoprecipitation technique has been widely exploited in pharmaceutical and agricultural research for drug encapsulation. It requires the solubilization of the polymer in an organic solvent that is partially miscible with water, like acetone. The organic phase is then added dropwise into the water under strong magnetic stirring and, after diffusion of the organic solvent in the aqueous media, polymer particles precipitate leaving a polymer dispersion. The main advantage of the methodology is that no surfactants and additives are needed that could affect the properties and biocompatibility of the product. Even in the salting-out technique the polymer is solubilized in a water-miscible organic solvent; however, the water phase contains high concentration of salting-out agent. Contrary to the nanoprecipitation, the solvent diffusion, in this case, is hindered by the presence of the salting-out agent in the aqueous phase. If the goal is the obtainment of a polymer dispersion, the emulsion thus formed is diluted with the sufficient amount of water to lower the concentration of the salting-out agent, thus allowing the diffusion of the organic phase into the media. Even though high concentration of salting out agents are required, better control of the particle size is achieved than with nanoprecipitation [158].

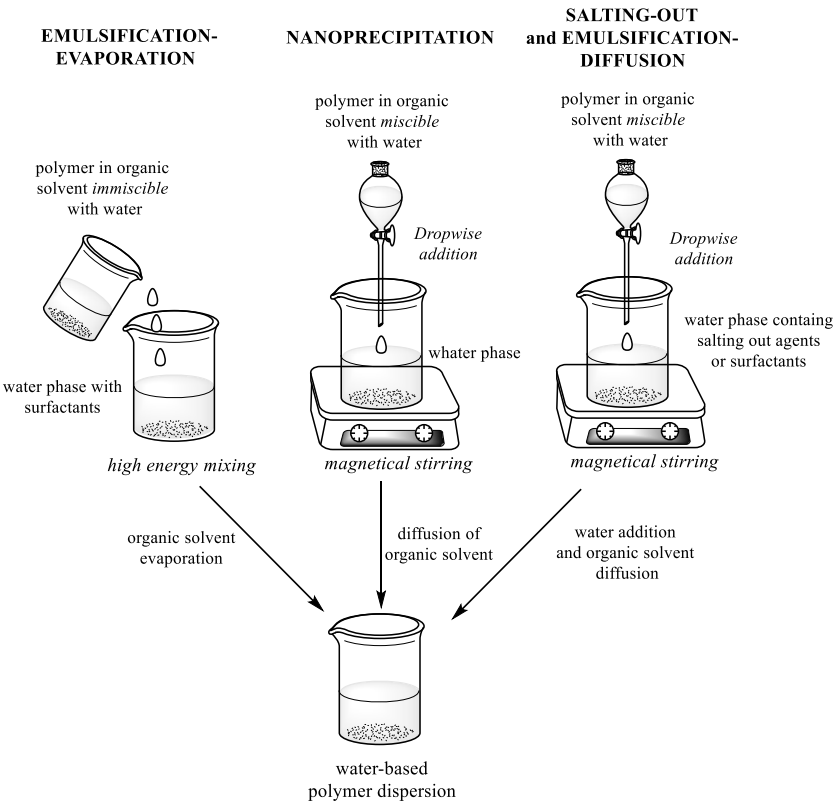

Figure 2.3: Comparison between emulsification-evaporation method, nanoprecipitation, salting-out and emulsification-diffusion methods.

The diffusion-emulsion method differs from salting out only in the use of an aqueous phase surfactant instead of a salting-out agent. Unlike the latter two methodologies, in nanoprecipitation there is no formal emulsion formation due to the fact that spontaneous precipitation of the polymer chains into a non-solvent phase occurs. With the nanoprecipitation and salting out techniques, usually dispersion with low final polymer content (< 5-10 % w) and micrometric range size particles are obtained. Indeed, these processes mainly aim at obtaining the polymer particles for drug encapsulation and release purposes. Nevertheless, for coating purposes, where the goal is the achievement of a dispersion with high polymeric content, the use of an emulsification-evaporation method is more indicated. Generally, the simplest procedure requires the solubilization of the polymer in a water-immiscible organic solvent, followed by subsequent dispersion of the organic phase into the aqueous medium. After that, the organic solvent is evaporated thus forming a polymer dispersion [203].

2.1.2. Surfactants

When preparing emulsions, it is always necessary to use a surfactant (also known as emulsifier) in order to disperse the two immiscible liquid phases [204]. Indeed, the selection of the proper emulsifier is essential to ensure the formation of the emulsion and its stability over time. Surfactants are amphiphilic molecules that are constituted by a hydrophilic head group and a hydrophobic tail. They are able to lower the surface tension between two liquids in order to form small droplets of dispersed phase. Moreover, when the emulsifier is absorbed on the surface of droplets it forms a protective layer, which prevents the droplets from merging together [205]. Surfactants are commonly classified according to the polarity of their head group: anionic, cationic, non-ionic and amphoteric [206] (Fig. 2.4).

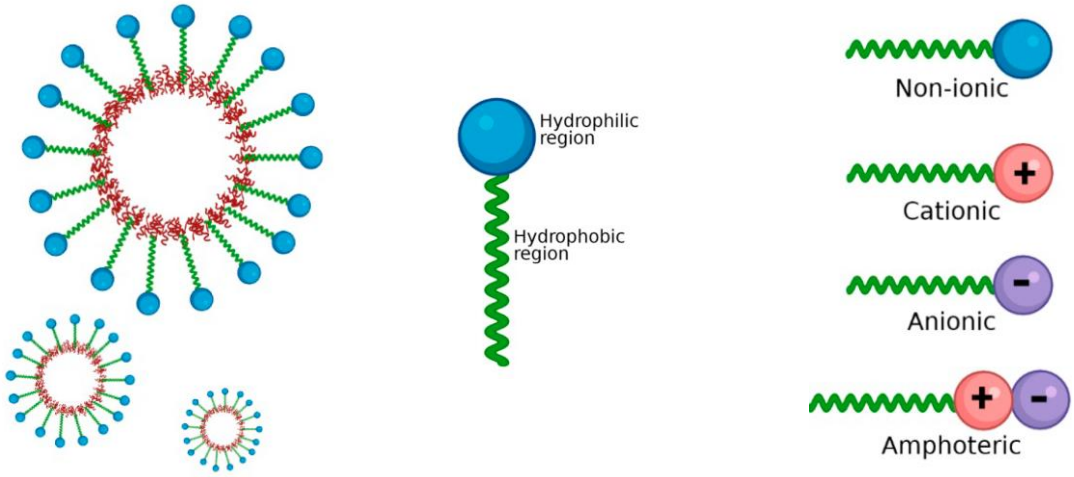

Figure 2.4: Micellar structure of the dispersed phase at the left, surfactant structure in the middle and type of emulsifier at the right.

When anionic, cationic or amphoteric emulsifiers are adsorbed on the emulsion droplet, an electrical double layer is formed, which can provide electrostatic repulsion between the particles. This repulsion is able to prevent the merging and the consequent destabilization of the dispersion. When charged emulsifiers, such as sodium dodecyl sulphate, are employed the system becomes sensitive to the presence of electrolytes. On the other hand, non-ionic surfactants, also named polymeric surfactants, like Pluronics, are extremely efficient in stabilizing the emulsion. Nevertheless, with non-ionic emulsifiers the production of small particles may be challenging without applying high energy. In this case, the presence of an

adsorbed surfactant or emulsifier layer prevents the merging of the droplets through steric repulsion. Generally, different typologies of emulsifiers can be used in mixture in order to have an optimal emulsification and stabilization of the emulsion. Besides, the influence of the emulsifier on the formation of polymeric film from latexes is deeply examined in Paragraph 1.5 of Chapter 1 concerning the film formation from aqueous-based polymeric dispersions.

Emulsifiers can be produced using either petrochemical and bio-based feedstock and, in recent years, due to the continuous consumption and depletion of fossil fuels, renewable substrates have been of growing interest for the production of bio-based surfactants [207].

2.1.2.1. Hydrophilic-lipophilic balance (HLB) value

The selection of the suitable emulsifier for a particular application is not a systemic process. Indeed, the industry often relies on the experience and recommendations and several time-consuming tests are needed in order to find the most suitable candidate. An empirical rule for the selection of emulsifiers based on the surfactant solubility was firstly provided by Bancroft. The rule establishes that the phase in which an emulsifier is more soluble constitutes the continuous phase [208]. Another criterion for the selection of the proper surfactant, based on the emulsifier chemical structure, was introduced by Griffith in 1949 with the use of the HLB (Hydrophilic-lipophilic balance value) [209]. The HLB value of a surfactant is a measure of the relative percentage of hydrophilic to lipophilic groups in the molecules. In particular, surfactants with HLB > 7 tend to form emulsions with oil droplets dispersed in water (oil-in-water emulsions) and HLB < 7 tend to form emulsions with water droplets dispersed in the oil media (water-in-oil emulsions). Griffith also proposed a method for calculating the HLB value, which is valid only for non-ionic surfactants. As a consequence, a general methodology to calculate the HLB value was reported by Davis in 1957 (equation 2.1) [210]. The effect of stronger and weaker hydrophilic groups is taken into account with this calculation, where m corresponds to the number of hydrophilic groups in the molecule, H_i is a tabulated value of the i^{th} hydrophilic group and n is the number of lipophilic groups in the emulsifier.

$$HLB = 7 + \sum_{i=1}^{m} H_i - n\ x\ 0{,}475 \qquad (2.1)$$

Furthermore, HLB values are additive, consequently the HLB value of a surfactant mixture can be calculated using equation 2.2., in which w_1 and w_2 are the weight of the surfactant 1 and 2, respectively, while w corresponds to the total weight of the surfactant mixture

$$HLB_{mixture\ 1,2} = \left(\%\frac{w_1}{w}\ x\ HLB_1\right) + \left(\%\frac{w_2}{w}\ x\ HLB_2\right) \qquad (2.2)$$

Generally, the HLB value is employed as a guide for the selection of the suitable surfactants' mixture. Two emulsifying agents that are at the opposite of the HLB scale are chosen and used in different percentages with the purpose of obtaining a wide range of HLB values. After that, the stability for the emulsion produced at each HLB number is assessed to determine the most efficient surfactant composition.
Nevertheless, the HLB concept possesses some limitations due to the fact that factors such as temperature, concentration of the emulsifier, possible interaction of other molecules, concentration of the continuous and dispersed phase are not taken into account.

2.1.3. Stabilizers

Stabilizers are non-surface-active agents which are able to contribute to the interfacial stabilization of an emulsion by interacting with the surfactant layer already located to the interface [211]. Over the years, due to the necessity of more eco-sustainable processes, the interest has shifted towards the use of bio-based and renewable stabilizers.
In particular, hydrocolloidal polymers have been widely employed as stabilizers due to their biodegradability, availability in nature as well as their promising physicochemical properties [212]. Hydrocolloids are a heterogeneous group of long-chain polymers (polysaccharides or proteins) that are capable of forming viscous

dispersions and/or gels in water. The majority of hydrocolloids can act as stabilizing agents in oil-in-water emulsions, even though only a few can act as emulsifiers [213]. Indeed, a distinction must be made between stabilizer and emulsifiers, the latter requiring substantial surface activity at the oil–water interface. The surface activity of hydrocolloids that act as emulsifiers is given by the presence of hydrophobic protein linked to the polysaccharide bone (such as arabic gum and pectines) or by chemical modification. In particular, in the latter case, hydrophobic groups are chemically inserted to the polysaccharide chain in order to provide the final molecules with an amphiphilic character. For instance, hydrophobically modified starch and cellulose have emerged as a possible alternative to fully fuel-based emulsifiers [214][215]. On the other hand, hydrocolloidal unmodified polysaccharide are able to function as stabilizers through interaction with the surfactant layer, thus increasing the steric hindrance around the dispersed droplets and preventing them from merging. Furthermore, these molecules can stabilise the formulation by working as a thickening or gelling agent in the aqueous media. In this way, the rheology of the continuous phase is modified and this leads to the slowing down or the prevention of creaming [212]. This rheological control mechanism is more efficient at low oil phase/water phase ratios, where individual droplets remain entangled in the biopolymer network. One of the most effective molecules in this type of stabilizing mechanism is xanthan gum. As previously described in Paragraph 1.3.2 of Chapter 1, xanthan gum is a natural polysaccharide whose chains are able to build up in water a 3D network that increases the viscosity of the water media even at low concentrations, hence slowing down creaming. The use of xanthan gum as stabilizers was initially studied using model oil-in-water emulsions [216][217]. It emerged that low concentration of xanthan induced creaming, whilst higher concentrations improved creaming stability due to the modification of the rheological properties of the continuous water media. It was also observed that the rate of creaming was increased by emulsion droplet flocculation. Subsequently, the mechanism of this flocculation has been identified as depletion flocculation [218]. In particular, the study conducted on sodium caseinate oil-in-water emulsions revealed that low concentration of xanthan gum caused fast creaming and phase separation due to depletion flocculation of the emulsion's droplets [219]. Indeed, large flocs move at a faster speed than the individual particles. Even though the increase in xanthan gum concentration caused a more extensive depletion flocculation, it was noticed an improvement in the creaming stability. This was ascribed both to the

incremented viscosity of the continuous phase and to the formation of a 3D gel-like network of emulsion droplets, with a consequent retard of creaming. In another study where xanthan gum was used as a stabilizer in combination with hydrophobically modified starch as emulsifier similar results were shown [220]. Besides, the influence of xanthan gum on rheological properties and stability of corn oil-in-water emulsions, stabilized by non-ionic surfactants, was subject of study [221]. It emerged that the addition of xanthan prevented the formulations from coalescence. Besides, an increase in xanthan caused a decrease in droplet size and an increment in the elastic properties of emulsions. Above 0.04% of polysaccharide concentration, rheological measurements indicated formation of weak gels due to droplet network association caused by depletion flocculation.

Another polysaccharide that has been explored as a stabilizer for oil-in-water emulsions is microfibrillated cellulose (MFC). Cellulose is the most abundant polymer on earth and it is constituted of glucan chains with repeating β-(1 /4)-D-glucopyranose units. These chains form parallel bundles, the microfibrils, which aggregate to form cellulose fiber. Through a fibrillation process, the cellulose fibers can be separated into a three-dimensional network of microfibrils with a large surface area. These entangled fibrils are called microfibrillated cellulose (MFC) [222]. Hydrophobized MFC has been reported to act as surfactant for the formation of water-in-toluene emulsions increasing the final stability of the preparation [223]. In this case, the MFC has been provided with activity at the interface as a result of its modification. Regarding the use of unmodified MFC, an interesting study reported the properties and stability of oil-in-water emulsions stabilized by this cellulose derivative [224]. With MFC all formulations possessed long-term stability over storage. It was hypothesized that the absorption of MFC at the interface provides a steric barrier preventing droplet coalescence through a Pickering mechanism. Additionally, it was noted that an increase in the stabilizer's concentration led to the formation of a 3D network able to entrap the dispersed droplets. In a previous study, the same authors examined the influence of the homogenization steps to obtain the MFC from mangosteen reed on the emulsion stability [225]. The study revealed that higher number of homogenization steps resulted in smaller droplets and greater stability against creaming.

Even though starch is the second most abundant biopolymer after cellulose, its use as stabilizer is not extensively reported in the literature [226][227]. On the other hand, it is widely employed as an emulsifier. In particular, the use of starch granules

as emulsifiers for the formation of Pickering emulsion has been widely explored [228]. Native starches extracted from different sources were tested and it emerged that their emulsifying capability was inversely related to the granules' size. Moreover, starch is often chemically modified with the introduction of a hydrophobic group, such as octenyl succinic anhydride (OSA), with the purpose of providing the molecule with surface active properties [229]. An interesting work reported the preparation of oil-in-water emulsions stabilized by gelatinized corn-starch [226]. In this case, the oil phase was dispersed into a starch dispersion, without the use of an emulsifier. It was hypothesised that the stability of the resulting formulation was due to degradation of starch during the homogenization process with the consequent formation of polysaccharide fragments and molecules. The starch fragments stabilised the emulsion through a Pickering mechanism, whilst the polysaccharide molecules formed a gel-like structure in the continuous phase entrapping the droplets and improving the formulation stability. Another later work reported the preparation of oil-in-water emulsions using gelatinized kudzu starch without a commercial or natural emulsifier [227]. The stabilisation mechanism proposed was the same as in the previous paper. In particular, the authors investigated the influence of the homogenization method on the stability of the preparation, discovering that the best results in terms of stability were achieved with the use of a rotor-stator homogenization followed by a high-pressure one.

2.2. RESULTS AND DISCUSSION

2.2.1 Influence of the preparation conditions on the stability of PLA dispersions in water

Several tests to prepare ethyl acetate/water (EtOAc/H_2O) emulsions of PLA with SDS as surfactant and starch as stabilizer were carried out (Table 2.1), by using Ultraturrax (UT) or Ultrasound processors (UH and UVC) as homogenizer.

Table 2.1: Experimental conditions adopted to prepare ethyl acetate-(EtOAc) in-water PLA dispersions with SDS as surfactant and starch as stabilizer.

Entry	Organic phase EtOAc/H_2O						Dispersion features		
	PLA (wt/vol %)[a]	Vol. (ml)	Vol. ratio	SDS conc. (wt. %)	Vol tot. (ml)	PLA/water[b] (wt %)	Homogenizer[c]	Stability[d]	Particles size[e] (nm)
1	11	45.0	1.3	0.8	80	14	UT	coa.	-
2	11	45.0	1.3	0.8	80	14	UH	yes	214 ± 2
3	11	45.0	1.3	0.8	80	14	UVC	yes	203 ± 7
4	11	62.5	1.8	0.8	97	20	UVC	cl.	225 ± 3
5	8	62.5	1.8	0.8	97	14	UVC	yes	178 ± 2
6	8	20.8	1.8	0.8	32	14	UVC	yes	167 ± 1
7	8	87.5	2.5	0.8	122	20	UVC[6]	cl.	202 ± 2
8	8	87.5	2.5	0.8	122	20	UH[6]	yes	130 ± 10
9	8	50.0	2.5	0.8	70	20	UVC	coa.	-
10	8	50.0	2.5	0.8	70	20	UH[6]	yes	138 ± 23
11	8	50.0	5.0	0.8	60	15	UH	coa.	-
12	8	50.0	2.1	0.3	74	17	UH	yes	158 ± 12
13	8	20.8	1.8	0.5	58	15	UVC	yes	183 ± 2

[a]Ratio between the weight of polylactic acid and the volume of EtOAc. [b]Ratio between the weight of polylactic acid and the volume of water. [c]UH= Ultrasonication with Hielscher, UVC= Ultrasonication with Vibracell, UT = Ultraturrax. [d]Assessed through visual criteria and DLS analysis both after the preparation and after 1 week. Stability as follows: coa. = coagulation, cl. = clot formation. [e]Determined through DLS analysis.

When Ultraturrax (UT) was used, the emulsion formed but it was unstable (entry 1, Table 2.1); during the subsequent evaporation of the organic solvent, the majority of the preparation coagulated. On the contrary, with the use of ultrasound processors, either Ultrasound Hielscher UP200St (UH) or Vibra-Cell Ultrasonic Liquid Processors VCX750–SONICS Materials (UVC), stable PLA emulsions in water were obtained (Fig. 2.5a). As a matter of fact, by solvent evaporation, these were converted into stable dispersions with size of 200–215 nm. No significant effect of the specific ultrasound processor used on the particle size was noticed (Table 2.1). Dry matter content was between 13 and 20 wt. %, which is much higher than any other reported result for stable PLA dispersions in water produced with emulsification-evaporation methods and non-chlorinated solvents [230][162].

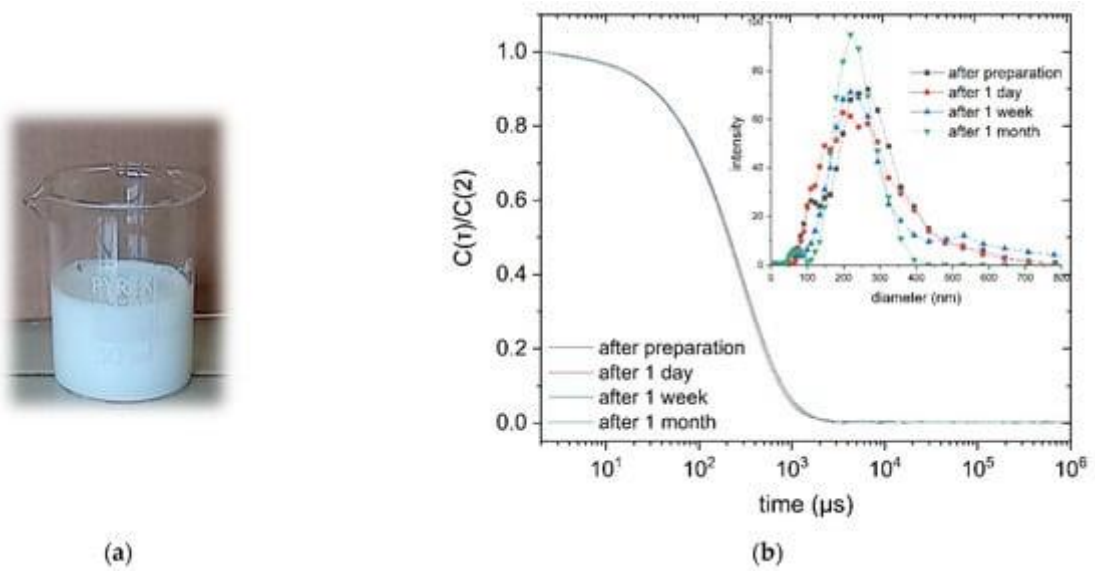

Figure 2.5: a) Picture of the PLA dispersion of entry 5, Table 2.1. b) comparison between DLS plots of the PLA dispersions prepared under the condition of entry 3, Table 2.1, after storing for increasing periods of time. Correlograms are normalized with respect to the intensity at time 2 μs. Insert refers to the particle size distribution as obtained by data fitting with a multimodal size distribution function.

Inspired by the good results obtained with ultrasound homogenizers, an attempt was made to further increase the PLA content in water by using a larger volume of organic phase, namely, 62.5 mL instead of 45 mL, to prepare the emulsion with the UVC homogenizer (entry 4, Table 2.1). However, even if the emulsion formed, the process was not effective since a cloth made of PLA formed on the stirrer during the subsequent EtOAc evaporation. When the process was replicated with the same oil and water phase volumes, but with 8% concentration of PLA instead of 11% in the organic phase, once again a homogeneous emulsion was obtained (entry 5, Table 2.1).

In this case, the emulsion was stable enough to be converted into a stable dispersion by EtOAc evaporation. Particle size was smaller than the one obtained in the previous test with higher PLA concentration (entry 5 vs entry 4, Table 2.1). Similar results were afforded when the total volume of the organic and water phases was reduced from 97 to 32 mL (entry 6, Table 2.1). The results suggest that the viscosity of the oil phase is the key parameter enabling dispersion in the case of the higher

oil/water phase ratio. Indeed, dispersion was achieved with PLA concentration of 11% and phase ratio of 1.3 or PLA concentration of 8% and phase ratio of 1.8. The decrease of the PLA concentration in EtOAc leads to a lower viscosity of the organic phase, thus reducing the energy input needed to disperse the organic phase into the aqueous one [231]; as a consequence, the treatment of a larger total volume becomes feasible. The further attempt to prepare a more concentrated PLA dispersion by increasing to 87.5 mL the volume of the 8% PLA solution (oil/water phase ratio of 2.5), once again gave an emulsion. However, this was not very stable and a clot formed on the stirrer during evaporation of the organic solvent, if the UVC homogenizer was used (entry 7, Table 2.1). On the contrary, with UH homogenizer, after solvent evaporation, the emulsion turned into a homogeneous dispersion with 20% dry matter content (entry 8, Table 2.1). Even when the preparation was performed in a smaller scale (with a lower total volume) but with the use of UVC homogenizer, a clot on the stirrer was formed during evaporation of the EtOAc (entry 9, Table 2.1). This result clearly indicates the higher efficiency of UH in transferring the energy and in treating larger both total volume and EtOAc/H_2O volume ratio than UVC does. Indeed, UH sonication was effective in treating EtOAc/H_2O volume ratio up to 2.5 (entries 2, 8, 10 and 11, Table 2.1), whilst the ratio was only up to 1.8 for preparations performed with UVC (entries 3, 4, 5, 6, 7 and 9, Table 2.1). In any case, the maximum EtOAc/H_2O volume ratio that could be treated is 2.5. As a matter of fact, no stable preparation could be obtained with a ratio of 5, even with the UH homogenizer, a relatively low total volume (60 mL) and a high concentration of stabilizer, 1.1% instead of 0.5% (entry 11, Table 2.1).

When the ratio between phases was lower than 2.5 for treatment with UH and not higher than 1.8 for UVC use, stable emulsions and then dispersions were obtained, even with SDS concentration lower than 0.8%. Indeed, good results were obtained with SDS 0.3% (entry 12, Table 2.1) plus 0.5% of starch.

2.2.2. Influence of ethyl acetate residua on the emulsion stability

The homogeneous emulsions obtained in the experiments described in Table 2.1, if left standing without stirring, coagulated in a reasonably short time. However, it was clear that they turned into stable dispersions after complete evaporation of the organic solvent (Fig. 2.5a). Dispersions can even be stored at room temperature or

in the fridge at +4 °C for days and months without sedimentation and significant change of the particles' size and of their distribution (Fig. 2.5b).

In order to better understand the emulsion preparation process, different samples were singled out at distinct times during the evaporation of the EtOAc and they were analyzed through DLS and head-space GC. Furthermore, the evolution of the dry matter content, while EtOAc evaporates, was followed. The experiment was carried out under the condition of entry 3 in Table 2.1. The evolution of the dry matter content shows an almost linear increase over time (Fig. 2.6a). On the contrary, the EtOAc residue initially decreases slowly, and then almost exponentially. The difference among the two kinetics clearly indicates that during the evaporation stage not only the organic solvent but also a portion of water is removed from the preparation. This is due to the minimum temperature of the azeotrope between water and EtOAc.

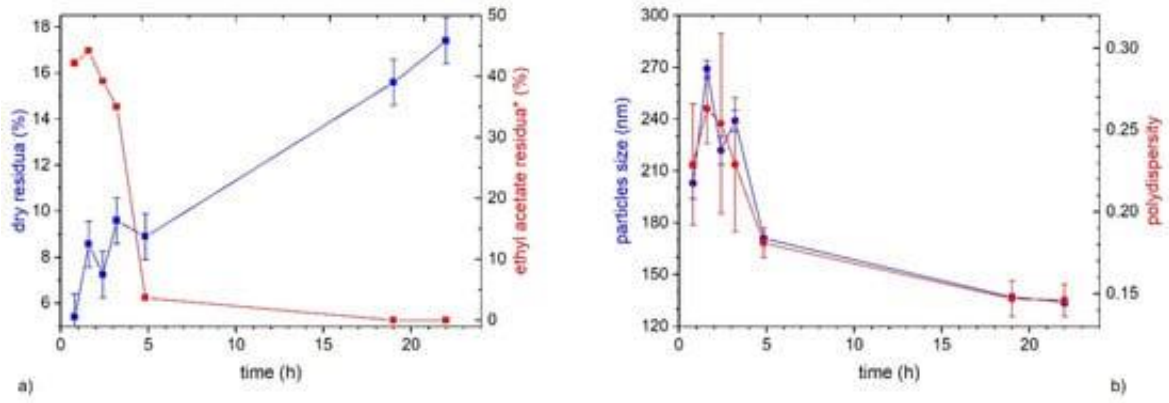

*Figure 2.6: a) Kinetics of ethyl acetate residue (red line) and dry residue (blue line) evolution. b) Kinetics of particles size (blue line) and polydispersity (red line) evolution over time. Data are related to test 3 in Table 2.1. * The highest data of ethyl acetate residua expressed in ppm are only indicative.*

In the initial period (0–3 h) when the EtOAc residuum is very high (~40%) but also later on, when it is lower, e.g., 37% at 5 h, the preparation is unstable and coagulates by standing. On the contrary, when the EtOAc residuum reaches the value of 80 ppm, after 19 h, the preparation is almost stable. In this case, the DLS correlogram exhibits just a slight decrease of the intensity during the analysis time and the emulsion was visibly stable. Besides, when the EtOAc residuum is only 33 ppm

(after 22 h), the dispersion is very stable, even after a month of storing in the fridge at 4 °C (Fig. 2.5). Overall, the data collected show that, in order to ensure the stability of the dispersion, the organic solvent must be completely removed (residue of EtOAc lower than 40 ppm).

During EtOAc evaporation, particle size and polydispersity evolve, both passing through a maximum after 90–100 min and then decreasing to reach the minimum after 1 day (Fig. 2.6b). The initial increase of size can be due to coalescence between distinct particles. Indeed, after preparation, the dispersed phase is made of drops of PLA solution in EtOAc. As the solvent evaporates, the particle volume decreases and therefore also its size. Furthermore, due to the evaporation of EtOAc, the concentration of PLA in the particle increases and, as a consequence, the viscosity of the oil phase increases also. As a result, the rate of coalescence between distinct particles decreases and becomes irrelevant once particles are solid.

2.2.3. Effect of stabilizer on PLA dispersions stability

With the purpose of studying the role of starch on the stability of the emulsion/dispersion, different trials to prepare the emulsion with only SDS as surfactant or with other polysaccharides than starch were performed (Table 2.2). Two different tests were carried out with only SDS as surfactant. The water phase amount, composition and the total amount of PLA were the same. The only difference between the two tests was the concentration of the oil phase, which was 11% and 8%, (entries 1 and 2, Table 2.2, respectively), and as consequence the oil phase amount and the oil/water phase ratio also has changed. In both cases, PLA dispersions unstable by DLS analysis were obtained. The comparison with the high stability of the dispersions prepared under comparable conditions with the additional presence of starch (entry 3 and 5 in Table 2.1, respectively) clearly indicates that the presence of such agent is of utmost importance for the stabilization of the resulting formulations. Usually, starch can act as an emulsifier only if hydrophobic modifications are introduced on its chain with the purpose of introducing substantial surface activity at the oil-water interface [232]. Gelatinized starch, as a non-surface-active polysaccharide, has been reported to act as stabilizer for the emulsion by

forming a secondary steric stabilization layer through interaction with the pre-adsorber emulsifier [233][211].

Table 2.2: Screening of different stabilizers for the preparation of PLA dispersions in the presence of SDS as surfactant.

	Aqueous phase		Organic phase		EtOAc/H_2O	Dispersion feature
Entry	Stabilizer	wt. %	PLA (wt/vol %)[a]	Vol. (ml)	Vol. ratio	Stability[b]
1	-	-	11	45.0	1.3	no
2	-	-	8	62.5	1.8	no
3	MFC	0.500	11	45.0	1.3	sed.
4	XG	0.090	11	15.0	1.3	no
5	XG	0.009	11	15.0	1.3	yes
6	XG	0.009	11	45.0	1.3	coa.

[a]Ratio between the weight of polylactic acid and the volume of EtOAc. [b]Assessed through visual criteria and DLS analysis both after the preparation and after 1 week. Stability as follows: coa. = coagulation, sed. = sedimentation.

After the result with starch, we decided to explore if similar results could be obtained with other polysaccharides. To this aim, microfibrillated cellulose and xanthan gum were tested. As previously anticipated in Paragraph 2.1.3, microfibrillated cellulose (MFC) has been reported to form in water a three-dimensional network capable of incorporating dispersed oil droplets, preventing their coagulation and sedimentation [224]. On the other hand, xanthan gum (XG) is widely used to increase the viscosity of the aqueous phase, hence preventing creaming of oil droplets [219]. However, in the case of the PLA, the attempt to employ MFC as stabilizer in a concentration of 0.5 wt.% in water, in the presence of SDS, gave a PLA dispersion that sedimented over time (entry 3, Table 2.2). On the other hand, any attempt to prepare PLA dispersions in the presence of higher MFC content was not successful because the mixtures could not be homogenized under ultrasound treatment due to the extremely high viscosity of the water phase.

Similar viscosity constraints were also observed with XG. Indeed, tests with XG as stabilizer provided stable dispersions only at XG concentration in water of 0.009 wt.% (entry 5, Table 2.2). The high viscosity of more concentrated XG solution, even

0.1 wt.%, prevented the effective emulsification of oil-and-water phases. Dispersion with 0.009 wt.% concentration of XG has nanoparticles with 192 nm diameter and dry residual of 14%. Both values are comparable to the ones achieved with starch as stabilizer, hence suggesting comparable mechanisms of stabilization for the two polysaccharides. Unluckily, when the preparation was performed at a larger scale (3 times higher) with XG, coagulation occurred (entry 6, Table 2.2). Overall, a PLA dispersion in water is formed in all the conditions listed in Table 2.2. However, only with starch as stabilizer is the formulation stable over time and it maintains its stability even when it is prepared at a higher scale, thus highlighting the key role of this polysaccharide in efficiently stabilizing the preparations, without preventing the effective homogenization of phases during the emulsion preparation.

Furthermore, the good stability of dispersions with starch, in spite of the lower viscosity of starch solutions with respect to XG, suggests that the viscosity is not the parameter that controls the dispersion stability.

2.2.4. Long term stability of the dispersions

The long-term stability of the dispersions was assessed by monitoring different formulations prepared under the same conditions of entry 3, Table 2.1 (from entry 1 to 5, Table 2.3) 12-21 months after the preparation. All the dispersions were stored in the fridge at +4°C. By visual analysis, all the formulations considered showed the presence of a white precipitate on the bottom, indicating sedimentation. Particularly, TGA analysis of the dispersions was conducted to monitor the variation of dry residua over time, while DSC analysis was performed to investigate the nature of the precipitate formed. All the data are reported in Table 2.3. It can be noticed that after 12 months the dry residues are only slightly decreased (entry 1,2, Table 2.3), while after 16-21 months they are more than halved (from 6.4 to 9 wt. %) (entry 3,4,5, Table 2.3). The DSC thermograms of the precipitates showed a glass transition temperature between 51.5 and 53.8 °C, in agreement with the PLA grade employed for the preparation. Consequently, the decline in the dry residue can be ascribed to the sedimentation of the PLA submicrometric phase. In particular, after 12 months, only 1-6 % of the PLA phase sediment, while after 21 months half of the PLA is precipitated (entry 1,2 vs entry 5, Table 2.3). Additionally, DSC analysis of the dried emulsion was conducted. The formulations analyzed after 12 months

showed a slight decline of the T_g temperature (from 51 to 47 °C). This can be assigned to a decrease in the molecular weight of PLA following hydrolytic degradation. After 16 months, the thermograms of the formulation analyzed cannot be interpreted or a T_g equal to 23 ° C is detected (entry 3,4,5, Table 2.3). In this case, the dispersed polymer is almost completely degraded.

Table 2.3: T_g of the dispersion after preparation, T_g of the dispersion over time, T_g of the precipitate and dry residue of the PLA dispersions prepared under the same conditions of entry 3, Table 2.1 over time.

Entry	Dry residue (wt. %)[a]	Dry residue over time (wt. %)[a]	Time (months)	T_g precipitate (°C)[b]	Amount of PLA precipitated (wt. %)	T_g dispersion over time (°C)[b]
1	16.0	15.8	12	51.6	1	46.7
2	17.0	16.0	12	52.1	6	47.2
3	15.0	9.0	16	53.8	40	nd[c]
4	14.2	7.0	20	51.7	50	23.3
5	14.0	6.4	21	51.5	54	nd[c]

[a]Determined through TGA analysis. [b]Assessed through DSC analysis. [c]n.d = non detectable.

Furthermore, DLS analysis was performed with the purpose of monitoring a variation of the particles size and polydispersity over time (Table 2.4).

Table 2.4: Particles size and polydispersity of PLA dispersions prepared under the same conditions of entry 3, Table 2.1 over time.

sample	Particles size (nm)[a]	Polydispersity[a]	Particles size over time (nm)[a]	Polydispersity over time (nm)[a]	Time (months)
1	202 ± 2	0,208 ± 0,016	268 ± 5	0,183 ± 0,009	12
2	194 ± 1	0,194 ± 0,015	261 ± 4	0,160 ± 0,021	12
3	217 ± 2	0,209 ± 0,014	289 ± 6	0,133 ± 0,028	16
4	225 ± 4	0,211 ± 0,011	300 ± 5	0,240 ± 0,024	20
5	223 ± 5	0,205 ± 0,027	313 ± 6	0,169 ± 0,041	21

[a]Assessed through DLS analysis

For each formulation analyzed during time, two samples were taken from the top and bottom of a standing flask. Since the samples taken from the same formulation showed similar characteristics regardless of the sampling point, it was decided to report in Table 2.4 the data relating to the sampling from the top of the formulation. It is possible to notice that over 12-21 months the particle size tends to increase, while the polydispersity usually decreases (from entry 1 to 5, Table 2.4). From this result it can be deduced that the dispersion is subject to destabilization by coagulation or Ostwald ripening. All the DLS correlograms displayed just a slight decrease of the intensity during the analysis time.

To sum up, after one year, the PLA formulations analyzed show the presence of a minimal amount of precipitate on the bottom due to sedimentation. The TGA, DSC, and DLS analysis revealed that the characteristic features of the formulation remain almost unvaried after one year from the preparation even if, to a small extent, the dispersed submicrometric phase is subject to coagulation or Ostwald ripening (entry 1,2, Table 2.4). On the other hand, after one year, the dispersions are unstable due to the high quantity of sedimented dispersed phase (entry 3,4,5 Table 2.4). Furthermore, in this case the PLA sub micrometric particles that did not sediment undergo significant hydrolytic degradation.

2.2.5. Screening of different emulsifiers for the formation and stability of the PLA Dispersion

In order to study the role of the emulsion stabilizer used in the formation and stability of the preparations, several surfactants in different combinations and concentrations were tested (Table 2.5). At first, SDS in combination with Span 80, SYN (a PEO-PPO block copolymer), alone and in combination with Span 80 and Tween 80 were tested in the absence of starch (from entry 2 to 9, Table 2.5). However, only SDS in combination with Span 80 (entry 2, Table 2.5) and SYN at 2.4% concentration (entry 4, Table 2.5) provided stable emulsions. In the case of SYN, an almost satisfactory emulsion was already obtained at 0.8% (entry 6, Table 2.5). However, PLA coagulated on the stirrer forming a clot during the subsequent solvent evaporation, when the concentration was other than 2.4% (entries 3, 5, 6 and 7, Table 2.5).

Table 2.5: Screening of different surfactants for the preparation of PLA dispersions.

Entry	Surfactant	Description	Aqueous phase			Dispersion stability[a]
			Surfactant (wt %)	HLB	Starch (wt %)	
1	SDS	Anionic surfactant	0.8	40	0	unstable
2[b]	SDS Span80	Anionic surfactant Non-ionic surfactant	2.5 0.5	34	0	stable
3	SYN	Block copolymer PEO/PPO	4.8	29	0	unstable
4	SYN		2.4	29	0	stable
5	SYN		2.0	29	0	unstable
6	SYN		1.6	29	0	unstable
7	SYN		0.8	29	0	unstable
8	SYN Span80	Block copolymer PEO/PPO Non-ionic surfactant	0.8 0.5	19	0	unstable
9	Tween 80	Non-ionic surfactant	0.5	15	0	partial
10	SYN	Block copolymer PEO/PPO	2.4	29	0.5	stable
11	SYN		0.8	29	0.5	unstable
12	Met. 388	Non-ionic compound	0.8	19	0.5	inverted
13	Tween 20	Non-ionic surfactant	0.5	17	0.5	partial
14	Tween 80	Non-ionic surfactant	1.0	15	0.5	partial
15	SA	Anionic polysaccharide	0.8	11	0.5	inverted
16	NaCMC	Anionic cellulose derivative	0.8	11	0.5	inverted
17	SSL	Anionic surfactant	0.8	9	0.5	inverted
18	Met. 368	Ester based	0.8	8	0.5	inverted

[a]Assessed through visual criteria and DLS analysis both after the preparation and after 1 week. Inverted = formation of water-in-oil emulsion instead of oil-in-water one. [b]Homogenization with UH, PLA/ EtOAc ratio (wt/vol. %) = 8, EtOAc/H_2O vol. ratio = 2.5, total volume = 70 ml.

The dispersion obtained with SYN possesses a particle size between 400 and 450 nm. This value is higher than the one obtained with SDS. On the contrary, the particle size observed with SDS and Span 80 was around 150 nm, which is comparable to the one with only SDS.

Met. 388, SA, NaCMC, SSL and Met. 368 (entries 12, 15, 16, 17 and 18, Table 2.5) tested in the presence of starch, all led to the formation of inverted emulsions (water in oil instead of oil in water). On the other hand, with the use of Tween 80 and Tween 20 (entries 9, 13 and 14, Table 2.5) all the preparations were unstable due to coagulation.

In order to rationalize the obtained results, they are visualized in Fig. 2.7: the formation and stability of the PLA preparations are plotted as a function of the surfactants' hydrophilic–lipophilic balance (HLB) values and their concentration in the water phase. The data highlight that for relatively low values of HLB (between 5 and 11) and low concentration in water (from 0.5 to 0.1 wt.%), an inverted emulsion (water-in-oil) is formed (red symbols, Fig. 2.7). When the hydrophilic–lipophilic balance (HLB) value is in the 15–20 range, without exceeding concentration values of 0.1 wt.% in water, the emulsion sometimes is still inverted and sometimes partially forms (respectively, red and orange symbols, Fig. 2.7). However, in this HLB range it is sufficient to increase the concentration of surfactant from 0.8 to 1.3 wt.% to obtain a direct emulsion (oil-in-water) (light green symbols, Fig. 2.7). Nevertheless, emulsions are not stable over time. Indeed, for hydrophilic–lipophilic balance (HLB) values higher than 19 and a concentration of surfactant higher than 1 wt.%, a direct emulsion was obtained with all tested surfactants, even if it is stable only in a few cases. In summary, two stability zones can be highlighted from the chart (dark green symbols, Fig. 2.7): (a) for a high HLB value (40), a relatively low concentrations of surfactant (0.8 wt.%) and starch as stabilizer; and (b) with modest HLB (29 and 34) and fairly high concentrations of emulsifier (2 and 3 wt.%). In the second case, the use of starch as stabilizer does not affect the stability of the preparations, suggesting that, in a certain range of HLB values and concentrations of emulsifier, no stabilizing agents are needed. As a drawback, the use of a higher amount of surfactant significantly affects the composition of the final coating, therefore most likely also the final properties of the layer.

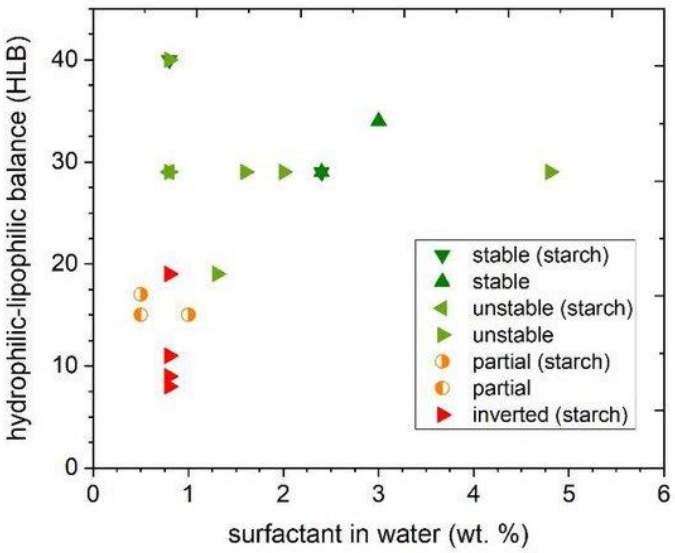

Figure 2.7: Influence of hydrophilic–lipophilic balance (HLB) and concentration of surfactant in water on the formation and stability of the formulations.

2.2.6. Characterization of the PLA dispersions

The dried dispersions were characterized through gel permeation chromatography (GPC) analysis in order to verify if the PLA was subjected to degradation during the preparation of the formulation and the subsequent storage. The comparison between the molecular weight of pristine PLA and PLA of dispersions showed minor differences (3–5%) in the range of the experimental error (Table 2.6). Furthermore, no significant change in polymer dispersity was detected, thus indicating the absence of significant degradation of the polyester during the processing in water for the dispersion preparation under ultrasound treatment and moderate heating and the subsequent storage for a few months.

When the dried dispersions in the form of film or powder were analyzed through GPC analysis, the samples were filtered after solubilization in trichloromethane due to the presence of an insoluble fraction. It must be taken into account that all the dispersion components except for starch (0.5 wt. %) are soluble in chlorinated solvents. With the purpose of further studying the formation of an insoluble fraction, dried samples of the PLA dispersions prepared and neat PLA were treated with DCM at reflux in a Soxhlet extractor. After 8 hours the amount of the insoluble residue was determined as shown in the Table below (Table 2.6).

Table 2.6: Molecular weight by GPC analysis of pristine PLA and PLA dispersions dried at different temperatures and amount of insoluble fraction after solubilization in DCM

Sample	Drying temperature (°C)	$\overline{M_n}$ (kDa)	Đ	Amount of insoluble residuum (wt. %)
PLA	-	113.8	1.46	0
PLA_SDS	rt	109.6	1.44	8.5
PLA_SYN	rt	119.5	1.38	7.5
PLA_SDS	60	96.8	1.46	3.6
PLA_SYN	60	102.2	1.32	4.9
PLA_SDS	80	92.3	1.45	n.d.
PLA_SYN	80	85.6	1.44	n.d.
PLA_SDS	100	99.6	1.44	n.d.
PLA_SYN	100	88.9	1.48	n.d.

n.d. = not determined

It is possible to notice from Table 2.6 that the pure PLA is completely soluble in dichloromethane, in fact the presence of an insoluble residue was not detected. On the contrary the emulsification process seems to generate an insoluble fraction (7.5-8.5 wt. %, sample processed at rt, Table 2.6). The latter is greater than the fraction of the component insoluble in chlorinated solvents (namely starch, 0.5 wt.%). This could be due to the production of radicals during ultrasound treatment with the consequent formation of a branched and then scarcely soluble PLA [234]. The role of starch in this phenomenon is minor because the formation of an insoluble residue also occurs in formulations that do not contain starch as a stabilizer (PLA_SYN, Table 2.6). When the dispersions are dried at 60 °C the amount of insoluble residua decreases (3.6-4.9 wt. %, Table 2.6). It has been shown that the temperature has a detrimental effect on the average molecular weight of the polymer (Table 2.6), as a consequence it can be speculated that higher temperatures promote hydrolysis of the branched polymer, thus partially restoring the solubility in DCM.

DSC analysis of neat PLA 4060D showed glass transition temperature at 54.1 °C and no melting or crystallization peaks (Fig. 2.8), in agreement with the amorphous nature of the resin declared by the producer (NatureWork processing guide NWPG002_020111; https://doi.org/10.1016/j.reactfunctpolym.2017.06.013, accessed on 1 September 2020).

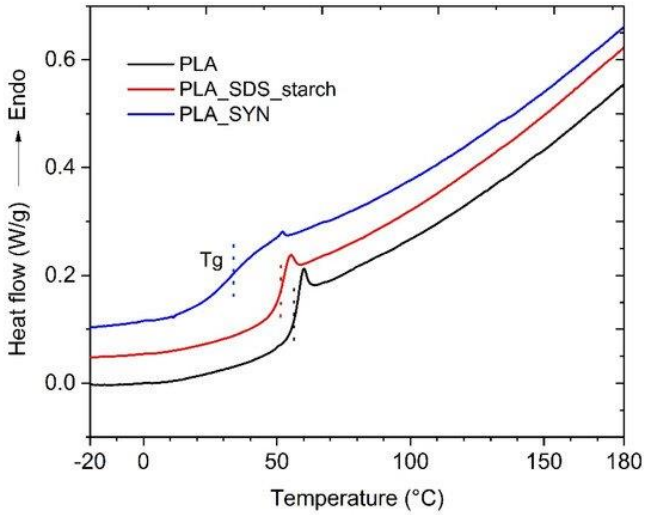

Figure 2.8: DSC thermograms at 10 °C/min of neat PLA, dried PLA dispersion with SDS and starch as surfactant and stabilizer, respectively, (entry 3, Table 2.1) and dried PLA dispersion with SYN (entry 23, Table 2.3). Second heating step. Thermograms were arbitrarily vertically shifted for clarity.

The analysis of dried dispersion with SDS and starch (entry 3, Table 2.1) showed only a modest shift of the T_g value towards a lower value (T_g = 51 °C) with respect to the pristine polyester, thus indicating a modest effect of the emulsion process even on the thermal properties of the resin. On the contrary, dispersion with SYN showed a significant decrease of ~20 °C in the glass transition temperature (T_g = 34 °C), indicating a plasticization of PLA by the PEO block of SYN [235]. This latter sample, in addition to the shift in the $T_{g's}$ mean value, showed a broadening of the transition, hence reflecting the variety of thermal motions available [236]. This last effect can be due to a non-homogeneous distribution of SYN in the PLA particles or even to a non-homogeneous distribution of SYN among particles, resulting in particles richer in the block copolymer and others with comparable depletion.

2.2.7. Preparation of films from PLA dispersions

PLA dispersions in water prepared with either SDS and starch as surfactant and stabilizer (PLA_SDS, entry 3,Table 2.1) or SYN as emulsifier (PLA_SYN, entry 29, Table 2.3) were cast on polytetrafluoroethylene (PTFE) capsules and left to dry.

When drying was performed at room temperature, a layer of powder was obtained. SEM analysis revealed the presence of submicrometric particles (Fig. 2.9a,b), whose dimension was comparable to the values by DLS data of the corresponding water dispersion (Paragraph 2.2.2). This result indicates that particles did not merge, most likely because the processing temperature was lower than the glass transition value of both dispersions (Paragraph 2.2.6). When drying was performed at 40 °C, particles started to merge, forming white continuous layers. However, these were brittle and fractured (Fig. 2.10a,b).

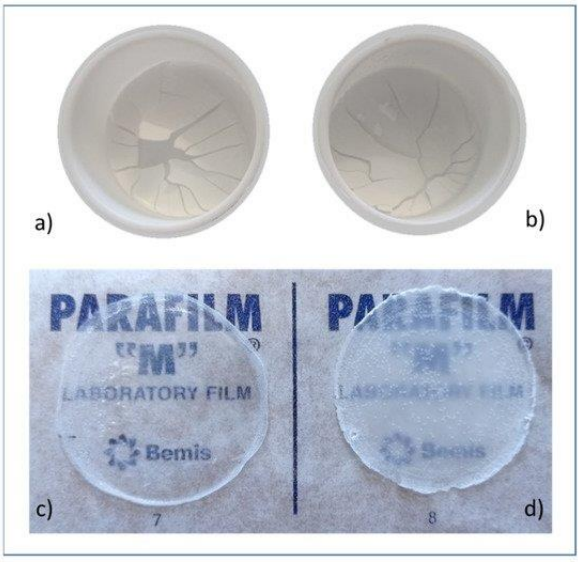

*Figure 2.10: Pictures of PLA films obtained by solution casting at 40 °C (**a**,**b**) and 60 °C (**c**,**d**) of water dispersions with SDS and starch (**a**,**d**) or SYN (**b**,**c**).*

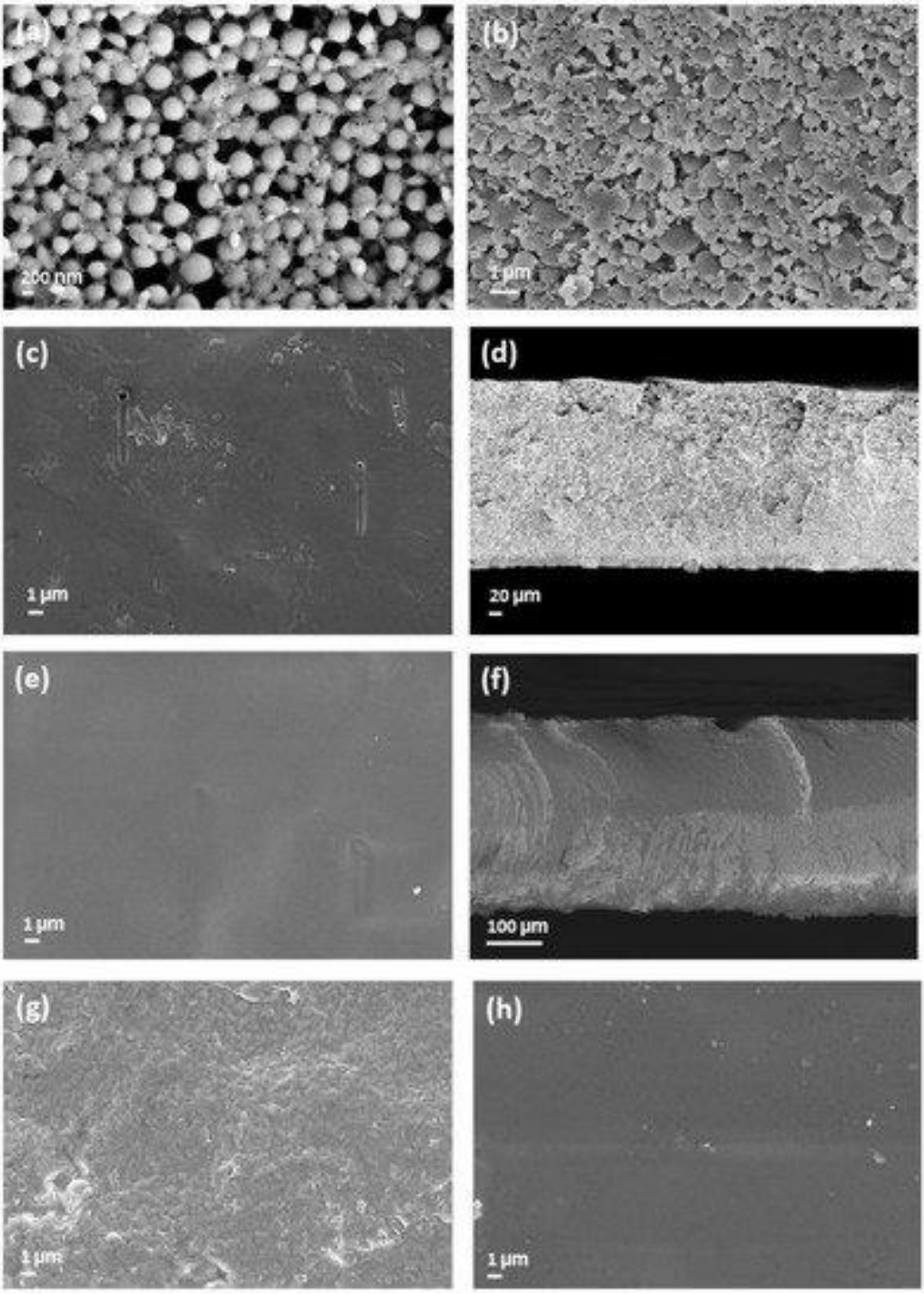

*Figure 2.9: SEM pictures of the filming tests performed with water dispersions of PLA at room temperature (**a**,**b**), at 60 °C (**c**–**f**) and at 80 °C (**g**,**h**). Pictures (**a**,**c**,**d**,**g**) refer to tests with the SDS formulation; (**b**,**e**,**f**,**h**), correspond to tests with the SYN formulation.*

A further increase of the temperature to 50 °C had a partial positive effect only in the case of the SYN dispersion, which has a glass transition temperature of 34 °C.

However, the formed film, even if partially transparent, was brittle and cracked. On the contrary, when films are dried at 60 °C, continuous free-standing films with thickness between 230 and 550 μm are afforded (Fig. 2.10c,d) with both formulations. The formulation with SYN gives almost transparent films, while in the presence of SDS and starch, opaque films are obtained. In both cases, individual particles cannot be distinguished by SEM observation of the film's surfaces (Fig. 2.9c,e,g,h) and section (Fig. 2.9d,f not shown), thus indicating effective film formation. Notice that 60 °C is higher than the glass transition temperature of both dispersions and of the pristine PLA. Processing at higher temperatures, up to 110 °C, provided films that look like the one obtained at 60 °C in the case of the SYN formulation. However, with the dispersions with SDS and starch, yellowing occurred at drying temperatures above 90 °C. Indeed, the SEM analysis of PLA dispersion in water prepared with SDS at 80 °C (Fig. 2.9g) shows the presence of granules that are probably due to the degradation of the surfactant/stabilizer.

Transmission measurements showed that PLA films with SDS and starch (thickness of 320 μm) possess a transmittance of 2.6% at 600 nm. The low transmittance is due to the whitish color of the film, probably given by the presence of starch. On the other hand, PLA film with SYN (thickness of 250 μm) showed a higher transparency (transmittance of 40% at 600 nm). However, the latter possesses a modest transparency considering that a pure PLA film prepared from EtOAc (thickness of 130 μm) has a transmittance of 72% at 600 nm.

ATR-IR analysis of the upper and lower surfaces of the films showed comparable band intensity, hence indicating a similar composition. As a consequence, significant surfactant segregation or blooming effects can be excluded (Fig. 2.11). However, films obtained at high drying temperatures (90 and 110 °C) showed a different composition between the upper and lower surface by ATR analysis (Fig. 2.11). In particular, an enrichment in stabilizer/surfactant is observed on the lower surface of the films. Indeed, the IR spectra of the bottom surface of PLA_SDS film prepared at 90 °C (Fig. 2.11a) shows a broad band between 3000 and 3500 cm^{-1}, which is typical of the starch's OH stretching. The enrichment of starch is further confirmed by the typical stretching band of sugar rings at around 1000 cm^{-1}. Similarly, the film from the PLA_SYN formulation obtained at 110 °C, in the bottom surface showed a more intense signal than the top surface. These are signals at

nearly 2800 cm^{-1} relative to CH_2 stretching and the one at nearly 955 cm^{-1}, which are both present in the ATR spectra of SYN.

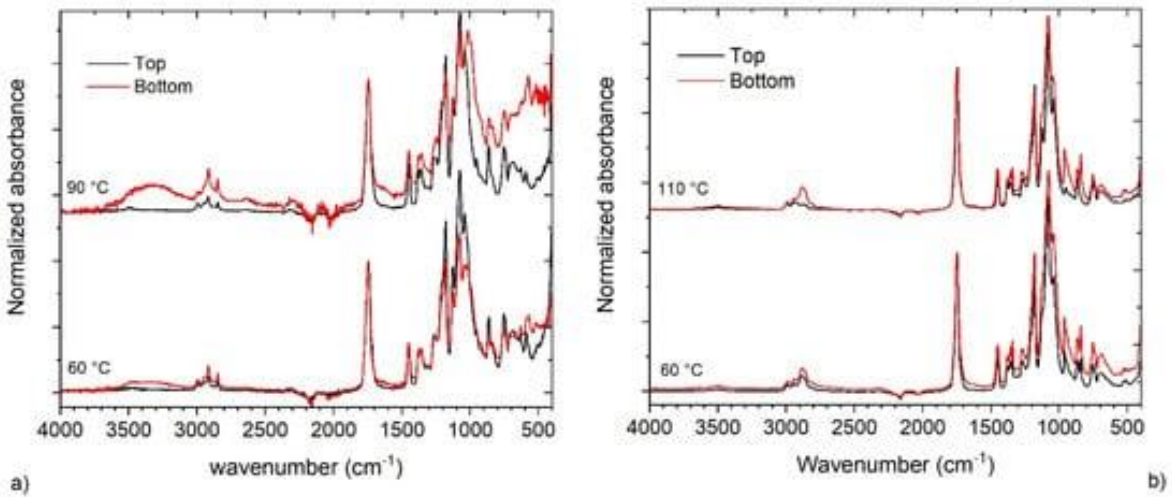

Figure 2.11: a) FT-IR spectra of the top and bottom surfaces of PLA_SDS films prepared at 60 and 90 °C. b) FT-IR spectra of the top and bottom surfaces of PLA_SYN films prepared at 60 and 110 °C.

The possible degradation of PLA during film formation was checked by GPC analysis (Table 2.6). A modest variation, even if detectable (10–15% decrement), was observed after drying at 60 °C. Higher processing temperature resulted in a more extended molecular weight decrement. No variation of the dispersity was detected as a result of a comparable decrement in both the $\overline{M_n}$ and $\overline{M_w}$ values, thus suggesting no preferential degradation of the high or low molecular weight fractions. In any case, no optimization of the drying time has been performed and it can be envisaged that better control over the molecular weight can be achieved by proper control of the heating time.

2.2.8. Preparation of PBSA dispersions in water

The extensibility of the aqueous dispersion preparation procedure developed to other biodegradable polyesters was examined. In particular, it was studied the possibility to prepare water-based dispersions of PBSA, a commercially available bio-based and biodegradable polymer. As previously anticipated in Paragraph 1.2.2

of Chapter 1, PBSA is a copolymer obtained through polycondensation of 1,4-butanediol (B) with succinic acid (S) and adipic acid (A). The relative content of succinate and adipate units, (BS/BA) of the PBSA used was 75/25 as determined by ^{1}H-NMR analysis [237] (Fig. 2.12). Particularly, the signals at 4.07, 2.58, and 2.29 ppm were ascribed to the α-methylene protons of the 1,4-butanediol unit (*a*), the one of the succinate units (*b*), and the one of the adipate unit (*c*), respectively. For the calculation of the BS/BA ratio the integral intensities of the protons *b* and *c* were normalized on the basis of the proton *a,* as shown in the ^{1}H-NMR spectra below.

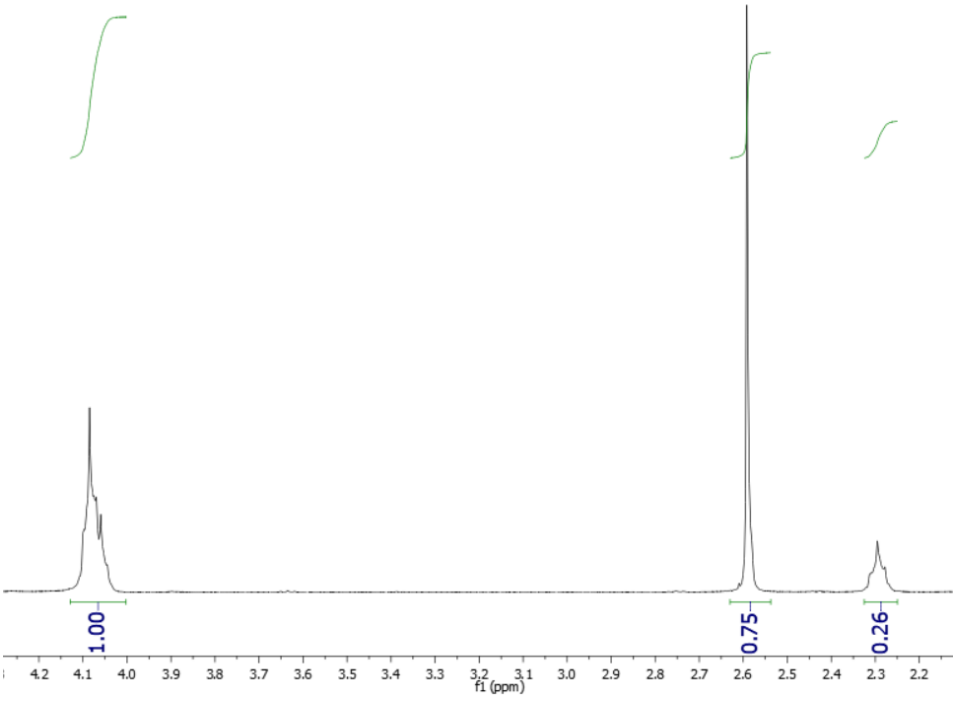

Figure 2.12: ^{1}H-NMR spectra of PBSA for the determination of the relative content of succinate and adipate units (BS/BA).

As it is possible to observe from the Table 2.8 below, to prepare the PBSA dispersions the same optimized conditions used to produce the PLA dispersions were employed (entry 3, Table 2.1 and entry 10, Table 2.5). Particularly, as surfactant, both SDS and SYN, that have previously given good results, were tested. The only difference is that as organic solvent dichloromethane (DCM) was employed instead of ethyl acetate due to the insolubility of the polymer in the latter organic solvent.

Table 2.8: Experimental conditions adopted to prepare DCM-in-water PBSA dispersions

	Aqueous phase			Organic phase	DCM/H_2O	Dispersion feature
Entry	**emulsifier**	**wt. %**	**PBS (wt/vol %)[1]**	**Vol. (ml)**	**Vol. ratio**	**Stability[2]**
1	SDS[3]	0.8	11	45.0	1.3	yes
2	SYN	2.4	11	45.0	1.3	Phase separation

[1]Ratio between the weight of PBS and the volume of DCM. [2]Assessed through visual criteria after the preparation.[3] The formulation contains also a 0.5 wt. % of starch in water.

In both conditions of entry 1 and 2 of Table 2.8, a polymer dispersion was initially formed even though some coagulum on the stirrer was noticed (Fig. 2.13). However, the formulation containing SYN as surfactant gave phase separation after 15 minutes (entry 2, Table 2.8). As regards the formulation with SDS (PBSA_SDS), it displayed a particle size of 319 ± 7 nm and a polydispersity of 0,177 ± 0,019 (entry 1, Table 2.8). Nevertheless, after 1 day a precipitate on the bottom of the flask formed, even though the formation of this deposit slowed down over time. After two weeks from the preparation the particle's dimension decreases (289 ± 8 nm), indicating that larger particles sediment preferably.

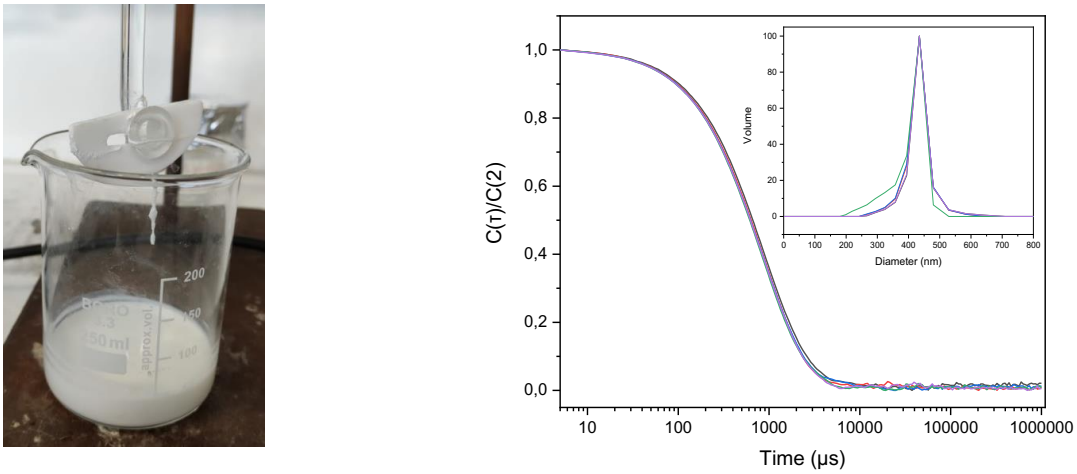

Figure 2.13: Pictures of the PBSA_SDS dispersion just prepared at the left and DLS plots of the PBS_SDS dispersion just prepared. Correlograms are normalized with respect to the intensity at time 2 μs. Insets refers to the particle size distribution.

2.2.9. Preparation of films from PBSA dispersions

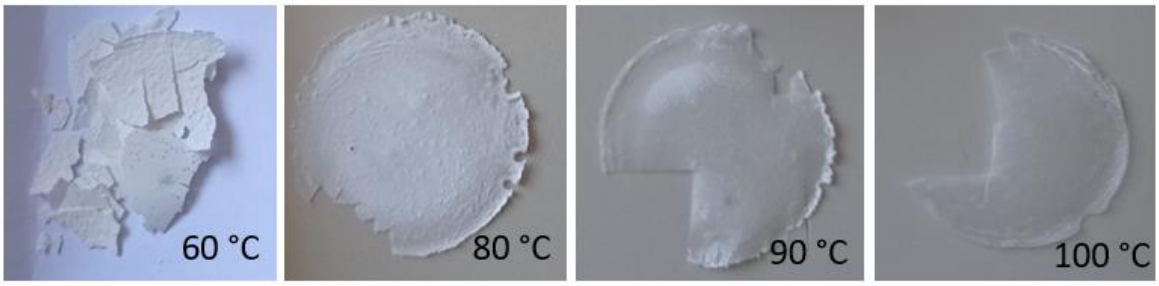

Figure 2.14: Pictures of PBSA films obtained by solution casting at 60, 80, 90 and 100 °C of PBSA_SDS dispersion. The films were cut in order to analyze the material.

With the purpose of preparing PBSA films, the PBSA_SDS dispersion produced was casted on PTFE capsules and left to dry. When drying was performed below 60 °C, a layer of powder was obtained (Fig 2.14). In Fig. 2.15 the ATR-IR spectra of the PBSA dispersion dried at rt and at 60 °C have been reported together with the spectra of pure PBSA for comparison. As described in literature, the ATR-IR spectrum of PBSA shows an absorption band at 2945 and 1330 cm^{-1} assigned to the stretching of the C–H bond. The intense band at 1710 cm^{-1} can be ascribed to the carbonyl C=O stretching. Furthermore, the peak at 1144 cm^{-1} is characteristic of C–O–C stretching vibration [238]. It can be noticed that the spectra of dispersion dried at rt or at 60 °C differ from that of pure PBSA. It is clear that both the emulsification process and the drying temperature modify the structure of the polymer, even though it is difficult to understand the nature of this modification. When the formulation is dried at 80 °C a whitish film is obtained. Nevertheless, by drying at 90-100 °C the dispersions, continuous and opaque films with thickness between 100 and 200 μm were formed. On the other hand, when the drying temperature is above 120 ° C the films become cracked and fragile. In order to investigate the homogeneity of the films obtained, ATR-IR analysis of the upper and lower surfaces was performed (Fig. 2.16a).

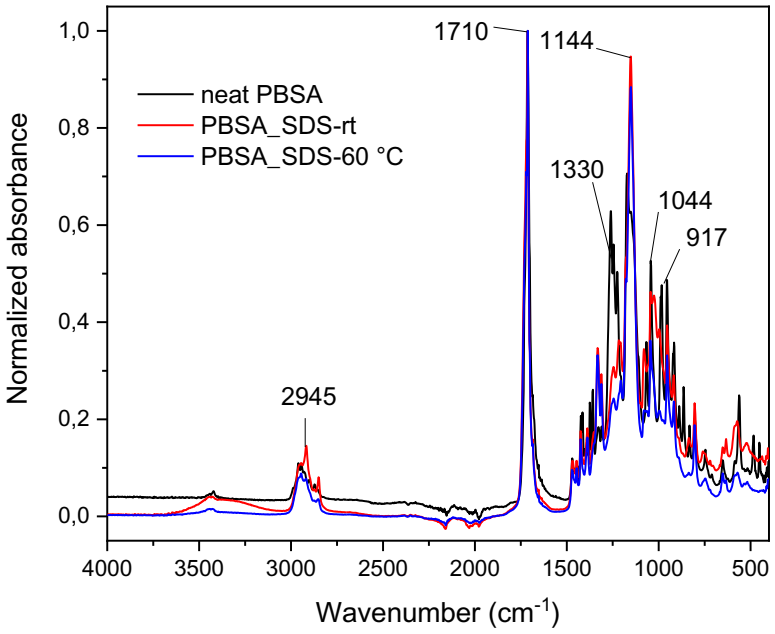

Figure 2.15: FT-IR spectra of the neat PBSA and the PBSA dispersions dried at room temperature and at 60 °C. The spectra were normalized with respect to the stretching carbonyl band at 1710 cm^{-1}.

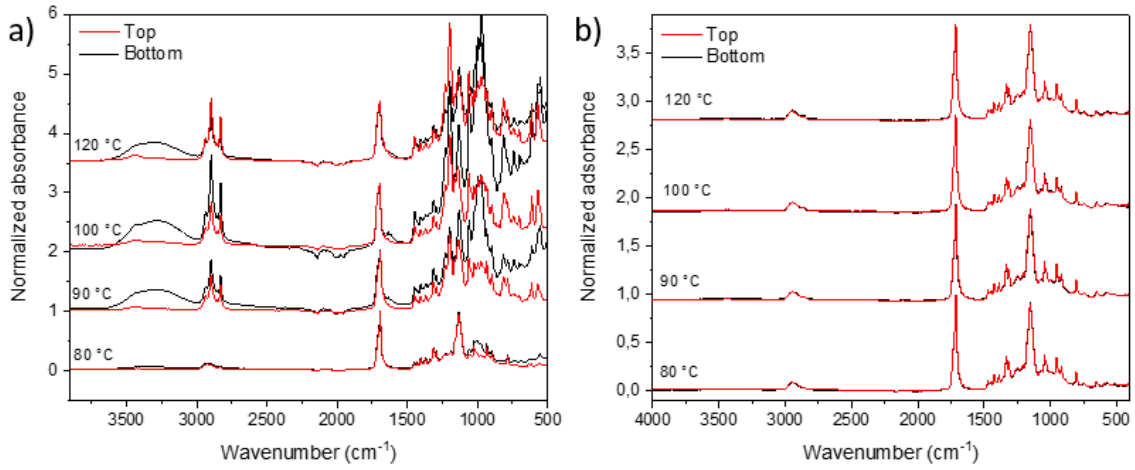

Figure 2.16: a) ATR-IR spectra of the top and bottom surfaces of PBSA_SDS films prepared at 90, 100 and 120 °C. b) ATR-IR spectra of the top and bottom surfaces of PBSA_SDS films prepared at 80, 90, 100 and 120 °C after washing in hot water.

It can be observed that the spectra of the upper and lower surfaces of the PBSA film differ from each other. In particular, a wide band between 3000 and 3500 cm^{-1},

typical of OH stretching, and the characteristic stretching band of the sugar rings at 1000 cm^{-1} appear at the bottom of the film. This can be due to the accumulation of the polysaccharide stabilizer, namely starch, on the bottom surface of the film. To confirm this hypothesis the ATR-IR analyses were repeated after washing the film in hot water (Fig. 2.16b). In this case, the signals relative to starch disappear and good homogeneity between the upper and lower surfaces of the film is observed, hence indicating that during drying segregation of the stabilizer occurs.

Furthermore, the surface and section of the PBSA films prepared at 90 and 100 °C were analyzed through SEM (Fig 2.17). It can be noticed that in both cases cracks and defects are present even if to a lesser extent in the film dried at 100 ° C (Fig 2.17b,c,d). From the section image it is clearly evident the inhomogeneity of the film (Fig. 2.17d). Probably, in this case, a MFFT cannot be detected due to the modification of the polymer during the preparation process or to the accumulation of starch onto the bottom surface.

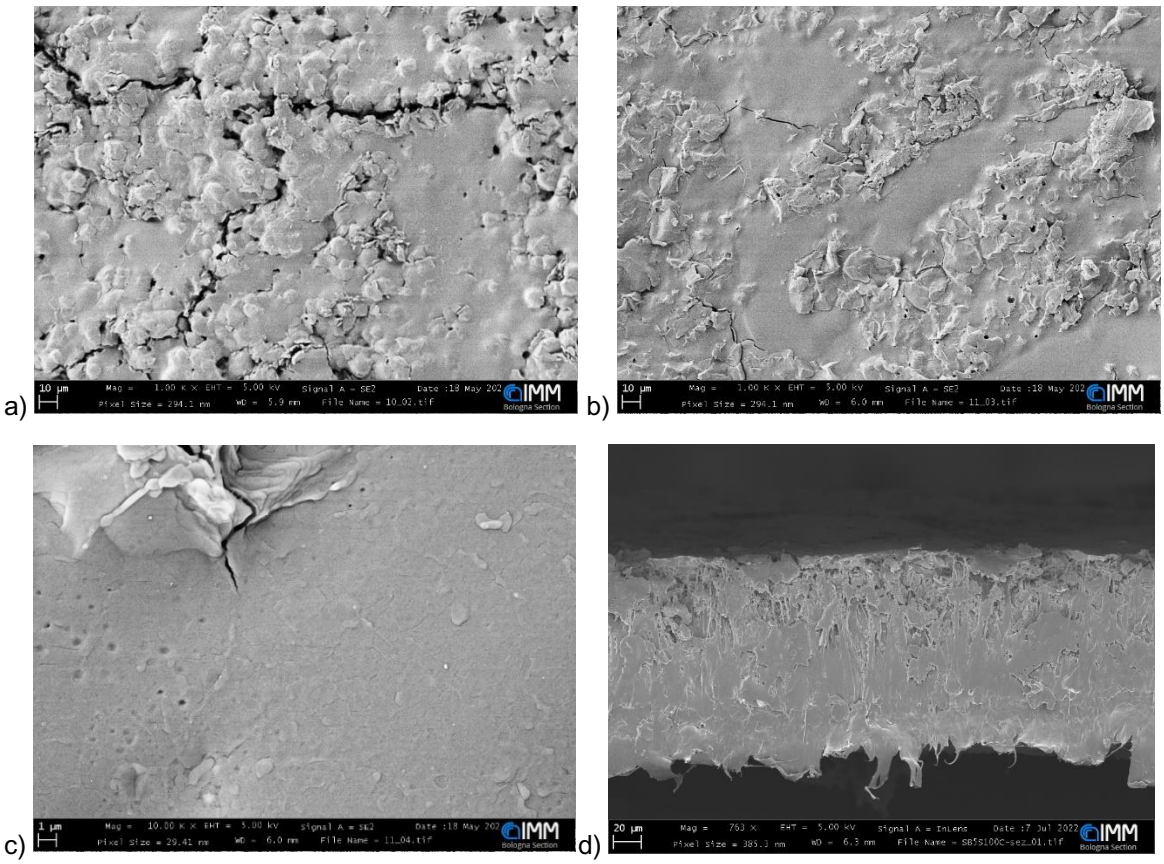

*Figure 2.17: SEM pictures of the filming tests performed with water dispersions of PBSA at 90°C (**a**) and 100 °C (**b,c,d**).*

2.2.9.1. Characterization of the PBSA films produced from water dispersions

With the purpose of investigating the thermal properties of the neat PBSA and the PBSA films, thermal gravimetric analysis (TGA) and differential scanning calorimetry (DSC) analysis were performed. To evaluate the thermal stability of the films, TGA analysis was carried out under standard conditions in nitrogen atmosphere (Table 2.9, Fig. 2.18).

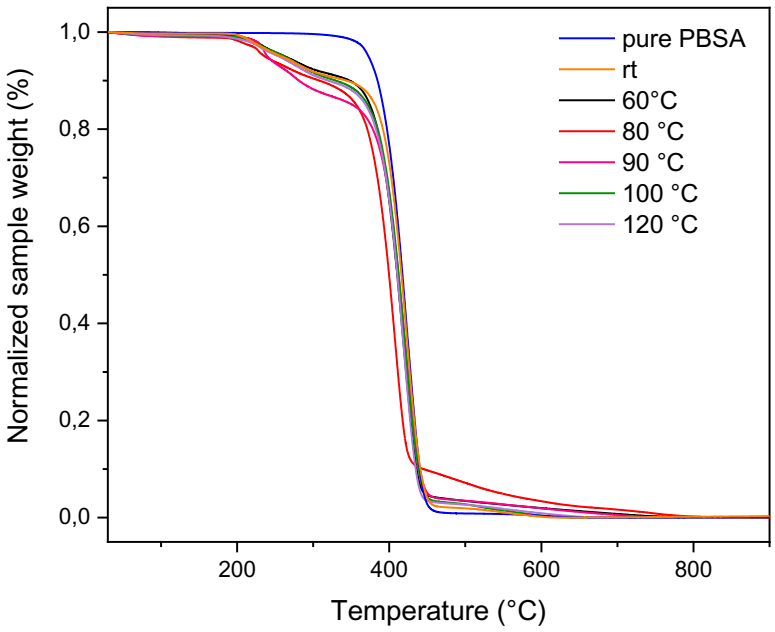

Figure 2.18: Comparison among the TGA curves of pure PBSA (blue line) and PBSA films prepared with PBSA_SDS dispersion at different drying temperatures.

The analysis revealed that neat PBSA degrades in a single step process and its T_{on} is close to 384 °C, thus indicating high thermal stability. Nevertheless, the dried dispersions display lower thermal stability (T_{on} from 187.3 to 213.4 °C), showing two distinct degradation steps. The first degradation step is too marked to be ascribed to the presence of the surfactant and stabilizer in the formulation (SDS at 0.8 wt.% and starch at 0.5 wt. %, respectively). This suggests that the emulsification process and the drying temperature promote some modification of the polymer, with a consequent modification of its thermal stability.

Table 2.9: First and second temperature of onset (T_{on}^1 and T_{on}^2), first and second temperature of maximum degradation rate (T_d^1 and T_d^2) and residuum after degradation (Res.) from TGA analyses of the pure PBSA (blue line) and PBSA films prepared with PBSA_SDS dispersion at different drying temperature.

Drying temperature (°C)	T_{on}^1 (°C)[a]	T_d^1 (°C)	T_{on}^2 (°C)[a]	T_d^2 (°C)	Res. (%)[b]
-	-	-	383.5	412.6	0.4
rt	187.4	209.0	385.7	413.3	2.7
60	196.9	221.3	278.9	411.7	1.8
80	196.0	217.2	369.7	400.6	0.9
90	213.4	224.9	384.4	413.3	2.6
100	194.9	221.4	382.4	413.1	1.8
120	195.7	219.9	381.6	411.2	2.4

[a]Temperature of the peak minimum in the first derivative TGA plots; [b]Residuum at 850 °C.

The DSC thermograms of the pure PBSA and PBSA films obtained at different temperature of drying are presented in Fig. 2.19 and the thermal properties are summarized in Table 2.10. The neat PBSA presents a T_g around -44°C followed by a T_{cc} and T_m at -4.0 and 86.3 °C respectively. It can be observed that with the emulsification process the cold crystallization peak disappears. It is not observed even after film formation from the emulsion, whatever the temperature adopted for drying. Besides, it has been reported that the melting points of PBA and PBS are 60 °C and 114 °C, respectively, and the melting point of the copolymer PBSA increases by raising the ratio of BS/BA from 50/50 [239]. Consequently, a small decrease of the melting point can suggest that a slightly preferential degradation occurred in the succinate units block [237].

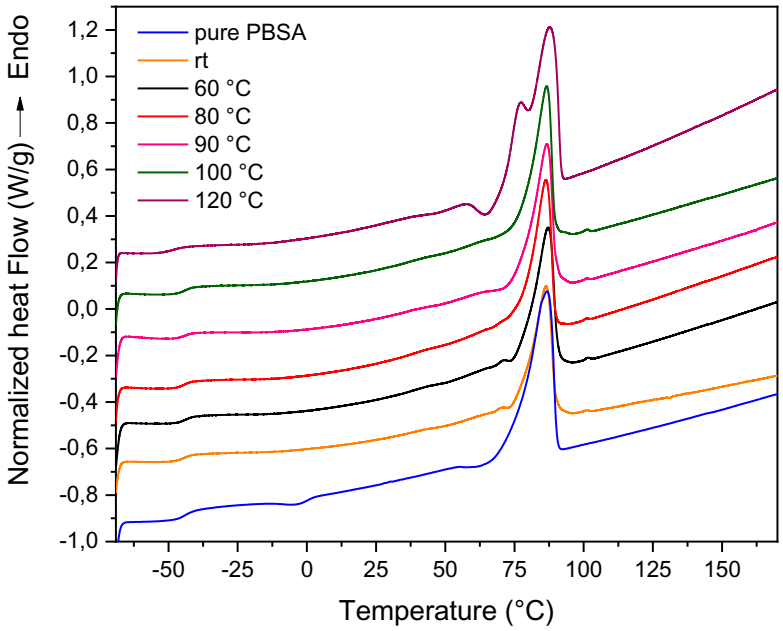

Figure 2.19: DSC analysis at 10°C/min relative to the second heating step of pure PBSA (blue line) and PBSA films prepared with PBSA_SDS dispersion at different drying temperatures. Thermograms were arbitrarily shifted for clarity.

Table 2.10: Glass transition temperature (T_g), cold crystallization temperature (T_{cc}), cold crystallization enthalpy (ΔH_{cc}), melting temperature (T_m^2) and melting enthalpy (ΔH_m^2) of the second heating step from DSC analyses of the pure PBSA and the PBSA films prepared from the PBSA_SDS dispersions at different drying temperatures.

Drying temperature (°C)	T_g (°C)[a]	T_{cc} (°C)	ΔH_c (J/g)	T_m (°C)[b]	ΔH_m (J/g)
-	-43.9	-4.0	-1.2	86.3	44.0
rt	-44.6	-	-	86.1	35.5
60	-43.4	-	-	86.8	34.5
80	-43.4	-	-	86.4	33.2
90	-43.9	-	-	86.4	33.9
100	-44.5	-	-	86.3	33.9
120	-47.5	-	-	87.3	50.0

[a]Values at the midpoint; [b]Values at the peak maximum.

The decrease in ΔH_m from pure PBSA to PBSA dispersion indicates a diminishment in the polyester crystallinity. The latter phenomena can be ascribed to a reduction of the polymer's molecular weight, which results in a decrease of crystallinity. In the

sample dried at 120 ° C the T_m and the ΔH_m increase; nevertheless the melting peak doubles suggesting the presence of a polymer fraction with lower melting temperature. Most likely by chain scission of polymer fractions with different amounts of the two blocks formed and at high processing temperature polymer mobility is enough to promote phase separation and consequent independent crystallization of the fractions of different composition. As a result, we can say that after the emulsion process the thermal transitions characteristic of the PBSA were modified.

2.3. CONCLUSION

In summary, a procedure based on emulsification-evaporation method, which gives aqueous PLA dispersions targeting coating applications has been developed. The procedure is based on the combination of an amorphous commercial PLA grade, ethyl acetate as solvent and surfactants all approved for food contact applications, so that the preparation is also suitable for this application's purpose. Formulations with dry matter content up to 20 wt.% were disclosed.

Emulsifiers with hydrophilic–lipophilic balance (HLB) in the 29–34 range at 2 and 3 wt.% concentration are needed to stabilize the formulations during the preparation stages. Surfactants with higher HLB (40) are also effective if starch is included as stabilizer. Emulsification needs high energy input by ultrasound sonication to achieve effective dispersion. Furthermore, the total treated volumes, the organic/water volume ratio and the viscosity of phases must be adjusted to the sonication capability to achieve the stability of the final dispersion. Overall, two different water-based formulations of PLA were developed: one with SDS as surfactant (0.8 wt. %) and starch as stabilizer (0.5 wt. %), called PLA_SDS, and the other one with SYN as (2 wt. %) and no stabilizer, named PLA_SYN.

In addition, it was discovered that, for long-term stability, the final dispersion formulation must contain negligible ethyl acetate residua (<40 ppm). Under this circumstance, dispersions do not sediment or cream and particle size does not appreciably change over 6 months at room temperature or in the fridge at 4 °C.

The obtained dispersions, consisting of submicrometric PLA particles, were successfully cast into films, with minimum formation temperature of 60 °C, which is a little above the glass transition temperature of the pristine PLA.

Encouraged by these results, the extensibility of the aqueous dispersion preparation procedure to PBSA, another biodegradable polyester, was examined. A PBSA dispersion was obtained under the same conditions employed for the preparation of the PLA_SDS formulation. The only difference is that as organic solvent dichloromethane (DCM) was used instead of ethyl acetate due to the insolubility of the polymer in the latter organic solvent. Nevertheless, the PBSA dispersion, also named PBSA_SDS, does not possess the same stability as the PLA ones, indeed the day after the preparation a sediment is formed. If the PBSA dispersion was cast and dried at temperatures higher than 100 °C a continuous and homogeneous PBSA layer by eyes inspection was obtained. However, SEM analysis reveled the presence of small cracks and defects in the films. Moreover, through IR and DSC analysis, it is clear that both the emulsification process and the drying temperature modify the structure of the polymer, even though it is difficult to understand the nature of this modification.

CHAPTER 3

Rheological response of PLA water-based dispersions thickened with xanthan gum and applications of these formulations as coatings for paper substrates

Most of the work described in this Chapter is adapted with permission from “Buoso, S.; Belletti, G.; Ragno, D.; Castelvetro, V.; Bertoldo, M. “Rheological response of polylactic acid dispersions in water with xanthan gum” *ACS Omega,* 2022, 7, 15, 12536–12548”. Copyright 2022 American Chemical Society.

3.1. INTRODUCTION

3.1.1. Biodegradable and renewable polymeric coatings on paper

Paper is a green and biodegradable material which due to its excellent properties like lightweight, recyclability and good mechanical resistance find numerous applications in packaging, printing, microfluidic industries and household products [240]. Paper possesses a porous structure formed by cellulose long-chain molecules, known as microfibrils, which are in a crystalline state interspersed with amorphous regions. For packaging purposes, in order to extend shelf-life of the product and maintain its characteristics unchanged, the control and full understanding of adsorption and transport of water, gases, and oils is of utmost importance. However, the hydrophilic nature of cellulose and its fiber network porosity limits the barrier properties of paper. Indeed, water from the environment or from the product can be easily absorbed by the paper packaging with a consequent loss of product shelf-life and reduced mechanical strengths of the packaging [241]. In order to provide the final packaging with the required barrier properties, paper is often combined with other materials, such as plastic and aluminium in a multilayer structure. For instance, when gas-barrier properties are required, the choice relies on ethyl vinyl alcohol (EVOH), a polymer with excellent barrier property towards oxygen [242]. Nevertheless, the hydrophilic character of this polymer favours the absorption of water, thus making necessary the addition of a further polymer layer. Usually the latter consists of polyolefins, rubber latex, and

fluorocarbon that are able to provide the final packaging with a good liquid and vapour water barrier [243][244][245]. The barrier efficiency of these materials, their low cost and great availability are the reasons why these polymers dominate the current packaging market. However, the majority of these materials are oil-based non-biodegradable and this limits the recycling and the eco-sustainability of the final packaging. For these reasons, in recent years, the research interest has shifted towards the use of naturally renewable polymer for packaging and coatings applications [246]. Indeed, numerous biopolymers, such as polysaccharides, proteins, lipids and polyesters have been applied as coatings on paper and paperboard [240]. For example, it has been demonstrated that a whey-protein-coating on paper increases the oil resistance and reduces the water-vapor permeability of the final packaging [247]. Similarly, paper coated with chitosan or chitosan/carnauba wax displayed good barrier properties towards oxygen, nitrogen, carbon dioxide [248]. However, due to their hydrophilic character, biopolymers show reduced total barrier performance as packaging material in comparison to synthetic polymers, due to the low resistance towards water vapour. Blending of the former with other polymers or fillers is a convenient method to improve the final performance without affecting the eco-sustainability to the process. For instance, soy protein coatings with layered silicates additives like montmorillonite showed increased water barrier properties [249]. As regards the use of biodegradable polyesters for paper coating, almost all the works reported in literature present the use of PLA or PHAs. Just recently, the use of poly (butylene succinate) PBS as coating for recycled paperboard for food packaging was reported [250]. The contact angle of water and avocado oil on the PBS coated was measured revealing both good water and oil barrier properties.

3.1.2. Processing of biopolymers for paper coatings

Usually, biopolymers are coated over paper and paperboard through melt processes, solvent casting or dispersion coating. Among the melt processes, extrusion coating, compression moulding coating, thermocompression coating are the most commonly employed. They involve the melting of the polymer followed by the deposition of the latter onto the chosen surface. Industrially, these methodologies possess numerous advantages like the continuity of the process, the

uniformity of the final coating and the absence of potentially harmful organic solvents. Indeed, the uniformity of the coating as well as its thickness are factors that largely influence the biopolymer barrier properties. By these routes, it is not possible to prepare very thin coating layers (<100 μm) and besides, biopolymers that lack thermoplastic character or that degrades at high temperature, like polysaccharides, proteins and lipids, are not suitable for these processes. On the other hand, even thermoplastic biopolymers, such as PLA and PHB, have shown a tendency to undergo thermal degradation above their melting temperatures and, for this reason, in order to be coated through melt processes, the modification of the polymeric bulk [251] or the addition of plasticizer and additives was proposed [252]. On the contrary, solvent casting techniques do not require the use of high temperatures and they allow the obtainment of minimal coating thickness (<20 μm), which is often desired to reduce material consumption and the cost of the items. In this case, the biopolymer is solubilized in a proper organic solvent and then applied onto the paper substrate by solvent casting, spin coating, spray coating, curtain coating, dip coating and wire or rod coating [253]. With solvent based methods the necessary barrier properties can be achieved with low coat weights (around 10 g/m^2) [240] even though sometimes two layers are required to eliminate the surface defects and to provide the paper a sufficient water vapor barrier. Moreover, the post-processing of a solvent coating technology involves evaporation of the solvent and drying steps, which are energy and cost consuming processes. Besides, it must be taken into account that halogenated solvents are often employed to solubilize the polymer and the release of toxic and harmful chemicals during the coating process represent a health and environmental threat. Indeed, in food packaging applications, these solvents can migrate into the packaging and the food, posing health risks. For this reason, many efforts have been devoted to replacing solvent-borne polymer coating with their waterborne counterparts [254]. Water, indeed, is considered as a cheap, safe, non-toxic and environmentally benign solvent. Even though the use of polymer water based dispersions for coating paper is known industrially, in the majority of the cases the latex consist of fossil based non-renewable polymers like acrylates [255]. On the other hand, only a few examples report the use of biopolymer latex for this application. In particular, the use of an aqueous latex of a poly ([beta]-hydroxyalkanoate) (PHA) to provide paper with water imperviousness was reported [256]. Furthermore, it was reported the application of PLA/montmorillonite latexes with a solid content around 25 % as coating for potential food paper packaging [92].

The water vapor transmission rates of the resulting coating were improved up to 85% in comparison with the pristine papers. However, even though in this case the coating application is solvent-free, the preparation of the PLA/montmorillonite requires the use of chlorinated toxic solvent.

3.1.3. PLA based coatings on paper

Biodegradable polyesters, such as PLA and PHAs are a class of biopolymers which was widely studied for potential application as paper coating for packaging [257]. Their accessible production either through fermentation and synthetic routes aroused the interest in spite of the higher cost in comparison with traditional oil-based polyesters. PLA coated paperboards were successfully prepared by bar coating of a chloroform polyester solution, increasing the elongation at break and the water resistance of the final paperboard [186]. Similar performances were reported by preparing the PLA-coated paper with thermocompression instead of solvent casting [258]. In both cases, the paperboards showed 2.3 times higher heat-sealing strength and equal or higher tensile strength than polyethylene (PE)-coated paperboards. Moreover, the manufacture of paper cups coated with PLA though solvent casting was efficiently reported [259]. In this case, water vapor permeability, water absorptiveness and contact angle of water drop were measured, indicating that water barrier properties of the paperboard were improved by the polyester coating. Besides, the thermal stability, mechanical properties and processability of PLA were enhanced by blending with a modified gelatine plasticizer without any loss of the biomass origin and compostable properties of the material [251]. Furthermore, both amorphous and semicrystalline PLA were employed for paper-based packages using montmorillonite (MMT) as fillers. The contact angle, water vapor and grease permeabilities of the resulting coatings were measured and compared to commercial materials finding comparable performances [260]. In particular, the barrier properties of PLA-MMT coated papers were found to be highly dependent on the crystallinity and concentration of PLA. Another interesting work, described the incorporation of ZnO nanoparticles to PLA through solubilization in a common green organic solvent in order to produce a biopolymer coated paper packaging with antimicrobial activity [261]. Similarly, PLA/nano-cellulose fibers (NCF) composites were applied onto paper through solvent casting, thus allowing the lowering of the

water vapor transmission rate (WVTR) [262]. Additionally, krafted paper was successfully coated with PLA with the purpose of providing a barrier to liquid water [263].

3.1.4. Rheological properties of coatings

Rheology is the science of flow and industrially it finds application in characterizing and predicting the product performance [264]. For example, rheology is often employed in the study of the formulation's viscosity at different shear rates. The dependence of the viscosity on the applied shear stress is usually reported in a flow curve and generally there are two general classes of fluid behaviour: Newtonian or non-Newtonian fluids. The viscosity of Newtonian fluids remains constant as the shear rate varies, while in non-Newtonian fluids the viscosity is not constant and can decrease (shear thinning) or increase (shear thickening) by varying the shear rate. It must be considered that the majority of industrial coatings are non-Newtonian fluids and, in this case, a single point measure of the viscosity does not represent the flow behaviour of the formulation. Indeed, for non-Newtonian fluids rheological measurements are of utmost importance in obtaining information on the behaviour of the system at different shear rates [265]. As a matter of fact, rheology is widely applied in the coatings industry, since the flow curve can provide information on the storage, handling and final application of the coating formulation. For example, in Fig. 3.1 a flow curve displaying the optimal viscosity values at the different shear rate associated with various processes is shown.

When a coating formulation is developed, the objective is to achieve a product that displays optimum viscosity at each shear rate with the purpose of meeting all performance requirements [266]. Typically, dispersion coatings need to have high viscosities in the low shear region to avoid settling and instability during storage and transport. On the other hand, they need to have low viscosities in the high shear rate region, which corresponds to the application [267]. Furthermore, the time-dependent viscosity build-up after exposure to high shear should be fast enough to prevent sagging but still slow enough to allow good flow levelling. Usually, suitable rheology control is achieved with specific additives, such as thickeners or viscosity reducing agents [266]. In particular, due to the relevance for this work, thickeners will be properly discussed in the next paragraph.

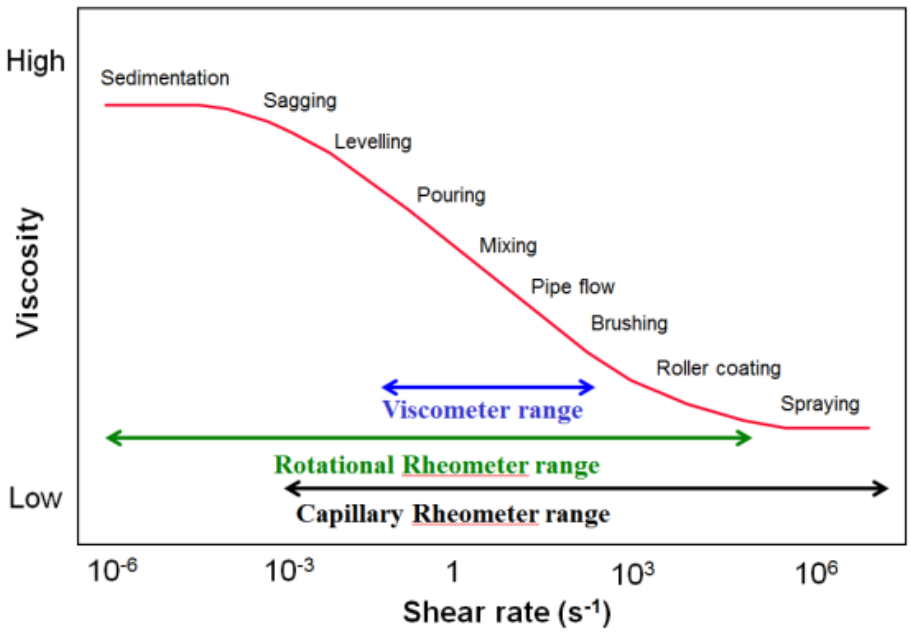

Figure 3.1: Typical shear rate ranges encountered during common coating processes [268].

When a water polymer dispersion coating is rheologically characterized, it is important to conduct in addition to viscosity measurements also viscoelastic ones. The latter analysis is relevant in studying the microstructure of the formulation and the dispersion state of the polymer particles [269]. The viscoelastic properties are usually determined through frequency sweep measurement with the purpose of assessing the time-dependent properties of the material. The analysis displays the magnitude of elastic modulus (G') and viscous modulus (G") in relation to the time of applied stress, which is reported as angular frequency. The dispersion state of the polymer particles and the nature of the continuous phase of the formulation are sensitive to such measurement. For instance, if the dispersion state is a gel-like network G' will exceed G" even at low frequencies [270]. Furthermore, colloidal suspensions show a complex phase behaviour which is controlled by the volume fraction (ϕ) of the dispersed particles [271].

In the literature the rheological studies involving PLA dispersions have been limited to highly viscous polymer melts in which the polyester was the matrix and the filler was the dispersed phase, aiming at a particle-modified PLA-based material [25][272].

3.1.5. Thickening agents

Thickeners are rheological additives, usually polymers, which act as viscosity-enhancing substances that build up structures in solution through their interaction with water and/or dispersed particles [267]. Polymers are able to modify the rheology of the system due to their high molecular weights, chain entanglement and polymer-solvent interactions [273]. In particular, polymer solutions show an increase in viscosity when the molecular weight (M_w) is incremented. Similarly, for a polymer with fixed molecular weight, the viscosity increases with the concentration. At a critical value, the dependence of the viscosity on the M_w and the concentration increments due to chain entanglement.

Traditionally, thickeners can be classified according to their origin: natural, naturally derived or synthetic [274]. As anticipated in Paragraph 1.3 of Chapter 1, polysaccharides like starches, cellulose and gums are natural thickeners which are widely employed in several application field, such as the textile, paint, paper, pharmaceutical and food industry; especially in those sectors where the restrictions on the possible substances used are necessary for the consumers' safety [52]. Indeed, since they are extracted from renewable and abundant sources, they are considered an eco-friendly and non-toxic alternative to synthetic thickeners. For instance, regarding the food sector, the combination of starch and xanthan gum resulted to be efficient as a thickener for sweet and sour sources [275][276]. As concerns the textile sector, alginates, guar and xanthan gum are revealed to be efficient modulators of the rheological properties of the printed paste with the purpose of obtaining sharp, clean drawing patterns in which dye migration is prevented [277]. Regarding the paint industry, an interesting work revealed the efficiency of sodium alginate as a thickening agent for a wall paint formulation after evaluating the interaction of the polysaccharide with the principal components of the paint [84]. Due to the relevance for this work, the use of xanthan gum as thickener will be further discussed in the next Paragraph (Paragraph 3.1.5.1).

Cellulose is the most widespread polysaccharide in nature, nevertheless its use as thickener is limited by its insolubility in water. For this reason, cellulose can be modified with the introduction of hydrophilic substituents with the purpose of using it as a thicken agent. In this way water-soluble cellulose ethers such as carboxymethyl cellulose (CMC), hydroxyethyl cellulose (HEC), methyl cellulose

(MC), ethyl cellulose (EC) and hydroxypropyl cellulose (HPC) can be synthesised [278]. Cellulose ethers can be biodegradable or not depending on the modification degree and they found large use as thickening agents for waterborne paints [279]. For example, recently, CMC was efficiently employed as a thickener in food nanoemulsions, increasing the physical stability of the formulation [280]. Besides, CMC was used, in combination with cellulose nanocrystals (CNCs), as thickener for textile printing ink, providing the formulation with the adequate viscosity without modifying the other desirable properties of the formulation [281]. Additionally, the use of modified starch like hydrolysed starch, hydroxypropyl starch and sodium starch octenyl succinate as viscosity control agents has been reported for personal care systems [282]. Generally, when polysaccharide or modified polysaccharide are employed as thickeners for polymer dispersion they display a simple thickening behaviour, also known as “volume restriction”. Specifically, they increase the system’s viscosity by restricting the volume available for the particles, without interacting with them [282]. On the other hand, synthetic polymer thickeners able to interact with themselves and with the dispersion particles were developed and they are commonly known as associative thickeners. Associative thickeners are a powerful class of rheology modifiers formed by water soluble polymers of low to moderate molecular weight modified with the insertion of small amounts of hydrophobic moieties. The hydrophobic parts of the thickener can aggregate in micellar-like structures that highly increase the viscosity of the system and, moreover, they can be absorbed onto the latex particles surface [283]. Thanks to the dynamic interactions of hydrophobic groups, the network of thickener and latex particles can be disintegrated under high shear rate and regenerated at rest [284]. Due to these pseudoplastic properties, associative thickeners are primarily used in paint and inks, even though other applications in personal care and enhanced oil recovery were also reported [285][286]. There are several typologies of associative rheology modifier, however the most common are hydrophobically modified ethoxylated urethane (HEUR) polymers [284], hydrophobically modified alkali-swellable emulsion (HASE) polymers [287], hydrophobically modified polyacrylamide (HMPAM) [288] and hydrophobically modified cellulosic (HMC) polymers [278]. However, these typologies of thickeners are fully or partially fossil-based and non-biodegradable and besides, even when renewable substrates are employed, the necessity of inserting hydrophobic modification reduces the eco-sustainability of the final product.

3.1.5.1. Xanthan gum as thickener

As previously discussed, xanthan gum has found large application as a thickening agent in several applicational fields due to its non-toxicity and biodegradability, as well as its physicochemical properties. The primary structure and its industrial applications were fully described in paragraph 1.3.2 of Chapter 1. Particularly, this biopolymer forms hydrocolloid solutions with high stability at high shear values and in a wide range of pH, temperature, and ionic strength [289][75]. The secondary structure of xanthan, depending on the temperature and ionic strength, undergo an order-disorder (helix-coil) transition [290]. Indeed, at room temperature and in distilled water, the polysaccharide chains are in a randomly broken helix configuration (disordered) in which there is a high extension due to the electrostatic repulsions from the charged groups on the side chains. If the temperature is increased, a change in rheological properties occurs since the configuration assumes a coil like state where the molecules are dissociated. On the contrary, if at room temperature the salinity is increased, a transition to an order helical conformation takes place [291]. In this state, as a consequence of the charge screening effects, the charged trisaccharide chains collapse onto the backbone stabilizing the final conformation. Since the electrostatic repulsion is screened, the xanthan gum chains realign and associate forming a gel-like structure. In this case, the transition to a disordered conformation requires the use of much higher temperatures (80-100°C). For this reason, the shear viscosity of xanthan solutions is relatively uninfluenced by temperature. Overall, xanthan gum chains, even at low concentrations, are able to build up a network that confers to the solution a pseudoplastic behaviour with predominant conservative properties [292][290]. Even though at low frequencies the predominance of the elastic (G') over the viscous (G'') modulus is similar to the behaviour of a gel, xanthan gum is a non-gelling agent in itself; consequently, its solutions are able to retain the flow properties required for their effective spreading over surfaces [61]. Thanks to its outstanding rheological properties, XG is commonly used as a thickening agent in food [293], cosmetic, agricultural, pharmaceutical [74], and petroleum industry applications [75], as well as in home and personal care product formulations [294]. Regarding the coating applications, xanthan gum has been successfully employed in edible coatings enriched with antioxidant and antibacterial agents with the purpose of extending the shelf-life of fresh cut fruits [295]. However, in the literature the use of xanthan gum

as a thickening agent for industrial coatings has not yet been reported. In spite of its relatively high price, this biopolymer may be considered as an interesting sustainable alternative to the current waterborne coating additives because of its effectiveness as a rheology modifier even at very low concentrations.

3.2. RESULTS AND DISCUSSION

3.2.1. Rheological response of PLA dispersions in water with xanthan gum

3.2.1.1. Preparation and characterization of the PLA Dispersion

A water dispersion of amorphous PLA in water, stabilized with starch and sodium dodecyl sulfate (SDS) as an emulsifier, was prepared by a two-step procedure, as sketched in Fig. 3.2, and was previously reported by in Chapter 2 (entry 3, Table 2.1) [95].

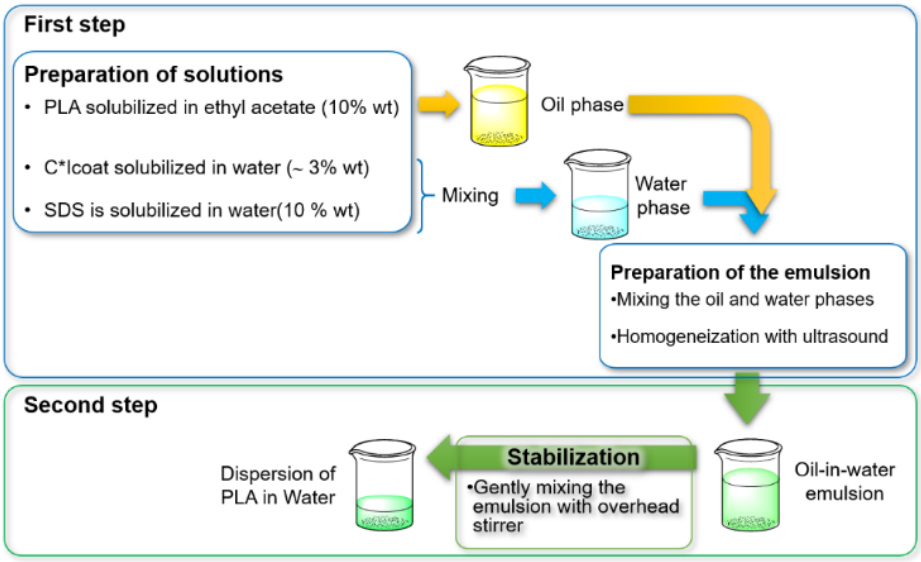

Figure 3.2: Cartoon of the procedure for the preparation of the PLA dispersion in water.

The obtained dispersion, with 15.0 ± 0.1% dry matter content, appears as a white, homogenous, clots-free liquid with water-like viscosity. Dynamic light scattering (DLS) analysis of the dispersion revealed sub-micrometer-sized particles with an average hydrodynamic diameter of 222 ± 2 nm and polydispersity of 0.230 ± 0.003 (Fig. 3.3a). A comparable size could be observed by scanning electron microscopy (SEM) analysis of the dried particles obtained from the dispersion (Fig. 3.3b).

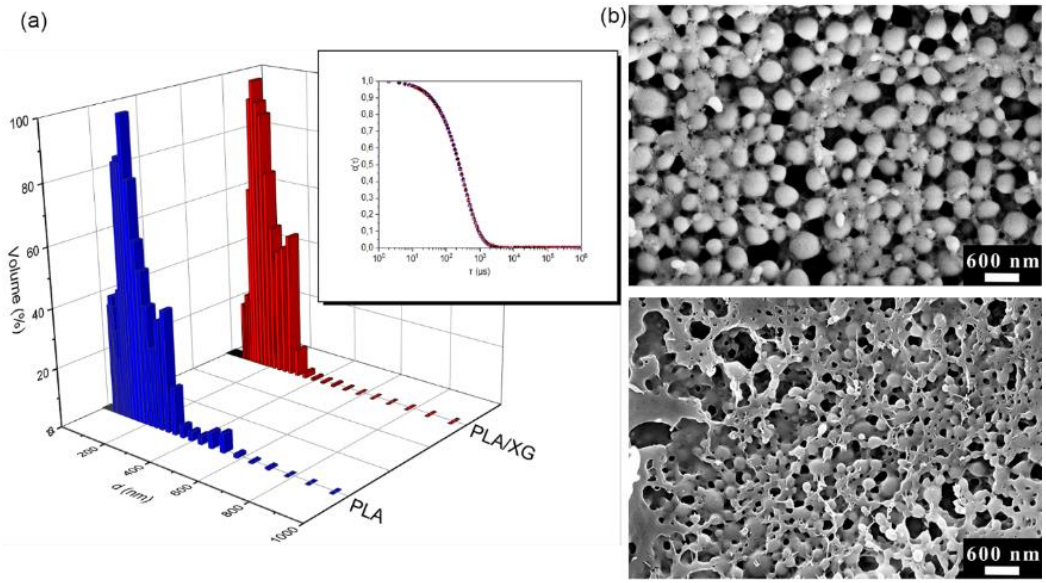

Figure 3.3: (a) DLS size distribution plots of PLA dispersions without xanthan gum (blue histogram) and with 0.35 wt. % xanthan gum (red histogram); inset: DLS correlation plots of the same dispersions. (b) SEM micrographs of PLA dispersion without xanthan gum (top) and with 0.35 wt. % (bottom) dispersions at 40k magnification. Error bars are calculated as standard deviation.

The negative *Z* potential of −35.30 ± 0.85 mV (Table 3.1), as expected from the presence of the anionic SDS surfactant on the particle's surface, resulted in the high stability of the dispersion. Indeed, no evidence of the onset of either coagulation or sedimentation processes was visually detectable over 6 months of storage both at room temperature and at 4 °C, as previously discussed in Paragraph 2.2.4 of Chapter 2.

Table 3.1: Z potential, mobility, and conductance of the PLA dispersion

Sample	Z potential (mV)	Mobility (V/cm)	Conductance (μS)
D0_15	-35.30±0.85	-2.76±0.07	22±0

These results are in agreement with the ones described in Paragraph 2.2.1 and 2.2.6 of Chapter 2.

3.2.1.2. Addition of XG to the PLA Dispersion

The addition of XG as a thickener to the PLA dispersions (Table 3.2) did not result in any appreciable change in their apparent properties, except for the higher viscosity. In particular, in Table 3.2 are reported all the PLA/XG dispersions prepared with given xanthan gum concentration (C_x) and particle concentration (C_p). No creaming, sedimentation, or coagulation formation was detected over a few months of observation, indicating that XG does not negatively affect the dispersion stability. Accordingly, the DLS correlation plots obtained from the dispersions with added XG are overlapping with those from the corresponding pristine PLA dispersions (inset in Fig. 3.3a): the DLS correlation curve shows a single inflection point, suggesting the absence of large clusters or of secondary phase domain formation. Particle size distribution by volume is almost bimodal for both dispersion types (with and without XG, Fig. 3.3a). The average particle size and polydispersity were found to not appreciably depend on either XG or particles' concentration (Table 3.3).

Table 3.2: Prepared dispersions of PLA/XG with given C_X concentrations of XG and given C_P concentrations of PLA, in water.

Acronym[a]	C_X (wt. %)	C_P (wt. %)[b]
D0_15	0	15.00±0.10
D15_15[c]	0.151	15.25±0.08
D25_15[c]	0.251	15.35±0.10
D35_15[c]	0.356	15.45±0.11
D50_15[c]	0.503	15.60±0.06
D65_15[c]	0.655	15.76±0.09
D75_15[c]	0.760	15.86±0.10
D50_5[d]	0.50	5.02±0.03
D50_10[d]	0.50	10.02±0.08
D50_12.5[d]	0.50	12.5±0.10
D50_13.5[d]	0.50	13.5±0.03
D50_20[d]	0.50	22.29±0.10
D75_5[d]	0.75	4.99±0.09
D75_10[d]	0.75	9.98±0.05
D75_20[d]	0.75	20.25±0.07

[a]Samples are labeled with the acronym D*x_p*, where *x* represents the concentration of XG in wt. % multiplied by 100, and *p* represents the concentration of PLA particles in wt. %. [b]Determined as weighed dry residue. [c]Dispersions prepared by varying the amount of XG added at constant dry residue. [d]Dispersions prepared by varying the dry residue at a fixed amount of XG (0.50 or 0.75 wt. %).

The addition of XG confers to the initial PLA dispersion a typical honey-like viscosity, a feature that will be discussed in-depth in the next Paragraph. SEM analysis of the dried PLA/XG dispersion shows a densely interconnected pattern (Fig. 3.3b), likely associated with the buildup of an interconnected network between XG and nanoparticles. Individual particles are still detectable but they are held together by XG resulting in a biphasic morphology. The presence of such a network becomes more evident at increasing XG/PLA mass ratio (Fig. 3.4a). Indeed, when the concentration of PLA decreases, its particles are hardly detectable within the XG network (Fig. 3.4b).

Table 3.3: Calculated volume fraction Φ, mean diameter <d> and polydispersity IPD sand viscosity η at shear rate 1 s^{-1} for all prepared dispersions of PLA/xanthan gum.

Acronym[a]	Φ	<d> (nm)[b]	IPD[b]	η (Pa s)[e]
D0_15	0.105±0.004	221.9±2.0	0.230±0.003	0.01±0.11
D15_15[d]	0.139±0.005	248.1±2.3	0.254±0.007	0.23±0.11
D25_15[d]	0.147±0.006	250.1±3.1	0.252±0.010	1.20±0.38
D35_15[d]	0.155±0.005	231.6±3.4	0.222±0.018	1.70±0.23
D50_15[d]	0.161±0.010	226.9±0.9	0.237±0.005	4.07±1.21
D65_15[d]	0.172±0.006	239.0±1.4	0.251±0.012	7.32±0.36
D75_15[d]	0.179±0.006	236.4±1.4	0.251±0.008	10.58±0.06
D50_5[e]	0.089±0.011	219.3±1.5	0.230±0.009	0.28±0.10
D50_10[e]	0.124±0.010	230.4±2.9	0.241±0.004	1.26±0.29
D50_12.5[e]	0.137±0.009	228.5±3.7	0.231±0.018	1.90±0.39
D50_13.5[e]	0.154±0.009	229.8±1.8	0.238±0.005	2.40±0.39
D50_20[e]	0.221±0.001	224.7±0.8	0.234±0.007	7.12±1.22
D75_5[e]	0.104±0.006	279.0±21.4	0.276±0.013	0.75±0.11
D75_10[e]	0.140±0.005	258.9±5.4	0.234±0.020	3.28±0.39
D75_20[e]	0.216±0.006	261.0±3.4	0.245±0.011	10.70±0.06

[a]Samples determined by the acronym Dx_p, where x represents the concentration of xanthan gum in wt. % multiplied by 100 and p represents the concentration of PLA particles in wt%. [b]Determined by DLS. [c]Value at $\dot{\Upsilon}$=1 s^{-1}, determined by steady shear experiments. [d]Dispersions prepared by varying the amount of xanthan gum added and maintaining the dry residuum constant. [e]Dispersions prepared by varying the dry residuum at a fixed amount of xanthan gum (0.50 or 0.75 wt. %).

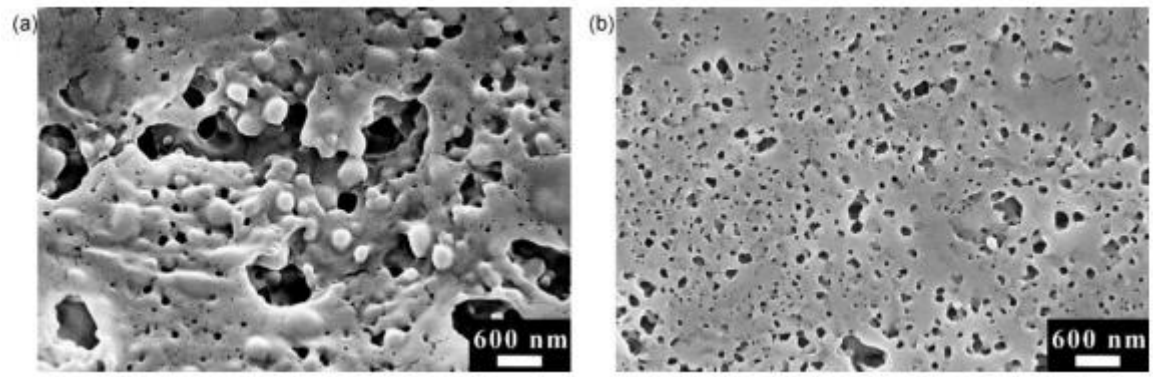

Figure 3.4: SEM micrographs of PLA/xanthan gum dispersions dried at room temperature: a) D75_15, b) D50_10. (See Table 3.2 for the decoding of the acronyms).

Even in the presence of XG, the molecular weight ($\bar{M}_n$) and dispersity of PLA were comparable to those of the pristine polymer (Table 3.4), an indication of the absence of any degradation phenomena throughout all the preparation steps, including the addition of the XG thickener.

Table 3.4: Average molecular weights (M_w and M_n) and polydispersity index (IPD) of PLA 4060D, dispersion D0_15, D25_15 and D35_15 by GPC analysis. See Table 3.2 for decoding of acronyms.

Sample	**M_w (kD)**	**M_n (kD)**	**IPD**
PLA 4060D	172	120	1.43
D0_15	160	112	1.42
D35_15	163	114	1.43
D25_15	158	111	1.42

3.2.1.3. Steady shear properties of PLA/XG Dispersions

Neat PLA dispersions in water show, within the concentration range of our interest, viscosity independent of the shear rate and similar to water (Fig. 3.5a, light-blue graph), as typically observed for low concentration of hard-sphere colloids [296]. On the contrary, when XG is added to the dispersion it conveys a shear-thinning behavior, and the Newtonian plateau is no longer observed. The flow curve profiles of the thickened dispersion show the same features as those of aqueous XG solutions (Fig. 3.6a), a behavior previously observed for aqueous dispersions of SiO_2 particles with XG [297]. However, the viscosity of the PLA/XG dispersion is higher (Fig. 3.6b) than that of the reference XG solution.

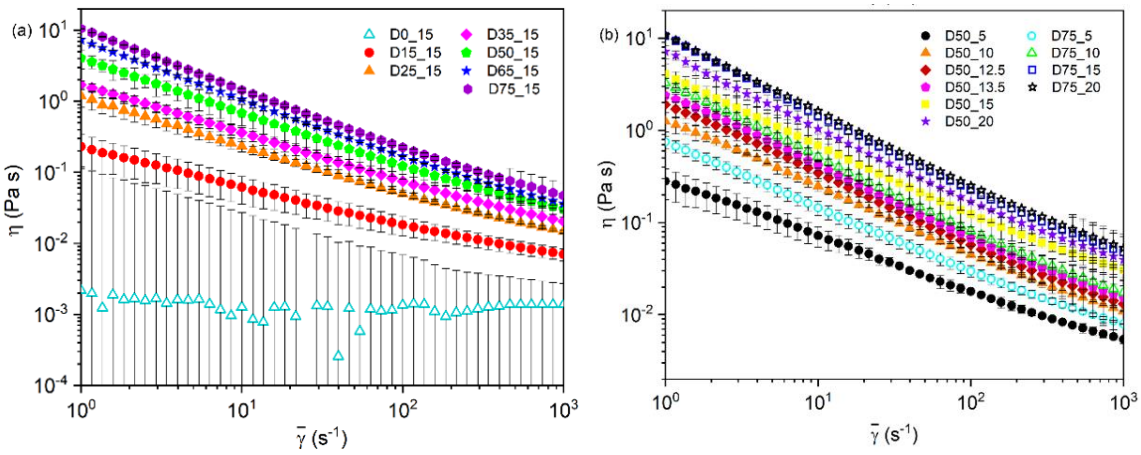

Figure 3.5: Viscosity as a function of shear rate for dispersions with (a) different concentrations of XG and constant content of particles; (b) different concentrations of particles and constant concentration of XG. See Table 3.2 for the decoding of the acronyms in the legend. Error bars are calculated as standard deviation.

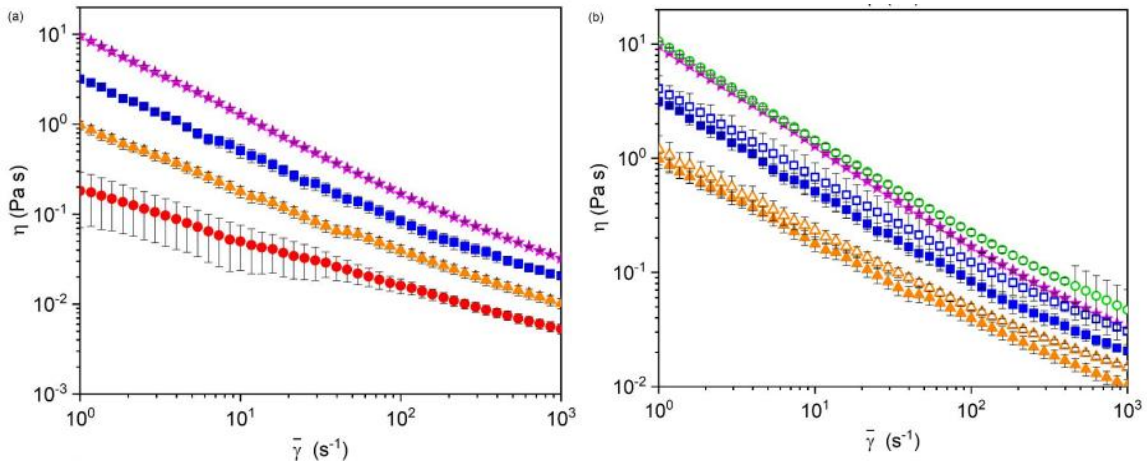

Figure 3.6: Viscosity plots at 25°C for. a) water solutions of xanthan gum at different concentration (circles 0.15%, triangles 0.25%, squares 0.55%, stars 1% wt.); b) comparison between the viscosity curves of xanthan gum solutions (full symbols) and PLA dispersions (empty symbols) with different concentration of xanthan gum (triangles 0.25%, squares 0.55%, circles 0.75%, stars 1% wt.). Error bars are calculated as standard deviation.

The increase of viscosity is higher than that expected from a simple additive contribution by the viscosity of the neat PLA dispersion. This indicates the occurrence of specific interactions between the particles and the polysaccharides. Accordingly, the viscosity of the PLA/XG mixed dispersions increases by increasing

either the XG or the PLA particle concentrations, with comparable dependence on the shear rate at all investigated compositions (Fig. 3.5).

3.2.1.4. Dynamic Viscoelastic Properties of PLA/XG Dispersions

Amplitude sweep experiments performed on samples with different concentrations of PLA or XG show, as expected, a low strain sweep region in which both storage and loss moduli are constant (Fig. 3.7). In this region, the former is larger than the latter, indicating a gel-like behavior. The difference between the two moduli increases with the content of XG when mixtures of comparable PLA content are considered, a clear indication of the key role of XG in inducing such gel-like behavior. At larger deformations, the storage modulus decreases at all investigated compositions, the onset of the deviation from the plateau occurring at progressively higher deformations with an increasing XG amount in the formulation. The inability of the system to completely recover the deformation within the experiment time frame corresponds to the typical behavior of solutions of high molecular weight polymers such as XG [298]. The loss moduli show a behavior similar to the storage moduli in the high-amplitude region at a low XG content. On the contrary, at a high XG content, a distinct peak is generally observed before the value starts decreasing, disclosing the presence of the so-called “weak strain overshoot”. This behavior is typical of metastable complex fluids such as XG and it has been correlated to a decrease of the structural relaxation time at large strain values [299][300]. The deviation from the plateau starts at lower deformation for the most concentrated solutions and it is faster for the storage than the loss moduli so that the two plots cross. The crossing point shifts at higher deformation for higher XG content, an indication that the system is able to dissipate progressively more energy and to recover elastically larger deformations when the concentration of XG increases. As a result, the linear viscoelastic region (LVR) becomes more extended, and the crossing point between storage and loss moduli shifts at higher strain as the concentration of XG increases [298].

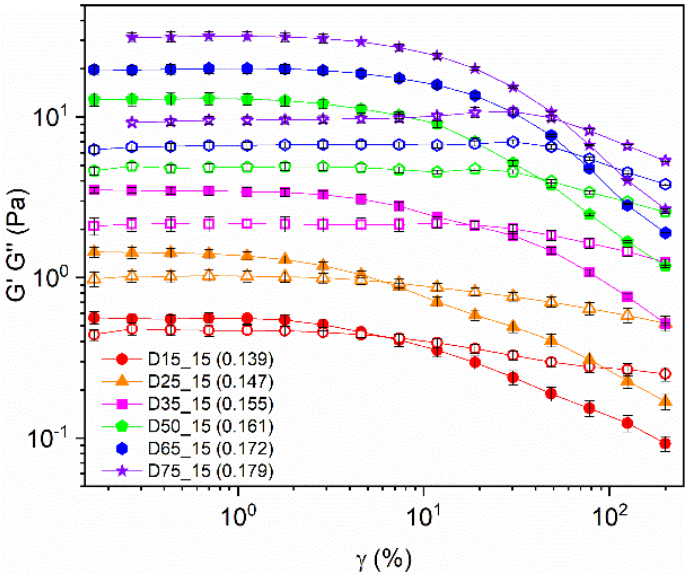

Figure 3.7: Storage (G'—full symbols) and loss (G''—empty symbols) moduli as a function of strain sweep for dispersions with 15 wt. % PLA particles and different XG concentrations (circles: 0.15, triangles: 0.25, squares: 0.35, pentagons: 0.50, hexagons: 0.65, stars: 0.75 wt. %). The values in parentheses refer to the volume fraction of PLA particles, resulting from different volume ratios of aqueous XG with 15 wt. % PLA in the formulations. See Table 3.2 for the decoding of the acronyms in the legend. Error bars are calculated as standard deviation.

The frequency dependence of the viscoelastic moduli at constant strain in the 0.5–1% range for dispersions with different XG contents shows an increase of both storage and loss moduli with both increasing concentration and increasing frequency (Fig. 3.8). The times of the experiment are too long to allow the system to relax; therefore, the crossover frequency can hardly be observed and only at the lower investigated concentrations. As a result, the systems exhibit a solid-like behavior throughout the investigated frequency range ($G'' > G'$).

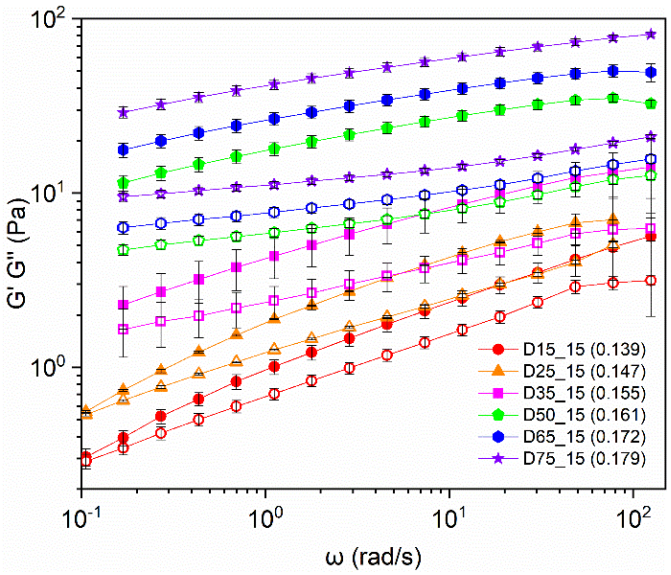

Figure 3.8: Storage (G'—full symbols) and loss (G—empty symbols) moduli as a function of frequency for dispersions with 15 wt. % PLA particles and different XG concentrations (circles: 0.15, triangles: 0.25, squares: 0.35, pentagons: 0.50, hexagons: 0.65, stars: 0.75 wt %). The values in parentheses in the legend refer to the volume fraction of PLA particles, resulting from different volume ratios of aqueous XG with 15 wt. % PLA in the formulations. See Table 3.2 for the decoding of the acronyms in the legend. Error bars are calculated as standard deviation.

The plots of oscillatory shear flow experiments on samples with a comparable XG concentration showed an increase of the moduli values with increasing PLA concentration in the 5-20 wt. % range (Fig. 3.9). In addition, higher moduli are shown by samples with PLA particles as compared to samples without PLA particles (Fig. 3.9 vs 3.10) at comparable XG concentrations.

This behavior indicates that not only XG but also the dispersed PLA particles contribute to the viscoelasticity of the system. Indeed, both storage and loss moduli vs. frequency plots exhibit values dependent on both PLA and XG contents. In other words, even if the neat PLA dispersion does not exhibit any elastic behavior, we can say that PLA particles enhance both elastic and viscous behavior of the thickened dispersion, in a similar way that XG does (Fig. 3.9). Therefore, the combined effects induced by the increase of both XG and dispersion particle concentrations result in a more pronounced viscoelastic behavior.

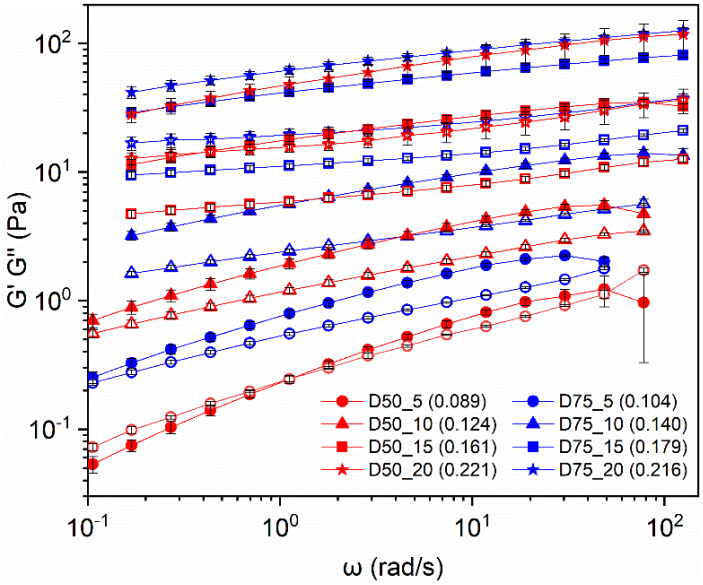

Figure 3.9: Storage (G'–full symbols) and loss (G"–empty symbols) moduli as a function of frequency for dispersions with different particle concentrations and fixed XG concentration (red symbols: 0.50 wt. %, blue symbols: 0.75 wt. %). The values in parentheses in the legend refer to the volume fraction of PLA particles in the samples. See Table 3.2 for the decoding of the acronyms in the legend. Error bars are calculated as standard deviation.

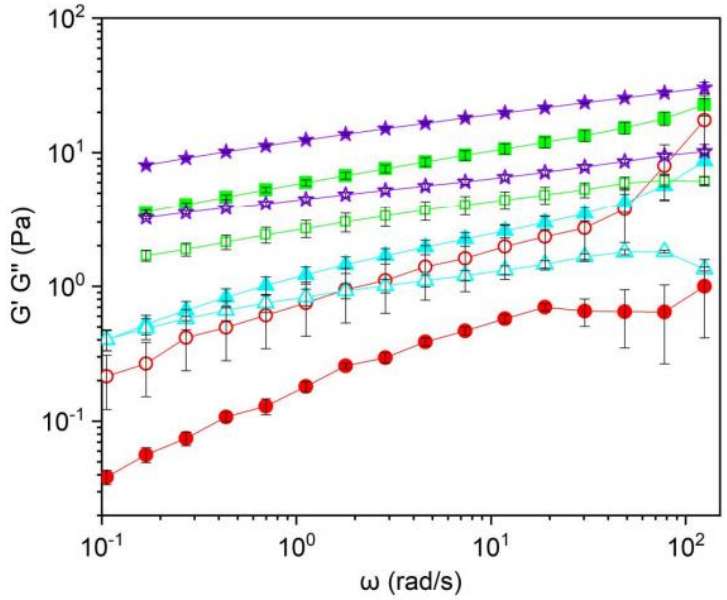

Figure 3.10: Storage (G'-full symbols) and loss (G"-empty symbols) moduli as a function of frequency of solutions with different xanthan gum concentration (circles 0.15, triangles 0.25, squares 0.50, stars 0.75 wt. %). Error bars are calculated as standard deviation.

The frequency dependence of the moduli is higher in the low concentration range; thus, the sample with the lowest concentrations of both PLA (5 wt. %) and XG (0.5 wt. %) is also the one displaying the crossover at the lowest frequency of about 1 rad/s, corresponding to a relaxation time of 5.5 s, indicative of a fluid-like behavior at low shear. None of the other samples presents the crossover within the investigated frequency range, indicating a more marked elastic behavior.

3.2.1.5. Volume Fraction

A critical discussion of the rheological behavior of the PLA dispersions described so far requires a clear understanding of the specific features of the system we are dealing with. The dispersed particles are made of amorphous PLA and its T_g of 54 °C is quite higher than the temperature at which the investigation was performed (25 °C). As a result, under the study conditions, the system can be approximated to a dispersion of hard spheres. The presence of SDS as the surfactant provides a negative surface charge to the particles, while XG in the continuous phase contributes to the negative charge of the mixed PLA/XG network and to the viscoelastic properties of the overall dispersion [301]. Consequently, the neat PLA dispersion can be described as negatively charged hard spheres dispersed in a continuous liquid phase, and the PLA/XG system as negatively charged hard spheres dispersed in a complex anionic fluid matrix [302].

The rheological results described so far indicate that the viscoelasticity of the dispersion with XG arises from the presence of the polysaccharide in the continuous phase, as it generally occurs for dispersions of solid particles in polymeric matrices [301]. However, even if dispersions of neat PLA (hard) particles do not exhibit any viscoelasticity, the same particles do affect the viscoelastic response of the overall system once dispersed in a polymeric XG solution. Therefore, both components must be considered at once for a comprehensive discussion of the system behavior.

A single parameter including both components may be the particle volume fraction, Φ, defined as the fraction of volume occupied by the particles, Φ_i, with respect to the whole volume of the system, Φ_{TOT}. It depends on the number of particles n in the system and on the volume occupied by a single particle V_P, with respect to the total volume of the system (equation 3.1)

$$\Phi = \frac{\Phi_i}{\Phi_{TOT}} = \frac{n\,V_P}{V_{TOT}} \qquad (3.1)$$

The total number of particles in dispersion is given by

$$n = \left(V_{TOT} - \frac{w_x}{\rho_x}\right) * V_P^{-1} = \left[V_{TOT} + \frac{\left(w_{dry} - w_{TOT}\right)}{\rho_x}\right] * V_P^{-1} \qquad (3.2)$$

Where w_x is the weight of the solvent, w_{TOT} is the total weight of the sample, w_{dry} is the weight of the sample without the solvent, and ρ_x is the density of the solvent. By substituting equation 3.2 in 3.1 and rearranging the equation for the volume fraction, equation 3.3 is obtained

$$\Phi = 1 + \frac{\rho_0}{\rho_x}\left(\frac{w_{dry}}{w_{TOT}} - 1\right) \qquad (3.3)$$

where ρ_0 is the density of the dispersion.

In this study, ρ_0 and w_{dry}/w_{TOT} were assumed as equivalent to the density and the dry residue, respectively, of the neat PLA dispersions in water, irrespective of the presence and concentration of XG, while ρ_x was assumed as equivalent to the density of the XG solution at a given concentration in the absence of the dispersed particles. The volume fraction, Φ, was hence obtained by substituting in equation 3.3 the experimentally determined values for the densities (Fig. 3.11) and the dry residues.

The obtained values for the dispersions were found to depend on the concentrations of both PLA particles (C_P) and XG (C_X) (Fig. 3.12). Hence, Φ can be used to describe the effects of the dispersion composition on the dispersion properties.

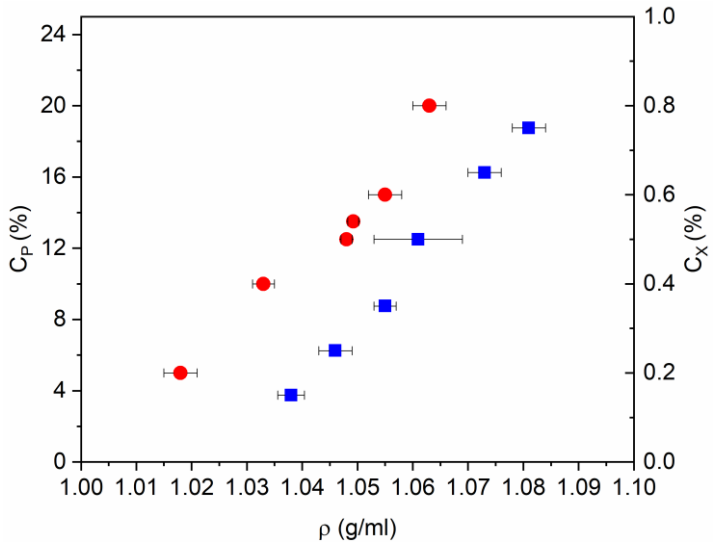

Figure 3.11: Left scale: dots: density of dispersions without xanthan gum and different concentration of particles C_P (5, 10, 12.5, 13.5, 15, 20 wt.%); right scale: squares: density of xanthan gum aqueous solutions at different concentration C_X (0.15, 0.25, 0.35, 0.50, 0.65, 0.75 wt. %). Error bars are calculated as standard deviation.

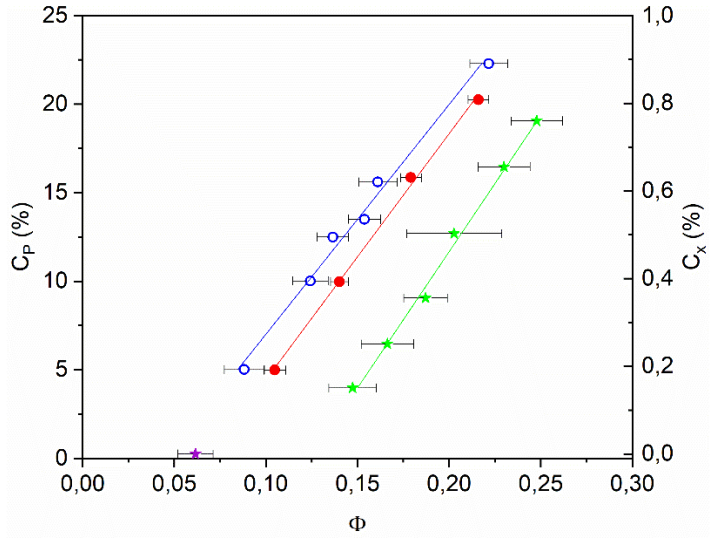

Figure 3.12: Left scale: volume fraction Φ of dispersions with different mass concentrations of particles, C_P, at a fixed XG concentration of 0.50 wt. % (blue triangles; D50_5-20, Table 3.2) and 0.75 wt. % (red dots; D75_5-20, Table 3.2), respectively. Right scale: volume fraction Φ of dispersions with different mass concentrations of XG, C_X, and fixed concentration of particles (green stars; D15-75_15, Table 3.2); violet star: volume fraction of the dispersion without XG and 15 wt. % of particles (D0_15, Table 3.2). Straight lines: linear fitting (see Table 3.5 for fitting data). Error bars are calculated as standard deviation.

The calculated Φ values range between 0.09 and 0.22, scaling linearly with both PLA and XG concentrations, as indicated by the R^2 values larger than 0.9 for the linear fits of the data plots (Tables 3.5).

Table 3.5: Best fitting parameters for the dependence of the volume fraction on sample's composition shown in Fig. 3.12.

$C = a + b\Phi$	a	b	R^2
C_P (C_X=0.50%)	0.046±0.006	0.0077±0.0004	0.98
C_P (C_X=0.75%)	0.068±0.003	0.0072±0.0002	0.99
C_X (C_P=15%)	0.130±0.001	0.0644±0.0023	0.99

Based on the new scale by the volume fraction, it is interesting to notice that the moduli vs. frequency plots shown in Fig. 3.9 scale monotonically although the compositions differ in both PLA and XG concentrations. Indeed, if the storage, loss, and complex moduli at a fixed frequency (0.169 rad/s) are plotted as a function of the volume fraction in the log–log scale (Fig. 3.13), an apparent linear trend is observed. This suggests that the amount of PLA particles in the dispersion affects its viscoelasticity by influencing the degree of crowding, intended as the total amount of species in the system, including the XG chains and the colloidal particles. Based on DLS analysis, XG does not adsorb irreversibly at the particle surface. Indeed, in such a case, even after dilution, particles would be larger in the presence of XG than in its absence. Therefore, the observed effect must be ascribed to the presence of obstacles hindering the diffusion of the XG chains. Such obstacles may consist solely of the PLA particles, although a contribution from weak van der Waals interactions or scattered hydrogen bonds between PLA particles and XG chains, which are negligible at a low concentration but become relevant as the concentration increases, cannot be excluded [303].

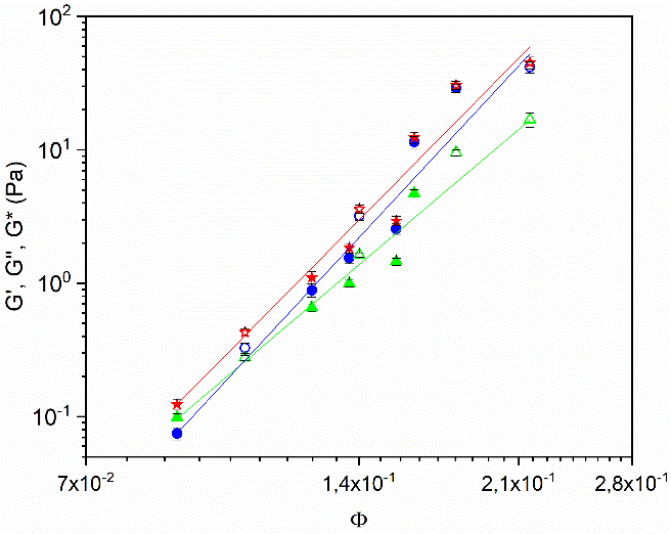

Figure 3.13: Complex (red stars), storage (blue circles), and loss (green triangles) moduli at 0.169 rad/s as a function of the volume fraction for dispersions with different particle concentrations and fixed XG concentration (full symbols: 0.50%, empty symbols: 0.75 wt. %) (D50_5-20 and D75_5-20, Table 3.2). Straight lines are a guide to the eye.

3.2.2. Coating on paper of the polyester dispersions thickened with xanthan gum

The application as coating for paper of the PBSA dispersion (PBSA_SDS) and the two different PLA formulations (PLA_SDS and PLA_SYN) previously developed was deeply studied. In order to coat the polyester formulations onto porous substrates, such as paper, the viscosity of the dispersion must be increased, otherwise the coated aqueous formulation would permeate into the pores of the paper substrate. It must be taken into account that viscosities lower than 3 Pa·s at a shear rate of 1s^{-1} are not indicated for paper substrates. For this reason, in the light of the previous studies, xanthan gum in the amount of 0.5 wt. % was added to the formulation to provide the selected viscosity. Indeed, the influence of the addition of 0.5 wt.% of xanthan gum on the PLA_SDS dispersion was deeply investigated (see Paragraph 3.2.1). As a consequence, the viscosity of all the other polyester dispersions thickened with 0.5 wt.% was measured with the purpose of verifying if the targeted value was reached (Table 3.6). From Table 3.6 it is possible to notice that all the thickened formulations possess a viscosity that is in the proper range.

Table 3.6: Particles dimension, polydispersity and dry residuum of the bare polyester dispersions and viscosity values of the dispersions thickened with 0.5 wt. % of XG.

Formulation	Particles dimension[a] (nm)	Polydispersity[a]	Dry residuum (wt. %)[b]	Viscosity (Pa·s)[c]
PLA_SDS	260.9 ± 3.6	0.173 ± 0.02	15.2	3.2
PLA_SYN	425.5 ± 9.2	0.277 ± 0.01	15.6	5.8
PBSA_SDS	262.0 ± 2.1	0.167 ± 0.03	19.9	6.6

[a]Assessed through DLS analysis. [b]Determined by TGA analysis. [c]Determined at a shear rate of 1 s^{-1}

3.2.2.1. Selection of the paper substrates

Two different paper substrates were considered: Gestar HDS and Repro red paper. Gestar HDS is an industrially produced flexible paper for packaging purpose and it is mineral coated and calendered on one side. On the other hand, Repro red is a laser printing and ink-jet paper. The specific characteristics of each paper substrate are listed in Table 3.6.

Table 3.6: Characteristic features of the evaluated paper substrates.

Paper type	Gestar HDS	Repro red
Thickness (μm)	54 ± 2	104 ± 4
Grammage (g/m^2)	59 ± 2	80 ± 2
Roughness (ml/min)	21 ± 5	250 ± 50

Firstly, the thickened PLA_SYN dispersion was coloured blue with the addition of a food dye and it was subsequently coated onto the two paper substrates available through the use of a doctor blade coater (Fig. 3.14). Nominal coating thickness was 90 μm. After coating the samples were dried onto a heating plate at 60°C. Indeed, it is necessary to work above the minimum film formation temperature (MFFT) of the PLA in order to allow the polymer particles to merge and form a homogenous coating (see Paragraph 2.2.7, Chapter 2). When Gestar HDS paper was used, the

formulation was deposited both on the mineral coated and uncoated side. Nevertheless, in both cases, inhomogeneous coatings were obtained (Fig. 3.14a). It must be taken into account that a good homogeneity and continuity of the deposited layer is essential to guarantee good barrier properties. On the contrary, with the use of paper Repro red good results were obtained as it is possible to notice from Fig. 3.14b. This is probably due to a combination of surface and thickness properties of this type of paper, the former allowing a better spreading of the formulation and the latter allowing a less curling of the substrate during drying.

a)  b) 

Figure 3.14: Picture of Gestar HDS (a) and Repro red paper (b) coated with the PLA_SYN dispersion thickened with 0.5 wt. % of XG. The samples were prepared with a doctor blade coater with 90 µm of coating thickness.

3.2.2.2. Selection of the coating methodology

After selecting the proper paper substrate, the attention was focused on the study of the most suitable coating methodology. Doctor blade coaters with nominal coating thickness of 60, 90 and 120 µm and threaded rods of different diameters were tested. The characteristics of each threaded rod are listed in Paragraph 7.1 of Chapter 7. In order to compare the different coating devices, a model formulation having a viscosity in the target range, namely a water solution at 12% of PVA GH 17R, was used (viscosity of 3 Pa·s at a shear rate of 1 s^{-1}). This solution was blue coloured with a food dye in order to visually evaluate the homogeneity of the deposited polymer layer. In this case, the coating was left to dry at room

temperature, since PVA is able to film at a lower temperature than PLA. The different devices were at first compared in terms of thickness of the produced coating, indicated as coating weights for surface unit (Table 3.7).

Table 3.7: Coating weight as a function of the coating device used for the deposition of a PVA solution in water at 12 % on Repro red paper.

Coating device	**Features of the device[a]**	**Coating weight (g/m^2)**
Doctor blade	60 µm	1.4
	90 µm	2.3
	120 µm	4.1
Threaded rod	3 mm	3.1
	4 mm	15.0
	5 mm	25.0

[a]For the doctor blades the thickness of the layer deposited by the devices are indicated, while for the threaded rods the diameters are listed.

As it is possible to observe from Table 3.7 the use of threaded rods with a 4-5 mm diameter allowed the obtainment of coating weights higher than those achieved with doctor blade coaters. It must be taken into account that higher coating weights are preferred when it is necessary to provide the paper substrates with good barrier properties. Consequently, the threaded rod was chosen as the most appropriate coating device. The threaded rod with 3 mm diameter was discarded due to the low coating weight achieved, which is comparable with the ones obtained with doctor blade coaters.

Overall, threaded rods with a diameter between 4 and 10 mm were used to prepare polyester coatings on paper with different coating weights. The samples were dried in the oven with the purpose of providing a more homogeneous heating in comparison with the hot plate. The dispersions bearing PLA were dried at 60 °C, while the PBSA dispersion was dried at 110 °C since it possesses a higher MFFT (see Paragraph 2.2.9, Chapter 2). All the samples prepared are listed in Table 3.8.

Table 3.8: Coating weight (CW) of the coated papers as a function of the formulation coated and the size of the threaded rod employed.

Entry	Formulation coated[a]	Threaded rod diameter (mm)	CW (g/m^2)[b]
1	PLA_SDS	4	20.75
2		10	44.44
3	PLA_SYN	4	5.69
4		5	13.22
5		7	29.18
6		10	38.5
7	PLA_SYN (x 2)	4	37.7
8		5	39.1
9	PBS_SDS	4	47.3

[a]All the formulations were thickened with 0.5 wt. % of XG; after coating the samples were dried in the oven for 1h at 60 °C. [b]Determined on 28,26 cm^2 of sample. [c]The sample was dried in the oven at 110°C for 1h.

In order to study the morphology of the prepared coatings SEM analysis was performed (Fig. 3.15 and 3.16). It can be seen that with the use of PLA_SDS and PBSA_SDS dispersions a porous morphology is obtained (Fig. 3.15c,d). Besides, when the largest rod diameter (10 mm) was used to deposit on paper the PLA_SDS dispersion (Fig. 3.15b), the coating is fractured and porous. This is probably due to a repulsion between the negatively charged polymeric colloidal particles and the paper substrate. Indeed, different additives (either anionic or cationic) are used during the papermaking process and the z-potential of the paper surface depends on the charge balance between the different additives. It can be hypothesized that the paper substrate used is formally negatively charged and that therefore there is an unfavorable interaction with the polymer particles.

On the other hand, with the PLA_SYN dispersion continuous and homogeneous coatings were achieved with both 4 and 5 mm diameter rods (Fig. 3.16a,b). It is clear that to obtain a homogeneous coating it is better to use uncharged colloidal polymeric particles obtained with a neutral surfactant such as SYN. Nevertheless, in the sample coated with the 4 mm rod the presence of small surface defects was noticed. When the diameter of the coating rod was increased up to 7 or 10 mm, thus

incrementing the coating weight of the deposited layer, a detrimental effect on the morphology of the coating was observed. This suggests that to obtain a homogeneous coating it is necessary, in addition to uncharged polymer particles, to deposit a small amount of dispersion. The hypothesis was confirmed by the fact that, if coating weights similar to the ones obtained with the higher diameter rods are achieved through two different depositions, continuous and homogeneous coatings morphology are obtained (Fig. 3.16c,d). Despite the continuity of the polymeric layer, the sample coated two times with the 5 mm diameter rod presents some micrometric spheres dispersed in a continuous matrix (Fig. 3.16d).

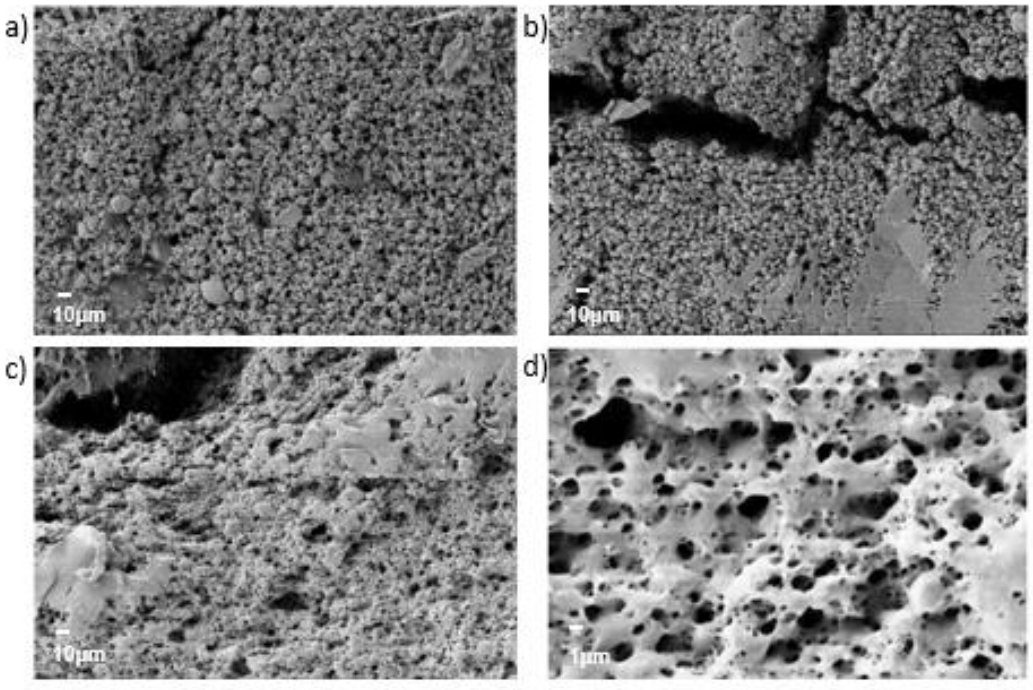

*Figure 3.15: Pictures of the coating trials performed with the PLA_SDS (**a**,**b**) and PBSA_SDS (**c**,**d**) dispersions deposited with threaded rods of 4 mm (**a**,**c**,**d**) and 10 mm (**b**) diameter.*

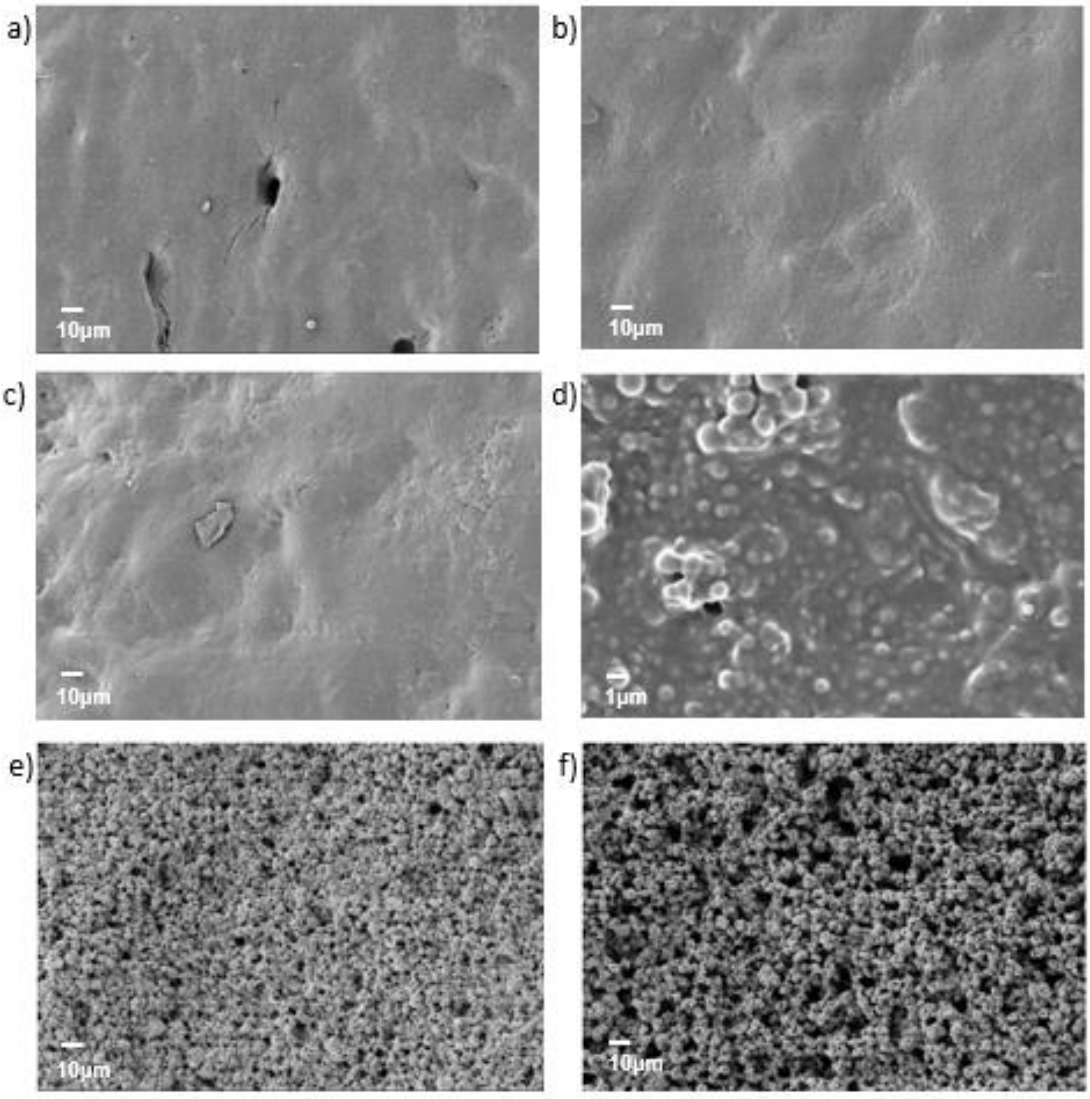

*Figure 3.16: SEM pictures of the coating trials performed depositing a single layer of the PLA_SYN dispersion and the threaded rod with a diameter of 4 (**a**), 5 (**c**), 7 (**e**) and 10 mm (**f**) and a double layer of the PLA_SYN dispersion with the threaded rod with a diameter of 4 (**b**) or 5 (**d**).*

3.2.2.3. Barrier properties to liquids of the polyester coatings on paper

Subsequently, the liquid barrier properties and the grease resistance of the coated samples prepared were studied. In this context, the liquid water permeability (LPW) index and the grease permeability (GP) were measured and correlated to the coating weights and morphology (CW) (Table 3.9).

Table 3.9: Coating weight (CW), liquid water permeability (LWP) index and grease permeability (GP) of the coated papers as a function of the formulation coated and the size of the threaded rod employed.

Entry	Formulation coated[a]	Threaded rod diameter (mm)	CW (g/m^2)[b]	LWP (g/m^2)	GP (s)
1	none	-	-	23.4 ± 2.1	19.3 ± 2.0
2	PLA_SDS	4	20.75	54.0 ± 4.9	113.0 ± 110.0
3		10	44.44	77.6 ± 1.5	112.0 ± 102.0
4	PLA_SYN	4	5.69	10.6 ± 2.3	504.3 ± 503.9
5		5	13.22	10.4 ± 2.6	806.0 ± 511.0
6		7	29.18	49.9 ± 5.6	119.0 ± 115.0
7		10	38.5	64.1 ± 1.3	37.0 ± 6.2
8	PLA_SYN (x 2)	4	37.7	6.8 ± 0.2	+1800
9		5	39.1	6.7 ± 3.0	+1800
10	PBS_SDS	4	47.3	82.3 ± 5.0	230.0 ± 99.6

[a]All the formulations were thickened with 0.5 wt. % of XG; after coating the samples were dried in the oven for 1h at 60 °C. [b]Determined on 28,26 cm^2 of sample. [c]The sample was dried in the oven at 110°C for 1h.

Liquid water permeability is a property that indicates the amount of water that material can absorb. A high LPW index corresponds to poor liquid water barrier and this can result in faster packaging deterioration and mechanical problems during handling or storage. The liquid water permeability index of non-coated and coated papers was determined using a modified ISO 535 procedure (see Paragraph 7.3.10 of Chapter 7).

Grease resistance is an important parameter for packaging materials that contain fats or oils. This property of non-coated and coated papers was determined using a modified TAPPI T454 test (see Paragraph 7.3.11 of Chapter 7). The test provides a comparison of the relative rates at which oils or greases penetrate papers. According to this, penetration time of 1800 s or higher corresponds to an excellent resistance to fats and oils [260].

In Fig. 3.17 the LPW indexes (Fig. 3.17a) and GP values (Fig. 3.17b) obtained after coating the paper substrates with different polyester dispersions and under different application conditions are compared.

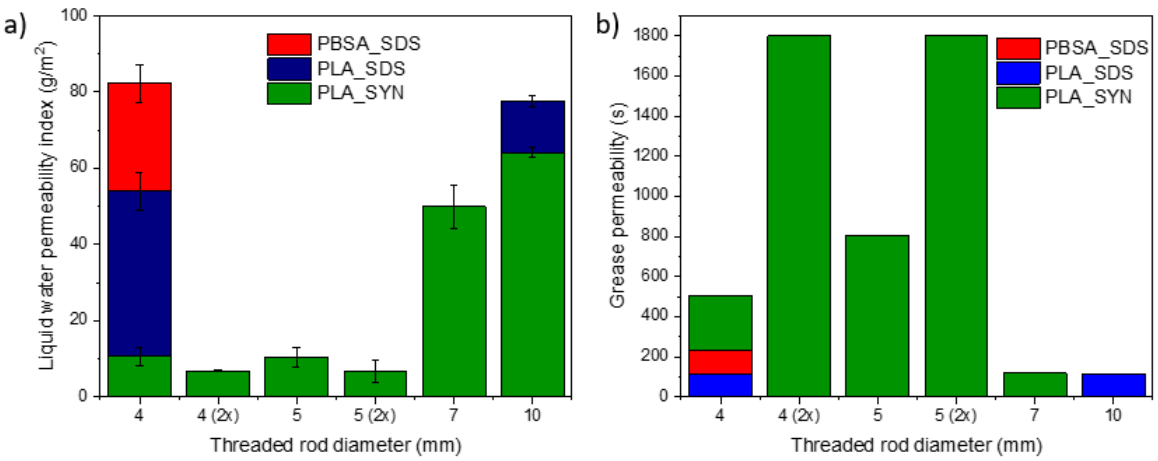

*Figure 3.15: Liquid water permeability index (**a**) and grease permeability (**b**) as a function of the threaded rods diameter and the formulation coated.*

When the PBSA_SDS and PLA_SDS dispersions are used as a barrier layer on paper, poor barrier properties to both water and grease are obtained (LPW indexes between 82 and 54 g/m^2 and GP values from 112 to 230 s) (entry 2,3 and 10, Table 3.9). The achievement of worse barrier properties with the PBSA_SDS dispersion (entry 10, Table 3.9), in comparison with the PLA_SDS one (entry 2 and 3, Table 3.9), can be explained by the fact that, when the PLA_SDS formulation was casted onto capsules and dried at 60 °C, homogeneous and continuous films were obtained (Paragraph 2.2.7 of Chapter 2), whilst, for the PBSA_SDS dispersion, even at the visually identified MFTT (100 °C), the presence of defects and cracks in the film was detected by SEM analyses (Paragraph 2.2.9 of Chapter 2). Overall, all the samples that contain SDS as surfactant display poor liquid barrier properties. This behaviour can be due to the observed porous and fractured morphology of the film that allows external agents, such as water and grease to penetrate. Indeed, this porous structure can act as a sponge able to adsorb water and grease generating LWP and GP values even higher than the one of uncoated paper (LWP index of 23.4 g/m^2 and GP index of 19.3 s,) (entry 1, Table 3.9). This hypothesis is supported by the observation that when a larger amount of PLA_SDS dispersion was deposited on the paper by using a rod with a larger diameter (10 mm) (entry 3, Table 3.9), a high LWP index was obtained (77.6 g/m^2), due to the larger thickness of the porous film which results in a larger pore volume to entrap water. In any case, alterations in the structure of the paper support due to the contact time with the water present in the formulation cannot be excluded. Indeed, the presence of cracks in the coating can

make the paper substrate accessible, which may have been so structurally modified by the water of the formulation. When a large amount of dispersion is deposited on paper at once, a corresponding large amount of water is deposited also and this may plasticize and swell paper. If in the subsequent drying stage paper is not properly pressed, it cannot recover the initial compact structure [304]. Increasing voids and surface roughness would form, hence avoiding the formation of a homogenous and continuous film on the surface.

Surprisingly, the grease barrier properties are not influenced by the use of a larger threaded rods in the case of the PLA_SDS formulation where GP values of 112-113 s are obtained in any case (entry 2,3, Table 3.9). Most likely, the higher viscosity of the grease compared to water causes a slowdown in the penetration into the depth of the porous structure.

On the other hand, when the PLA_SYN dispersion was used with both 4 and 5 mm diameter rods, good barrier properties to liquid were obtained (LPW index of nearly 10 g/m^2) with an overall improvement of more than 50% with respect to the uncoated paper (entry 4 and 5, Table 3.8). Indeed, the morphology of the PLA_SYN film is more compact and defect free than the one with PLA_SDS thus providing a much more effective barrier to water. In the case of the GP barrier, moderate values are achieved (from 504 to 806 s) (entry 4 and 5, Table 3.9), thus indicating a worse barrier of the layer to grease than water. The use of rods with larger diameter, namely 7 or 10 mm, to deposit the PLA_SYN formulation, led to the deterioration of the barrier properties to both water and grease (LPW index of 49.9 and 64.1 g/m^2 and GP values of 119 and 37 s, respectively) (entry 6 and 7, Table 3.9). However, the sample presented a porous morphology by SEM analysis. On the contrary, when PLA_SYN dispersion was deposited in two different steps to form a final coating weight comparable with the one obtained with the 7-10 mm diameter rods very good barrier properties were achieved (LWP indexes 6.7-6.8 g/m^2 and GP values of +1800 s) (entry 8 and 9, Table 3.9) and the barrier properties were improved in comparison to the use of a single layer coating (LPW index of 10.4-10.6 g/m^2) (entry 4,5, Table 3.9). Indeed, in these cases a continuous and homogeneous coatings morphology was observed through SEM analysis (Fig. 3.16c,d). Besides, the presence of micrometric spheres dispersed in a continuous matrix observed through SEM analysis in the sample coated two times with the 5 mm diameter rod seem to not negatively affect the barrier properties (Fig.3.16d).

3.3. CONCLUSION

In summary, the rheological properties of aqueous polyester dispersions thickened by the addition of xanthan gum (XG) were studied. The understanding and control of the rheological properties of the thickened formulations is an important starting point to explore the potential of these colloidal dispersions as coating for paper substrates. For a deep study of the rheological properties, a PLA dispersion prepared with SDS as surfactant, starch as a stabilizer PLA_SDS was taken as a model. The PLA_SDS/XG formulations examined were found to remain stable over time irrespective of the presence of XG, thus indicating the suitability of XG as a thickener for this system. The results of the rheological analysis performed in steady and oscillatory conditions on dispersions with PLA content ranging between 5 and 22 wt. % and XG between 0 and 0.76 wt. % showed a transition from the very low viscosity of the neat PLA dispersions, typical of diluted colloids, to the honey-like viscosity and strong viscoelastic behavior of the dispersions obtained upon the addition of XG, even at low concentrations. All of the PLA_SDS/XG formulations analyzed showed a gel-like behavior throughout the explored frequency range, with the exception of the most diluted sample (PLA 5 wt. %), which revealed a fluid character before the crossover frequency. Both storage and loss moduli of PLA_SDS/XG samples vary monotonically with the concentration of either PLA particles or XG, thus indicating the participation of both components in the gel network.

Overall, from the rheological studies it emerged that, for all the polyester dispersions prepared (namely PLA_SDS, PLA_SYN and PBSA_SDS), the right viscosity for application on paper substrates can be obtained by adding a 0.5 wt. % of XG. Two different types of paper were selected as promising substrates for the coating and the best results in terms of coating homogeneity were obtained with Repro red paper. Besides, among the coating methodologies tested, threaded rods with diameters between 4 and 10 mm were chosen due to the possibility of depositing coating weights higher than the doctor blades coaters. The polyester dispersions previously prepared, (PLA_SDS, PLA_SYN and PBSA_SDS) were used to coat paper substrates and the liquid water permeability (LPW) index and the grease permeability (GP) of the resulting coatings were measured. Both the SEM analysis and the liquid barrier properties measurements revealed that the use of formulations

containing a negatively charged surfactant (PLA_SDS and PBSA_SDS) and the deposit of high quantity of dispersions led to the obtainment of a porous morphology with a consequent deterioration of the barrier properties. On the contrary, if higher coating weights are achieved by depositing a dispersion containing neutral surfactant (PLA_SYN) for two consecutive times a good homogeneity of the coated layer is revealed by SEM analysis. In this case excellent barrier properties were achieved (LWP indexes in the 6.7-6.8 g/m^2 range and GP values of +1800 s).

CHAPTER 4

Preparation of PLA/PVA blends from PLA aqueous dispersions

4.1. INTRODUCTION

4.1.1. Polymer blends

The combination of the characteristic features of different polymers with the purpose of creating a final material with tailored and advanced physicochemical properties has always attracted the research interests. With this objective in mind, over the years, several combination methods of different monomers involving random, block and graft copolymerization were disclosed. Alternatively, polymer blending emerged as a convenient route for the development of new materials, which incorporates the characteristic properties of two or more existing polymers. This approach is usually less time consuming and cheaper than the development of new monomer and polymerization routes [305].

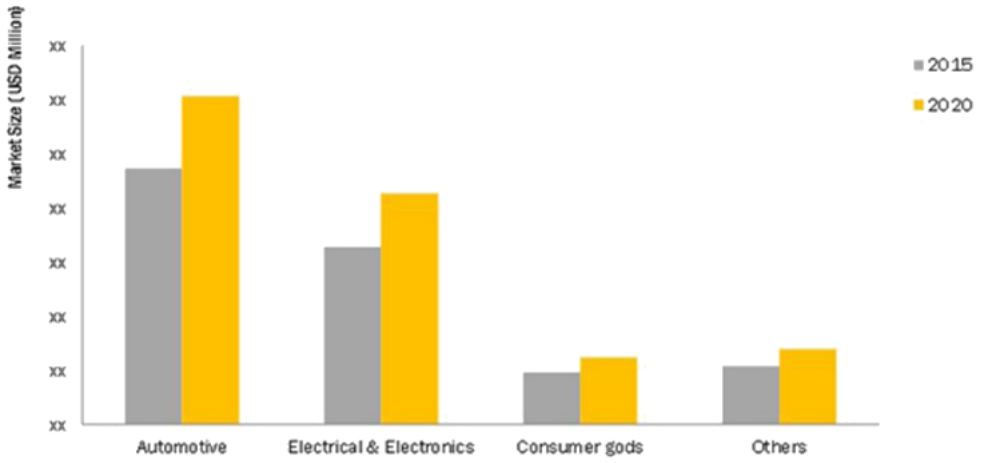

Figure 4.1: Polymer blends and alloys market by application [https://www.marketsandmarkets.com/Market-Reports/polymer-blends-alloys-market 88629095.html].

Nevertheless, many physical blends of different high molecular weight polymers resulted to be immiscible, leading to the formation of manufacts with low mechanical properties. In spite of this, many physical polymer blends are commercialized and the global polymer blends and alloys market was estimated to grow from USD 3.3 Billion in 2015 to USD 4.2 Billion by 2020, as shown in Figure 4.1. Polymer blends find commercial applications in the automotive, electrical and electronic, packaging, building and household industries [306]. Due to their multicomponent nature, the recycling of these materials might present some challenges and, for this reason, increasing attention has been paid to biodegradable and bio-based polymer blends. For example, PLA/PBAT blends are commercialized by BAF under the name of Ecovio®. The main areas of use for these biodegradable blends are plastic films such as organic waste and carrier bags as well as agricultural films.

Polymer blends can be classified in the following categories: immiscible, miscible compatible and compatibilized. Miscible polymer blends are homogeneous mixtures that display a single-phase structure and a single glass transition temperature in between the T_gs of both blend components. The latter value is in a close relation to the blend composition and can be calculated with Flory-Fox equation (equation 4.1), where $T_{g,mix}$ correspond to the glass transition temperature of the mixture and $T_{g,i/x}$ and $w_{i,x}$ are the glass transition temperature and the mass fraction of the *i* and *x* component of the blend, respectively.

$$\frac{1}{T_{g,mix}} = \frac{w_i}{T_{g,i}} + \frac{w_x}{T_{g,x}} \qquad (4.1)$$

Miscibility is governed by the change of free energy of mixing (ΔG_{mix}), as shown in equation 4.2, where ΔH_{mix} is the enthalpy (or heat) of mixing; T is the absolute temperature and ΔS_{mix}, the entropy of mixing.

$$\Delta G_{mix} = \Delta H_{mix} - T\Delta S_{mix} \qquad (4.2)$$

The necessary condition for miscibility of the polymers is the negativity of the variation of free energy mixing ($\Delta G_{mix} < 0$). The gain of entropy when two high molecular weights molecules are blended is negligible, consequently, in order to obtain full miscibility, the heat of mixing (ΔH_{mix}) must be negative (exothermic process). For this to happen it is necessary the presence of specific interactions between the blend components such as hydrogen bonding, ion-dipole, dipole-dipole and donor-acceptor interactions. In order to obtain a stable one-phase system, in addition to the negative variation of the energy of mixing, equation 4.3 must be satisfied. The expression describes the criteria for phase stability of binary mixtures of composition φ at fixed temperature T and pressure P.

$$\left[\frac{\partial^2 \Delta G_{mix}}{\partial {\varphi_i}^2}\right]_{T,P} > 0 \qquad (4.3)$$

For instance, in Figure 4.2 is shown an example of an immiscible system A ($\Delta G_{mix} > 0$), and a fully miscible system B in which $\Delta G_{mix} < 0$. On the other hand, C is a partially miscible system that satisfies $\Delta G_{mix} < 0$ for all composition range, even though for some composition immiscibility takes place due to the fact that $\left[\frac{\partial^2 \Delta G_{mix}}{\partial \varphi i^2}\right]_{T,P} < 0$.

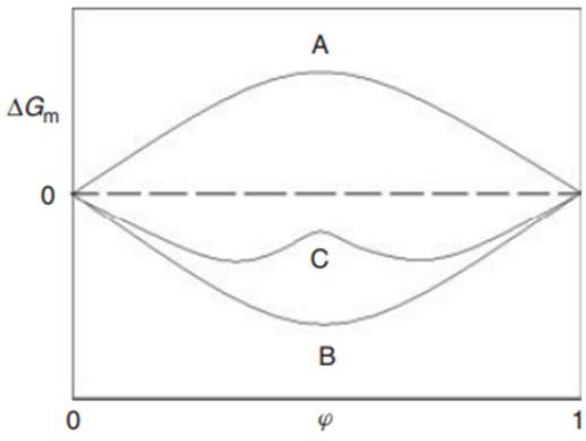

Figure 4.2: Schematic phase diagram for binary blends.

A well-known example of a miscible blend over a very wide temperature range and in all compositions is polystyrene/poly(dimethyl phenylene oxide) (PS/PPO), in

which the heat resistance and the toughness of PPO are combined with the good processability and the low cost of PS [307]. Regarding biodegradable blends, in order to accelerate the biodegradation of PLA, the latter was successfully mixed with used poly(aspartic acid-*co*-lactide) (PAL), forming miscible blends which are able to produce homogeneous film without negatively affecting the mechanical properties of PLA [308]. It must be taken into account that miscibility in polymer blends is not a requirement; nevertheless, with the purpose of enhancing the final properties, interfacial adhesion between the polymer components is highly desirable.

On the other hand, immiscible polymer blends possess large size domains of dispersed phase. The morphology of immiscible blends is influenced by several factors such as the process methodology, the composition of the mixture, the rheology of the blend's components and interfacial tension between phases. Overall, there are three types of morphology: the matrix-dispersed particle (sea–island), lamellar, and co-continuous ones (Figure 4.3). Particularly, the dispersed morphology enhances impact properties whilst the lamellar morphology increments barrier properties. As concerns the co-continuous morphology, its mechanical properties are between those of the blended polymers [309]. The morphology is greatly influenced by the blend concentration; indeed, at low concentration of either component, the dispersed phase forms nearly spherical drops. When the concentration is increased the dispersed phase can assume the form of cylinders, fibers, and sheets (Fig. 4.3). In the middle range of concentration, the morphology is co-continuous [310].

In the case of immiscible blends formed by two components, two distinct glass transition temperatures (T_gs) corresponding to the pure polymers are detected. If the components are also incompatible, the adhesion at the interface is poor and this leads to a decrease of the mechanical properties. However, in these cases, the final performance of the blends can be greatly improved through compatibilization. After compatibilization, the coarse morphology of the immiscible blend becomes finer and this contributes to the enhancement of the blend performance. Indeed, the compatibilizer can improve the adhesion between the blend components by facilitating better stress transfer from one phase to the other one. When the stress transfer between blended components is effective, the final blend's performances are improved [311]. On the other hand, compatible polymer blends are immiscible

mixtures that display macroscopically uniform physical properties caused by sufficiently strong interface interactions between the polymer blend components.

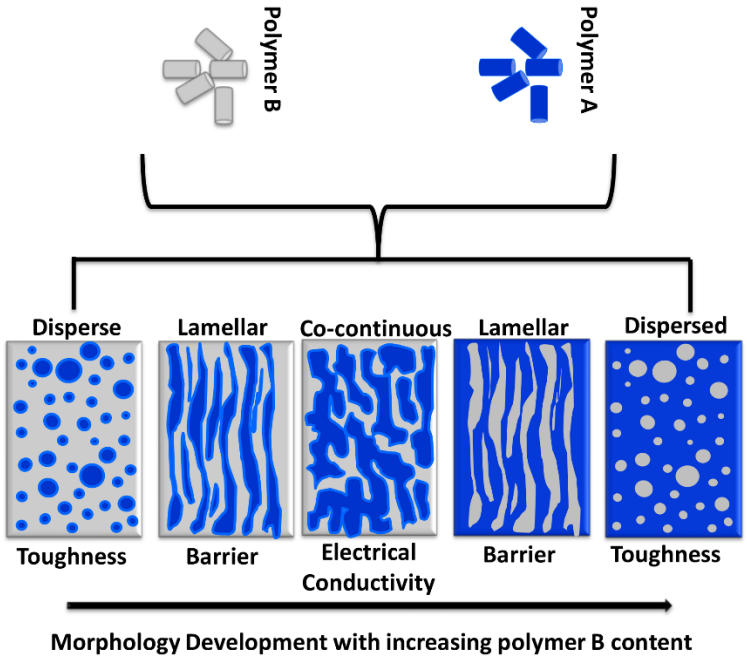

Figure 4.3: Types of polymer blend morphology and influence of the blend composition on its morphology and properties [312].

Among biodegradable polymer blends, starch/PLA blends have been often studied. The thermodynamic immiscibility between the components leads to poor adhesion between them and consequent scarce and irreproducible performances [313]. As a consequence, various compatibilizers and additives have been investigated to improve the interfacial interactions. Compatibilization can be obtained with several methodologies; the most common of which is the addition of a third component, that can be a functional polymer or a copolymer. Generally, a copolymer can act as a compatibilizer due to the fact that one block is miscible with one component of the blend and the other block is miscible with the other blend component. Diblock, triblock and graft copolymers are extensively used to compatibilize immiscible polymer blends [314]. For instance, polyvinyl alcohol (PVOH) containing non-hydrolysed residual groups of poly(vinyl acetate) (PVAc) proved to be an efficient compatibilizer for PLA/starch blends due to its to good affinity with starch [315]. With the purpose of overcoming PLA brittleness, this polymer was blended with poly (butylene succinate) (PBS); nevertheless, the immiscibility between these two

polymers leads to product defects in terms of strength and clarity. With the purpose of solving this incompatibility issue, a triblock copolymer poly(l-lactide-*b*-butylene succinate-*b*-L-lactide) (PLLA-*b*-PBS-*b*-PLLA) was proposed as a compatibilizer, plasticizer and nucleating agent for the PLA/PBS blends, thus improving, toughness, and clarity of the polymeric mixture [316]. Moreover, the use of PCL-PEG block copolymer as a compatibilizer in PLA/PCL binary blends was efficiently reported. In this case, the miscibility of the PLA phase with the PEG segment of the compatibilizer allowed the improvement of mechanical properties of the blend [317].

In general, a functional compatibilizer is a polymer that possess reactive functional groups (like anhydride, epoxy, isocyanates, etc.,) able to react with other functional group (such as hydroxyl, carboxyl, etc.,) of the blended components with the purpose of forming in situ graft and/or block copolymers. This methodology is often referred to as reactive compatibilization. For example, recently, the obtainment of super toughened PLA-blends through compatibilization of PLA/thermoplastic polyurethane (TPU) blends with a polyurethane elastomer prepolymer (PUEP) as reactive compatibilizer was reported. In this case it was demonstrated that the isocyanate (−NCO) group in PUEP is able to react with the –OH groups at both PLA and PU side, thus forming a polyurethane (PU)-PLA copolymer that significantly improves the interfacial compatibility of PLA/TPU blends [318].

4.1.2. Preparation process for polymer blends

Generally, there are several different methodologies that can be used for the preparation of polymer blends: melt mixing, solution blending, latex mixing and emulsion blending.

Melt blending is the most widely employed mixing methodology for the preparation of polymeric blends. In this case, all the components of the mixture are molten and mixed together. The main advantage is that there is no use of harmful organic solvents; however, the treatment at high temperature might cause polymer degradation. For instance miscible and partially miscible PLA and poly(ethylene glycol) (PEG) blends were efficiently prepared by melt blending and extruded into films [319]. Besides, melt mixing allows also exploiting co-polymerization reactions between the blend components in order to achieve greater homogeneity. For example, PLA was melt-blended with epoxy resin to study the effects of the reaction

on the mechanical and thermal properties of the PLA. It was demonstrated, through NMR analysis, that a reaction between the -COOH groups of PLA and the epoxy groups of the resin occurred. This reaction improved the interfacial crosslinking, morphology, thermal properties, and mechanical properties of the PLA/epoxy resin blends [320].

For the polymers that suffer from thermal degradation, solution blending represents a promising alternative for the production of polymeric mixtures. The methodology involves the solubilization of the components blended in a common solvent (co-solvent). The solution is then casted and, after evaporation of the solvent, a polymeric film mixture is obtained. However, not all polymers are readily soluble in common, safe solvents and many crystalline polymers require warming of the solution and control of the temperature during casting. Generally, this technology is used for the production of thin film since making thick shapes by casting is often difficult. Besides, it must be considered that the nature of the multi-polymeric resulting film is strongly influenced by the solvent used and the casting conditions. For example, biodegradable blends of polycaprolactone (PCL) and chitosan were prepared by casting from acetic acid/water solutions. In this case the solvent composition greatly influences the morphology of the final blends [321].

On the other hand, latex blending consists in physically mixing two or more types of latexes to obtain a final formulation with improved or combined properties [322]. The main advantages of this methodology are the simplicity of procedure and the low environmental impact of the process due to the use of water as solvent. Besides, the presence of surfactants in the latex formulations may decrease the interfacial tension between polymers thus lowering the coarsening rate of the domain structures [323]. In particular, binary latex blend systems constituted by natural rubber and acrylates [324][325], styrene/butadiene [326] latexes have been studied with the purpose of improving physical properties and barrier properties.

On the contrary, emulsion blending is a promising approach for the combination of water-soluble biopolymer with hydrophobic polymers. In this case, an oil-in-water emulsion is prepared by mixing an organic solution of the hydrophobic polymer with a water phase containing the biopolymer. After evaporation of the organic solvent a latex composed by both polymers is obtained. This approach allows the blending of thermally sensible polymers that cannot be solubilized in a common solvent. For instance, the emulsion blending was exploited for the preparation of gelatin/(PBSA)

bio-based and biodegradable blends [173]. Regarding PLA, mixtures of the latter and hydrophobic polymers such as chitosan [168][169], lignin [327] and nanocellulose [171][328] were efficiently prepared though emulsion blending.

Blends of hydrophobic and hydrophilic polymers can also be prepared by a mixed approach between latex mixing and emulsion blending. In these cases, a water solution of the hydrophilic polymer is then mixed with the hydrophobic polymer latex to produce composites with combined properties. For instance gelatinized starch plasticized with glycerol was added to natural rubber latex (NRL) achieving a composite with lower water absorption characteristics, biodegradability, and tensile strength but improved elongation at break [329]. Subsequently, a modification of the natural rubber dispersion with dimethyl aminoethyl methacrylate was proposed. The latter acts as a compatibilizer through hydrogen bonding with starch, thus allowing an improvement in the mechanical and barrier properties in comparison with the unmodified natural rubber latex [330]. Interestingly, with this methodology, the preparation of chitin/NRL blends with enhanced antibacterial activity was reported [331]. Furthermore, deproteinized NRL was blended with a water solution of hydroxypropyl methyl cellulose (HMC) in order to produce adhesive patches for the release of nicotine [332].

4.1.3. PLA-based blends

As previously discussed in Paragraph 1.2.1 of Chapter 1, PLA has emerged among the family of biodegradable polyesters as a promising alternative to fossil-based polymers due to its biodegradability, compostability, safety and production at an industrial scale. However, this biopolymer still lacks some of the required properties for many practical applications. As a consequence, blending PLA with other biodegradable polymers is considered a necessary measure to obtain industrial manufacts with tailored properties [313]. For instance, the thermal stability of PLA is generally not high enough for its use as an alternative for many commercial polymer's applications. Indeed, blending enantiomeric PLAs was proposed as a possible solution to improve its thermal properties [333]. In particular, the PLLA/PDLA blend has a melting temperature that is nearly 50 °C higher than those of pure PLLA and PDLA thanks to the formation of a stereocomplex between chains with opposite configurations. Moreover this stereocomplex shows higher hydrolysis

resistance due to the strong interaction between PLLA and PDLA chains [334]. Furthermore, PLA possesses a low degradation rate and, for this reason, lowering its hydrolytic degradability is of utmost importance for some applications. For example, as previously mentioned, poly(aspartic acid-*co*-lactide) (PAL) was blended to PLA in order to accelerate the degradation rate [308]. Moreover, PLA is a hard and brittle polymer, and for this reason its blending with other polymers results necessary in order to improve tensile mechanical properties (tensile modulus, stress at break and elongation at break) of the final material. For instance, by addition of PBAT the elongation at break increases from 14% (pure PLA) to 50% (PLA/PBAT blends) [335]. The blending of PLA with PVA will be deeply discussed in the next paragraph due to its relevance for this work.

4.1.3.1. Binary blends of PLA and PVA

As discussed in paragraph 1.1.1 of Chapter 1, poly(vinyl alcohol) is a biodegradable, biocompatible and non-toxic polymer that finds applications in numerous industrial fields. The addition of PVA has been proven to have a positive effect on the biodegradability of PLA, thus accelerating degradation [336]. Moreover, the hydroxyl groups of PVA can react or form hydrogen bonds with the ester groups of PLA, thus favouring the compatibility and blending with other components. Furthermore, the solubility of PVA in water has been exploited for the preparation of porous scaffold from PLA/PVA blends through a green process that just involves etching the material with water. Besides, PVA is a promising candidate to overcome PLA brittleness due to its high strength and flexibility, indeed pure PVA has a tensile strength of 48.4 MPa, elongation at break 220.7% and Young's modulus 707.9 MPa [337].

The main strategies adopted for the preparation of PLA/PVA blends are melt processes and solvent mixing. Particularly, melt processes are most commonly employed; indeed through this methodologies compatible PLA/PVA mixtures were prepared using a PVA with a high hydrolysis degree (97-99%) [338]. This compatibility was ascribed to the formation of interpolymer hydrogen bonds in the amorphous region of PLA/PVA blends for PVA content higher than 50 wt. %. Another interesting work described the preparation through melt spinning of

nanofibrillary structures from PLA/PLA blends [339]. PLA nanofibrils were obtained by solubilizing PLA/PVA 70/30 blends in water in order to remove the PVA matrix. It was found that increasing the amount of PVA greatly improves the thermal stability of the polymeric mixture. Besides, the effect of molecular weight and hydrolysis degree of PVA on the thermal and mechanical properties of PLA/PVA blends was an object of study [336]. For this purpose, PLA/PVA mixtures with ratios 80/20, 90/10, 97/3 were prepared by a melt blending method. For all ratios a single T_g was observed through DSC analysis, thus highlighting the formation of compatible blends. It emerged that PVA with higher M_w and hydrolysis degree (HD) conferred to the blend higher thermal stability. On the other hand, the mechanical properties of the blends resulted to be greatly influenced by the PVA content rather than its M_w and HD. In particular, quantities around 3% of PVA do not affect the tensile strength, while at higher PVA percentages the tensile strength decreases. Furthermore, melt blending of PLA with poly(vinyl acetate) (PVAc) by using a single-screw extruder was reported [340]. The resulting polymer mixtures were made by a homogenous phase as highlighted from the presence of a single T_g, thus indicating miscibility between the two components. For PVAc contents between 5 and 30%, the resulting blends showed higher values of tensile strength. Besides, enzymatic degradation tests indicated that by adding PVAc to PLA, a significant increase in the degradation rate was obtained. Moreover, another research group reported the preparation of PLA/PVA blends with a composition of 70/30, 60/40 and 50/50 wt.% through twin-screw extruder and injection moulding [341]. The aim of this work was to prepare porous structures by an etching process in hot water to remove PVA. The SEM analysis revealed that, as the PVA content increases, the morphology converts from a sea-island one to a co-continuous morphology. Additionally, a single glass transition temperature that obeyed the Flory-Fox rule was detected. Furthermore, the use of lacti-glyceride as plasticizer and compatibilizer for PLA/PVA blends was reported and their properties were compared to the blends obtained with glycerol as plasticizer. It was shown that with lacti-glyceride better thermal processability, mechanical properties and surface hydrophobicity were obtained [342].

Regarding the preparation of PLA/PVA blends through solvent mixing, hexafluoro isopropanol was efficiently employed as a solvent [343].The PLA/PVA blends thus produced showed at every composition two distinct T_gs though DSC analysis, hence highlighting incompatibility between PLLA and PVA amorphous regions. The FTIR

and the ^{13}C solid-state NMR analyses confirmed the formation of interpolymer hydrogen bonding in the amorphous region, which is indicated as the driving force leading to some degree of component compatibility in the immiscible systems. As concerns the mechanical properties, when the contents of the two polymers were close, the tensile strength and the elongation at break were at a minimum. Indeed, the mechanical properties decrease for PVA content between 0 to 50 wt.% and then increase with an increment of the PVA content due to the crystallization of PVA and PLA as isolated phases. Similarly, another research group exploited hexafluoro isopropanol as a solvent for preparing PLLA/PVA blends with PVA with high HD (99%). Also in this case, two different phases, one rich in PLLA and the other of PVA, were revealed [344]. Furthermore, the young's modulus, tensile strength and percent elongation at break of the blends incremented with increasing PVA content from 50 to 90 wt.%. Besides, the preparation of PLA/PBA blends from dioxane/water solutions through solvent casting was reported [345]. Sodium tetraborate as crosslinking agent, glycerol as plasticizer and colloidal silver (Ag^0) as antimicrobial agent were incorporated in the polymer's solution. It was found that for PVA contents between 70 and 90 wt.% the blends were partially compatible. The PVA/PLA films containing Ag^0 presented lower mechanical properties in comparison to PVA films Ag^0 loaded, thus indicating a partial incompatibility of the blends.

Generally, for PLA/PVA blends the preparation process seems to have a great influence on the morphology and the compatibility between the phases. Indeed, with melt process miscibility between the two blend components is observed, as revealed by the presence of a unique T_g. Contrastingly, with the use of hexafluoro isopropanol or dioxane/water solutions as co-solvents, immiscible or partially compatible PLA/PVA blends were obtained after solvent casting. On the other hand, rarely in literature the use of latex mixing and emulsion blending methods for the preparation of PLA/PVA blends has been reported. Specifically, in an interesting work aimed at the production of ternary chitosan/PVA/PLA blends, the preparation of a binary PLA/PVA blend through emulsion blending was reported [169]. However, the PLA/PVA blend prepared (50/50) was impossible to handle or mechanical characterize due to its extreme fragility. On the contrary, a mixed approach between latex mixing and emulsion blending has not been yet reported for the preparation of PLA/PVA blends.

4.2. RESULTS AND DISCUSSION

4.2.1. Characterization of the different PVA grade available

Three different PVA grades were purchased and characterized in order to select the most suitable PVA type for the preparation of PLA/PVA blends. In particular, PVA GH 17R solution at 12% in water from Mitsubishi Chemicals Performance Polymers, PVA 4-88 and PVA 6-88 from Kuraray Chemical were available. With the purpose of being analysed, PVA GH 17R solution at 12% was first lyophilized.

Attenuated Total Reflectance Fourier transform Infrared spectroscopy (ATR-FTIR) was employed to characterize the presence of specific chemical groups in the starting material (Figure 4.4). In all cases, the typical signals of the PVA were observed. In particular, according to the literature [346], the large band observed between 3700 and 3000 cm^{-1} corresponds to the O-H stretching of the functionalities involved in intermolecular and intramolecular hydrogen bonds. The vibrational band between 3000 and 2840 cm^{-1} is relative to the C-H stretching of the alkyl groups, while the peaks between 1750-1735 cm^{-1} corresponds to the C=O stretching of the residual acetate groups.

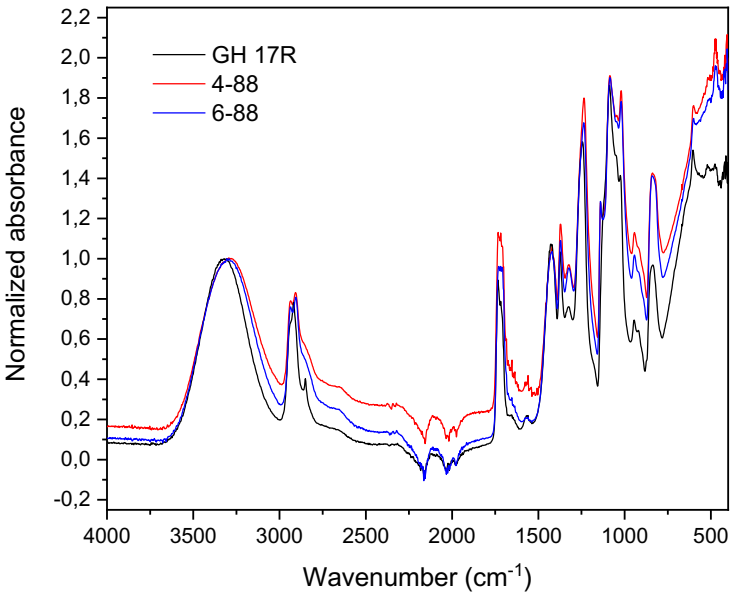

Figure 4.4: ATR-FTIR spectra of PVA GH 17R (in black), PVA 4-88 (in red) and PVA 6-88 (in blue). Spectra were normalized over the 3000-3700 cm^{-1} region.

Generally, the intensity of the signals at 1750-1735 cm^{-1} is weak for PVA that possess high hydrolysis degree, highlighting that only few acetate groups are present in the polymeric chain.

As previously mentioned in Paragraph 1.1.1 of Chapter 1, PVA is synthesised by polymerization of vinyl acetate followed by subsequent controlled partial alkaline hydrolysis. The hydrolysis degree (HD) significantly influences the physicochemical properties of the resulting PVA. The ATR-FTIR analysis provides a semi-quantitative method to estimate the relative HD of different PVAs type through comparison of the intensity relative to the O-H broad band (3000-3700 cm^{-1}) and the one relative to C=O peak (1735-1750 cm^{-1}). In this case the broad band between 3000 and 3700 cm^{-1} was taken as a reference and the ATR-FTIR spectra of the PVAs available were normalized with respect to this band. From the ATR-FTIR analysis it is possible to deduce that PVA 4-88 possesses the lowest HD. Indeed, it shows the highest intensity of the 1750-1735 cm^{-1} signals. On the contrary, PVA GH 17R exhibits the highest HD among the three PVA grades considered.

Subsequently, in order to accurately determine the HD value, ^{1}H-NMR analysis of the three different PVA grades was performed (Fig. 4.5). As reported by literature the acetylation degree (AD) was first determined by comparing the signal of the CH_3 unit of the polyvinyl acetate (PVAc) at nearly 1.8-2.0 ppm with the signals correspondent to the CH of the PVA and PVAc main chain, at 3.75 and 3.9 ppm, respectively [347] (Fig. 4.5 and equation 4.1).

$$AD\ (\%) = \frac{(integral\ value\ of\ CH_3\ signal)/3}{(integral\ value\ of\ CH\ signal)/2}\ x\ 100 \qquad (4.1)$$

Afterwards, once the AD has been calculated, it is possible to obtain the HD using the following equation (equation 4.2).

$$HD = 100 - AD\ (\%) \qquad (4.2)$$

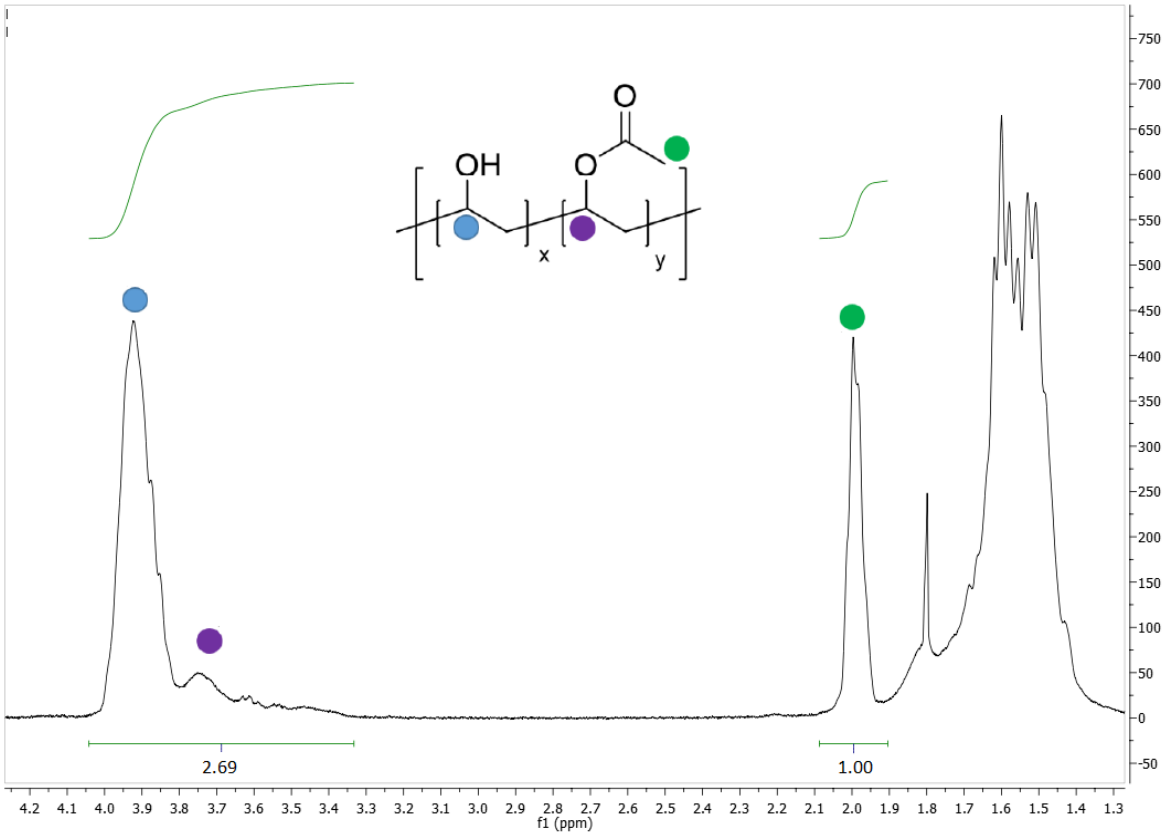

Figure 4.5: Representative ^{1}H-NMR spectra of PVA GH 17R for the determination of the hydrolysis degree (HD).

In this way the HD of all the PVA grades available was determined, as reported in Table 4.1.

Table 4.1: Hydrolysis degree of the different PVA grades

PVA grade	Hydrolysis degree (HD)[a]
GH 17R	75.2
4-88	73.1
6-88	73.6

[a]Determined through ^{1}H-NMR analysis.

Overall, it is possible to affirm that all the PVA grades possess a comparable HD (between 73.1 and 75.2). The obtained data were in accordance with the semi-quantitative results by ATR-FTIR analysis. Indeed, PVA GH 17R showed the highest HD (75.2 %), while PVA 4-88 exhibited the lowest value (73.1 %).

With the purpose of investigating the thermal properties of the materials, thermal gravimetric analysis (TGA) and differential scanning calorimetry (DSC) analysis were performed. In particular, to evaluate the thermal stability of the PVAs, TGA analysis was carried out under standard conditions in nitrogen atmosphere (Table 4.2, Fig. 4.6).

Table 4.2: Water content (%), first temperature of onset (T_{on}^1) at which the degradation begins, first temperature of maximum degradation rate (T_d^1), second temperature of onset (T_{on}^2), second temperature of maximum degradation rate (T_d^2) and residuum after degradation (Res.) from TGA analyses of the different PVA grades.

PVA grade	Water content (%)[a]	T_{on}^1 (°C)	T_d^1 (°C)[b]	T_{on}^2 (°C)	T_d^2 (°C)[b]	Res. (%)[c]
GH 17R	6.0	286.1	335.50	415.0	445.1	2.0
4-88	3,3	304.1	328.4	423,4	451.3	2.6
6-88	2.0[d]	302.1	329.9	432.4	452.9	1.9

[a]Weight loss % between 30 and 130 °C; [b]Temperature of the peak minimum in the first derivative TGA plots; [c]Residuum at 850 °C; [d]Weight loss % was in the range 30-200 °C.

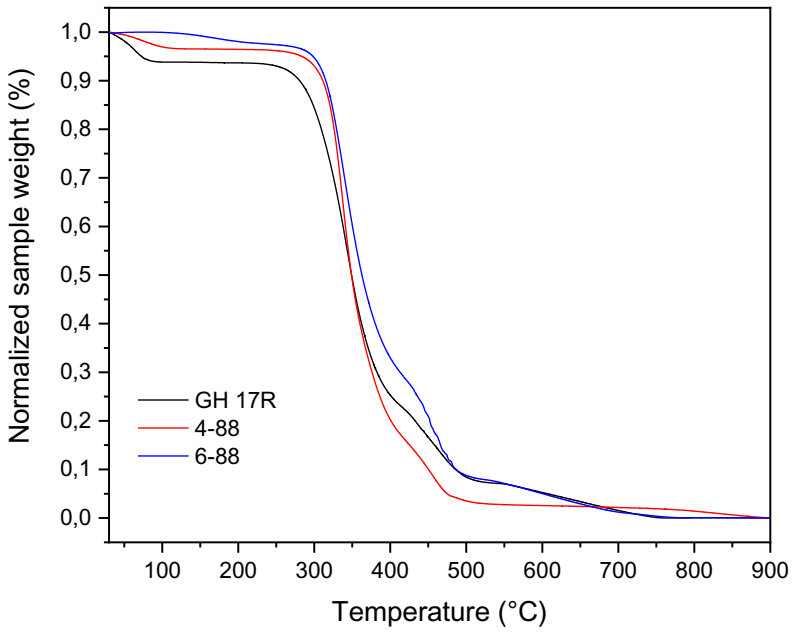

Figure 4.6: Comparison among the TGA curves of PVA GH 17R (black line), PVA 4-88 (red line) and PVA 6-88 (blue line).

The TGA analysis revealed three different degradation steps [348]. The first one occurs at a temperature range of 30-120°C and it is ascribed to the removal of the

absorbed water. The percentage of absorbed water was observed to depend on the hydrolysis degree determined by ^{1}H-NMR and ATR-FTIR analysis, since PVA GH 17R having the highest hydrolysis degree shows the highest amount of absorbed water (6,0 wt. %). Besides, for PVA 6-88 it can be noticed that the absorbed water is more retained inside the polymer, indeed the interval of the first weight loss step extends up to 200 °C instead of 130 °C (Table 4.2). This suggests a degree of crystallinity greater than the other polymer, since the crystal structure is able to retain water molecules more efficiently. The second degradation step (T_{on}^1 and T_d^1**)** represents the most significant weight loss and it is ascribed to the elimination of the side OH and acetate groups. The last step is associated with the breakage of the polymeric chain due to a cleavage of the C-C bonds. The TGA analysis revealed that the three PVA grades possess a similar temperature of maximum degradation rate (T_d), even though for PVA GH 17R the degradation begins at a lower temperature as it can be observed from the lower T_{on} (286 °C in comparison with 302-304 °C of the other two PVA grades).

On the other hand, the DSC thermograms of the second heating step of the three PVA grades are reported in Fig. 4.7. For all the samples, a shift of the baseline (between 66 and 73 °C) indicating a glass transition and an endothermic peak (in the temperature range 158-185 °C) assigned to the melting of the crystalline domain were revealed, suggesting the presence of a semicrystalline structure for all polymers.

The data obtained from the DSC analysis (Table 4.3) highlighted that, among the PVA grades, GH 17R showed a slightly higher T_g (72.9 °C against 66-67 °C). On the other hand, PVA 6-88 presents the highest melting temperature (184.4 °C) in comparison with the other starting materials. Moreover, its higher melting enthalpy (24.3 J/g) indicates a higher degree of crystallinity than the other PVA grades. These data explain the higher ability to retain water of this polymer as revealed through TGA analysis.

Subsequently, PVA solutions in water at 12 wt. % were analysed with a rheometer in order to determine their viscosity (Table 4.4). Except for PVA GH 17R, which had already been purchased in solution in water at 12 wt. %, the other two PVAs (4-88 and 6-88), in the form of powder, were suitably dissolved in water with specific procedures described in Paragraph 7.3.13 of Chapter 7 with the aim of preparing solutions in water at the same concentration of the PVA GH 17R solution.

Table 4.3: Melting temperature of the first heating step (T_m^1), melting enthalpy of the first heating step (ΔH_m^1), crystallization temperature (Tc), crystallization enthalpy (ΔH_c), glass transition temperature (T_g), melting temperature (T_m^2) and melting enthalpy (ΔH_m^2) of the second heating step from DSC analyses of the PVA grades.

PVA grade	T_m^1 (°C)	ΔH_m^1 (J/g)	T_c (°C)	ΔH_c(J/g)	T_g (°C)[a]	T_m^2 (°C)[b]	ΔH_m^2 (J/g)
GH 17R	194.3	50.3	109.4	-12.2	72.9	158.7	18.2
4-88	194.4	36.1	129.6	-18.8	66.4	176.9	16.4
6-88	191.6	39.6	134.1	-26.2	67.7	184.4	24.3

[a]Values at the midpoint; [b]Values at the peak maximum.

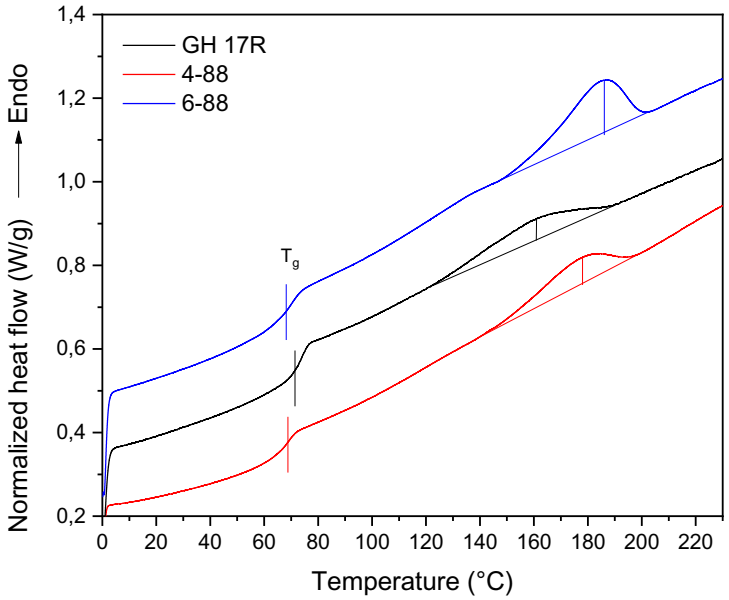

Figure 4.7: DSC analysis at 10°C/min of PVA GH 17R (black line), PVA 4-88 (red line) and PVA 6-88 (blue lines) relative to the second heating step. Thermograms were arbitrarily shifted for clarity.

Table 4.4: Viscosity values of the PVA solutions in water at 12 wt. %.

PVA grade	Viscosity[a] (Pa x s)
6-88	0.09
GH 17R	2.4
4-88	0.01

[a]Determined at a shear rate of 0.1 s^{-1}

From the rheological analysis, all samples exhibit Newtonian behavior up to a shear rate of 100 s^{-1}. At higher strain rates, a shear thinning behavior is observed, in which the viscosity curve deviates from linearity towards lower values. It emerged that the solution of PVA GH 17R showed the highest viscosity (4.3 Pa·s), whilst PVA 4-88 and 6-88 solutions exhibited a very low viscosity (between 0.01 and 0.09 Pa·s). As a consequence, considering the comparable HD of the PVA types, it can be affirmed that the viscosity of the solution is indicative of the average molecular weight of the polymer, thus identifying the PVA GH 17R as the PVA examined with the highest molecular weight [349].

4.2.2. Preparation of film of PLA/PVA blends from PLA aqueous dispersion

PLA/PVA blends were prepared from aqueous dispersion of PLA by exploiting a two-step procedure, as depicted in Scheme 4.1. The first step involves the preparation of a water-based PLA dispersion, using the procedures previously described in Paragraph 2.2.1 and 2.2.5 of Chapter 2. Two different PLA formulations were produced for the preparation of PLA/PVA blends: one containing SDS as surfactant and starch as stabilizer (PLA_SDS, dry matter content of 15.2 %) and the other one containing SYN as surfactant (PLA_SYN, dry matter content of 16.1 %). The DLS analysis of the PLA_SDS and PLA_SYN dispersions (Fig. 4.8) showed the presence of sub-micrometric particles with an average hydrodynamic diameter of 289.1 ± 5.5 and 415.4 ± 7.1 and a polydispersity of 0.194 ± 0.021 and 0.290 ± 0.009, respectively.

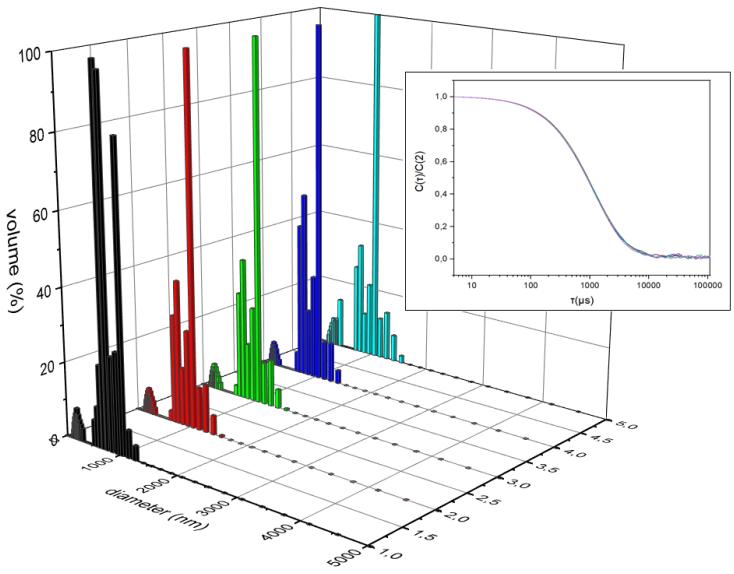

Figure 4.8: DLS size distribution plots of the five repeated measurements relative to the PLA_SYN dispersion employed for the preparation of PLA/PVA blends; inset: DLS correlation plots of the same dispersion.

In the second step, a PVA solution in water was properly added to both PLA dispersions and the mixtures were magnetically stirred for 4 h. Due to the hydrophilic nature of PVA, the latter is solubilized in the continuous water phase of the dispersion, whilst PLA constitutes the dispersed phase in submicrometric particles form. Subsequently, the PLA/PVA blend was casted onto polystyrene (PS) capsules and left to dry at 60 °C in the oven.

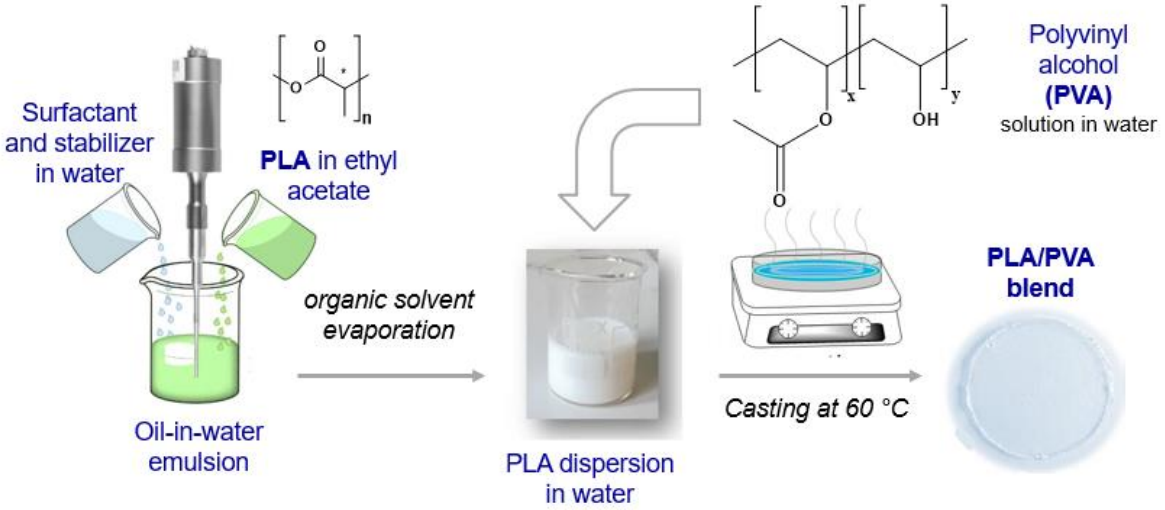

Scheme 4.1: Cartoon of the procedure for the preparation of film of PLA/PVA blends from aqueous PLA dispersions.

4.2.3. Selection of the most suitable PVA grade for the preparation of PLA/PVA blends

After having characterized the three different types PVAs, solution of the latter at the highest possible concentration (12 wt. % for PVA GH 17R and 4-88, 30 wt. % for PVA 6-88) were prepared and added to PLA_SDS and PLA_SYN dispersions in the right proportion to obtain 3 different PLA/PVA 50/50 blends. The resulting PLA/PVA latexes were casted onto a polystyrene dish and left to dry at 60 °C. The latter was selected as a proper drying temperature since from previous studies this was identified as the MFFT for PLA aqueous dispersions. On the other hand, PVA solutions in water are able to form homogeneous and continuous films even at room temperature.

With the purpose of selecting the most suitable PVA grade for the preparation of the blends, the homogeneity and continuity of the formed PLA/PVA 50/50 films was visually evaluated (Fig. 4.9). In general, it can be noticed that films prepared with the PLA_SYN dispersion are more opaque than the one containing the PLA_SDS formulation. This can be due to a larger PLA phase size. Indeed, the particle size of the PLA_SYN is almost double that of PLA_SDS.
Films with PVA 4-88 (Fig. 4.9e,f) resulted to be fragile and fragmented. Similar results, albeit to a lesser extent, were observed with the use of PVA 6-88 (Fig. 4.9c,d). On the contrary, films prepared with PVA GH 17R (Fig. 4.9a,b) resulted to be homogeneous and soft. For this reason, this PVA grade was selected for the preparations of PLA/PVA blends in proportion 25/75, 50/50 and 75/25.

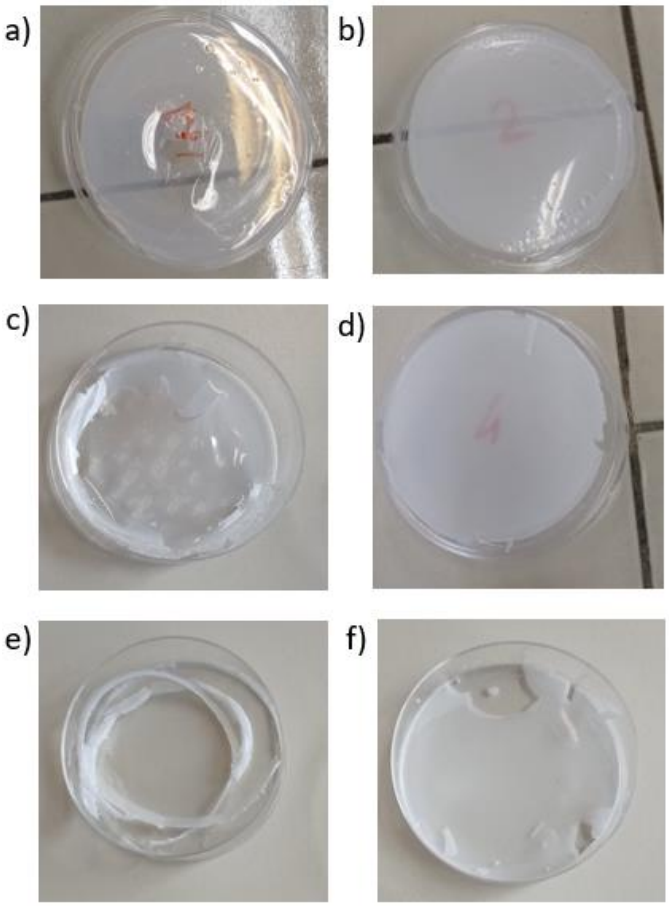

*Figure 4.9: pictures of PLA/PVA 50/50 blends prepared with the PLA_SDS dispersion (**a,c,e**) and the PLA_SYN (**b,d,e**) with PVA GH 17 R (**a,b**), PVA 6-88 (**c,d**) and PVA 4-88 (**e,f**).*

4.2.4. Characterization of emulsified blends and blends films

4.2.4.1. Steady share properties of aqueous PLA/PVA dispersions

First, the rheological behaviour of the PLA/PVA blends in water was studied by performing steady shear measurements (Fig. 4.10). As previously reported in Paragraph 3.2.1.3 of Chapter 3, the PLA dispersions (green line in charts) showed a viscosity almost independent of the shear rate and similar to water, as typically observed for low concentration of hard-sphere colloids [296]. In the presence of PVA, the viscosity plots are comparable to the one of the pure polymers showing Newtonian fluid behaviour up to shear rates of 100 s^{-1}. After that a shear thinning behaviour was observed, in which the viscosity curve deviates from linearity towards lower values. It can be noticed that the viscosity increases exponentially with the

PVA content. In comparison with the mixtures containing PLA_SDS (Fig. 4.10a), the one with PLA_SYN displays a slightly higher value of viscosity (Fig. 4.10b). Besides, in Fig. 4.11 the viscosity values of the PLA/PVA latexes at shear rate of 0.1 s^{-1} as a function of the PVA content are reported (green and red lines) together with the viscosity values of the PVA solution in water at the same dilutions used in the preparation of the PLA/PVA mixtures (black line). In the latter case, the viscosity of the PVA water solutions increase exponentially with the PVA content, albeit to a lesser extent than the PLA/PVA latexes. This indicates that the interaction between PLA particles and PVA chains also contributes to the viscosity of the system.

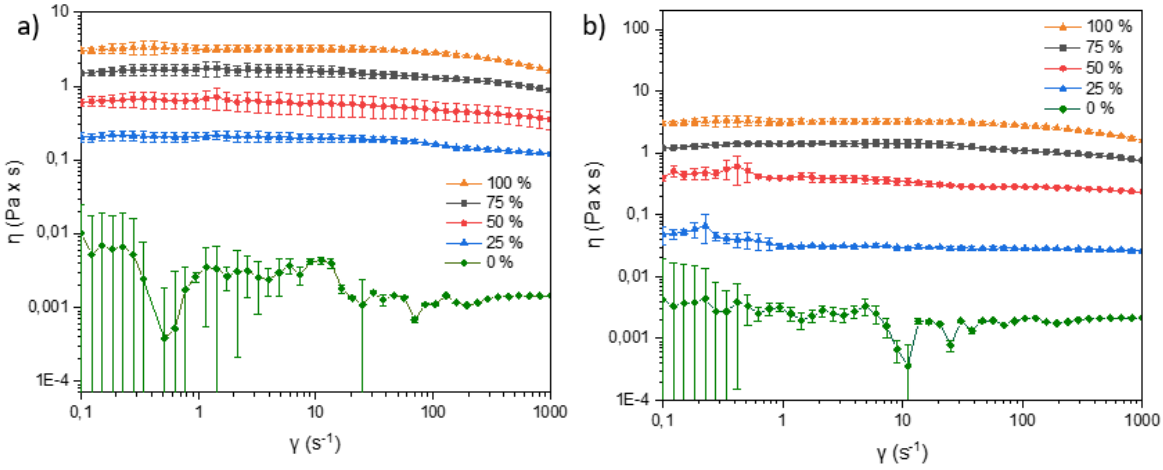

*Figure 4.10: Viscosity as a function of the shear rate for PLA_SDS (**a**) and PLA_SYN (**b**) dispersions with different PVA content (0,25,50,75 and 100 wt. %).*

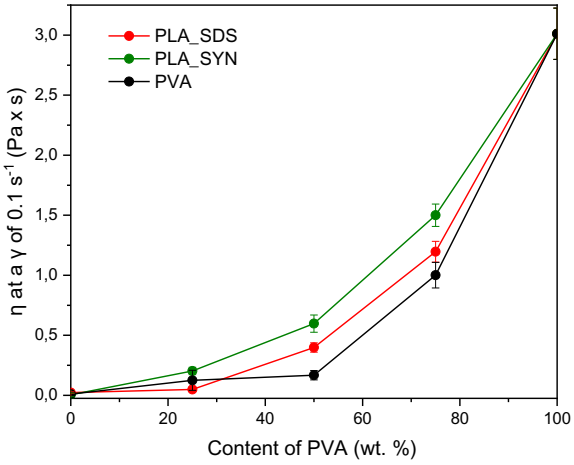

Figure 4.11: Viscosity values at a shear rate of 0.1 s^{-1} of PLA/PVA mixtures with PLA_SDS (in red) and PLA_SYN (in green) dispersions as a function of the PVA content together with the viscosity values of PVA solutions in water at the same dilutions used in the preparation of the PLA/PVA mixtures (in black).

4.2.4.2. Characterization of the PLA/PVA films

PLA/PVA 25/75, 50/50, 75/25 emulsified blends prepared with either PLA_SDS and PLA_SYN dispersions were casted on PS capsules and left dry in the oven at 60 °C. Opaque, homogeneous and continuous films with a thickness between 100 and 250 µm were obtained for all composition (Fig. 4.12). The only exception is PLA/PVA 75/25 film with PLA_SDS dispersion, which is fragile and fragmented (Fig. 4.12d). Films prepared with PLA_SYN dispersion resulted to be softer and less fragile to the touch in comparison to the ones containing PLA_SDS dispersion.

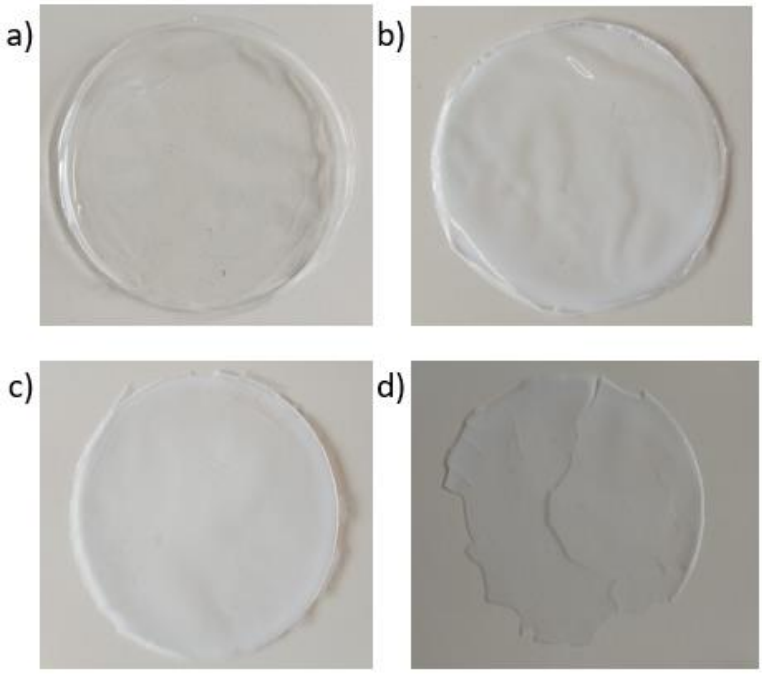

Figure 4.12: Pictures of PLA/PVA films prepared from PLA_SDS dispersion with a PVA content of 100 (a), 75 (b), 50 (c) and 25 (d) wt. %.

4.2.4.2.1. Attenuated total reflectance Fourier transform infrared spectroscopy (ATR-FTIR)

ATR-FTIR analysis of the upper and lower surfaces of the films was performed in order to investigate the homogeneity of the prepared blends (Fig. 4.13). The upper and lower surfaces of each film showed comparable band intensity, thus indicating a similar composition and no phase separation during the drying stage. Indeed, in

case of dispersion instability sedimentation or creaming (Paragraph 2.2.7, Chapter 2) may occur which can lead to a different PLA content at the lower or upper surface of the film, respectively. The intensity of the large band at 3700-3000 cm^{-1} and the peak at 3000 and 2840 cm^{-1} relative to the O-H and C-H stretching of PVA increases with the increment of the PVA content. At 1750-1735 cm^{-1} it is possible to observe the C=O stretching of both PLA and PVA. Indeed, as the PVA content of the blend increases, the band around 1750-1735 cm^{-1} becomes broader. In previous studies a shift of the carbonyl band of PLA to lower frequency was ascribed to the presence of hydrogen bonding between PLA and PVA [343]. However, in our case, the broadening of the PLA's C=O band with an increased amount of PVA is also due to overlapping between the carbonyl signals of the two polymers, and thus it is not possible to observe other phenomena (Fig. 4.14).

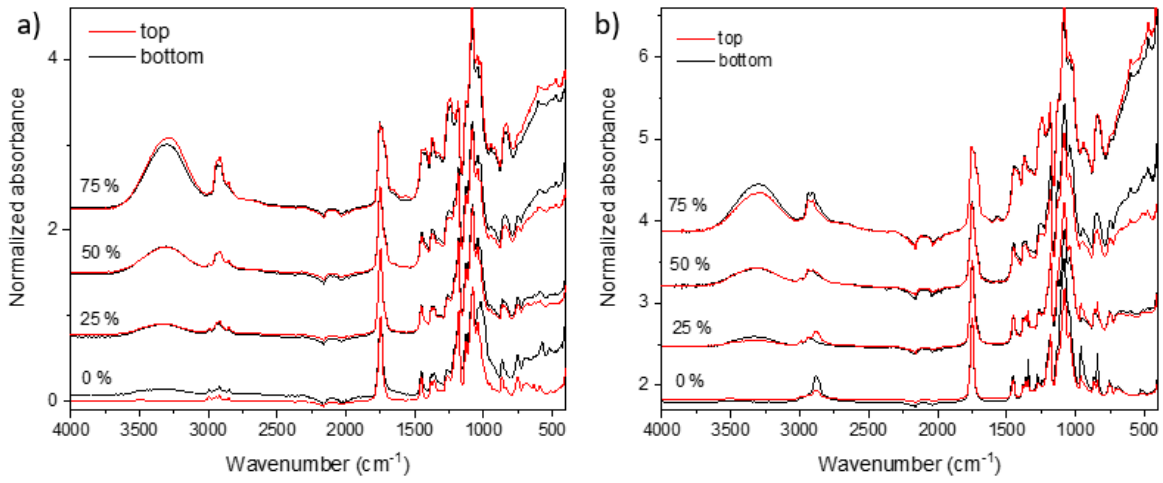

*Figure 4.13: ATR-FTIR spectra of the top and bottom surfaces of PLA/PVA films prepared from PLA_SDS (**a**) and PLA_SYN (**b**) dispersions with a PVA content of 0, 25, 50 and 75 wt. %.*

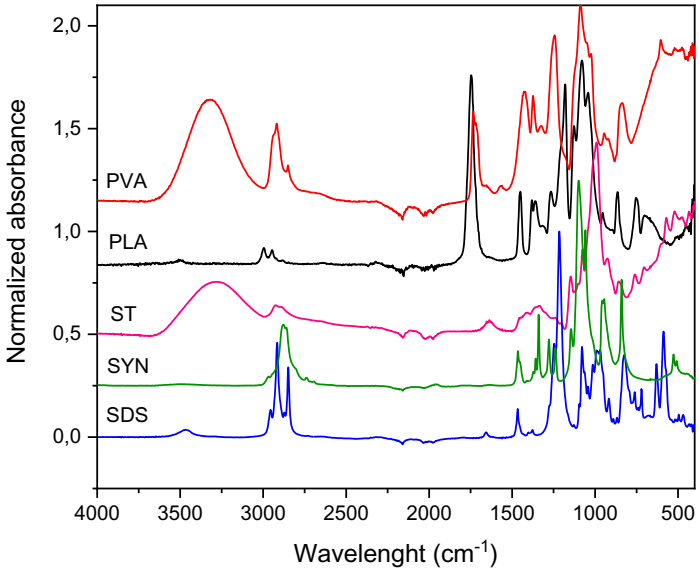

*Figure 4.14: ATR-FTIR spectra of PLA, PVA, Starch C*Icoat (ST), Synperonic PE/F68 (SYN) and sodium dodecyl sulfate (SDS).*

On the other hand, the signals ascribed to the CH_2 stretching of the emulsifiers (SDS and SYN) can be noticed, when they are not superimposed with the peak of the C-H stretching of PVA, between 2750 and 3000 cm^{-1}. In the blends containing PLA_SDS dispersion the presence of starch as stabilizer can be highlighted by the broad band around 3500-3000 cm^{-1} relative to the O-H group (often superimposed by the O-H stretching of PVA) and the typical stretching band of sugar rings at 1000 cm^{-1}. It is possible to observe that, as previously reported, the neat PLA_SDS and PLA_SYN dispersion films prepared at 60 °C show an enrichment of stabilizer and surfactant on the lower surface of the films. Due to the overlap between the surfactant signals with those of the PVA, it is not possible to estimate whether blooming effect occurs in the PLA/PVA blends. Nevertheless, strong polymer segregation in the mixtures can be excluded.

4.2.4.2.2. Blend morphology by scanning electron microscopy (SEM) analysis

Figure 4.15, 4.16 and 4.17 shows the surface and cross section SEM images of the pure PLA dispersions, pure PVA and PLA/PVA blends. As previously anticipated in

Paragraph 4.1.1, polymer mixtures can display three types of morphology: the matrix-dispersed particle (sea–island), lamellar, and co-continuous [312]. In all the PLA/PVA mixtures prepared the presence of the sub-micrometric dispersed particles into a continuous matrix is observed (Fig. 4.15). The type of morphology does not depend on the blend composition. This is probably due the fact that PVA is added into a water phase containing dispersed solid submicrometric particles of PLA, consequently PVA should form the continuous phase and PLA the dispersed one.

As it is possible to notice from Fig. 4.15, the dimension of the submicrometric dispersed phase ranges between 200 nm and 1 μm and it increases as the PVA content increments. For PLA/PVA 75/25 blend containing the PLA/SDS formulation (Fig. 4.15a), the dimension of the dispersed phase is in good agreement with the one revealed in pristine PLA_SDS dispersion (nearly 200 nm). On the contrary, the PLA_SYN/PVA 75/25 mixture exhibits a lower particle size than the original PLA aqueous dispersion (200 nm against 450 nm) (Fig. 4.15f). In both PLA/PVA 50/50 blends, the particle size of the original dispersions is almost maintained (Fig. 4.15c,d), while the same cannot be said for the PLA/PVA 25/75 blends, which display the presence of micrometric dispersed phase domains in both PLA formulations (Fig. 4.15e,f).

Generally, it is possible to notice that in the mixtures with PLA_SYN (Fig. 4.15b,d,f) there is a better adhesion at the interface in comparison to the blends with PLA_SDS dispersion (Fig. 4.15a,c,d). Clearly, the nature of the surfactant seems to play an important role in this behaviour.

Indeed, in some cases, namely blends PLA_SDS/PVA 75/25 and 50/50 (Fig. 4.16c,d,e,f) a porous morphology is observed. This might be due to the repulsion between the anionic charges of the surfactant on the surface of the PLA particles generating voids in the structure. Accordingly, when the PLA_SDS content is low (25 wt. %) no voids are observed and the adhesion between the particles and the continuous matrix looks good (Fig. 4.16e,f). On the other hand, from the SEM analysis, it is evident that the use of a non-ionic surfactant allows a greater adhesion, and most likely also higher miscibility at the interphase (Fig. 4.15b,d,f). Among the mixtures prepared with the PLA_SYN dispersion only the PLA/PVA 50/50 presents a slightly porous morphology (Fig. 4.17e,f). In this case, some cavities might be generated from the detachment of dispersed particles during sample preparation for

SEM analysis, suggesting a lower adhesion between the polymer phases for this specific composition.

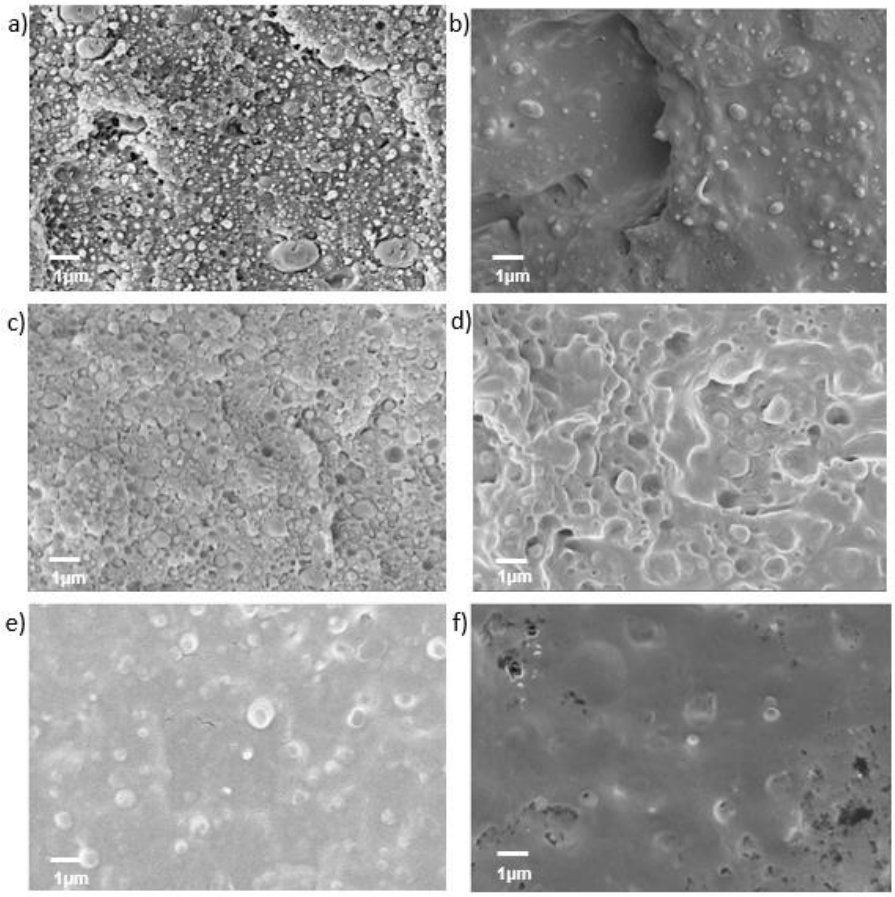

*Figure 4.15: SEM pictures of sections of PLA/PVA films prepared from PLA_SDS (**a**,**c**,**e**) PLA_SYN (**b**,**d**,**f**) dispersion with a PVA content of 25 (**a**,**b**), 50 (**c**,**d**) and 75 (**e**,**f**).*

Additionally, it is possible to observe that the surface and section of PVA without the addition of PLA are smooth and continuous (Fig. 4.17i,l), while the pure PLA_SDS and PLA_SYN dispersions present some discontinuities (Fig. 4.16a and 4.17a, respectively). Notice that the two formulations were dried in polystyrene capsules while for the previous studies the dispersions were dried in teflon capsules (see paragraph 2.2.7, Chapter 2). The capsule's material could have affected the phase morphology due to the different surface wettability of polystyrene and teflon. Indeed, many papers report the influence of surface on the miscibility between blend components and the derived morphology of the resulting films [350][351][352][353][354]. As regards the surfaces used for the preparation of the PLA/PVA blend, teflon is considered an inert material and thus it possesses a lower surface wettability than polystyrene. Possibly, the lower wettability favours the formation of a continuous film

due to the greater surface tension of the formulation on the substrate, which favours a cohesion among the particles. Moreover, the capsules materials and the surfactant used in the formulation could have an influence on the release kinetics of trapped air bubbles. Indeed, the film prepared from the PLA_SYN dispersion (Fig. 4.17a,b) appears to be more cohesive than the one prepared with the PLA_SDS formulation (Fig. 4.16a,b).

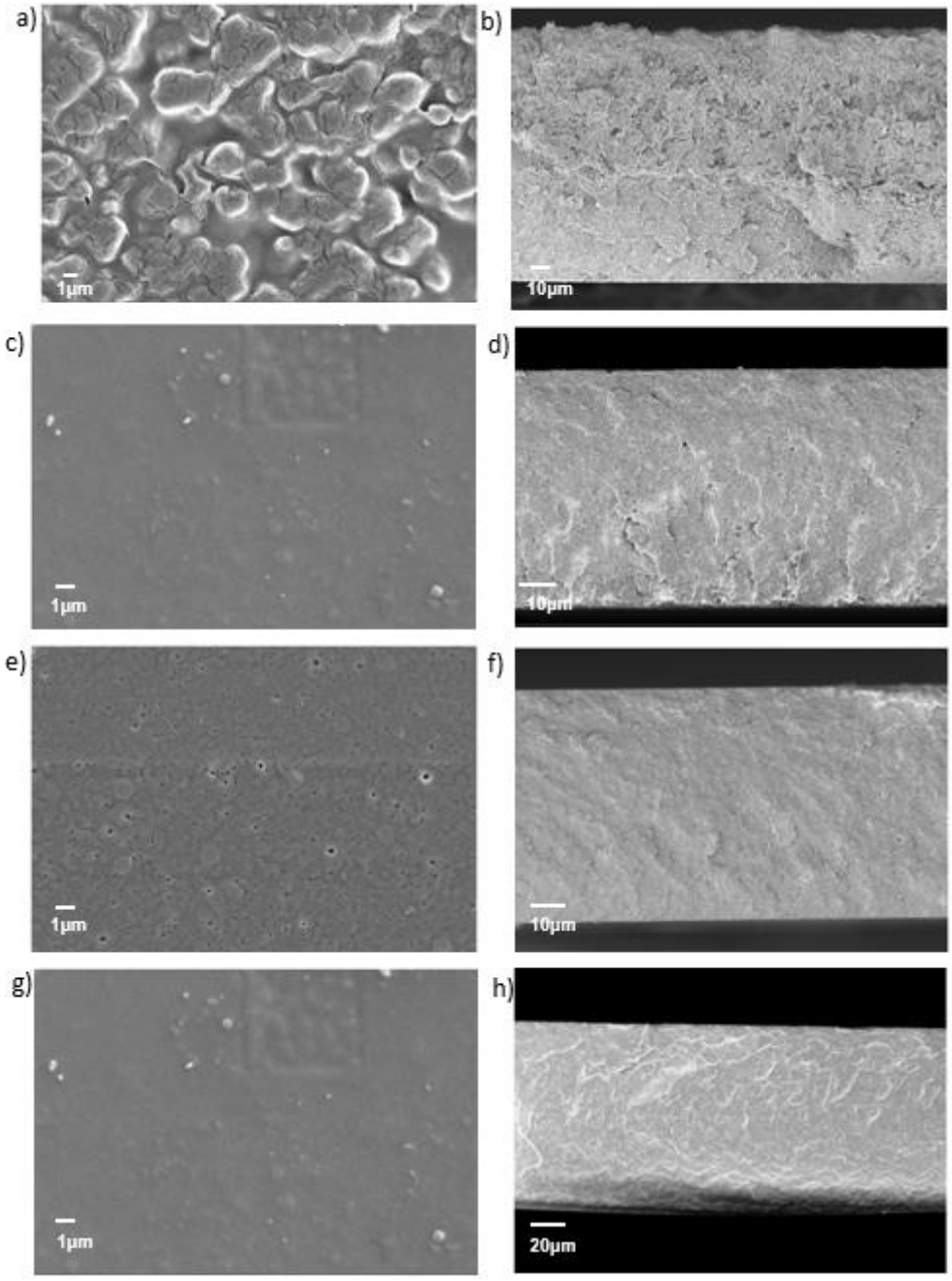

*Figure 4.16: SEM pictures of surfaces (**a**,**c**,**e**,**g**,) and sections (**b**,**d**,**f**,**h**,) of PLA/PVA films prepared from PLA_SDS dispersion with a PVA content of 0 (**a**,**b**), 25 (**c**,**d**), 50 (**e**,**f**) and 75 (**g**,**h**).*

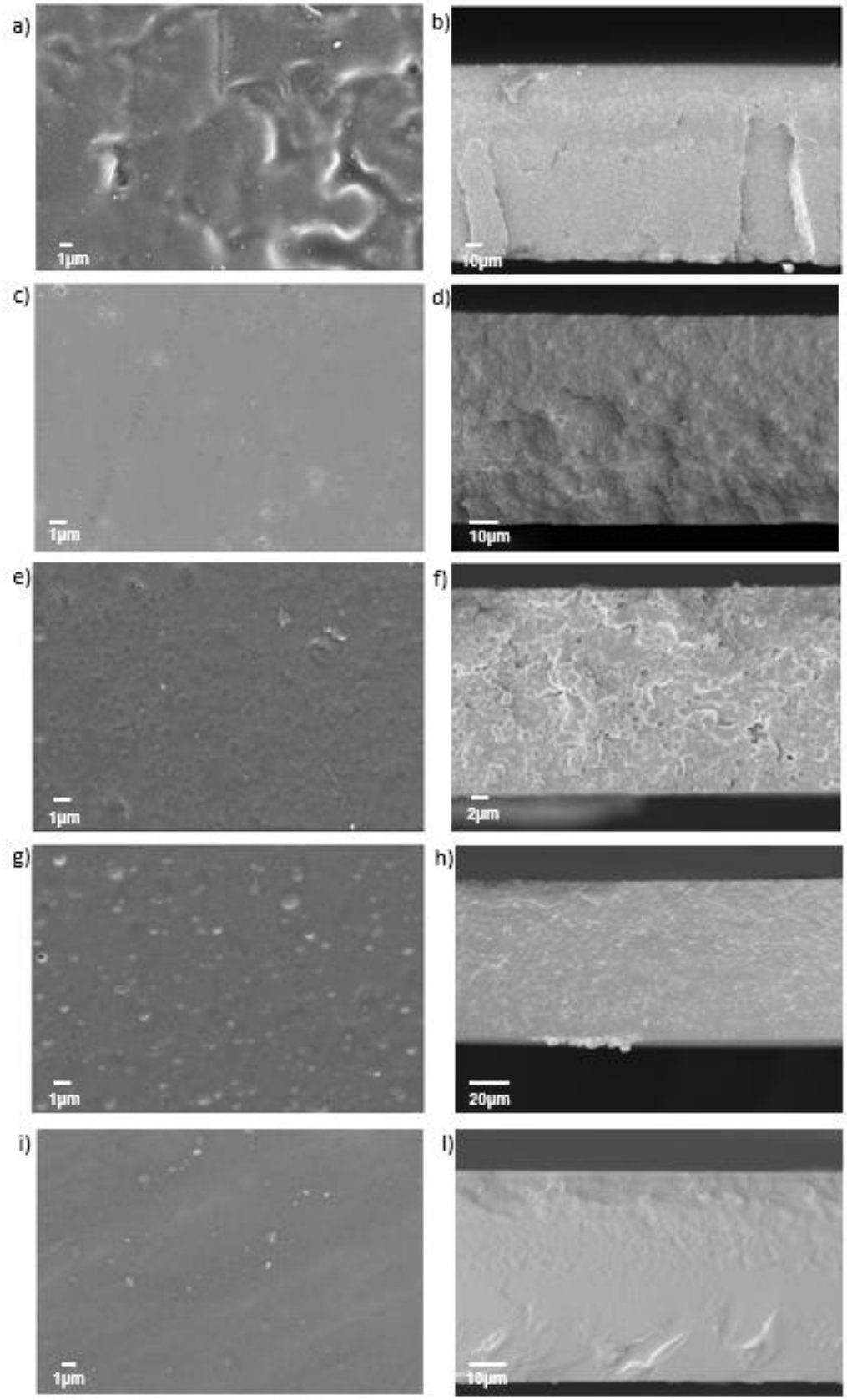

*Figure 4.17: SEM pictures of surfaces (**a**,**c**,**e**,**g**,**i**) and sections (**b**,**d**,**f**,**h**,**l**) of PLA/PVA films prepared from PLA_SYN dispersion with a PVA content of 0 (**a**,**b**), 25 (**c**,**d**), 50 (**e**,**f**), 75 (**g**,**h**) and 100 wt. % (**i,l**).*

4.2.4.2.3. Thermal analysis

Thermal stability of pure PLA dispersions, PVA and PLA/PVA blends was evaluated by TGA analysis. Tables 4.5 and 4.6 summarize the thermal parameters while Fig. 4.18 and 4.19 shows respectively the 1st derivatives of the thermograms of the pure components and of the PLA/PVA mixtures. As it is possible to observe from Fig. 4.18, the TGA curve of pure PLA shows a unique degradation peak, corresponding to the breaking of the ester bond with consequent depolymerization (T_d between 375.16 °C) [355]. However, PLA_SDS dispersions display an additional small degradation peak at lower temperatures (T_d between 212 and 216 °C) that can be ascribed to the presence of SDS as surfactant by comparison with the thermogram of the latter (Fig. 4.19a and Fig. 4.18 respectively). The intensity of this peak increases when the dispersion is dried at 60°C instead of room temperature (Fig. 4.18a). This is probably due to surfactant segregation (as highlighted through ATR-FTIR analysis): the emulsifier is expelled from the sample thus increasing the intensity of the relative degradation peak. Even the PLA_SYN dispersion presents an additional degradation step (Fig. 4.19b). However, this is at higher temperatures with respect to the main one (T_d in the 403-405 °C range) and it can be assigned to the presence of SYN as an emulsifier by comparison with the thermogram of the latter (Fig. 4.18). In this case, there are no evident differences between the formulation dried at room temperature and the one dried at 60 °C, thus suggesting that the drying temperature has no or poor influence on the segregation of the emulsifier (Fig. 4.19b). On the other hand, SYN is expected to be more compatible than SDS with the blend components, thus reducing or avoiding segregation.

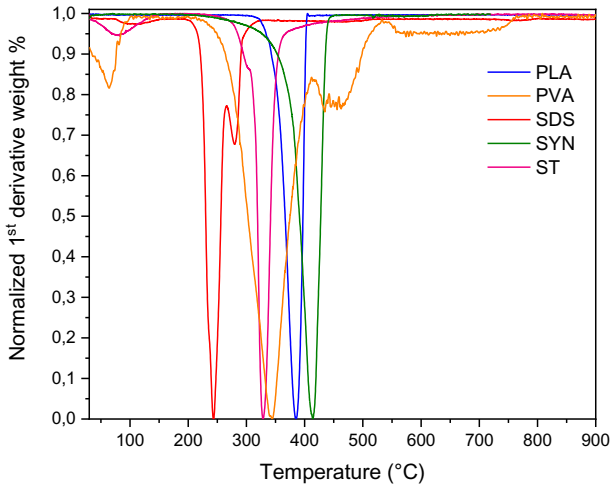

*Figure 4.18: Comparison among the 1st derivative of the TGA curves of PLA, PVA, Starch C*Icoat (ST), Synperonic PE/F68 (SYN) and sodium dodecyl sulfate (SDS).*

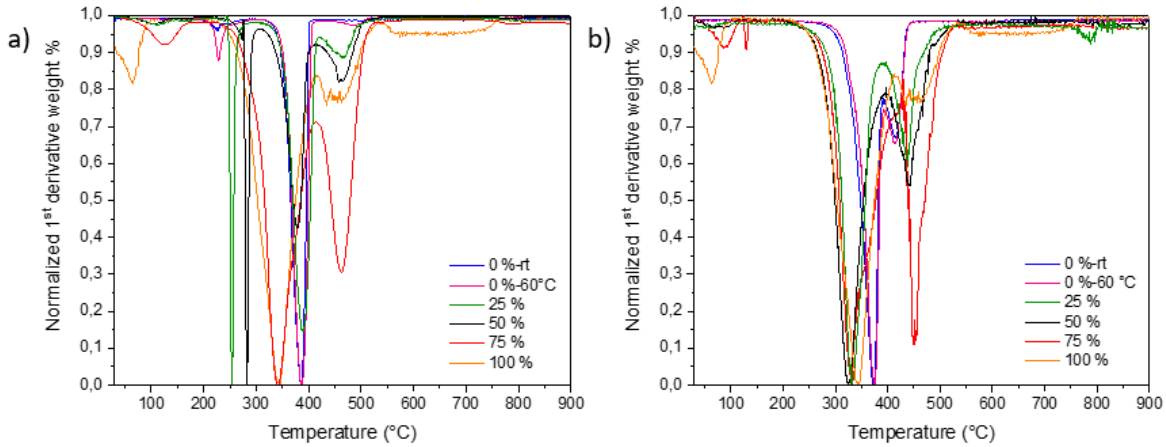

*Figure 4.19: Comparison among the 1st derivative of the TGA curves of PLA/PVA blends prepared from the PLA_SDS dispersion (**a**) and PLA_SYN dispersion (**b**) with a PVA content of 0 (dried at rt or at 60°C), 25, 50, 75, 100 wt. %.*

In all prepared PLA/PVA mixtures, a weight loss peak is observed in the 30-180 °C range, which corresponds to the loss of the absorbed water (Fig. 4.19). Its intensity increments with the PVA content. This is due to the fact that PVA, which is more hydrophilic, displays a greater water content than PLA. In the blends, this peak is also shifted towards higher temperatures, hence suggesting that in the PLA/PVA mixture water is more retained.

Table 4.5: Water content (%), first, second and third temperature of onset (T_{on}^1, T_{on}^2 and T_{on}^3), first, second and third temperature of maximum degradation rate (T_d^1, T_d^2 and T_d^3) and residuum after degradation (Res.) from TGA analyses of the PLA/PVA blends prepared with the PLA_SDS dispersion.

PVA content (wt. %)	Water content[a] (%)	T_{on}^1 (°C)[b]	T_d^1 (°C)	T_{on}^2 (°C)[b]	T_d^2 (°C)	T_{on}^3 (°C)[b]	T_d^3 (°C)	Res. (%)[c]
0-rt	-	200.7	212.0	350.9	373.9	-	-	2.4
0-60 °C	-	205.8	216.5	352.8	375.7	-	-	4.0
25	1.9	237.5	243.2	353.6	378.9	439.0	457.4	5.2
50	2.5	267.5	273.0	346.5	369.1	493.2	459.6	4.6
75	2.9	297.6	335.3	-	-	-	-	6.6
100	6.0	286.1	335.5	422.0	447.3	-	-	2.0

[a]Weight loss % between 30 and 180 °C; [b]Temperature of the peak minimum in the first derivative TGA plots; [c]Residuum at 850 °C.

In general, two or three degradation steps were observed in the PLA/PVA blend thermograms (Fig. 4.19) with peak position in the first derivative plots depending on the blend composition. In the case of the PLA_SDS/PVA blends the onset of degradation increases almost linearly with the blend composition (Table 4.5) moving from ~ 200 °C, in the case of PLA_SDS, to 286.1°C for pure PVA. On the other hand, for PLA_SYN/PVA blends the onset of degradation decreases almost linearly with the blend composition shifting from 328 °C in PLA_SYN dispersion to 286.1 of the pure PVA (Table 4.6).

By comparing the thermograms of the blends at different compositions with those of the pure components (Fig. 4.19 and 4.18 respectively), it is evident that when PVA is in large excess the thermogram is similar to the one of pure PVA: the first degradation process being almost superimposed to the one of the neat polymer. With both PLA formulations, the second degradation step in the 25/75 PLA/PVA blends is larger than in the pure PVA suggesting that the degradation of PLA has been shifted at higher temperature. Surprisingly, the peak shift and area are lower when the PLA amount in the blend is higher (75 and 50 wt. %), in agreement with

the observed different morphology and miscibility at the different compositions. Moreover, the PLA_SDS/PVA 75/25 and 50/50 blends degrade by a three-steps process instead of two (Fig. 4.19a). The first one is at a lower temperature than that of the pure components. These blends showed, through SEM analysis, the presence of a porous structure. Indeed, the presence of the first degradation process can be due to some components enriched at the air interface in the PLA/PVA mixtures that are easily exudated through the structure's pores. The second peak is completely superimposed to the one of pure PLA and it is therefore attributed to PLA domains not mixed with PVA. The other two peaks are attributed to neat PVA or mixtures of PVA and PLA. The lower stability of PVA in the blends might be ascribed to a different phase organization due to interactions with PLA or to a lower crystallinity degree.

Table 4.6: Water content (%), first and second temperature of onset (T_{on}^1 and T_{on}^2), first and second temperature of maximum degradation rate (T_d^1 and T_d^2) and residuum after degradation (Res.) from TGA analyses of the PLA/PVA blends prepared with the PLA_SYN dispersion.

PVA content (wt. %)	Water content[a] (%)	T_{on}^1 (°C)[b]	T_d^1 (°C)	T_{on}^2 (°C)[b]	T_d^2 (°C)	Res. (%)[c]
0-rt	-	328.0	361.3	393.5	403.8	2.4
0-60 °C	-	335.1	363.4	399.0	404.3	1.5
25	-	292.4	322.4	404.9	429.3	1.3
50	1.4	280.5	315.0	411.8	433.3	4.1
75	2.5	288.3	318.2	433.3	444.3	6.4
100	6.0	286.1	335.5	422.0	447.3	2.0

[a]Weight loss % between 30 and 180 °C; [b]Temperature of the peak minimum in the first derivative TGA plots; [c]Residuum at 850 °C.

The results of DSC measurements of pure PLA dispersions, PVA and PLA/PVA blends prepared with PLA_SDS and PLA_SYN are listed in Tables 4.7 and 4.8, respectively.

Table 4.7: Crystallization temperature (T_c) and crystallization enthalpy (ΔH_c) of the cooling step and glass transition temperature (T_g), melting temperature (T_{m^2}) and melting enthalpy (ΔH_{m^2}) of the second heating step from DSC analyses of the PLA/PVA blends prepared from the PLA_SDS dispersion.

PVA content (wt. %)	T_c (°C)	ΔH_c (J/g)	$T_g{}^1$ (°C)[a]	$T_g{}^2$ (°C)[a]	$T_m{}^1$ (°C)[b]	$\Delta H_m{}^1$ (J/g)
0-rt	85.6	-0.5	56.8	-	89.9	0.3
0-60 °C	86.1	-1,3	55.7	-	90.1[d]	0.7
25	86.4	-1.0	56.2	71.0	90.3	1.3
50	-	-	56.7	70.3	-	-
75	-	-	57.3	71.4	-	-
100	-	-	-	71.5	-	-

[a]Values at the midpoint; [b]Values at the peak maximum; [c]Calculated through the Flowry-Fox equation; [d]A second T_m at 101.2 °C with ΔH_{m^1} of 0.3 is detected.

Table 4.8: Glass transition temperature (T_g), melting temperature (T_{m^2}) and melting enthalpy (ΔH_{m^2}) of the second heating step from DSC analyses of the PLA/PVA blends prepared from the PLA_SYN dispersion.

PVA content wt. %	$T_g{}^1$ (°C)[a]	$T_g{}^2$ (°C)[a]	$T_m{}^1$ (°C)[b]	$\Delta H_m{}^1$ (J/g)	% PVA in PLA phase[c]
0-rt	12.9	-	41.1	3.8	-
0-60 °C	13.3	-	53.3	3.2	-
25	24.7	72.8	-	-	56.7
50	-	71.7	52.3	1.8	-
75	36.3	70.1	53.3	1.9	77.8
100	-	71.5	-	-	-

[a]Values at the midpoint; [b]Values at the peak maximum; [c]Calculated through the Flory-Fox equation.

One of the most relevant criteria for determining the miscibility of components is the shift in the glass transition temperature (T_g) of a polymer blend. As previously

anticipated in Paragraph 4.1.1, miscible binary blends show a single T_g relative to a unique polymer phase. This T_g, which is at an intermediate temperature between the T_g values of each pure polymer, must obey the Fox equation. The latter describes the relationship between the T_g value of the blend, its composition and T_g values of the pure components. When the components are immiscible two T_gs corresponding to the ones of the pure polymers are detected. In this case, two different polymer phases coexist. Nevertheless, if two polymers are only partially miscible, the T_g value of each component should be influenced by the other one and this behaviour is usually composition dependent [7].

In all the DSC thermograms of the PLA/PVA blends, two different T_gs are observed, hence revealing the presence of two distinct polymer phases, in agreement with SEM observation (Tables 4.7 and 4.8). This is due to the preparation methodology used in which the PVA is inserted in aqueous dispersion containing sub-micrometric PLA particles. Indeed, one phase should be constituted by the PLA submicrometric particles and the other one by a continuous matrix of PVA. In the case of the blends containing the PLA_SDS formulation, the T_g values are similar to the one of the pure PLA dispersions and PVA. For high PVA content, the T_g of the PLA phase tends to slightly shift towards the other component (Table 4.7 and Fig. 4.20). However, the shift is small and it is not possible to determine if the phenomenon is due to a partial miscibility at the interphase or to the uncertainty of the measurement. On the contrary, in the blends containing the PLA_SYN formulation, the shift of the PLA T_g towards the PVA is so relevant that it can be clearly ascribed to partial miscibility between the two polymers (Table 4.8). Indeed, it must be taken into account that through SEM analysis the PLA_SYN/PVA blends displayed a good adhesion at the interface in contrast with the poor adhesion in the PLA_SDS/PVA mixtures.

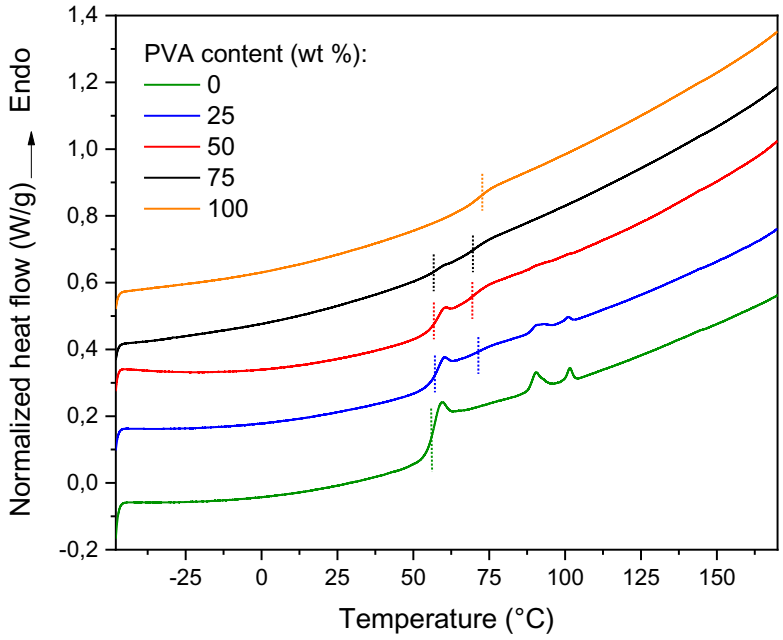

Figure 4.20: DSC analysis at 10°C/min of blends prepared with PLA_SDS dispersion with a PVA content of 0, 25, 50, 75 and 100 wt. % relative to the second heating step. Thermograms were arbitrarily shifted for clarity.

As concerns the PLA_SYN/PVA blends 50/50 the unique T_g revealed is similar to the one of the pure PVA. Consequently, the presence of a single T_g does not indicate the existence of a single polymeric phase. In this case, a second T_g corresponding to the PVA-rich phase can be hidden by the peak between 52 and 53 °C, which corresponds to the melting of the crystalline phase of the emulsifier, namely SYN.

This situation can be simplified by assuming the presence of 2 different polymer phases: one of pure PVA and one PLA phase enriched with PVA (Fig. 4.21b).

The entity of the T_g shift towards the other component of the mixtures can provide an idea on the degree of miscibility. In particular, in Fig 4.22, it is possible to observe the T_g shift of the PLA_SYN/PVA blends as a function of the PVA content.

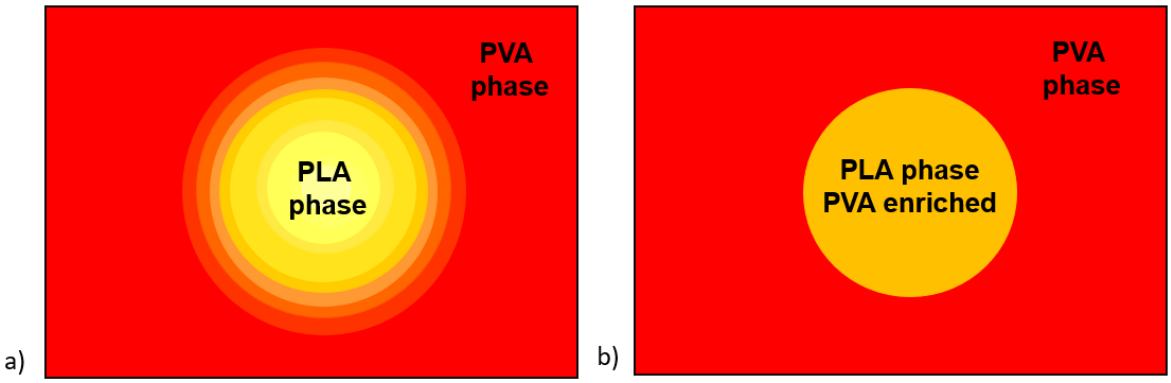

Figure 4.21: Cartoon of the structure phases present in the PLA/PVA blends

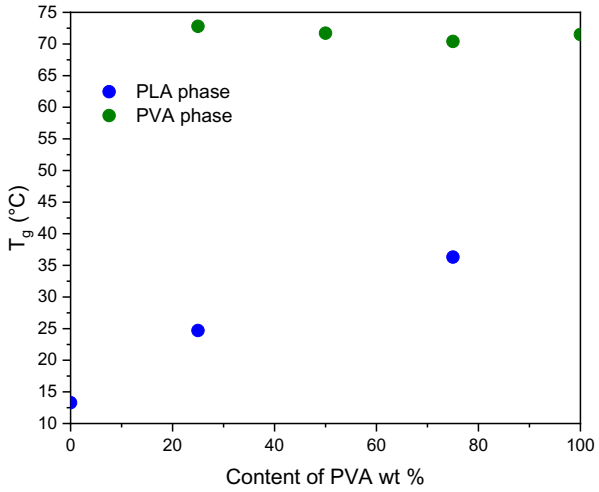

Figure 4.22: Glass transition temperature values as a function of the PVA content (wt. %) in PLA_SYN/PVA blends.

Moreover, the shift of the T_g corresponding to PLA can be correlated to the average content of PVA in the PLA phase PVA-enriched through the Fox equation. The results are reported in Table 4.8, where it is possible to observe that the PVA content in the PLA phase PVA-enriched is 57 and 78 % for the 75/25 and 25/75 PLA/PVA blends composition, respectively. In order to understand the different composition, it can be useful to go back to the phase morphology of the blend and to remember that at the 75/25 composition the dispersed phase could be difficulty observed and, when it was detectable, it was made by particles larger than the original in the PLA dispersion (Fig. 4.15f). This suggests that particles have been enlarged by the incorporation of PVA. No similar effect was observed in composition 25/75, where

most likely a gradient concentration into the dispersed phase particles was established with a minor effect in the dispersed phase volume (Fig. 4.15b).

Furthermore, an increase or decrease of the crystallization temperature (T_c) may indicate that the crystallization of this polymer becomes difficult or easier upon blending [356]. Also changes in the melting temperature (T_m) of the components depending on composition can suggest the presence of an interaction between the polymer phases [357]. While the PLA used is amorphous and therefore it does not display a crystallization or a melting temperature, pure PVA is a semi-crystalline polymer with a T_m of 158.7 °C and a T_c of 109.4 °C. However, due to the poor thermal stability of some PLA/PVA mixtures, the DSC analysis was carried out up to 170 °C. Under these conditions, the T_m and T_c relative to the PVA cannot be detected. As a consequence, these data are not available to evaluate the influence of the blending on the crystallization and melting temperature of the polymers.

From table 4.7 it is possible to observe that the PLA_SDS dispersion displays a crystallization temperature in the 85-86 °C range and a melting temperature of 89-90 °C, whose enthalpies increase when the dispersion is dried at 60°C. This crystallization and melting peaks are evident even when the PVA content is relatively low (25 wt. %) while they disappear for higher PVA contents. They can be ascribed to SDS by comparison with the DSC curve of the pure emulsifier. SDS may form separated domains in the case of low PVA content but it can be better dispersed in this polymeric matrix when present in larger amounts. Regarding the mixtures containing PLA_SYN dispersion, all the blends analysed as well as the pure PLA formulation, exhibit a melting peak around 51 and 52 °C that corresponds to the melting of the crystalline phase of the surfactant (Table 4.8). In Paragraph 2.2.6 of Chapter 1, the PLA dispersions analysed displays only a T_g through DSC analysis, with no evidence of peaks relative to the emulsifier. Probably, in this case, segregation and migration of the surfactant occurs because of the PVA presence.

Overall, from the results of the DSC analysis it can be concluded that PLA/PVA blends prepared from PLA aqueous dispersions are characterized by a phase separated domain morphology made of a continuous phase of pure PVA and a dispersed phase made of a mixture of the two polymers. These results are in agreement with the one reported for PLA/PVA mixtures prepared by solvent blending [7][8]. On the contrary, for PLA/PVA blends prepared though melting methods full miscibility between the pure components was observed [9][10][11][12].

Therefore, the here observed morphology should be ascribed to the preparation process rather than to thermodynamic reasons, even if the miscibility is affected by the hydrolysis degree of PVA as well as by the stereochemistry of the PLA chains, and no one of the cited studied, where miscibility was observed, were performed by using exactly the same combination of polymers used in this work.

4.2.4.2.3. Mechanical properties

Pure PLA is a rigid and fragile material while pure PVA is more flexible. The stress-strain plots of the pure polymers are reported, together with the PLA/PVA blends prepared, in Fig. 4.23. Furthermore, the relationship between the mechanical properties (Young's modulus, elongation at break and stress at break) and the composition of the PLA/PVA prepared are shown in Fig. 4.24 and 4.25 (blue line for the blends containing PLA_SYN dispersion and red line for the ones containing PLA_SDS dispersion). It is possible to notice that native PLA (green star) possesses a lower elongation at break in comparison with PVA even though it displays a higher Young's modulus and stress at break. Moreover, the PLA_SYN formulation presents a higher elongation at break and a lower Young's modulus in comparison with PLA4060D, hence indicating that SYN acts also as a plasticizer. The mechanical properties of a polymer blend are influenced by the mechanical properties of the individual component as well as by the compatibility between the two polymer phases and by the blend morphology.

As regards the blends prepared with PLA_SDS dispersion, only PLA/PVA 25/75 could be cut for mechanical properties (Fig. 4.23, 4.24 and 4.25). Indeed, among the mixtures prepared with PLA_SDS dispersion, this composition was the only one that through SEM analysis showed a good adhesion at the interface. All other compositions and the pure PLA_SDS dispersion were too fragile and it was not possible to prepare the samples for the analysis. The measured sample displayed a stress-strain curve typical of brittle materials whose rupture occurs without evident changes in elongation rate. Indeed, blends containing the PLA_SDS dispersion showed a porous structure through SEM analysis (Fig. 4.15e). As previously hypothesized, these poor mechanical properties can be due to the presence of voids

in the structure generated by the electrostatic repulsion between the PLA nanoparticles stabilized by SDS.

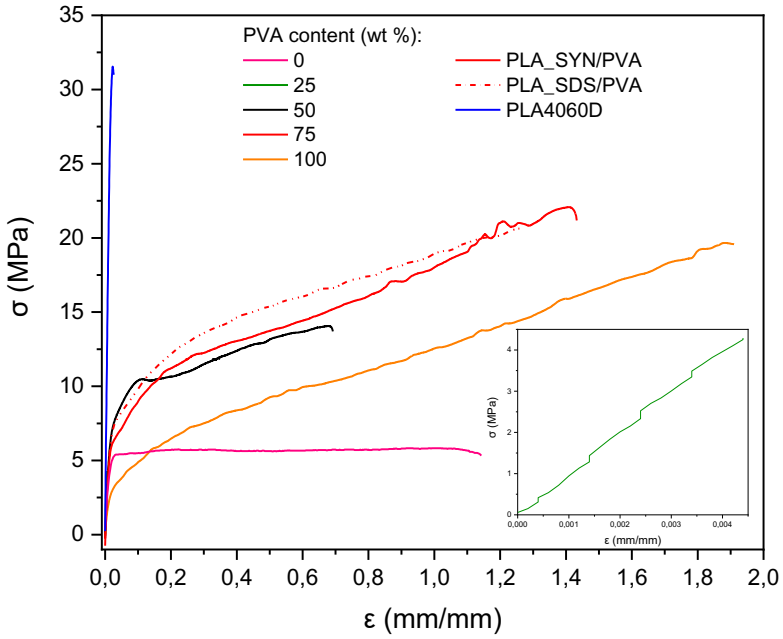

Figure 4.23: Representative stress-strain curves for the PLA4060D (blue line) and the PLA blends prepared from the PLA_SYN (solid line) and PLA_SDS dispersions (dashed line) with a PVA content of 0, 25, 50, 75, 100 wt. %. Inset bottom right is the result for the PLA_SYN/PVA 75/25 mixture (green line).

On the other hand, in the case of mixtures containing PLA_SYN, all prepared blends could be analysed. Clearly, the dispersed PLA phase renders the material more rigid and less deformable (Fig. 4.24 and 4.25). Indeed, the blends present a higher Young's modulus and a lower elongation at break in comparison with the pure PVA (Fig. 4.24 and 4.25a). In particular, this behaviour is more evident in the PLA/PVA 75/25 blend. On the other hand, the stress at break increases with the percentage of PVA in the mixture. From the stress-strain curves (Fig. 4.25b) it is possible to see that the PLA/PVA 50/50 blend displays a yield strength after which plastic behavior occurs. All the other samples show an initial elastic behavior followed by an elastic-plastic deformation.

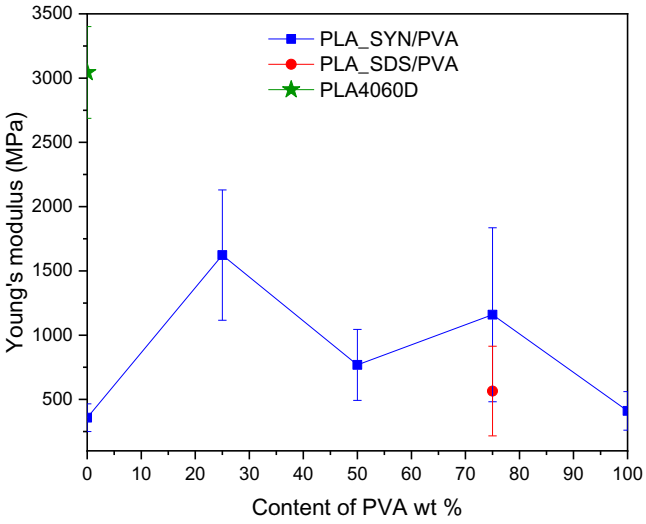

Figure 4.24: Young's modulus as a function of the PVA contents in the PLA/PVA blends prepared with the PLA_SDS (in red) and PLA_SYN dispersions (in blue).

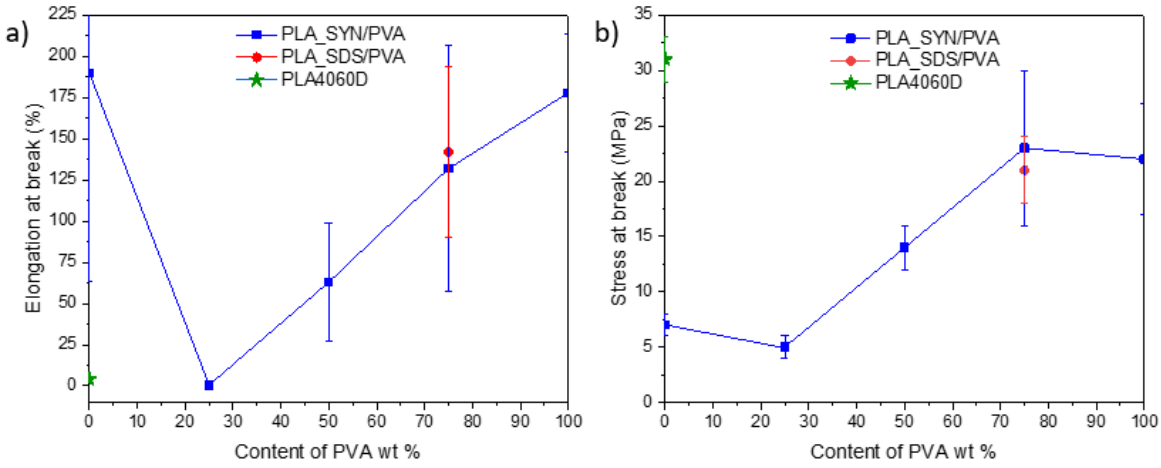

*Figure 4.25: Elongation at break (**a**) and stress at break (**b**) as a function of the PVA contents in the PLA/PVA blends prepared with the PLA_SDS (in red) and PLA_SYN dispersions (in blue).*

4.3. CONCLUSION

In this work, PLA/PVA blends were obtained exploiting a mixed and innovative approach between latex mixing and emulsion blending. The procedure involves the addition of a PVA water solution to a PLA aqueous dispersion containing PLA

submicrometric particles in water media. After casting the PLA/PVA latexes thus prepared onto PS capsules and drying at 60 °C, PLA/PVA films are obtained.

Three different PVA grades with comparable HD (73-75 %) were available and among these, PVA GH 17R, was chosen due to the greater homogeneity and continuity of the PLA/PVA 50/50 films formed. After selecting the most suitable PVA grade, PLA/PVA blends in proportion 25/75, 50/50, 25/75 were prepared using PLA dispersions containing SDS or SYN as surfactant. All the PLA/PVA mixtures showed, through SEM analysis, the presence of the submicrometric PLA particles dispersed into a continuous PVA matrix, in agreement with the preparation method that requires the addition of PVA into a water phase containing dispersed solid submicrometric particles of PLA.

In particular, the use of a non-ionic surfactant (SYN) for the preparation of the PLA formulation allowed a greater adhesion and miscibility at the polymer interphase. On the other hand, when a negatively charged emulsifier (SDS) was present in the PLA dispersion, the blends containing a moderate/high amount of PLA_SDS formulation (from 50 to 75 wt.%) showed a porous morphology rich in voids which causes the presence of an additional peak of thermal degradation at a lower temperature than the one of the pure components. This reduced thermal stability observed by TGA analysis might be due to the exudation through the pores of the structure of some components enriched at the air interphase. Furthermore, the presence of voids and defects in the blends structure render the final materials so fragile that the preparation of the PLA_SDS/PVA samples for the mechanical tests is not feasible. The only exception is constituted by the PLA_SDS/PVA mixture with the lowest amount of PLA_SDS dispersion (25/75), which shows good compatibility at the interphase and measurable mechanical properties. The mechanical analyses conducted highlighted that, the dispersed PLA phase confers to the final PLA/PVA blends a higher rigidity and a reduced deformability, as typically observed for polymer blends with a matrix-dispersed particle (sea–island) morphology. Indeed, the PLA/PVA mixtures analysed display a higher Young's modulus and a lower elongation at break in comparison with the pure PVA and PLA dispersion.

All the prepared PLA/PVA blends showed, through DSC analysis, the presence of two distinct polymer phases as evidenced by the two T_gs detected. Particularly, a shift of the PLA phase's T_g towards the one of the PVA is observed. While for the PLA_SDS/PVA mixtures this shift is so small that it is not possible to distinguish it

from the measurement error, for the PLA_SYN/PVA blends the shift is so relevant that it can be clearly ascribed to partial miscibility between the two polymers. For this reason, the system can be described as a dispersed phase of PVA-enriched PLA immersed in a continuous PVA matrix. These results were in agreement with the SEM analysis, which showed a good interphase adhesion in the PLA_SYN/PVA blends in contrast with the poor adhesion observed in the PLA_SDS/PVA mixtures. Consequently, for the PLA_SYN/PVA blends, the PVA content in the PVA-enriched PLA phase, was estimated with the Fox equation, revealing a content of 57 and 78 % for the 75/25 and 25/75 PLA/PVA blends composition, respectively. These results reflect the morphology of the blends, in which the dispersed phase exhibited a larger particle dimension than the one present in the original PLA dispersion when the composition was 25/75. As a consequence, a PLA particle enlargement due to incorporation of PVA at higher PVA content in the blends was hypothesised.

Overall, the use of PLA aqueous formulations containing non-ionic surfactants is of utmost importance in guaranteeing a good miscibility at the polymer interphase as well as good mechanical properties.

In conclusion, the innovative and green approach reported for the preparation of PLA/ PVA blends constituted an important tool for preparing polymer blends in which PLA is dispersed in a submicrometric phase in a continuous water-soluble polymer matrix.

CHAPTER 5

Bio-based and biodegradable polymers in electronics

Most of the work described in this Chapter is adapted with permission from “Cocchi, M.; Bertoldo, M.; Seri, M.; Maccagnani, P.; Summonte, C.; Buoso, S.; Belletti, G.; Dinelli, F.; Capelli, R.; Fully Recyclable OLEDs Built on a Flexible Biopolymer Substrate, *ACS Sustainable Chem. Eng.* 2021, 9, 38, 12733–12737” and “Marchi, L.; Dinelli, F.; Maccagnani, P.; Costa, V.; Chenet, T.; Belletti, G.; Natali, M.; Cocchi, M.; Bertoldo, M.; Seri, M.; Sodium alginate as a natural substrate for efficient and sustainable organic solar cells, *ACS Sustainable Chem. and Engin.,* 2022.

5.1. INTRODUCTION

5.1.1. “Green” Electronics

Electronic devices such as batteries, computers, mobile phones, Liquid Crystal Displays (LCDs) or Light Emitting Diodes (LEDs) are part of our daily life and contribute to making modern life as we know possible. Even though electronic products that are increasingly energy efficient during use are being developed, a great amount of energy is consumed for the production of these devices, thus generating an imbalance. The current global demand of electronics is leading not only to an energy imbalance, but also to the generation of an enormous amount of electronic waste (e-waste) and to the fast consumption of natural elements, like indium and gallium, whose exhaustion is estimated in 20 years [358]. Indeed, according to the US Environmental Protection Agency (EPA), each European citizen produces on average 5 kg of e-waste annually, for an estimated total of 7×10^6 tons [359]. Besides, due to the hazardous nature of some electronic device’s components, like cadmium and mercury, the disposal of the e-waste represents a serious risk for the human health and environment. The collection and transportation of the e-waste with the purpose of recycling is the most costly step of the recycling

chain (more than 80% of the total cost) [360]. Once transported to the recycling facility, the e-waste is subjected to a pre-treatment and a feed back to market phases [361]. The pre-treatment step mainly consists in sorting and separating by components and material the incoming e-waste. Usually, in this step the electronic device is disassembled in order to separate valuable components or remove hazardous substances. Generally, the pre-treatment involves a subsequent size reduction of the e-waste through the use of shredders. After that, ferrous metals, aluminium and plastic are separated through magnetic, eddy-current and density separation. In the second step of the recycling chain, the materials separated in the pre-treatment step that have the potential to be reinserted in the market, for instance for the reuse in new products, will be sold to the same industries that produce those materials. On the contrary, plastic recycling is more challenging than the metal one due to the fact that e-waste is composed of a great variety of several plastics that must be classified and separated [362]. Besides, plastic usually contains impurities like paint, flame retardant and different additives that make the recycled material less valuable and thus less profitable.

It must be taken into account that materials that cannot be recycled in the process are incinerated to create energy or disposed of in landfills. Nevertheless, the majority of electronic devices contain halogenated flame retardants that can form dioxins during incineration, posing a problem for the health and the environment [363]. Due to the diverse structure and composition of electron devices, the development of advanced recycling methodologies suitable for all the different items represents a huge challenge. Besides, the electronic devices differ not only for their material composition but also for their recycling economy. Indeed, some products contain large amounts of valuable materials and consequently recycling generates value and profit. In other cases, the devices are made of materials that have no reselling value and hence their recycling becomes a cost. Moreover, some products contain hazardous components that need to be disassembled and treated in specialized waste treatment facilities. Furthermore, it must be considered that the small amounts of e-waste collected is one of the major factors that hinder the development of advanced recycling technologies [364].

For all these reasons, the interest in the production of “green electronics” made of recyclable and renewable material that can be easily disassembled with safe procedures has increasingly grown. According to European Standard EN13432, at least 90% of all materials used in green electronics must be converted within 6

months of abandonment into harmless components, such as water, carbon dioxide, and biomass, through the action of fungi or microorganisms under certain defined conditions of temperature, humidity, and oxygen concentration [365].

Furthermore, green electronics aim at generating environmentally friendly technologies that can be integrated into living tissues with the purpose of reaching biochemical monitoring, diagnostic and drug delivery tasks [366]. For this reason, flexible, highly conformable and thin devices are needed. Consequently, due to the soft nature of carbon-based materials, organic based technologies were developed for the production of flexible electronics. Organic electronics based on polymers or organic small molecules as semiconductor elements were first presented in the mid 1970's/early 1980s with the purpose of addressing the energy and cost inefficiency issues posed by their inorganic counterparts [358]. Even though the performance and stability of organic semiconductors are not comparable to their inorganic counterparts, their flexible nature confers to them an incredible advantage. Indeed, the applications of flexible electronics extend beyond the biomedical sector; for instance, flexible organic light-emitting devices (OLED's) are the base of the latest generation of foldable commercial displays for mobile phones. In particular, the goal of green electronics is to use highly abundant and economic organic substances that can be produced though synthetic routes that do not use toxic solvent or generate harmful waste. Besides, in the electronics sector many efforts have been made to replace fossil-based materials with renewable and biodegradable ones that can be reconverted and recycled with sustainable processes [367]. The use of biodegradable and biocompatible polymers is particularly convenient in devices for biomedical applications, where the resorption of the system in the body limits the need to surgically remove it post-diagnosis, monitoring, or therapy [368]. Nevertheless, in this work, the bio-based and biodegradable polymer was employed to facilitate the fabrication and the disassembly of the device through green methodologies.

5.1.2. Biodegradable and renewable materials for electronic devices

The replacement of conventional materials with greener ones has been addressed with regard to all the components of electronics devices namely, the substrates, the active layers and the conductive contacts. However, from a quantitative point of

view, the most relevant component is represented by the substrates, which typically accounts for more than 90 % of the total volume [369]. Its substitution would therefore furnish the largest environmental impact, provided that non-toxic and harmless substances are employed.

For example paper has been efficiently employed as substrate for printed electronics [370]. Indeed, the high surface roughness of commercial papers is ideal for energy storage systems where large surface area is essential for easy absorption of electrolyte and binding with nanomaterials. However, the porosity and high roughness of the paper could be detrimental to thin film devices, especially those utilizing organic materials as semiconducting or dielectric layers. Usually, to solve this problem the paper substrate is coated with substances that guarantee planarization like wax, kaolin, starch and polymers such as polyethylene, polypropylene, polyurethane, and PVA [371]. Nevertheless, some of these coatings are not from renewable sources and cannot be processed through environmentally friendly methods. Furthermore, a relatively simple methodology for the preparation of transparent paper substrates directly from thin (400 μm to 1 mm) wood slices cut perpendicularly to the direction of growth was reported with the purpose of expanding the potential application of paper in electronic devices [372].

Moreover, bio-based fibers made of chitin (poly-β-(1,4)-N-acetyl-d-glucosamine) were employed as substrates for electronic items. Chitin is the second most abundant natural biopolymer in nature after cellulose. It forms the basic structural material in the exoskeleton of marine crustaceans and arthropods (e.g. crab, shrimp, lobster) and can be also found in some fungi, algae, and similar microorganisms [373]. For instance, the strong adhesion of chitin nanofibril to Au surfaces was exploited to prepare a flexible green electronic circuit [374]. In this case, the device could be used as an ultrafast and sensitive humidity sensor due to the destruction of the contacts between Au nanosheets that followed the swelling of the polymer in the presence of humidity.

Additionally, silk films and fibers were revealed to be suitable natural paper-like substances for the preparation of electronic items. Silk is mainly derived from domesticated *Bombyx mori* silkworm cocoons and exists as a self-assembled fiber, consisting of a core protein fibroin (70%), surrounded by a glue glycoprotein sericin (30%) [375]. Due to its great availability from different sources and low cost as well as its biocompatibility and biodegradability, silk sources were applied in electronics

for the biomedical and food industry [376]. For example, an array of passive metamaterial antennas fabricated on all protein-based silk substrates were transferred and adhered to the surface of an apple for food monitoring purposes [377]. Moreover, fibroin, an insoluble protein present in the silks produced by a variety of moth genera and insects, was exploited in the production of paper-like substrates for green electronics. Silk fibroin was indeed successfully employed as a dielectric layer to fabricate biodegradable resistive memory devices [378]. The device hence produced exhibited good mechanical properties as well as good flexibility and switching performances.

Even though cellulose, chitin, silk, fibroin and its derivative are the most diffused bio-based substrates used in green electronics, also the use of other biodegradable polymers such shellac, gelatin, chitosan, alginates and dextran was reported [379]. Particularly, in the next Paragraph, the use of sodium alginate as substrate for electronic items will be examined due to the relevance for this thesis.

Besides, it should be taken into account that only a few papers report the use of bio-based and biodegradable polymers as substrates as well as the possibility of disassembling the device with the aim of recovering valuable materials [380][381].

5.1.2.1. Sodium alginate substrates in electronic devices

As previously discussed in Paragraph 1.3.3 of Chapter 1, alginate, or alginic acid, is a linear polysaccharide extracted from brown algae. It is a biocompatible and biologically inert polymer whose hydrogels can undergo degradation via alginate lyase and can be dissolved slowly at neutral pH. Due to these properties, alginates hydrogels have been widely applied in the biomedical sector (e.g., in wound healing applications) and recently its potential as a constituent of electronic devices have been disclosed [382]. Its characteristic features make this biopolymer a promising candidate for biosensor due to its ability to provide a stable support for encapsulated cells and other components [383]. For instance, the use of sodium alginate (SA) as substrate for flexible conducting films were reported [384]. Particularly, SA alginate films with a 20 μm thickness were produced through solvent-casting. Subsequently, coating of a smooth ultrathin Au layer (<10 nm) via sputtering was performed. The conductive properties of the films were comparable to indium-tin oxide (ITO) and the

films could be dissolved in water thus allowing the recovery of Au by centrifugation. Besides, the fabrication of electrodes for supercapacitors with SA as an additive in order to confer higher specific surface areas was reported [385]. Higher amounts of SA increased micropores and surface grooves, improving the performance of the device. Furthermore, sodium alginate was integrated with graphene for the production of flexible temperature sensor fitting on human skin [386]. The system displayed good sensitivity, high accuracy, short response time and high stability. Moreover, the preparation of stretchable and conductive nanocomposite based on alginate hydrogels and silver nanowires (AgNWs) was reported [387]. In particular, the nanocomposite was prepared through cross-linking of alginates in the presence of AgNWs. The material showed higher electrical, ionic conductivity, higher stretchability and lower modulus than conventional conducting rubbers. The nanocomposite electrode thus fabricated was used to make wearable electronics, such as a wearable antenna and a skin-mountable supercapacitor hence demonstrating the efficiency of the sodium alginate-based nanocomposite as a soft conducting material for wearable electronics.

5.1.2.1.1. Alginate lyases

Alginate lyases are a type of polymer lyases that can be isolated from both microbial and animal sources, in particular from a wide range of marine and terrestrial bacteria [388]. Specifically, polysaccharide lyases are enzymes which are able to cleave particular activated glycosidic bonds that can be found in acidic polysaccharides, thus lowering the molecular weight with the consequent formation of oligosaccharides [389]. Indeed, for some applications the high viscosity of some polysaccharide's solution might represent an issue and hence it is necessary to depolymerize in order to obtain a final lower viscosity. The main advantages of enzymatic depolymerization over the chemical one is the high selectivity and the consequent obtaining of products with stereospecific structures [390]. Additionally, enzymatic reactions need mild conditions thus reducing the formation of undesired by-products and avoiding the use of toxic reagents and solvents.

Regarding alginate lyases, during the years, several hundred typologies of these enzymes that differ in specificity and properties have been isolated and characterized. Alginate lyases can be divided into two main different groups based

on their substrate specificity: the polyG lyases and the polyM lyases [391]. The first one is specific for the G-block of the alginate, the second one for the M block. Even though this classification is commonly accepted, there are alginate lyases that are active toward both G and M block (polyMG lyases). Overall, these enzymes are able to recognize and act on four different types of bonds: M-M, M-G, G-M, and G-G. Particularly, alginate lyases with different specificities are useful for the determination of the substrate's sequence and for the preparation of oligosaccharides with tailored structures. On the other hand, if the action mechanism is considered, these enzymes can be classified into endolytic and exolytic alginate lyases [392]. While endolytic lyases act on the glycosidic linkages inside alginate polymer with a consequent production of unsaturated oligosaccharides, exolytic lyases are able to further degrade the latter products into monomers. Alginate lyases are therefore able to degrade alginate though a β-elimination mechanism, cleaving the glycosidic bond between monomers, thus producing an unsaturation between the C4 and C5 of the sugar rings. By resolving the 3D structure of several alginate lyases it was possible to study more in detail the catalytic mechanism, which comprises 3 steps (Scheme 5.1) [393]. In the first one, the negative charge on the carboxylate anion is removed through neutralization with a salt bridge (possible with a histidine or lysine residua). In the second step, a base-catalysed removal of the proton on C5 occurs. In these cases, one amino acid residue acts as a proton abstractor while the other one as a proton donor. In the last step, the transfer of electrons from the carbonyl group results in the formation of a double bond between C4 and C5 and cleavage of the glycosidic bond.

The production of alginate's oligosaccharides has attracted increasing attention due to the promising applications of these products in the food and pharmaceutical industry. For example, they are employed as anticoagulants and tumour inhibitors as well as growth promoters for plants [394]. Additionally, also the alginate lyases recently found interesting application in the pharmaceutical industry for the treatment of cystic fibrosis in combination with antibiotics [395]. Indeed, they are efficient in the degradation of polysaccharide bacterium's biofilm in bacterial mucoid biofilm-dependent diseases. Besides, the synergistic effects of endo and exo lyases have been recently exploited for the production of bioethanol through the saccharification of alginate. As a matter of fact, with the increasing consumption of

fossil fuels, renewable sources like alginates were increasingly studied as alternative starting material for the production of bioethanol [396].

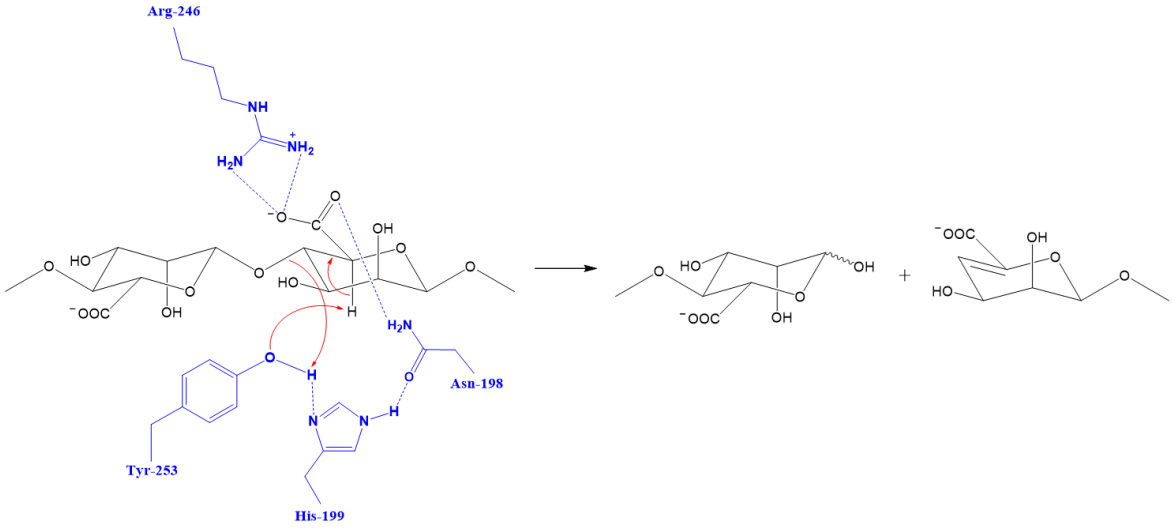

Scheme 5.1: Action's mechanism of alginate lyases [397].

5.1.3. Electronic devices with renewable and biodegradable substrates

Numerous efforts have been made in order to employ renewable and biodegradable substrates for the production of green devices such as sensors, batteries, solar cells, organic field-effect transistors, light-emitting devices. However, in the next paragraphs the attention will be focused in particular to Organic Light Emitting Diodes (OLEDs) and Solar Cells (SC) with bio-based and biodegradable substrates due to their relevance for this thesis.

5.1.3.1. Organic Light Emitting Diodes (OLEDs)

Organic light-emitting diodes (OLEDs) are light-emitting diodes (LEDs) in which the emissive electroluminescent layer is constituted of an organic compound that emits light in response to an electric current [398]. Due to their high luminous efficiency, low manufacturing cost, flexibility, lightness and thinness they are widely employed in commercial digitals displays. In general, OLEDs show a sandwich-like structure, formed by a substrate, anode, hole injection layer, emitting layer, electron injection layer, and metal cathode. Owing to the structure and mechanism of hole-electron

recombination, the balance between the hole and electron injection layers is of utmost importance for guaranteeing the efficiency of the device. Flexible OLEDs are usually fabricated through a bottom-up approach, in which all the functional and active layers, from metals to semiconductors, are sequentially grown directly on a flexible and transparent polymeric substrate. Usually, flexible OLEDs are fabricated on polyethylene terephthalate (PET) and polyethersulfone (PES) substrates [399][400]. Nevertheless, these substrates are derived from fossil-based sources and they are not biodegradable.

In literature, the use of renewable and biodegradable substrates for the construction of OLED devices has been limited mainly to cellulose derivatives. In particular, in order to be part of an OLED device, cellulose-based substrates must possess a low roughness combined with low coefficient of thermal expansion to avoid unreliability and damage to the active materials during the fabrication process under high temperatures [379].

The first example of OLED constructed on a biodegradable substrate involved the use of bacterial cellulose membranes produced by gram-negative acetic acid bacteria (*Gluconacetobacter xylinus*). However, with the purpose of achieving the necessary conductive properties, an indium tin oxide thin film was deposited onto the substrate. With this device the maximum luminance obtained with was 1200 cd/m^2, while the lowest resistivity reached was 4.90×10^{-4} Ω·cm [401]. Furthermore, the preparation of an OLED with a cellulose nanocrystals (CNC)-based substrate was reported [381]. A maximum luminance of 74 591 cd/m^2 and a current efficiency of 53,7 cd/A at a luminance of 100 cd/m^2 was achieved. Interestingly, in the latter the possibility of device disassembly and the recovery of the valuable material was reported. The CNC substrates could be indeed dissolved by simple immersion of the OLED device in water. Additionally, by dissolution in water, the device is separated into the organic semiconducting materials and metal layers which can be filtered out and recycled.

Besides, the use of nanopaper as substrate for an OLED was reported and the resulting device demonstrated stable performances in both the flat and bent state [402]. However, the substrate presented a substantially reduced transparency in the green-blue visible region, a strong limitation for the OLED performance.

Moreover, natural silk fibroin was employed as a substrate for flexible OLEDs devices. Indeed, the use of a silk fibroin (SF) film embedded with silver nanowires

(AgNWs) as conductive substrate was described [403]. In particular, the flexible OLED based on AgNWs/SF substrates displayed a current efficiency of 19 cd/A. In order to improve the planarization of the silk fibroin substrate, the latter was combined with a photopolymer [404]. The resulting OLED showed a remarkable maximum luminance and current efficiency of 45545 cd/m^2 and 37.7 cd/A, respectively.

Additionally, the use of a chitin nanofiber transparent paper for the fabrication of an OLED device was reported. The device showed performances comparable to that of a reference device constructed on synthetic plastic film. Nevertheless, in this case, a thin layer of poly(methyl methacrylate) (PPMA), which is non-biodegradable, was employed to provide planarization. Furthermore, hexafluoro isopropanol, a harmful organic solvent, was used for the preparation of chitin paper [405].

5.1.3.2. Solar cells

Solar cells are devices that are able to convert solar energy, a renewable source, into electrical energy based on the photovoltaic effect. Particularly, they are composed of different layers namely the substrate, the charge transporting layer, the active layer and the electrode. Similarly to OLEDs, also flexible solar cells are constructed though bottom up approaches [406]. Nowadays, several technologies based on silicon, perovskite and organic semiconducting materials are used to produce highly efficient solar cells. Commonly, solar cells are built on transparent substrates as glass or polyethylene terephthalate (PET) [407]. The latter is a thermoplastic polymer characterized by excellent optical and mechanical properties and, in contrast to glass, allows the obtainment of flexible devices. Nevertheless, life-cycle assessment of solar cells revealed that both incineration and disposal in landfills have a detrimental environmental impact due to the emission of photochemical oxidants, water depletion, and ecotoxicity [408]. For this reason, the attention has been focused not only in enhancing the efficiency of these devices but also to the production of renewable and recyclable photovoltaic with the purpose of reducing e-waste. In this context, the use of flexible and transparent film made from cellulose for the fabrication of organic solar cells was reported [409]. The substrate was obtained by combining *O*-(2,3-Dihydroxypropyl) cellulose with stiff tunicate cellulose nanocrystals to increase the mechanical properties of the layer while

keeping good adhesiveness, high transparency and surface smoothness. A thin layer of tin-doped indium oxide was deposited onto the cellulose-based paper and a solar cell was then fabricated. The device thus produced showed an efficiency of 4.98%, suggesting a potential application in the fields of biodegradable and wearable electronics or optoelectronics.

Besides, the construction of organic solar cells fabricated on optically transparent cellulose nanocrystal (CNC) substrate was described [380]. In this case, the biopolymer was not deposited on glass or indium tin oxide to provide mechanical stability and conductive properties. The organic solar cells fabricated on the CNC substrates displayed a power conversion efficiency of 2.7%. Interestingly, in the latter work the possibility of disassembling the device and the recovery of the valuable material was reported. Particularly, the device was first solubilized in water to dissolve the CNC that can be hence recovered. After that, the insoluble fraction was rinsed two times with chlorobenzene, noticing that the solid residuum left was composed of Ag and MoO_3.

Furthermore, Ag nanowire (AgNW)-regenerated cellulose film (RCF) was used as substrate and anode for the production of perovskite solar cells [410]. AgNW was incorporated in order to provide the substrate with conductive properties. With the purpose of solving the loss of transparency after this incorporation, a treatment with HNO_3 was performed to increase the bonding strength between AgNWs and cellulose. The resulting solar cell exhibited good performances, showing an open circuit voltage of 1.02 V and a short-circuit current density of 9.58 mA/cm^2. Similarly, a AgNW composite with antioxidant-acid-modified chitosan was used as substrate and anode for the construction of perovskite solar cells [411]. A power conversion efficiency of 7.9%, which corresponds to nearly 75% of that of the reference device with an indium tin oxide electrode, was achieved.

Moreover, a “top-down” and green approach for the preparation of an anisotropic paper material with high flexibility and transparency was devised [412]. The anisotropic transparent paper was used as a substrate for a gallium-arsenide solar cell with a significant efficiency enhancement of 14%.

5.2. RESULTS AND DISCUSSION

This work was done in collaboration with various institutions such as three different institutes of the CNR (Italian National Research Council), namely ISOF (Institute for Organic Synthesis and Photoreactivity), IMM (Institute for Microelectronics and Microsystems), and INO (National Institute of Optics), and the engineering department of the University of Modena (UNIMORE).
The goal of this research was the development of a flexible OLED (Organic Light Emitting Diode) and a OSCs (Organic Solar Cell) with an eco-sustainable preparation methodology and with the possibility of recycling the noble metals of the electronic device through a green and efficient procedure.
In particular, our contribution as UNIFE and ISOF-CNR consisted of developing a green and sustainable method for the effective recovery and recycling of the electronic devices built on a sodium alginate layer.

5.2.1. Fully recyclable OLEDs built on a flexible biopolymer substrate

5.2.1.1. Production and characterization of OLEDs built on a flexible sodium alginate substrate

As is possible to observe from Fig. 5.1b, the electronic device is composed by a sodium alginate foil (110 μm), an anode layer constituted by an 8 nm Au film, a cathode consisting of a 0.55 mm thick LiF layer and a 100 nm thick Al film, an emitting layer (EML) formed by a 30 nm thick blend film [8 wt. % (3Z)-4-(Hydroxy-κO)-3-penten2-onato]{bis[2-(2-pyridinyl)phenyl]}iridium (Irppy2(acac)) and 92 wt. % bis-4-(Ncarbazolyl)phenyl)phenylphosphine oxide (BCPO)]. The EML was located between exciton blocking layers of 50 nm thick 4,4',4''-tris(Ncarbazolyl)triphenylamine (TCTA) and 25 nm thick 1,3,5-tris(N-phenylbenzimidazole-2-yl)benzene (TPBi).
As UNIFE and ISOF-CNR we were in charge of the preparation of the sodium alginate (SA) substrate which has been obtained by casting a 4 wt. % water solution of a pharmaceutical-grade product, used as purchased, into polystyrene Petri dishes [384] (see Paragraph 7.3.16 of Chapter 7). In order to have a more complete view of the work, the main performances of the OLEDs produced are discussed below.

However, since our contribution to this research was more focused on the recycling of the electronic device, for further details regarding the manufacture and characterization of OLEDS, it is possible to refer to the published paper regarding this work [369].

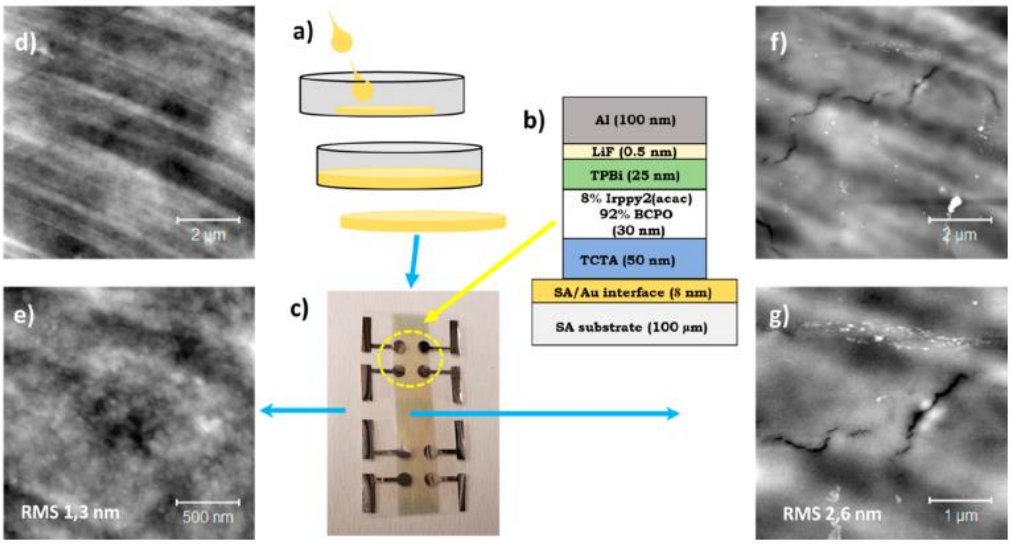

Figure 5.1: a) Scheme of the process employed to realize the freestanding SA foils. b) Layout of the device structure. c) Photograph of an array of eight OLEDs: the Au stripe and the Al pads are visible on the SA foil. d, e) AFM images of the pristine SA foil. f, g) AFM images of the Au stripe surface. The false-color z scale is the same for all of the images and is equal to 20 nm, from black to white.

In Fig. 5.1c, an array of height OLEDs is shown. The gray pads are the Al cathodes, whereas the yellow stripe is the Au anode. This stripe has been sputtered on the foil side that has been in contact with the Petri dish bottom, as by atomic force microscopy (AFM) it has been shown to be 1 order of magnitude smoother than the other [384]. Indeed, Fig. 5.1d shows that the SA surface presents some features with a maximum height of 15 nm. This is due to the fact that it is a replica of the Petri dish bottom, in which the solution has been poured. In Fig. 5.1e, a 2 × 2 μm^2 image obtained by enlarging within the stripes is reported. This area has a root-mean-square (RMS) roughness of 1.3 nm. A better control over the roughness could be achieved using a smoother mold; nevertheless, it is an acceptable value in order to grow a smooth stack of the active layers.

As described above, the anode is an Au stripe with a sheet resistance of 17 Ω/□, realized with a nominal thickness of 8 nm. This thickness value is chosen to combine a good electrical conduction and a minimum reduction of the transparency in the

visible range [413]. The Au surface exhibits a morphology similar to that of pristine SA (Fig. 5.1f,g) with a slight increase in roughness (2.6 nm, RMS). The presence of spikes, which may generate short-cut points as in the case of indium tin oxide (ITO) [414], was not observed. Very thin Au layers grown on a smooth polymeric surface such as SA, have been observed to form clusters with a preferential lateral direction [415]. Accordingly, the typical granular structure of Au films grown on hard inorganic substrates is not observed [416]. As reported elsewhere, for a thickness equal to or below 5 nm, the Au/SA interface is represented by an intermixed region, which forms during the sputtering process [417]. In this case, some cracks can be observed with a depth of below 3 nm. They form on the top of the intermixed region, where the Au film grows more homogeneously. Their presence, however, does not affect the electrical properties of the Au/SA stripe under bending conditions [384].

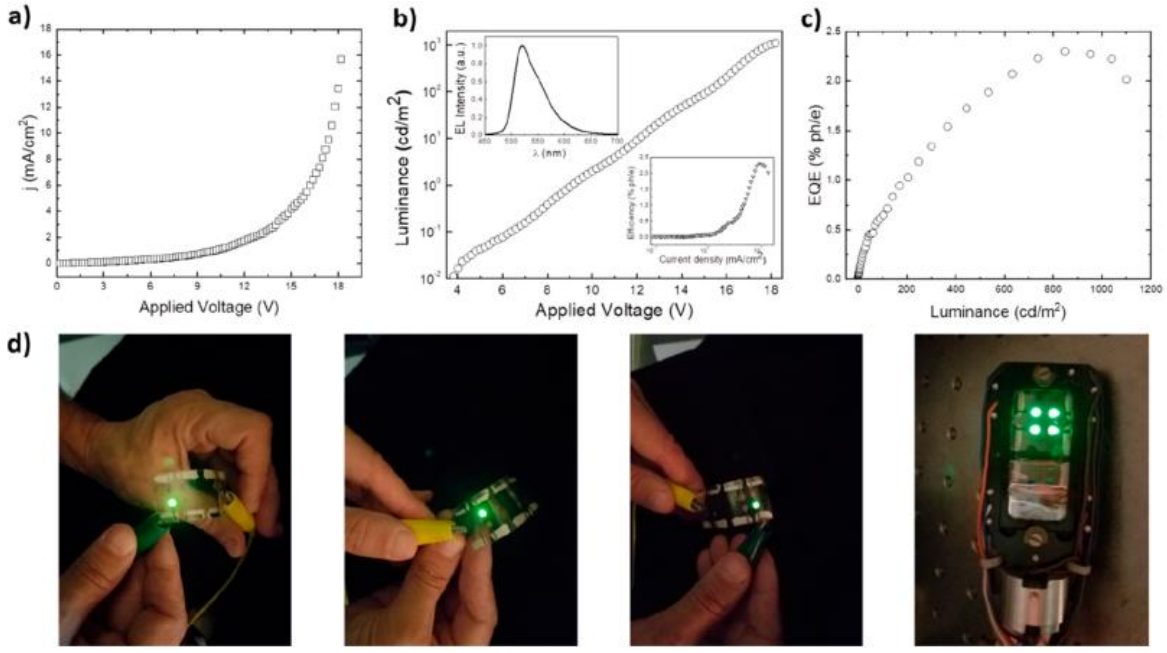

Figure 5.2: (a) Current density versus voltage curve. (b) Electroluminescence versus voltage characteristics (main panel), an external quantum efficiency versus current density curve (bottom inset), and an electroluminescence spectrum (top inset). (c) External quantum efficiency versus luminance curve. (d) Photographs of working OLEDs, operated in air and under bending conditions.

In Fig. 5.2a, a current density (*J*) versus voltage curve of a working OLED is reported. In Fig. 5.2b, the electroluminescence (EL) versus voltage curve together with an EL spectrum (top inset) and the external quantum efficiency (EQE) versus current density curve (bottom inset) are reported for the same device. As expected,

the EL spectrum reproduces the phosphorescence behavior of the emitter ($Ir(ppy)_2(acac)$). A maximum value of 1100 cd/m^2 for the luminance at 18 V and a maximum external efficiency of 2.3% at about 10 mA/cm^2 have been measured. Finally, an EQE versus luminance curve is shown in 5.2c.

5.2.1.2. Disassembly and Recycling of the OLEDs built on sodium alginate

In order to prove the concept of ambient sustainability of the electronic device described above, an original method using an eco-friendly process that allows a selective and effective recovery of all the components was devised. With the purpose of carrying out a quantification of the materials recovered, a model system that reproduces the structure of an OLED, as reported in Fig. 5.1b, but on a much larger scale was realized. The disassembly method developed is a two-step process and is based on the use of nontoxic solvents, such as water and ethanol (Fig. 5.3). Ethanol is currently available from renewable resources (i.e., bioethanol). The model system has a total active surface of 3.20 cm^2, allowing a semiquantitative evaluation of the recovery efficiency. To this purpose, the size of the SA substrate and the extension of the OLED stack area have been precisely measured. The thickness values of the Au and Al layers have been obtained through a calibration of the deposition rates as described in Paragraph 7.3.17 of Chapter 7.

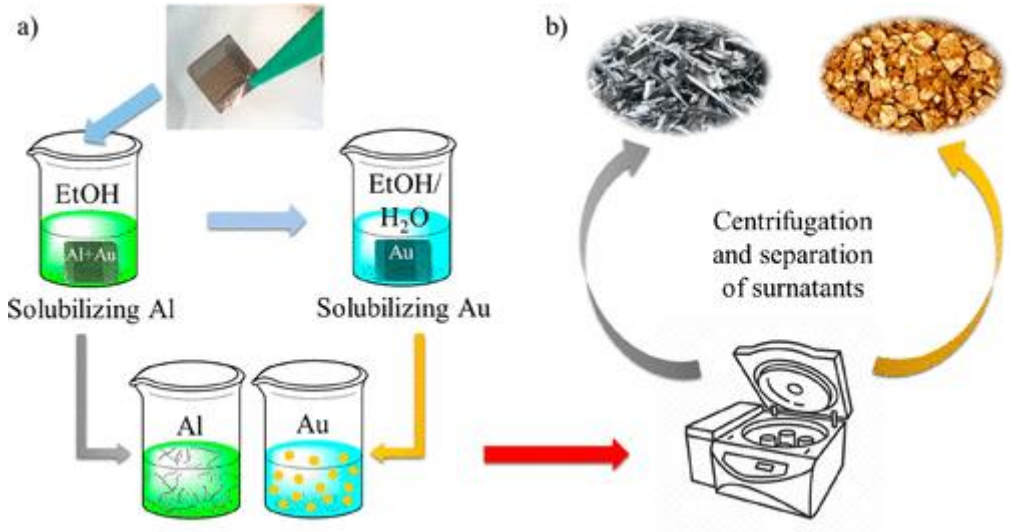

Figure 5.3: Procedure used to disassemble the device, from a) to b). The model system is first dipped into ethanol to solubilize Al and then in ethanol/water to solubilize Au. After centrifugation, the metals are finally recovered as precipitates, while the active components are solubilized in the solvents.

In the first step, the sample is dipped into 5 mL of ethanol at room temperature. Aluminum (Al) can be fully separated from the surface after 15 min of stirring with a magnetic bar or after 10 min in an ultrasonic bath (Elmasonic S40, 220–240 V, 50/60 Hz). Following this step, the SA foil with only Au left on top is withdrawn from the ethanol bath. Al and the active organic layers are thus dispersed and solubilized in the solvent, respectively.

In the second step, the Au/SA bilayer can be separated in an ethanol/water (1/2) mixture. The sample is gently shaken at room temperature for a few minutes, with the help of a clump. Au can be hence dispersed in the liquid phase, while the SA film is only slightly swollen. The ethanol/water ratio of the mixture has been optimized to promote the Au separation while the SA solubilization is minimized. A higher presence of SA in the solution would increase the viscosity and would not allow an effective recovery of Au in the following centrifugation step. Consequently, the SA film can also be entirely recovered, as it is possible to observe from Fig. 5.4b.

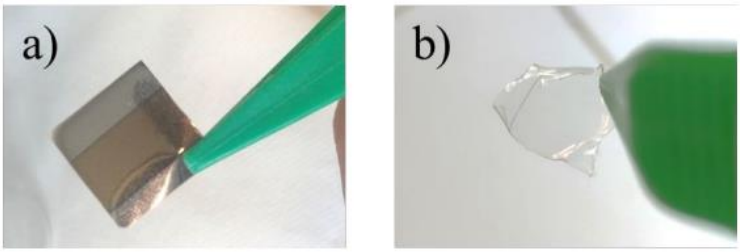

Figure 5.4: a) Photograph of the model system prepared for the disassembling test. b) Photograph of the SA layer recovered after the disassembling process.

The metals, separated in two different beakers, can be finally recovered from the two liquid phases with a centrifugation at 10000 rpm for 2 min (DIAB D30249 centrifuge), followed by decantation of the two supernatants. Al and Au are collected as precipitates on the bottom of the two tubes, dried under vacuum for 3 days, weighed, and analyzed with inductively coupled plasma–optical emission spectrometry (ICP-OES). The active organic components can be recovered from the supernatant after the evaporation of the solvents.

The values obtained have been compared with the deposited values, estimated from geometric considerations as described in Table 5.1. The data indicate that recovery

efficiencies of 77% and 87% for Al and Au, respectively, have been obtained. These results can be considered very promising, as the uncertainty in the initial amounts present on the model system is relatively high.

Table 5.1: Amounts of metals initially present in the model system (3.20 cm^2) and recovered from disassembly.

Metal	Volume occupied (mm^3)[a]	Density (g/cm^3)	Initial amount (mg)[b]	Recovered amount (mg)	Percentage recovered (%)[c]
Al	0.027	2.7	0.073	0.056	77
Au	0.00133	19.3	0.026	0.022	87

[a]Determined through measurements of the height, width and thickness of the samples. [b] Weight of the metal in the sample before the disassembling process, determined by multiplying the volume occupied for the density. [c]Weight of the metal recovered from the disassembling process, determined with ICP-OES, $ppm_{Metal} = mg_{Metal}/mL_{SOLUTION} * 10^3$; $mg_{Metal} = ppm * mL_{SOLVENT} / 10^3$.

5.2.2. Sodium alginate as a natural substrate for efficient and sustainable organic solar cells

5.2.2.1. Production and relative performances of Bulk heterojunction (BHJ) organic solar cells (OSCs) built on a flexible sodium alginate substrate.

The structure and main characteristics of the OCSs will only be briefly described in this paragraph since our contribution as UNIFE and ISOF-CNR, as previously discussed, has been focused on the development of a sustainable method to disassemble and recycle the device. In order to have a more complete view of the work, the main performances of the OCSs produced are briefly discussed below. For further details regarding the manufacture and characterization of OCSs, it is possible to refer to the published paper regarding this work [418].

As is possible to observe from Fig. 5.5a, the electronic device is composed by a sodium alginate foil (110 μm), an anode layer constituted by an ~8 nm Au film, an anode buffer layer consisting of ZnO (~ 40 nm), an active layer formed by a BHJ

blend, a cathode buffer layer of MoOx (10 nm), and an Ag cathode with average thickness of 91 nm. In total, three different BHJ blends, P3HT:$PC_{61}BM$ (1:1 wt/wt), PTB7:$PC_{71}BM$ (1:1.5 wt/wt) and PTB7-Th:$PC_{71}BM$ (1:2 wt/wt), have been used to investigate the behaviour of SA based solar cells with active layers having specific chemical, optical, morphological and electrical characteristics (Figure 5.5b). For comparison, analogous reference systems built on glass/ITO were also produced and tested. The SA substrate was prepared by using the same conditions employed for the preparation of the OLEDs described in Paragraph 7.3.16 of Chapter 7.

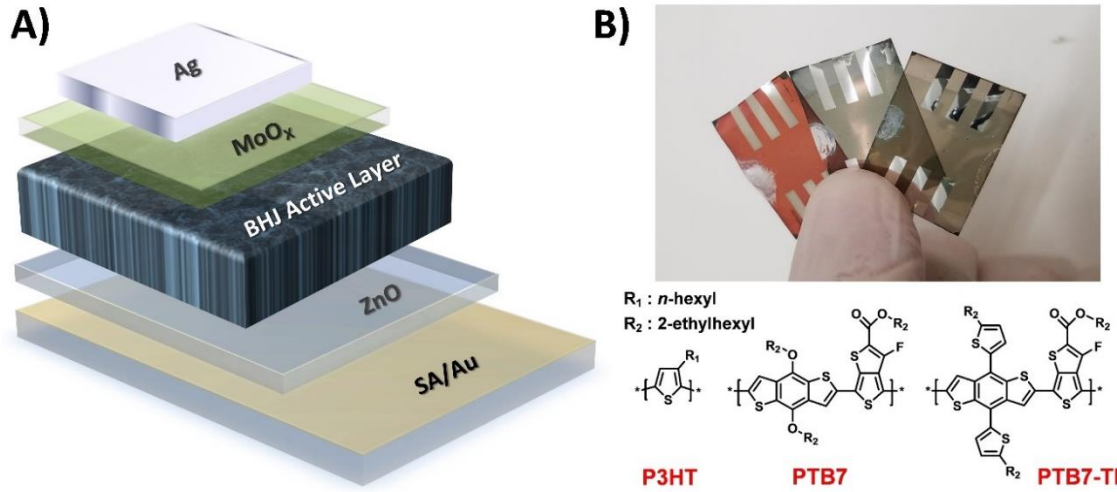

Figure 5.5: a) Device structure of SA-based inverted OSCs; b) Top: complete SA-based OSCs (from the left: P3HT:$PC_{61}BM$ (1:1 wt/wt), PTB7:$PC_{71}BM$ (1:1.5 wt/wt) and PTB7-Th:$PC_{71}BM$ (1:2 wt/wt) based devices) and, Bottom: chemical structure of the used donor materials.

In general, the photovoltaic performance of SA based OSCs were slightly lower than those obtained for analogous reference systems built on glass/ITO. Nevertheless, except for the P3HT:$PC_{61}BM$ based devices, the power conversion efficiency (PCE) reduction of PTB7:$PC_{71}BM$ and PTB7-Th:$PC_{71}BM$ devices, passing from glass/ITO to SA/Au, was lower than 20 %. This is a remarkable result if compared to similar studies on natural/bio-based substrates reported in literature [379,419]. Besides, this confirms the potential of SA substrates and in particular their excellent compatibility with solution-processed devices, allowing the effective deposition of multiple overlying layers.

The lower solar cell short-circuit density (J_{SC}) of SA based devices in comparison with the glass/ITO systems (4.1 *vs.* 7.2 mA/cm^2), should be ascribed to optical

losses due to the substrate and to the slightly different conditions of the thermal annealing employed for the production of the BHJ active layer. Indeed, the resulting films were annealed at 80 °C for 10 min in air (instead of 110 °C for 10 min used for the devices with glass/ITO as a substrate) in order to prevent possible deformations of the underlying natural support.

It was observed that the main limiting factor SA-based devices, compared to the reference ones built on glass/ITO, was represented by the J_{SC}. Open-circuit voltage (V_{OC}) and fill factor (FF) values, except some small fluctuations, remained substantially unchanged suggesting that SA/Au has almost no impact on some key related aspect, such as: *i*) energy level alignment within the device, *ii*) quality of thin-films and internal interfaces, without formation of defects and traps responsible for charge recombination/accumulation, and *iii*) charge transport/extraction efficiency within the different layers and at the electrodes, without changes of the internal resistances (series and parallel) [420].
As expected, the observed J_{SC} reduction can be mainly ascribed to the lower optical transparency of SA/Au compared to glass/ITO (average transmittance of ~ 76% and 93%, respectively); that hindering the light transmission toward the active blend, led to devices with reduced photocurrents.

Besides, a preliminary investigation on the stability of SA-based devices was conducted by monitoring the shelf-life degradation of PTB7 and PTB7-Th OSCs. For this purpose, SA-based solar cells were kept in a glove-box for 2 months (not in dark), in absence of oxygen and humidity, and then re-measured to evaluate the evolution of their photovoltaic parameters. The absence of well-known degradation agents such as water and oxygen, allowed to ascribe eventual losses mainly to morphological/chemical changes related to the SA substrate and/or to its adjacent interfaces. Interestingly, after 2 months of shelf storage the solar cells built on SA, based on both PTB7:$PC_{71}BM$ and PTB7-Th:$PC_{71}BM$ blends, showed a power conversion efficiency (PCE) drop ≤ 8%, suggesting a good device lifetime under these conditions.

5.2.2.1. Enzymatic promoted depolymerization of the sodium alginate substrate

Theoretically, the easiest and more sustainable route to separate the Au anode from the sodium alginate substrate of the OCS is to solubilize the polysaccharide in

neutral water for the recovery of the inorganic elements in solid form. However, the high viscosity of the alginate solution prevents the subsequent effective separation by centrifugation or filtration. In the OLEDs disassembly described in paragraph 5.2.1.2, the Au/SA bilayer was separated with a mixture of water and ethanol. The mixture of solvent/non solvent was optimized to promote the swelling but not the solubilization of the sodium alginate, thus avoiding viscosity issues. Nevertheless, the possibility to develop an alternative method based on the reduction of the viscosity of the sodium alginate solution by an enzymatically promoted depolymerization of the polysaccharide was explored. Alginate lyases, an enzyme able to cleave glycosidic bonds of the polysaccharide was used [421].

The cleaving condition was previously optimized and then used in the third step of disassembling a complete OCS device. With this aim, the alginate lyase depolymerization of a model solution of sodium alginate in water was first examined. In particular, the 4 wt. % sodium alginate water solution which was used to prepare the device substrate was taken as a reference. In literature, an interesting work disclosed the preparation of sodium alginate oligosaccharide through enzymatic depolymerization, describing the use of nearly 1.5 enzymatic units for a 5 wt. % water solution of 1.5 g of sodium alginate in 30 ml of water [422]. Based on this, it was estimated that for the depolymerization of 4 g of a 4 wt. % sodium alginate solution a minimum of 0,16 enzymatic units were required.

5.2.2.1.2. Experimental factorial design on the enzymatically catalyzed sodium alginate depolymerization

It must be taken into account that there are two variables involved in the enzymatic depolymerization of sodium alginate on which the attention has been focused, namely the temperature and the concentration of the enzyme. In order to examine the influence of those variables and to find the optimal experiment conditions, an experimental design was conducted. Usually, conventional methods of optimization require many experiments that are time and cost consuming. On the other hand, the response surface methodology (RSM), which is the graphical result of the experimental design, is an innovative powerful tool for the determination of the optimum reaction conditions with a consequent reduction in the number and cost of experimental tests [423].

There are different designs that can be implemented in a reaction of this type, and here is adopted the simplest one: a 2² factorial experimental design (Fig. 5.6).

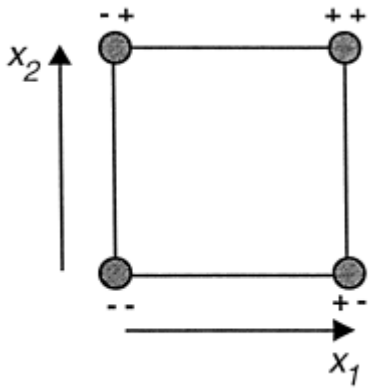

Figure 5.6: The experiments in a design with two variables (x_1 and x_2)[424].

In particular, the 2² factorial experimental design was employed considering the two independent variables mentioned above: amount of enzyme in enzymatic unit (E) and temperature (T). These variables are varied in two levels (+1, -1) and a central point (0). The chosen range of enzyme amount was between 0,1 and 1 unit while the selected temperature range was between 25 and 55 °C. Considering these variables, 5 different trials listed in Table 5.2 were planned. The response was related to the sodium alginate solution viscosity (Pa·s).

Table 5.2: 2² factorial design independent variables and their selected levels with real (in brackets) and coded values.

Run	**Coded and real variables**	
	T (°C)	**E (U)[a]**
1	-1 (25)	-1 (0.1)
2	+1 (55)	-1 (0.1)
3	-1 (25)	+1 (1)
4	+1 (55)	+1 (1)
5	0 (40)	0 (0.55)

[a]The amount of enzyme refers to the treatment of 4 g of sodium alginate solution in water at 4 wt. %.

With the purpose of selecting the appropriate reaction time, a kinetic evaluation was carried out by monitoring the viscosity of the sodium alginate solution over time after

treatment with alginate lyase. The viscosity of the solution was determined through rheological measurement under steady state conditions. The range of the shear rates examined (from 0.123 and 0,278 s^{-1}), the pre-shear given (10 s^{-1}) and the waiting time before the start of the measurement (700 s) were properly designated to conduct the analysis in the Newtonian plateau of the viscosity curve.

A kinetic evaluation was conducted under the same conditions of the central point of 2^2 factorial experimental design (run 5, Table 5.2). In Fig. 5.7 the kinetics of viscosity of the sodium alginate solution after treatment with alginate lyases are reported. Initially the reaction was monitored for 72 h (red line in Fig. 5.7) and samples were singled out after 2, 4, 6, 8, 24, 32, 48, 56 and 72 h. In this case, before measuring the sample after 2 h, the mixture was manually stirred with a metallic bar seeing that the high viscosity of the reaction media made the magnetic stirring very difficult. After the manual stirring the viscosity rapidly decreased as highlighted by the graph (Fig. 5.7) and, after 3 hours, a plateau in the viscosity was reached.

In the light of these results, the kinetic analysis was repeated under the same operative conditions except for the fact that after the enzyme addition the mixture was manually stirred with a metallic bar for 30 s (black line, Fig. 5.7). In this case the reaction was monitored over 5 h and samples were taken every 30 min. It is possible to notice that in this case the plateau is reached faster (after 1.5 h). It should be considered that in the chosen reaction time the viscosity must not reach a plateau in order to appreciate a significant variation of this parameter as a function of the variables examined. For this reason, a reaction time of 15 minutes was chosen.

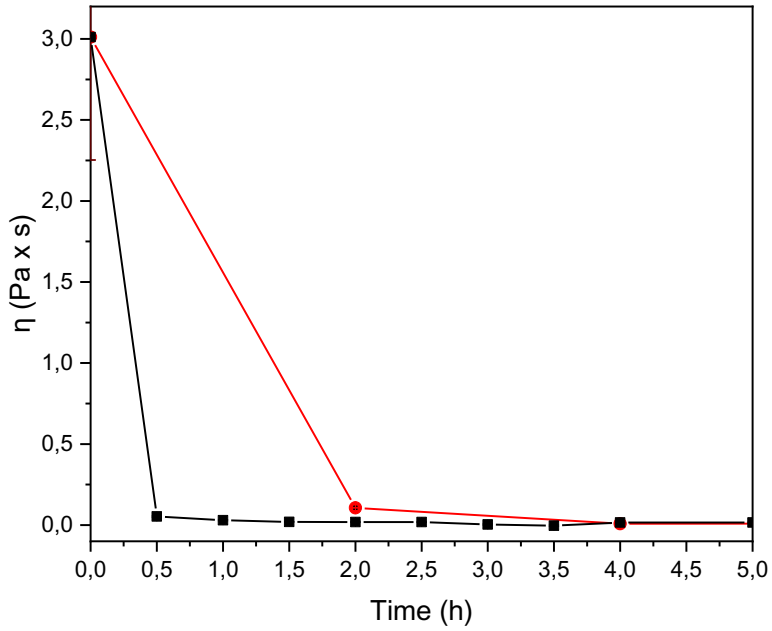

Figure 5.7: Kinetics of viscosity (η) of the SA solution at 4 wt. % in water after treatment with alginate lyases when the reaction media is manually stirred after nearly 2h (red line) or after the addition of the enzyme (black line). The viscosity reported is an average of the values at the different shear rates examined.

Since the reaction showed a fast kinetics with 0.55 enzymatic units, the chosen range of enzymatic quantity (U) for the 2^2 factorial experimental design was scaled down. Taking this into account, the new examined independent variables, their levels with real and coded values are presented in Table 5.3. All experiments were carried out in triplicate, totalling 15 experiments.

The reaction time and amount of the sodium alginate solution at 4 wt. % were fixed, respectively at 15 min and 4 g. The 2^2 factorial experimental design matrix with coded and real values and responses ((viscosity values of the sodium alginate solution)$^{-1}$ or 1/η) for the conditions tested are shown in Table 5.3. The η values for each run were determined through rheological measurements. Indeed, in Fig. 5.8 all the viscosity curves relative to the different experiments are reported. It must be taken into account that good depolymerization yields lead to lower viscosity of the final solution. As a consequence, with the purpose of determining an optimum maximum of the response, the inverse of the final viscosity (1/η) was considered. The good reproducibility of the experimental data can be observed by the low pure error ((41.01/1486.42) × 100 = 2.75%) confirming the good experimental

reproducibility of the tests, which is a consequence of the good reproducibility of the runs carried out at the central point (Table 5.3, runs 13 to 15).

Table 5.3: 2^2 factorial design variables (coded and real) and responses in terms of experimental $(viscosity)^{-1}$ of the sodium alginate solution in water.

Run	Coded and real variables		Experimental η (Pa·s)	Experimental 1/η ($Pa^{-1}·s^{-1}$)	Mean experimental 1/η ($Pa^{-1}·s^{-1}$)
	T (°C)	E (U)[a]			
1	-1 (25)	-1 (0.1)	2.07	0.48	0.46 ± 0.03
2	-1 (25)	-1 (0.1)	2.34	0.43	
3	-1 (25)	-1 (0.1)	2.18	0.46	
4	+1 (55)	-1 (0.1)	1.97	0.51	0.52 ± 0.16
5	+1 (55)	-1 (0.1)	1.46	0.69	
6	+1 (55)	-1 (0.1)	2.74	0.36	
7	-1 (25)	+1 (0.5)	0.072	13.80	15.43 ± 2.20
8	-1 (25)	+1 (0.5)	0.056	17.93	
9	-1 (25)	+1 (0.5)	0.069	14.57	
10	+1 (55)	+1 (0.5)	0.040	25.16	26.97 ± 1,87
11	+1 (55)	+1 (0.5)	0.037	26.84	
12	+1 (55)	+1 (0.5)	0.035	28.90	
13	0 (40)	0 (0.3)	0.076	13.14	17.15 ± 3.49
14	0 (40)	0 (0.3)	0.051	19.43	
15	0 (40)	0 (0.3)	0.053	18.90	

[a]The amount of enzyme refers to the treatment of 4 g of sodium alginate solution in water at 4 wt. %.

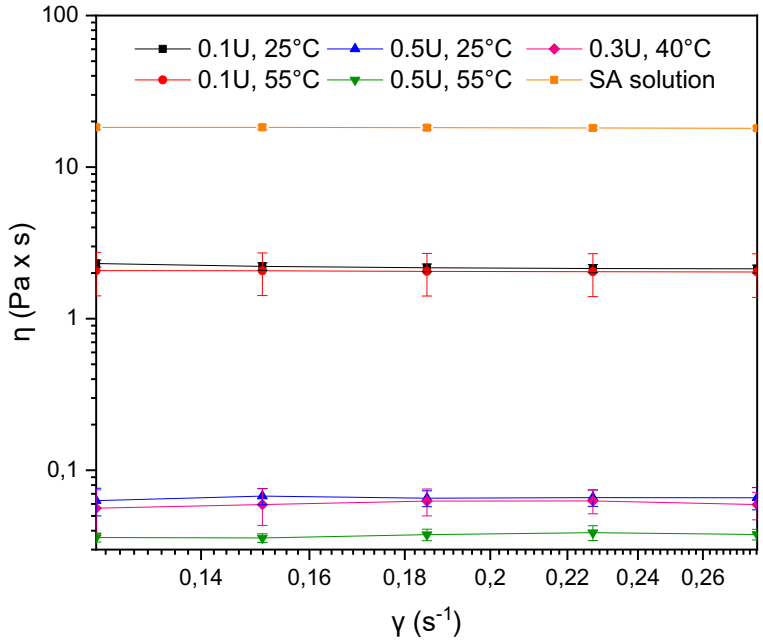

Figure 5.8: Viscosity curves as a function of the shear rate for the experiment conducted for the 2² factorial design.

With the results of the 2^2 factorial design, the estimated effect for each variable on the final viscosity was determined and reported in Table 5.5. Both the factors examined (temperature and amount of enzyme) and the interaction between temperature and amount of enzyme were statistically significant ($p \leq 0.05$) for the solution viscosity in the range analyzed.

Table 5.5: Estimated effects for the 2^2 factorial design for the optimization of the viscosity of the sodium alginate solution.

Factor	Effect	Standard Error	Calculated t	P value
Mean	12.11	0.91	13.30	$4.01\ 10^{-08}$
Temperature	2.90	1.02	2.85	0.0158
Enzyme	10.36	1.02	10.18	$6.21\ 10^{-07}$
Temperature x Enzyme	2.87	1.02	2.82	0.0168

Analysis of variance (ANOVA) was conducted in order to verify if the empirical model can reproduce the experimental data (Table 5.4). From this analysis, an *F* test was performed, which indicates whether there are significant differences between the means. The results found ($p \leq 0.05$) in this test were $F_{tabled} = 3.58$ and $F_{calculated} = 39.86$. It can be noticed that the $F_{calculated}$ is 11.1 times higher than F_{tabled}, consequently there are statistically significant differences between the averages. Additionally, the percentage of the total variance model was evaluated through the R^2, revealing a value of 91.5%. Overall, the results showed good agreement of the model with the experimental data. Moreover, the R^2 value indicated that equation 5.1 successfully explain the variability of the experimental values:

$$y_1 = 12.11 + 2.90x_1 + 10.35x_2 + 2.87x_1x_2 \qquad (5.1)$$

where y_1 is the inverse of the viscosity of the sodium alginate solution or 1/η, x_1 is the temperature and x_2 corresponds to the enzyme amount.

Table 5.4: Analysis of variance (ANOVA) of the estimated model for the optimization of the viscosity of the sodium alginate solution.

Source of variation	**Sum of squares**	**Degrees of freedom**	**Mean squares**	**F_{calc}**
Regression	1486.42	3	495.47	39.86[a]
Residuals	136.73	11	12.43	
Lack of Fit	95.72	1	95.72	23.34[a]
Pure Error	41.01	10	4.10	
Total	1623.15	14		

[a] $F_{tab0.95;3;11} = 3.58$.

The obtained statistical model (eq. 5.1) was used to describe the inverse of the predicted viscosity of the sodium alginate solution (column 4, Table 5.3) and allowed the construction of the response surface, which is illustrated in Fig. 5.9.

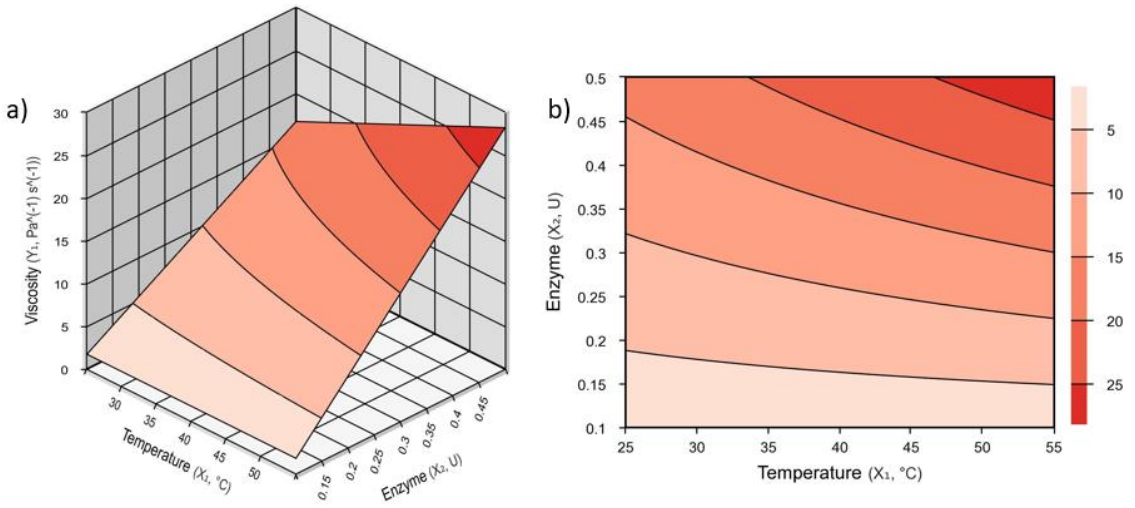

Figure 5.9: Response surface (a) and contour plot (b) for the enzymatic depolymerization of sodium alginate. Experimental conditions were described in Table 5.3. The lighter area represents the lowest 1/η (<5 $Pa^{-1}\cdot s^{-1}$) of the sodium alginate solution, whereas the darker area represents the highest 1/ η (<5 $Pa^{-1}\cdot s^{-1}$).

From Table 5.3 it can be deduced that the temperature had a moderate positive effect on decreasing the solution viscosity. With the same amount of enzyme, an increase in temperature led to higher 1/η values (run 1-3 vs 4-6 and run 7-9 vs 10-12, Table 5.3). Higher reaction temperatures increase collision of substrate molecules with the enzyme, improving at the same time the solubility of the substrates. Nevertheless, when the temperature of the tests containing the lowest amount of enzyme (0.1 U) was increased, the increment in 1/η values was moderate (run 1-3 vs 7-9, Table 5.3). Indeed, the parameter that had a significant positive effect on 1/η was the enzyme amount. This can be seen in the runs with 0.5U of alginate lyases (run 7-12, Table 5.3) that led to significantly higher 1/η in comparison with the runs conducted at lower enzyme amount (run 1-6, Table 5.3). High enzyme amount usually accelerates the reaction rate; however, the high cost of these biocatalysts usually poses a limitation on the used amount. By comparing entry 1,2,3 and 13,14,15 of Table 5.3 it can be observed that an increase in both temperature (40 °C against 25 °C) and enzyme amount (0.3U against 0.1U) had a positive effect of the final 1/η which increases from nearly 5 to 17 $Pa^{-1}\cdot s^{-1}$.

Overall, run 10,11 and 12 of Table 5.3 showed excellent 1/η values (higher than 25 $Pa^{-1}\cdot s^{-1}$), using the highest temperature (55 °C) and enzyme amount (0.5U).

Consequently, the experimental conditions of run 10,11 and 12 of Table 5.3 were tested on a simplified model of the electronic device consisting of a sodium alginate

foil over which a Au layer was deposited. Since the weight of gold can be neglected, once the device was weighed it was solubilized in an eppendorf in order to obtain a solution of SA at 4% wt. After treating the mixture with the proper amount of alginate lyases at 55 °C for 15 min, the solution was centrifuged for 10 min at 10.000 rpm. Surprisingly, under these conditions, it was not possible to separate the Au from the device due to the high viscosity of the solution (nearly 6 Pa·s). Probably in the eppendorf the sodium alginate film is not properly solubilized and diffusion issues of the enzyme arise. Further tests to investigate this phenomenon are currently ongoing. In the meantime, an additional trial was conducted duplicating the amount of alginate lyase employed (Table 5.6). In this case the depolymerization of the device substrate was efficient (0.039 Pa·s), allowing the recovery of the Au through centrifugation. If the amount of enzyme is increased there is a greater number of active sites which are able to accelerate the degradation even if the film is not properly dissolved.

Table 5.6: Trials conducted on an electronic device model.

Run	Amount of device (mg)	Amount of enzyme (µl)	Final viscosity (Pa·s)
1	50.5	31	6.2
2	51.2	64	0.039

5.2.2.3. Disassembly and recycling of the OCS device built on sodium alginate

The SA-based OCS was disassembled by an ad-hoc developed 3 steps process. The methodology aims at separating all OCS components for the quantitative recovery of the noble metals. Each step was optimized to avoid or minimize the use of toxic substances. In particular, the last step was conducted with no use of any synthetic chemical by exploiting an enzymatic promoted bioprocess in water. In the whole procedure, when possible, chemicals already produced on industrial scale from renewable resources, such as ethanol and acetic acid, have been selected in place of solvents from fossil oil and mineral acids, respectively. Besides, ammonia which is employed in the process instead of other mineral basis, is produced directly from hydrogen and nitrogen [425], which can be both obtained by sustainable processes [426].

The overall disassembling process is schematically represented in Fig. 5.10.
In the first step the electrical contacts made of Ag on a thin layer of molybdenum oxide are peeled off by sonicating the full device in ethanol, a solvent that does solubilize neither SA [413][427] nor the organic active polymers [428]. A solid powder of Ag with MoO_x was hence recovered after centrifugation. The latter was purified by exploiting the selective solubility of MoO_x under basic conditions in NH_3 [429]. The ICP-MS analysis of the residuum showed no detectable molybdenum and a good recovery of Ag (Table 5.7). Based on the inductively coupled plasma-mass spectrometry (ICP-MS) analysis of all fractions from the disassembling, it resulted that the largest loss of Ag occurred during purification from MoO_x. In fact, 5% of Ag was detected in the basic washing solution (Table 5.7). However, this value can be underestimated since some Ag could be lost because adsorbed onto the MoO_x precipitate that forms during the acid mineralization attack performed before the ICP-MS analysis.

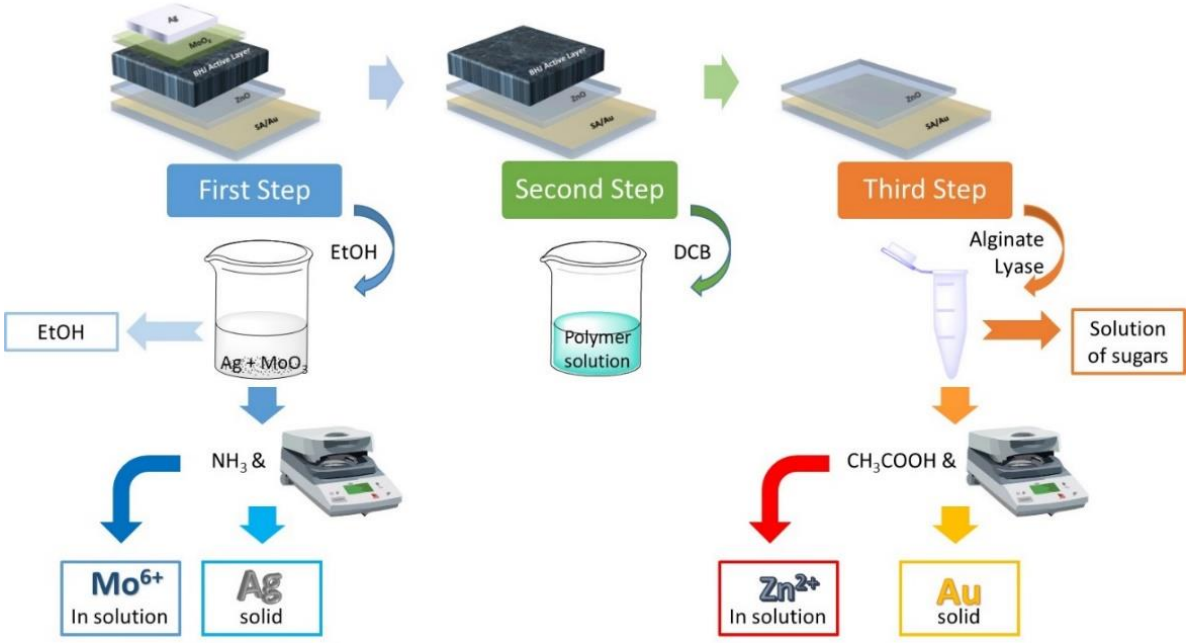

Figure 5.10: Scheme of the 3 steps disassembling process aiming at separating all components of the SA-based multilayer OCS.

The second step of the disassembling process consisted in the selective washing of the active polymer layer with the solvent used for its deposition, namely 1,2-dichlorobenzene. Unfortunately, no halogen free alternative solvent suitable to this aim exists [430]. However, the process was very effective since the amount of Ag

and Au detected in the residuum after solvent evaporation was almost negligible for both metals (Table 5.7). The last step of the disassembling process is the enzymatically catalyzed separation of Au and ZnO from the sodium alginate film (Fig. 5.10). For this purpose, the layers remaining after the second step were treated in water in the presence of the enzyme (alginate lyase). After incubation at the optimized conditions described in paragraph 5.2.2.1.1 (55 °C, 15 minutes), the viscosity of the solution is below 0.06 Pa·s and the inorganic components can be effectively separated by centrifugation. Indeed, after washing the precipitate with an acetic acid solution to leach out the ZnO [431], ICP analysis revealed a quantitative recovery of gold (Table 5.7). The recovery percentage higher than 100% is due to the uncertainty in the initial amounts of present on the device. Furthermore, no zinc was detected as impurity in gold. Zinc was detected in both the water solution with the depolymerized alginate and the leaching acid solution.

Table 5.7: Ag, Au, Mo and Zn amount by ICP-MS analysis of the fractions from the disassembling process sketched in Fig. 5.10 and the corresponding recovery ratio, calculated with respect to the metal amount in the device.

Sample	**Au (μg)**	**Recovery (%)**	**Ag (μg)**	**Recovery (%)**	**Zn (μg)**	**Recovery (%)**	**Mo (μg)**	**Recovery (%)**
Ag	0.2	0.7	69.2	80.5	0	-	0	-
Mo^{6+} solution	0	-	4.6	5.4	0	-	0.92	32.7
EtOH	0	-	1.5	1.8	0	-	0.29	10.3
Residuum DCB	0.2	0.2	0.2	0.2	0	-	0	-
Au	29.5	108.5	0.5	0.6	0	-	0	-
SA solution	0.2	0.7	0.1	0.1	8.17	12.3	0.12	4.3
Zn^{2+} solution	< 0.1	0.1	0	-	4.97	7.5	0	-
Total	29.9	110.2	76.1	88.6	13.1	20%	1.33	47%

5.3. CONCLUSION

In summary, in this work, the use of sodium alginate to realize transparent, flexible, and ready to use freestanding substrates for electronic devices was reported.

Sodium alginate allows to solve the planarization and stability limitations of other natural materials, the use of which has been proposed in green electronics and optoelectronic applications.

In particular, an OLEDs operating under bending conditions, built directly on top of a freestanding sodium alginate foil was successfully realized for the first time. The electroluminescence (EL) performances of the device thus produced are comparable with those of the best biopolymer OLEDs reported in literature (maximum value of 1100 cd/m^2 for the luminance at 18 V and a maximum external efficiency of 2.3% at about 10 mA/cm^2). A recovery of nearly all of the valuable materials can be obtained through the use of an environmentally safe disassembly method, thus avoiding the production of electronic or chemical waste. The two-step procedure developed is based on the use of nontoxic solvents, such as water and ethanol. In the first step the OLED is dipped into ethanol to recover the organic layers solubilized in the solvent and the Al cathode after centrifugation of the solution. In the second step, the remaining device is immersed in ethanol/water (1/2) mixture, where the SA is slightly swollen and the Au is dispersed in the liquid phase. Considering that a higher presence of SA in the solution would increase the viscosity and would not allow an effective recovery of Au through centrifugation step, the ethanol/water ratio of the mixture has been optimized to promote the Au separation minimizing the SA solubilization at the same time.

In addition, sodium alginate was exploited for the preparation of flexible, efficient and stable solution-processed (organic solar cells) OSCs. These devices disclosed showed PCE values up to 7.2%, compared to 8.5% obtained for analogous structures built on glass/ITO substrates. Even in this case a disassembly procedure to separate and recover all the components has been disclosed. The methodology has been designed with the objective of avoiding or reducing as much as possible the use of toxic and hazardous substances as well as the use of chemicals produced from fossil sources. The device is dipped in different solvents capable of selectively solubilizing specific components of the OCS. However, in this case, the Au anode was not separate from the SA foil by immersion in an ethanol/water mixture but an alternative method based on the enzymatic promoted depolymerization of sodium alginate in water was devised. As an enzymatic catalyst, alginate lyases, an enzyme able to cleave glycosidic bonds of the polysaccharide, was selected. The cleaving conditions were previously optimized on a model system, consisting of a SA solution in water at 4 wt. %. Particularly, a 2^2 factorial experimental design was employed to

evaluate the effect of temperature and enzymatic catalyst amount on the final viscosity of the SA solution. Probably due to an incomplete solubilization of the SA films that causes diffusivity issues, unsatisfactory results were achieved when the optimized conditions were employed in the third step of disassembling a complete OCS device. Nevertheless, to obtain an efficient SA depolymerization it was sufficient to duplicate the amount of alginate lyases employed.

Chapter 6

General conclusions

This Chapter will not enter into the specific conclusions of each previous Chapter but it will try to provide the reader with a broader conclusion on the work done in this PhD thesis. Overall, in this work, green water-based methodologies for the process of biodegradable and biobased polymers for coating and electronic applications were successfully developed.

As regard the application potential of the polyester dispersions in the coating sector and in polymer blend preparation, the formulations containing a non-ionic surfactant, like SYN, revealed to be more efficient in comparison to the one bearing an anionic surfactant such as SDS. This is probably due to the fact that the anionic charge on the polymer particles provided by SDS creates an electrostatic repulsion among the particles that limits the compatibility at the interface with other polymers as well as the merging for the formation of a continuous film.

In this PhD thesis, the PLA aqueous formulations developed were added both with xanthan gum (green route, Scheme 6.1), in order to obtain formulations to coat paper substrates, and with PVA (blue route, Scheme 6.1) to produce polymer blends with better mechanical properties. Both the addition of xanthan gum (Chapter 3) and PVA (Chapter 4) to the PLA formulations (PLA_SDS and PLA_SYN) caused an increase of the viscosity of the system, thus rendering the formulations suitable for coatings onto porous substrates. However, when xanthan gum is used as a thickening agent it is possible to achieve higher viscosity ranges (1-10 Pa·s at a shear rate of $1s^{-1}$) with smaller additions (from 0.05 to 0.75 wt. %). On the contrary, with the addition of PVA (from 25 to 75 wt. %) viscosities between 0.2 and 2 Pa·s at a shear rate of 0.1 s^{-1} are achieved. The steady shear properties determined through rheological analysis, revealed that PLA/XG latexes display a shear-thinning behavior, while the PLA/PVA ones show an almost Newtonian trend over the shear rate examined. For the use as coatings, depending on the optimal viscosity of application required in the coating process, this difference in rheological behavior could be exploited. Even though some PLA/PVA formulations exhibit a proper viscosity to allow the coating on paper, the latter were not applied for this purpose due to the poor barrier properties against liquid water that PVA possesses.

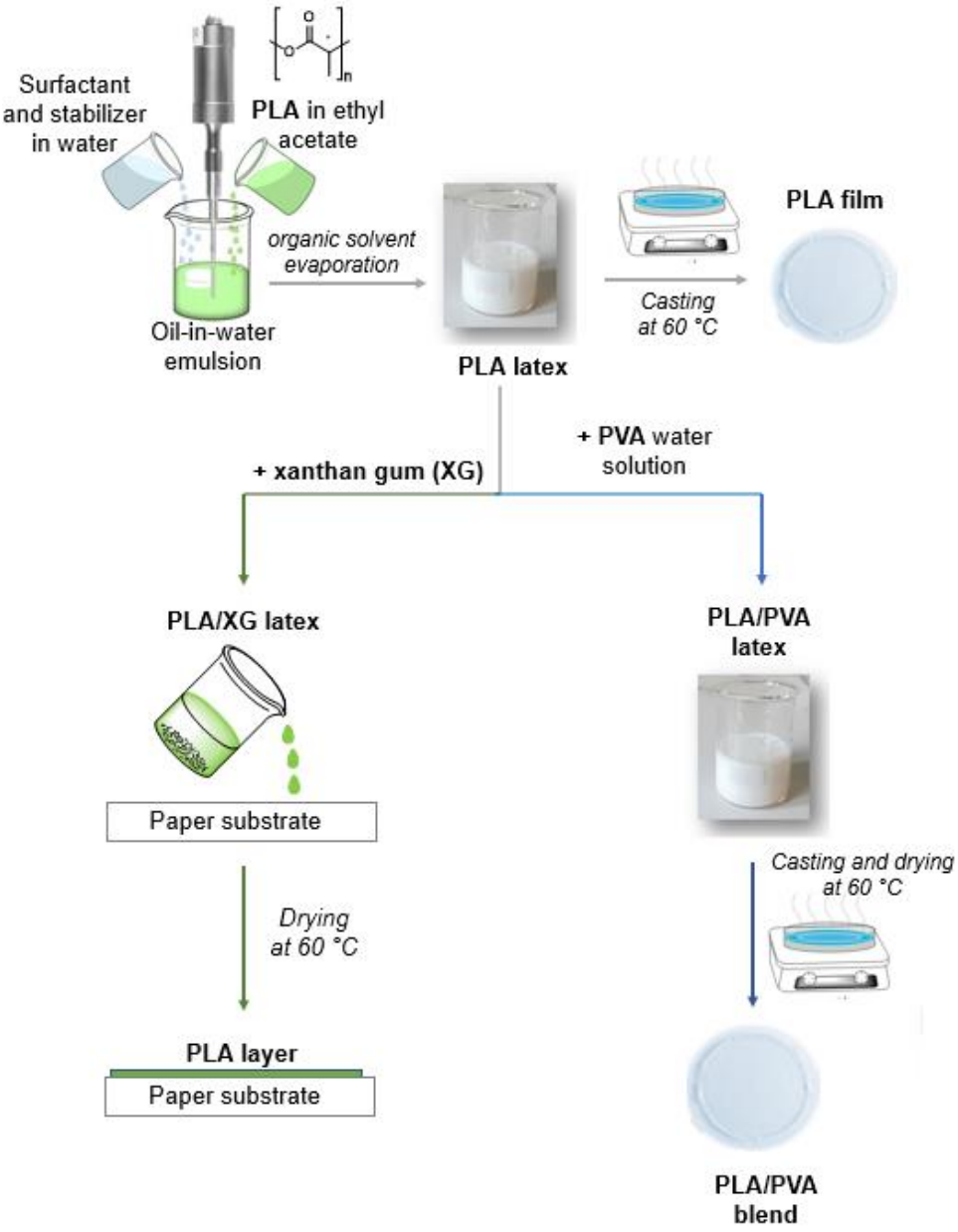

Scheme 6.1: Scheme of the preparation of aqueous dispersion of PLA and PLA films (grey route) and scheme of the addition of both xanthan gum (green route) and PVA (blue route) to the PLA dispersions for the obtainment of formulations to coat paper substrates and PLA/PVA blends, respectively.

Nevertheless, if oxygen barrier properties are requested, the inclusion of PVA in the PLA latex could represent a valid strategy for the preparation of gas resistant coatings. Moreover, the presence of a submicrometric dispersed structure in the PVA matrix could translate into an improvement of the PVA oxygen properties.

For future studies, other biopolymer soluble in water could be added into the PLA dispersions in order to obtain polymer latexes suitable as barrier coatings. For instance, whey-protein and chitosan could be promising candidates, considering that in some works present in literature, they improved the paper packaging performances showing good gas barrier properties and resistance to grease [432][248].

In the PLA/PVA blends, the submicrometric phase of PLA acted as a reinforcement in the continuous PVA matrix, increasing the rigidity and deformability of the system. In comparison with the PLA films, the greater mechanical properties of the PLA/PVA layers make the formulations more suitable for coatings for rigid rather than flexible packaging.

As regards the development of a water-based process to produce bio-based and biodegradable substrates for electronic devices, successful results were obtained through casting a sodium alginate water solution. The freestanding sodium alginate foils thus realized were used to build organic light emitting diodes (OLEDs) operating under bending conditions and flexible, efficient and stable solution-processed organic solar cells (OSCs) (Scheme 6.2).

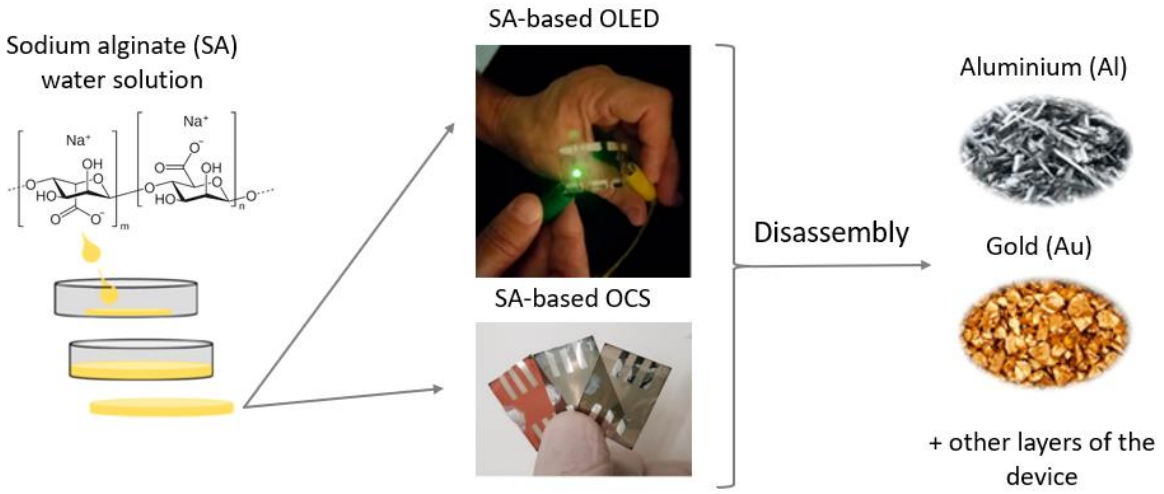

Scheme 6.2: Production and disassembly of OCSs and OLEDs built on a sodium alginate substrate.

Furthermore, a disassembly procedure to separate and recover all the components of the electronic devices has been developed, thus avoiding the production of electronic or chemical waste. In the OLED disassembly, though a solubilization step

in a mixture of ethanol and water, the valuable metals are recovered together with the swollen sodium alginate substrate. On the other hand, in the OCS disassembly, the sodium alginate is completely solubilized in water after a step of enzymatically catalyzed depolymerization.

In conclusion, the results reported in this PhD thesis open up new opportunities for the preparation of aqueous polyester coatings formulations and blends through green and eco-friendly methodologies. Moreover, the results achieved constitute an important tool for the fabrication of flexible electronic devices with a bio-based and biodegradable structure for an environmentally sustainable circular economy.

CHAPTER 7

Experimental section

7.1. Materials

Polylactic acid Ingeo PLA 4060D (PLA) was supplied by NatureWorks LLC (Minetonka, MN). PLA 4060D is an amorphous polymer with a L-lactide content around 88 wt. % and a weight-average molecular weight (M_w) of 1.15 × 10^5 g/mol [433]. Sodium dodecyl sulfate, sodium carboxymethylcellulose (NaCMC), Tween 80, Tween 20, stearoyl-2-lactylate (SSL) and Span80 were purchased from Sigma-Aldrich. Starch C*Icoat 07525 (starch) and xanthan gum Satiaxane CX 2 QD (XG) were provided by Cargill Deutschland GmbH. A solution of starch at 3 wt. % in ultrapure water was prepared by heating under reflux 6 g in 200 ml for nearly 1 hour. Synperonic™ PE/F68 (SYN) was generously supplied by Croda Chemicals. Metolad 368 (Met. 368), Metolad 388 (Met. 388), Leukonol LB-2 (Leu.) and Tafigel AP 15 (Taf.) were kindly provided by Münzing Chemie GmbH. Microfibrillated cellulose MFC Exilva F 01-L (MFC) was kindly supplied by Borregaard. Pharmaceutical grade sodium alginate was supplied by Farmalabor Srl (BT, Italy). Alginate lyase powder (≥10,000 units/g solid) was purchased from Merck (Merck, Darmstadt Germany). Ethyl acetate (purity ≥ 99.5%), acetic acid (ReagentPlus >99%), ammonium hydroxide solution (NH_3), (ACS reagent 28-30%). 1,2-dichlorobenzene (ReagentPlus 99%) and ethanol (99.8%) were purchased from Sigma-Aldrich and used without further purification. Poly(vinyl alcohol) POVAL 6-88 (PVA 6-88) and POVAL 4-88 S2 (PVA 4-88) grades were supplied by Kuraray Chemical. Poly(vinyl alcohol) Gohsenol GH-17 R (PVA GH 17R) solution in water at 12 wt. % was supplied by Mitsubishi Chemicals Performance Polymers.

7.2. Instruments, devices and analysis methods

As coating devices for the tests conducted in Chapter 3, a quadruple film applicator with width of 60 mm and gap clearances of 30, 60, 90, 120 μm supplied by ERICHSEN GmbH & Co. KG (Hemer, Germany) and threaded rods of different diameters were available. The characteristics of each threaded rod are listed in the Table below (Table 7.1).

Table 7.1: Diameter, distance between threads and thread height of the threaded rods available.

Threaded rod size	Diameter (mm)	Distance between threads (mm)	Thread height (mm)
S	3	0,9	0,37
M	4	0,9	0,57
L	5	1,2	0,86
XL	7	1,6	1,1
XXL	10	2,1	1,3

To weigh the starting materials Entris Sartorius and Sartorius BP61S laboratory balances were used. To prepare solutions and mixtures, IKA magnetic stirrer RCT basic was employed. Ultrapure water was produced with Millipore Direct-Q 3UV.

For homogenization of oil and water phases during the emulsification process for the preparation of aqueous polyester dispersions, Ultrasound Hielscher® Up200St (UH) equipped with a 14 mm diameter probe, Vibra-Cell™ Ultrasonic Liquid Processors VCX750 (UVC) provided with a 13 mm diameter probe and IKA ULTRA-TURRAX® T 25 basic (UT) equipped with a S 25 N - 18 G dispersing tool were used.

Emulsions and dispersions were stirred with an overhead stirrer Argo Lab AM20-D equipped with PTFE blade.

The residual amount of EtOAc present in the emulsion was quantitatively determined by gas chromatography/mass spectroscopy analysis (GC/MS). A triple quadrupole GC/MS instrument from Agilent Technologies (Agilent Technologies, Inc., Santa Clara, CA, USA) equipped with a 20 × 0.18 mm, 0.18 µm column was employed, using hydrogen at 0.8 mL/min as carrier gas with a 10:1 split ratio. For the analysis, 100 µL of the emulsion was added to a 20 mL chromatography vial and incubated at 85 °C for 30 min for head-space extraction. The GC oven was programmed at 40 °C for 3 min, followed by a stepped increase of 10 °C min^{-1} to 50 °C, where it was held for 5 min, and then the temperature was increased by 30 °C/ min to 230 °C/min, where it was held for 3 minutes. The quantitative determination of EtOAc traces was conducted by using the selected ion monitoring (SIM) at the

m/z values 88/73. Calibration was performed by injecting solutions of EtOAc in N, N- dimethylacetamide at known concentrations into the GC/MS instrument.

A Perkin Elmer Lambda 650 UV–Vis spectrophotometer was used to record the transmittance of free-standing PLA films produced from the aqueous polymer dispersions, as described in Paragraphs 2.2.7 and 2.2.8 of Chapter 2. Measurements were accomplished in transmission mode. Film thickness was measured with an electronic outside micrometer able to perform measurement between 0.001 and 25 mm.

The diameter of the polymer particles was determined by dynamic light scattering (DLS) analysis at 25 °C using a NanoBrook Omni Particle Size Analyser (Brookhaven Instruments Corporation, USA) equipped with a 35 mW red diode laser (nominal 640 nm wavelength) and BI-SCP cell in backscattering (173 °). In order to give reliable results, dilute suspensions (0.15 % v/v) were analysed. For data elaboration, the reflective index of the dispersion medium and of the dispersed phase were assumed to be 1.330 and 1.596, respectively. Each measurement was repeated 5 times on the same sample and the reported data were the average over the five measurements. The standard deviation δ (equation 7.1) was assumed as data error, where N is the number of measurements, x_i the value of the i^{th} measurement and μ the arithmetic mean. All the DLS data were analysed by a multimodal function. Particles were assumed to be uniform spheres.

$$\delta = \sum_{i=1}^{N} \frac{\sqrt{(x_i - \mu)^2}}{\sqrt{N - 1}} \qquad (7.1)$$

The Z-potential of the PLA_SDS dispersion was determined by Phase Analysis Light Scattering (PALS) at 25 °C using a NanoBrook Omni Particle Size Analyser (Brookhaven Instruments Corporation, USA) equipped with a 35 mW red diode laser (nominal 640 nm wavelength). The analyses were carried out on samples at 0.25 wt. % and the reported data are the averages over five repeated measurements.

Size-exclusion chromatography (SEC) analysis were performed with a Jasco (Jasco Europe srl, Cremella, Italy) instrument comprising a PU-2089 Plus quaternary pump and injector with a 20 mL loop, two in series PLgel MIXED-D columns (Agilent

Technologies Italia S.p.A., Cernusco sul Naviglio, Italy; linearity range 200 to 2,000,000 g/mol based on polystyrene equivalent) placed in a Jasco CO-2065 column oven set at 30 °C, a Jasco RI-2031 Plus refractive index detector, and a Jasco UV-2077 Plus multi-channel UV-Vis detector. The samples in the form of films or powders were dissolved in trichloromethane (HPLC grade Sigma-Aldrich) with the aid of sonication and filtered through a 0.2 mL pore size PTFE filter to remove the insoluble fraction before injection as 5 mg/mL solutions; elution was performed with trichloromethane at 1 mL/min flow rate. The ChromNav Jasco software was used for data acquisition and analysis based on a calibration curve obtained by running a set of four monodisperse polystyrene standards (19,000, 50,000, 233,000, and 300,000 g/mol, respectively) and performing a 4^{th} order fit.

Differential scanning calorimetric analysis was conducted on a DSC 8000, PerkinElmer Inc. USA instrument equipped with IntraCooler II cooling device and Pyris software for instrument control, data acquisition and analysis. The instrument was calibrated in temperature and energy with high-purity indium and lead as standards. 3-10 mg of sample were analyzed in aluminum pans under dry nitrogen atmosphere (30 mL/min).

Scanning electron microscopy analysis (SEM) was accomplished with a Zeiss EVO 40 microscopy equipped with a LaB6 source. Samples in the form of powder or film were gold sputtered before observation. Film sections were obtained by fracture in liquid nitrogen.

FT-IR spectra were recorded on Agilent Cary 630 FTIR spectrophotometer with ZnSe ATR element. Background and sample spectra were collected by accumulating 32 scans.

The rheology measurements were performed with Anton Paar MCR 102 Rheometer, equipped with a cone-plate geometry CP50-1 (49,975 mm of diameter) probe and Anton Paar software for data acquisition and analysis. A solvent reservoir was attached to prevent the sample from drying.

For the determination of the hydrolysis degree of the different PVA types employed in Chapter 4, the ^{1}H-NMR spectra of the three different polymers were recorded on Varian Mercury Plus 300 in D_2O at room temperature.

7.2.1. Characterization methods

The dispersions' stability was assessed through visual criteria and DLS analysis both after the preparation and after 1 week. Dispersions were assumed stable if no phase separation was observed and if the particle size variation was lower than the standard deviation on the particle size value.

For the samples described in Chapter 2, The dry residuum of each dispersion was determined after heating the sample at 200 °C for 30 minutes in the oven, while for the samples described in Chapter 3, the dry residue (C_X) was determined by drying 250 mg (w_{TOT}) of sample in an oven at 200 °C for 20 minutes, followed by weighing (w_{dry}) (equation 7.2):

$$C_X = \frac{w_{dry}}{w_{TOT}} \cdot 100 \qquad (7.2)$$

When DSC analysis was conducted on the samples described in Chapter 2, the latter were at first heated up from 25° C to 200 ° C to erase the thermal history and to remove any trapped volatile substance such as residual solvents. After that, samples were cooled down to -70 °C (cooling step), maintained at -70 °C for 5 minutes and finally heated up again to 200 °C (second heating step). As regards the sample of Chapter to containing PBSA, the maximum temperature was fixed at 170 °C instead of 200 °C. When DSC analysis was conducted in the samples described in Chapter 3, samples were at first heated up from 25° C to 200 ° C to erase the thermal history and to remove any trapped volatile substance such as residual solvents. After that, samples were cooled down to -70 °C (cooling step), maintained at -70 °C for 5 minutes and finally heated up again to 200 °C (second heating step). For the DSC analysis of the PVAs available employed in Chapter 4, the samples were first heated up from 25 to 220 °C to erase the thermal history and to remove any trapped volatile substances. After 2 min at 200 °C, samples were cooled down to 0 °C (cooling step), maintained at 0 °C for 2 min and finally heated up again to 240 °C (second heating step). On the other hand, for the DSC analysis of the PLA/PVA blends, the samples were first heated up from 0 to 170 °C to erase the thermal history and to remove any trapped volatile substances. After 1 min at 170 °C, samples were cooled down to -50 °C (cooling step), maintained at -50 °C for 2

min and finally heated up again to 170 °C (second heating step). In all the analysis, the heating and cooling steps were all performed at 10°C/min.

The density of the emulsions and solutions described in Chapter 3 was determined by measuring the weight of a precise volume of sample (2-5 mL) in a controlled temperature system. Each measure was repeated ten times, and the data was taken as an arithmetic average value on the calculated density. Data error was calculated as standard deviation.

As regards the rheology measurements performed in Chapter 3, steady shear experiments were performed at 25 °C by recording the flow curves in the range of shear rates from 1 to 1000 s^{-1}. Each measurement on a given sample was repeated at least three times and an arithmetic mean was performed on the collected data. The error was calculated as standard deviation. Before each oscillatory measurement, a pre-shear at 100 s^{-1} for 60 s followed by a 300 s rest was applied to erase the effect of loading. Amplitude oscillatory sweep tests were performed in order to determine the linear viscoelastic range (LVR). The viscoelastic response in the strain range from 0.01 to 200 % was measured at ω=1 rad s^{-1}. Frequency sweep tests were performed at a strain amplitude within the previously determined linear viscoelasticity range. Each measurement on a given sample was repeated at least three times and an arithmetic mean was performed on the collected data. The error on the viscoelastic moduli was calculated as standard deviation. Further elaboration of the collected data was performed with the OriginPro 2018 software. The rheological measurements of the PVA types available and the PLA/PVA aqueous dispersions (Chapter 4) were performed at 25 °C by recording the flow curves in the range of shear rates from 0.1 to 1000 s^{-1}. Before each measurement a pre-shear at 100 s^{-1} for 60 s followed by a 120 s rest was applied to erase the effect of loading. When PLA/PVA dispersions were analyzed a water reservoir was attached to prevent samples from drying. Each measurement on the PLA/PVA formulations was repeated three times and the arithmetic mean was calculated on the collected data. The error was calculated as standard deviation. As regards the rheology measurements of the sodium alginate solutions viscosities (Chapter 5), steady shear experiments were performed at 25 °C by recording the flow curves in the range from 0.123 and 0,278 s^{-1}. Before each measurement a preshear at 10 s^{-1} for 60 s followed by a 700 s rest was applied to erase the effect of loading. The majority of the measurements on a given sample was repeated at least three times and an

arithmetic mean was performed on the collected data. The error was calculated as a standard deviation.

7.3. Preparation procedures

7.3.1. Preparation of PLA dispersions with sodium dodecyl sulfate as surfactant and starch as stabilizer

6.47 g of starch water solution at 3% conc. was diluted with 28.5 mL of ultrapure water (starch conc. 0.5 wt.%) and 0.28 g of SDS was added (SDS conc. 0.8 wt.%). In the meantime, 5 or 7 g of PLA was solubilized in 45 or 87.5 mL of ethyl acetate (EtOAc) (11 or 8 wt./vol.%, respectively) under vigorous stirring for 4 h at room temperature. After that, proper amounts of the oil and water phases were mixed, in an ice bath, with the use of a homogenizer to obtain the emulsions. Different tests were carried out by changing the volume ratio between the two phases as well as the total phase volume (entries 1–13, Table 2.1 of Chapter 2). For homogenization, ULTRA-TURRAX (UT) or two different ultrasound probes (UVC and UH) were tested. Homogenization conditions were as follows: (a) UH for 30 s at amplitude 50% + 1 min 30 s at amplitude 80%; (b) UVC for 30 s at amplitude 50% + 2 min of overhead stirrer at 200 rpm + (30 s at amplitude 90% + 2 min of overhead stirrer at 200 rpm) three times; (c) UT for 1 min 30 s at 1100 rpm. Afterwards, the resulting emulsions were stirred for 20 h at room temperature and 200 rpm under the aspiration of a laboratory hood (suction speed: 0.5 m/s). A similar procedure was adopted in tests of entry 11 and 12 in Table 2.1 except that the amount of the starch solution used was 0.38 g (starch conc. 1.1 wt.%) in test 11 and the amount of SDS employed in test 12 was 0.10 g (SDS conc. 0.3 wt.%).

7.3.2. Preparation of PLA dispersions with SDS and different polysaccharides as stabilizers

Different amounts of starch, MFC or XG and 0.28 g of SDS were solubilized in 35 mL of ultrapure water (Table 2.2 of Chapter 2). In the case of MFC, the polysaccharide suspension was treated with UT at 10000 rpm for 4 min before addition of SDS. In the meantime, 5 g of PLA was solubilized in 45 or 62.5 mL of

EtOAc (11 or 8 wt./vol.%, respectively) under vigorous stirring for 4 h at room temperature. After that, the oil and water phases were mixed together, in an ice bath, with the aid of the UVC homogenizer [30 s at amplitude 50% + 2 min of overhead stirrer at 200 rpm + (30 s at amplitude 90% + 2 min of overhead stirrer at 200 rpm) three times]. Afterwards, the resulting emulsion was stirred for 20 h at room temperature at 200 rpm under the aspiration of a laboratory hood (suction speed: 0.5 m/s).

7.3.3. Preparation of PLA dispersions with different surfactants than SDS

The proper amount of emulsifier was solubilized into 35 mL of ultrapure water. In the case of the presence of starch as stabilizer in the formulation, the 35 mL included 6.47 g of starch solution at 3% conc. (starch conc. 0.5 wt.%). The type of surfactant employed and its concentration in the water phase are listed in Table 2.3 of Chapter 2.

Moreover, 5 g of PLA was dissolved in 45 mL of EtOAc under vigorous stirring for 4 h at room temperature. When Span 80 was employed as surfactant, the latter was solubilized in the organic phase together with PLA. After that, the oil and water phases were mixed together and homogenized while standing in an ice bath to obtain the emulsions. Homogenization was carried out with UH or UVC ultrasound homogenizer under conditions “a” or “b” mentioned in Paragraph 7.3.1, respectively. Afterwards, the resulting emulsions were stirred overnight at 200 rpm under the aspiration of a laboratory hood (suction speed: 0.5 m/s).

7.3.4. Preparations of PLA films from dispersions

1.7–3.0 g of PLA dispersions prepared under the condition of entry 3, Table 2.1 of Chapter 2 (PLA_SDS) or entry 4, Table 2.3 of Chapter 2 (PLA_SYN), were transferred into a PTFE capsule (diameter 3.7 cm) and allowed to dry for 2–3 h at the selected temperature until solidification occurred. The drying temperature was room temperature and then the latter was gradually increased by 10 °C starting from 40 up to 110 °C.

7.3.5. Preparation of PBSA dispersions with sodium dodecyl sulfate as surfactant and starch as stabilizer

6.47 g of starch solution at 3% conc. was diluted with 28.5 mL of ultrapure water (starch conc. 0.5 wt.%) and 0.28 g of SDS was added (SDS conc. 0.8 wt.%). In the meantime, 5 g of PBSA was solubilized in 45 mL of dichloromethane (DCM) (11 wt./vol.%) under vigorous stirring for 4 h at room temperature. After that, the oil and water phases were mixed, in an ice bath, with the use of a UVC homogenizer [30 s at amplitude 50% + 2 min of overhead stirrer at 200 rpm + (30 s at amplitude 90% + 2 min of overhead stirrer at 200 rpm) three times] to obtain a PBSA emulsion. Afterwards, the resulting emulsion was stirred for 20 h at room temperature at 200 rpm under the aspiration of a laboratory hood (suction speed: 0.5 m/s).

7.3.6. Preparations of PBSA films from dispersions

1.7–3.0 g of PBSA dispersions prepared under the condition described in Paragraph 7.3.5, was transferred into a PTFE capsule (diameter 3.7 cm) and allowed to dry for 2–3 h at the selected temperature until solidification occurred. The drying temperature was room temperature and then the latter was gradually increased by 20 °C starting from 60 up to 120 °C.

7.3.7. Preparation of water dispersions of PLA at 200 g scale

A 3 wt. % solution of starch in ultrapure water was prepared by heating at a reflux temperature for 1 h. About 51.8 g of this solution was diluted to 280 g with ultrapure water and then 2.24 g of SDS was added. Meanwhile, 40 g of PLA was solubilized in 360 mL of ethyl acetate under vigorous stirring for 4 h. After parting both the oil and the water phases each in 8 equal fractions, 8 equal mixtures were prepared by mixing one to one the oil and of the water phases, followed by homogenization and ultrasound treatment (Vibra-Cell Ultrasonic Liquid Processor VCX750, maximum power output: 750 W, equipped with a 13 mm diameter probe) in four continuous steps of 30 sec each. The power amplitude was 50% in the first step and then 90%. Steps were spaced out by 2 min during which the mixture was kept under mechanical stirring with an overhead stirrer. Each one of the resulting emulsions

was separately collected in a 2 L reactor and the organic solvent, ethyl acetate, was distilled off at 40 °C and 0.85 bar for 4 h while keeping the emulsion under stirring at 120 rpm, resulting in a residual ethyl acetate content <40 ppm by GC analysis and dry matter content ≥15 wt. % at 200 °C.

7.3.8. Preparation of water dispersions of polyesters with XG

Dispersions with PLA and XG contents in the 5–22 and 0.15–0.76 wt. % range, respectively, were prepared (Table 3.2 of Chapter 2). They are identified with the acronym D*x*_*p*, where *x* stands for the concentration of XG given as 100× wt. % and *p* for the wt. % concentration of PLA in the final aqueous dispersions. Aqueous dispersions with 15 wt. % PLA and different amounts of XG (0.15, 0.25, 0.35, 0.50, 0.65, and 0.75 wt. %) were obtained from the pristine PLA dispersion by adding an appropriate amount of XG, stirring the mixture at 200 rpm overnight at room temperature, and then keeping the dispersion under mild vacuum until air bubbles were removed.

Dispersions with concentrations of PLA particles lower than 15 wt. % (5, 10, 12.5, and 13.5 wt. %, respectively) were obtained by diluting the pristine PLA dispersion with ultrapure water before the addition of XG. Dispersions with 20 wt. % PLA were obtained by processing the 15 wt. % dispersion through an ultrafiltration cell (Millipore Amicon 8003) equipped with a 100 kDa (membrane filter Ultracel 100 kDa Millipore) until the desired concentration of particles was reached (few minutes). Two dispersions were obtained by thickening with XG at 0.50 and 0.75 wt. %, respectively. Reference XG aqueous solutions at 0.15, 0.25, 0.50, and 0.75 wt. % were prepared by stirring a suitable amount of the thickening agent in ultrapure water for a couple of hours.

For the preparation of the polyester dispersions thickened with xanthan gum for the coating tests, at first PLA dispersions were prepared under the conditions of entry 3, Table 2.1 of Chapter 2 (PLA_SDS) and entry 4, Table 2.3 of Chapter 2 (PLA_SYN), while the PBSA dispersion was prepared following the procedure described in paragraph 7.3.5. Subsequently, 0.5 wt. % (25 mg) of xanthan gum were added to 5 g of polyester aqueous dispersion and the mixture was magnetically stirred overnight. The stirring speed must be low (60-80 rpm) in order to avoid the excessive formation of air bubbles in the formulations.

7.3.9. Application of the XG thickened polyester dispersions onto paper substrates

A paper rectangle (12 x 30 cm) without wrinkles was first fixed onto a stable surface. Afterwards, the chosen thickened polyester dispersion was poured onto the top of the sheet of paper forming a horizontal line. Subsequently, the selected threaded rod was placed over the formulation line and was swiped along the entire length of the paper sample. The coated paper was dried in the oven for 1.5 h at 60 °C (in the case of the PLA formulations) or at 100 °C (in the case of the PBSA dispersion).

7.3.10. Liquid water permeability (LWP) of coated paper

The liquid water permeability index of coated and non-coated papers was determined using a modified ISO 535 procedure. The apparatus used for the test consists of a rigid base and a rigid metal cylinder with an internal diameter of 3.5 cm and with a means of securely attaching it to the base plate. The height of the glass cylinder is sufficient to provide a water depth of 10 mm. In particular, the paper samples were first cut in a circle of 6 cm diameter (28.26 cm^2) and accurately weighed. After that, the test piece was placed with the surface to be tested uppermost on the base plate. The glass cylinder was placed with the machined edge in contact with the test piece and it was clamped sufficiently firmly to prevent any leakage of water between it and the test piece. Subsequently, 9.6 ml of ultrapure water was poured into the cylinder, hence providing a water depth of 10 mm, and the time was started immediately. After 20 s the excess of water was poured off and the cylinder was quickly unclamped and removed. The test piece was rapidly removed and placed, test face uppermost, on a sheet of dry blotting paper. 30 s after the commencement of the test, a second sheet of blotting paper was placed on top of the test piece and the excess water was removed, using a glass bar (1 cm diameter) with two rolls (once forward and once back) without exerting any pressure on the roller. The sample was then accurately weighted and the LWP index was calculated as follows (equation 7.3):

$$LPW\ \left(\frac{g}{m^2}\right) = \frac{weight\ test\ piece\ after\ the\ procedure - initial\ weight\ test\ piece}{area\ test\ piece} \qquad (7.3)$$

Each measurement was repeated three times and the arithmetic mean was calculated on the collected data. The error was calculated as standard deviation. For each determination new ultrapure water was used.

7.3.11. Grease permeability (GP) of coated paper

Grease resistance of coated and non-coated papers was determined using a modified TAPPI (Technical Association of the Pulp and Paper Industry) test T 454 om−10. Particularly, the test specimen was placed onto a clean white sheet of paper. Subsequently, 5 g of dry sand was placed in an iron tube (25 mm diameter) onto the test specimen to obtain a heap. 1.1 mL of peanut oil was then added dropwise to the heap of sand. The time in seconds was measured and indicated as the result after which the first peanut oil penetration appears on a white sheet of paper present underneath the test specimen. According to this method, a time of 1800 s corresponds to a high penetration resistance to fats and oils. Each measurement was repeated three times and the arithmetic mean was calculated on the collected data. The error was calculated as standard deviation.

7.3.12. General procedure for the preparation of PVA solutions in water

For the preparation of the aqueous solutions starting from powdered PVA 4-88 and 6-88, the procedures provided by Kurakay chemical were followed. 125 ml of cold water (10-20 °C) was charged into a jacketed 1L reactor and, subsequently, the stirrer was switched on at a not too vigorous speed in order to avoid foam formation. After that, 30 g of PVA 4-88 and 6-88 (for solutions at 12 wt. %) or 75 g of PVA 6-88 (for a solution at 30 wt. %) in powder was slowly added into the reactor with a funnel. The other 125 ml of water was used to wash the areas of the reactor above the water line in order to solubilize all the PVA. The temperature was then increased up to 95 °C and everything was stirred slowly for 2h. Subsequently, before discharging the reactor, the temperature was lowered to 25°C. The solutions, as described in the Kurakay's procedure, gave rise to skinning.

7.3.13. Preparation of film of PLA/PVA blends from PLA aqueous dispersions

PLA/PVA blends were prepared from PLA aqueous dispersion by exploiting a two-step procedure. The first step involves the preparation of a water-based PLA dispersion, using the procedures previously described in Paragraph 7.3.1 and 7.3.3 Particularly, PLA dispersions were prepared under the same conditions of entry 3, Table 2.1 of Chapter 2 (PLA_SDS) or entry 4, Table 2.3 of Chapter 2 (PLA_SYN). In the second step, a PVA solution in water was properly added to both PLA dispersions (PLA_SDS and PLA_SYN) and the mixtures were magnetically stirred for 4 h. Subsequently, 5.6 g of the resulting PLA/PVA latexes was casted onto polystyrene (PS) capsules (10 cm of diameter) and left to dry at 60 °C in the oven.

7.3.14. PLA/PVA blend specimens' preparation for the mechanical tests

As described in Paragraph 7.3.13, the PLA/PVA films were obtained in the form of 100 mm diameter disks.

PVA films were prepared by casting 5.6 g of a solution at 12 wt. % in water onto PS dishes with a 100 mm diameter. In this case, the water present in the formulation was evaporated at room temperature.

PLA4060D and PLA_SYN films were produced with the use of a hot 50 ton press able to work on a maximum area of 40x40 cm. After heating the press plate at 180 ° C, 6 g of material (PLA4060D granules or PLA_SYN dried dispersion) was poured in the center. Subsequently, the dishes were put in contact and, after 2 min, a pressure of 280 was applied. After 1 min, the pressure was lowered to 0 bar and a 280-bar pressure for 1 min was applied (this step was repeated 2 times). Lastly, the plates were opened and the film was removed and allowed to cool at rt.

Each film was sprayed with a water-based white paint to allow the acquisition of the deformation by Digital Imaging Correlation (DIC), (Dantec Dynamics, Skovlunde, Denmark). For a correct DIC reading of the pure PVA sample, before the spraying phase with the white water-based paint, the film was opacified by spraying with water and talc powder. The non-influence of the paint on the film thickness was verified with the stereomicroscope Leica MZ6, equipped with a Leica EC3 camera

(Leica Microsystem, Wetzlar, Germany). After these steps, each disk was press-dried to prevent wrinkling. Subsequently, test specimens were cut in 10x100 mm rectangles, with a scalpel, according to ASTM D882 standard. The thickness of each sample was measured using a digital micrometer (Mitutoyo 293, 2 μm resolution). Afterwards, the samples were conditioned at 25 °C, under pressure, in a dryer containing saturated solution of $Mg(NO_3)_2$ to keep a relative humidity in the 50 ± 5 %, as reported in ASTM D882 standard.

7.3.15. Tensile testing on the PLA,PVA and PLA/PVA samples

Mechanical tests in simple tension were performed using a universal testing machine (INSTRON 4467, USA), equipped with a 500 N load cell. Trials were carried out on five specimens for each formulation at room temperature with a 5 mm/min crosshead speed and with a gauge length of 50 mm. For each material a suitable preload was fixed and listed in Table 1. DIC was used to evaluate the strain until 0.2% for the determination of the Young's modulus.

Table 7.2: Materials preloads

PLA formulation	**PVA content (wt. %)**	**Preload [N]**
-	0	1
PLA_SYN	25	0.5
PLA_SYN	50	1
PLA_SYN	75	≈2.5
PLA_SDS	75	≈2.5
-	100	≈2.5

7.3.16. Preparation of sodium alginate foils

Sodium alginate (SA) foils were obtained by casting a 4 wt. % water solution of SA, used as purchased, into PS Petri dishes. SA was solubilized in ultrapure water at a concentration of 4 wt. % at room temperature. The solution was left to stand overnight to allow bubble escaping and then it was casted into polystyrene Petri

dishes. The evaporation of water excess and the final drying were performed at room temperature under a controlled environmental condition (humidity ~40%, and temperature ~23 °C). The SA film thickness can be adjusted varying the total amount of the solution poured into the Petri dish. Substrates with balanced mechanical properties, in terms of stability and flexibility, and a transparency superior to 90% over the whole visible range can be realized by casting 30 g of SA solution into a 9 cm ϕ Petri dish. This volume yields a foil thickness of around 130 μm.

7.3.17. Calibration of the metal film thickness of the electronic devices

For a precise evaluation of the Au and Al thickness, a calibration procedure has been performed. Firstly, a metal film with a nominal thickness of 20 nm was made on a SiO_2 substrate, keeping the deposition parameters fixed at the values used for the manufacture of OLEDs. After that, the film thickness has been measured with an Atomic Force Microscopy (AFM). Considering τ that is given by the product between the deposition rate and the deposition time, the deposition $\tau\ R\ t$ rate R has been then evaluated as follows:

$$\tau = \mathrm{Rt} \rightarrow \mathrm{R} = \frac{\tau}{\mathrm{t}} \qquad (7.4)$$

7.3.18. Model system for the OLED disassembly and material recovery quantification

A special sample has been prepared for use in disassembling tests (Fig. 7.1). It consists of two devices that have been cut before use. The amount of metals present in each device, which has a total surface of 3.2 cm^2, was estimated using geometric considerations (Table 7.3).

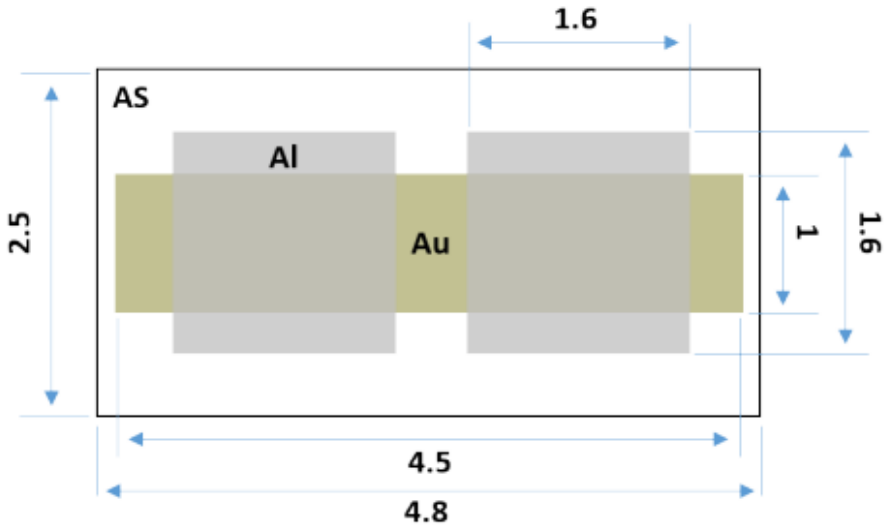

Figure 7.1: Scheme of the model system prepared for the disassembling tests. SA (130 μm) / Au (8 nm) / TCTA (70 nm) / Al (85 nm). All the dimension values are given in cm.

Table 7.3: Amounts of metals initially present in the model system (3.20 cm^2) and recovered from disassembly.

Metal	Volume occupied (mm^3)[a]	Density (g/cm^3)	Initial amount (mg)[b]	Recovered amount (mg)	Percentage recovered (%)[c]
Al	0.027	2.7	0.073	0.056	77
Au	0.00133	19.3	0.026	0.022	87

[a]Determined through measurements of the height, width and thickness of the samples. [b] Weight of the metal in the sample before the disassembling process, determined by multiplying the volume occupied for the density. [c]Weight of the metal recovered from the disassembling process, determined with ICP-OES, $ppm_{Metal} = mg_{Metal}/mL_{SOLUTION} * 10^3$; $mg_{Metal} = ppm * mL_{SOLVENT} / 10^3$.

7.3.19. Metal recovery analysis from OLED disassembly

A quantification of the metals recovered after disassembly has been performed with an inductively coupled plasma - optical emission spectrometer (ICP-OES, Varian 700-ES series), using the solutions, suitably diluted, which were obtained by dissolving the samples in concentrated HNO_3.

7.3.20. Kinetic analysis of the alginate lyase catalysed depolymerization of sodium alginate

In a 50 ml flask,15 g of SA water solution at 4 wt. % was added and the mixture was left at a temperature of 40 ° C for 15 minutes. After that, 206 µl of an alginate lyase solution containing an activity level of 10 U/ml and 168 µl of water were added. Subsequently, the reaction was manually stirred with a metal bar for 30 s and then the mixture was magnetically stirred. Every 30 min, 1ml of reaction sample was taken out to measure, through rheological analysis, the viscosity.

7.3.21. Experimental design for the optimization of the sodium alginate solution's viscosity

The enzymatic depolymerization was optimized with the use of the Response Surface Methodology (RSM). A 2^2 factorial experimental design was employed considering two levels (+1, -1) and one central point (0). The independent variables involved were the amount of enzyme (E) and temperature (T). The independent variables, their levels with real and coded values are presented in Table 5.3 of Chapter 5. All experiments were carried out in triplicate, totalling 15 experiments. The statistical analysis was carried out by using the online software Protimiza Experimental Design (http://experimentaldesign.protimiza.com.br/), considering a significance level of 95% ($P < 0.05$).

For each experiment, in an ordinary vial, 4 g of SA water solution at 4 wt. % was added and the mixture was left at the selected temperature for 15 minutes. After that, the proper amount of enzyme solution containing an activity level of 10 U/ml was added. Considering that the different experiments required different amounts of enzymatic solution, in most of the tests an appropriate amount of water was also added in order to uniform the total amount of water inserted in the reaction media. In particular, the amount of enzyme solution and water for each experiment are reported in Table 7.4. After addition of the enzyme, the mixture was manually stirred with a metallic bar and then magnetically stirred for 15 min. Subsequently, 1 ml of reaction sample was taken out to measure through rheological analysis the experimental viscosity.

Table 7.4: Amount of enzyme solution and water to be added in the experimental design tests.

Run	Enzyme amount (U)	Amount of enzyme solution (µl)	Amount of water (µl)
1,3	0.1	10	40
5	0.3	30	20
3,4	0.5	50	-

7.3.22. OCS's disassembly

The process consists of three steps.

First step. The top layer of the device, consisting in six stripes of Ag and MoO_3, was delaminated by immersion in 5 mL of ethanol in an ultrasound bath for 30 minutes. The other layers of the device were not affected by the treatment and the device was collected, washed with 1 mL of fresh ethanol and dried at room temperature. The delaminated layer portions were separated via centrifugation (Centrifuge DIAB D30249, 15 000 rpm for 5 minutes), decantation, and then washed three times with water. The dried solid was finally washed three times for 30 min with 1 mL of NH_3 0.5 M in an ultrasound bath (Ultrasound bath Elmasonic S40, 220-240V, 50/60Hz). The remaining solid was solubilized with 1 mL of HNO_3 at 80°C for 3 h, diluted to 10.0 mL with ultrapure water and analyzed with ICP-MS.

Second step. The second layer consisting in a mixture of photoactive polymers was washed-off by gently shaking the device in 5 mL of 1,2-dichlorobenzene and then rinsing with some fresh solvent. The solvent turns green/blue while the device discolored indicating the solubilization of the organic layer. The solvent was evaporated and the residuum was digested with 2 mL of HNO_3/H_2O_2 3:1 at 130°C for 4 h, diluted to 10.0 mL with ultrapure water and analyzed by ICP-MS

Third step. The device (~80 mg) was cut in small pieces, left to swell in 2 mL of water in an Eppendorf and then placed at 55°C for 15 minutes. Subsequently, alginate lyase was added (98 µL of a 5 U/mL enzyme solution) and the mixture was manually stirred with a metallic spatula for nearly 30 s. After incubation for another 15 minutes at 55°C, the mixture was centrifuged at 15000 rpm for 5 minutes, thus allowing the supernatant to be separated and removed from the residuum. The residuum was washed 3 times with fresh water then with 0.5 M acetic acid in

ultrasound bath and finally again with water. The solid residuum was dried, digested with 1 mL of freshly prepared aqua regia (HNO_3:HCl 1:3 by volume) for 3 h at 70°C, diluted with ultrapure water up to 10.0 mL and analyzed by ICP-MS.

References

1. Andrady, A.L.; Neal, M.A. Applications and societal benefits of plastics. *Philos. Trans. R. Soc. B Biol. Sci.* **2009**, *364*, 1977–1984, doi:10.1098/rstb.2008.0304.
2. Sudesh, K.; Iwata, T. Sustainability of biobased and biodegradable plastics. *Clean - Soil, Air, Water* **2008**, *36*, 433–442, doi:10.1002/clen.200700183.
3. Innocenti, F.D. *Biodegradability and Compostability, biodegradable polymer and plastics*; 2003;
4. Vroman, I.; Tighzert, L. Biodegradable polymers. *Materials (Basel).* **2009**, *2*, 307–344, doi:10.3390/MA2020307.
5. Kab, H. *Bioplastics*; 2010; Vol. 100; ISBN 0471238961.
6. Tang, X.; Alavi, S. Recent advances in starch, polyvinyl alcohol based polymer blends, nanocomposites and their biodegradability. *Carbohydr. Polym.* **2011**, *85*, 7–16, doi:10.1016/j.carbpol.2011.01.030.
7. Avérous, L. Polylactic acid: Synthesis, properties and applications. *Monomers, Polym. Compos. from Renew. Resour.* **2008**, 433–450, doi:10.1016/B978-0-08-045316-3.00021-1.
8. Aslam, M.; Kalyar, M.A.; Raza, Z.A. Polyvinyl alcohol: A review of research status and use of polyvinyl alcohol based nanocomposites. *Polym. Eng. Sci.* **2018**, *58*, 2119–2132, doi:10.1002/pen.24855.
9. DeMerlis, C.C.; Schoneker, D.R. Review of the oral toxicity of polyvinyl alcohol (PVA). *Food Chem. Toxicol.* **2003**, *41*, 319–326, doi:10.1016/S0278-6915(02)00258-2.
10. Gaaz, T.S.; Sulong, A.B.; Akhtar, M.N.; Kadhum, A.A.H.; Mohamad, A.B.; Al-Amiery, A.A.; McPhee, D.J. Properties and applications of polyvinyl alcohol, halloysite nanotubes and their nanocomposites. *Molecules* **2015**, *20*, 22833–22847, doi:10.3390/molecules201219884.
11. Ben Halima, N. Poly(vinyl alcohol): Review of its promising applications and insights into biodegradation. *RSC Adv.* **2016**, *6*, 39823–39832, doi:10.1039/c6ra05742j.
12. A. Salvini, L. M. Saija, S. Finocchiaro, G. Gianni, C. Giannelli, G.T. A New Methodology in the Study of PVAc-Based Adhesive Formulations. *J. Appl. Polym. Sci.* **2009**, *114*, 3841–3854, doi:10.1002/app.
13. Matijašić, G.; Gretić, M.; Vinčić, J.; Poropat, A.; Cuculić, L.; Rahelić, T. Design and 3D printing of multi-compartmental PVA capsules for drug delivery. *J. Drug Deliv. Sci. Technol.* **2019**, *52*, 677–686, doi:10.1016/j.jddst.2019.05.037.
14. Jiang, S.; Liu, S.; Feng, W. PVA hydrogel properties for biomedical application. *J. Mech. Behav. Biomed. Mater.* **2011**, *4*, 1228–1233, doi:10.1016/j.jmbbm.2011.04.005.
15. Amass, W.; Amass, A.; Tighe, B. A review of biodegradable polymers: Uses, current developments in the synthesis and characterization of biodegradable polyesters, blends of biodegradable polymers and recent advances in biodegradation studies. *Polym. Int.* **1998**, *47*, 89–144, doi:10.1002/(SICI)1097-0126(1998100)47:2<89::AID-PI86>3.0.CO;2-F.

16. Lim, L.T.; Auras, R.; Rubino, M. Processing technologies for poly(lactic acid). *Prog. Polym. Sci.* **2008**, *33*, 820–852, doi:10.1016/j.progpolymsci.2008.05.004.

17. Castro-Aguirre, E.; Iñiguez-Franco, F.; Samsudin, H.; Fang, X.; Auras, R. Poly(lactic acid)—Mass production, processing, industrial applications, and end of life. *Adv. Drug Deliv. Rev.* **2016**, *107*, 333–366, doi:10.1016/j.addr.2016.03.010.

18. Lasprilla, A.J.R.; Martinez, G.A.R.; Lunelli, B.H.; Jardini, A.L.; Filho, R.M. Poly-lactic acid synthesis for application in biomedical devices - A review. *Biotechnol. Adv.* **2012**, *30*, 321–328, doi:10.1016/j.biotechadv.2011.06.019.

19. Tawakkal, I.S.M.A.; Cran, M.J.; Miltz, J.; Bigger, S.W. A review of poly(lactic acid)-based materials for antimicrobial packaging. *J. Food Sci.* **2014**, *79*, doi:10.1111/1750-3841.12534.

20. Ahmed, J.; Varshney, S.K. Polylactides-chemistry, properties and green packaging technology: A review. *Int. J. Food Prop.* **2011**, *14*, 37–58, doi:10.1080/10942910903125284.

21. Jabeen, N.; Majid, I.; Nayik, G.A. Bioplastics and food packaging: A review. *Cogent Food Agric.* **2015**, *1*, 1117749, doi:10.1080/23311932.2015.1117749.

22. Tyler, B.; Gullotti, D.; Mangraviti, A.; Utsuki, T.; Brem, H. Polylactic acid (PLA) controlled delivery carriers for biomedical applications. *Adv. Drug Deliv. Rev.* **2016**, *107*, 163–175, doi:10.1016/j.addr.2016.06.018.

23. Auras, R.; Harte, B.; Selke, S. An overview of polylactides as packaging materials. *Macromol. Biosci.* **2004**, *4*, 835–864, doi:10.1002/mabi.200400043.

24. Madhavan Nampoothiri, K.; Nair, N.R.; John, R.P. An overview of the recent developments in polylactide (PLA) research. *Bioresour. Technol.* **2010**, *101*, 8493–8501, doi:10.1016/j.biortech.2010.05.092.

25. Murariu, M.; Dubois, P. PLA composites: From production to properties. *Adv. Drug Deliv. Rev.* **2016**, *107*, 17–46, doi:10.1016/j.addr.2016.04.003.

26. Farah, S.; Anderson, D.G.; Langer, R. Physical and mechanical properties of PLA, and their functions in widespread applications — A comprehensive review. *Adv. Drug Deliv. Rev.* **2016**, *107*, 367–392, doi:10.1016/j.addr.2016.06.012.

27. Mehta, R.; Kumar, V.; Bhunia, H.; Upadhyay, S.N. Synthesis of poly(lactic acid): A review. *J. Macromol. Sci. - Polym. Rev.* **2005**, *45*, 325–349, doi:10.1080/15321790500304148.

28. Wanamaker, C.L.; Bluemle, M.J.; Pitet, L.M.; O'Leary, L.E.; Tolman, W.B.; Hillmyer, M.A. Consequences of polylactide stereochemistry on the properties of polylactide-polymenthide-polylactide thermoplastic elastomers. *Biomacromolecules* **2009**, *10*, 2904–2911, doi:10.1021/bm900721p.

29. Vahabi, H.; Rohani Rad, E.; Parpaite, T.; Langlois, V.; Saeb, M.R. Biodegradable polyester thin films and coatings in the line of fire: the time of polyhydroxyalkanoate (PHA)? *Prog. Org. Coatings* **2019**, *133*, 85–89, doi:10.1016/j.porgcoat.2019.04.044.

30. Rafiqah, S.A.; Khalina, A.; Harmaen, A.S.; Tawakkal, I.A.; Zaman, K.; Asim, M.; Nurrazi, M.N.; Lee, C.H. A review on properties and application of bio-based poly(Butylene succinate). *Polymers (Basel).* **2021**, *13*, 1–28, doi:10.3390/polym13091436.

31. Wallace H. Carothers and J. A. Arvin Polymerization and ring formation. ii. poly-

esters. *J. Am. Chem. Soc.* **1929**, *51*, 2560–2570.

32. Aliotta, L.; Seggiani, M.; Lazzeri, A.; Gigante, V.; Cinelli, P. A Brief Review of Poly (Butylene Succinate) (PBS) and Its Main Copolymers: Synthesis, Blends, Composites, Biodegradability, and Applications. *Polymers (Basel).* **2022**, *14*, doi:10.3390/polym14040844.

33. Xu, J.; Guo, B.H. Poly(butylene succinate) and its copolymers: Research, development and industrialization. *Biotechnol. J.* **2010**, *5*, 1149–1163, doi:10.1002/biot.201000136.

34. Seggiani, M.; Gigante, V.; Cinelli, P.; Coltelli, M.B.; Sandroni, M.; Anguillesi, I.; Lazzeri, A. Processing and mechanical performances of Poly(Butylene Succinate–co–Adipate) (PBSA) and raw hydrolyzed collagen (HC) thermoplastic blends. *Polym. Test.* **2019**, *77*, 105900, doi:10.1016/j.polymertesting.2019.105900.

35. Nikolaivits, E.; Pantelic, B.; Azeem, M.; Taxeidis, G.; Babu, R.; Topakas, E.; Brennan Fournet, M.; Nikodinovic-Runic, J. Progressing Plastics Circularity: A Review of Mechano-Biocatalytic Approaches for Waste Plastic (Re)valorization. *Front. Bioeng. Biotechnol.* **2021**, *9*, 1–31, doi:10.3389/fbioe.2021.696040.

36. Labet, M.; Thielemans, W. Synthesis of polycaprolactone: A review. *Chem. Soc. Rev.* **2009**, *38*, 3484–3504, doi:10.1039/b820162p.

37. Chee, W.K.; Ibrahim, N.A.; Zainuddin, N.; Abd Rahman, M.F.; Chieng, B.W. Impact toughness and ductility enhancement of biodegradable poly(lactic acid)/poly(ε-caprolactone) blends via addition of glycidyl methacrylate. *Adv. Mater. Sci. Eng.* **2013**, *2013*, doi:10.1155/2013/976373.

38. Thakur, M.; Majid, I.; Hussain, S.; Nanda, V. Poly(ε-caprolactone): A potential polymer for biodegradable food packaging applications. *Packag. Technol. Sci.* **2021**, *34*, 449–461, doi:10.1002/pts.2572.

39. Grossen, P.; Witzigmann, D.; Sieber, S.; Huwyler, J. PEG-PCL-based nanomedicines: A biodegradable drug delivery system and its application. *J. Control. Release* **2017**, *260*, 46–60, doi:10.1016/j.jconrel.2017.05.028.

40. Cohn, D.; Hotovely Salomon, A. Designing biodegradable multiblock PCL/PLA thermoplastic elastomers. *Biomaterials* **2005**, *26*, 2297–2305, doi:10.1016/j.biomaterials.2004.07.052.

41. Wu, C.S. Physical properties and biodegradability of maleated-polycaprolactone/starch composite. *Polym. Degrad. Stab.* **2003**, *80*, 127–134, doi:10.1016/S0141-3910(02)00393-2.

42. Malikmammadov, E.; Tanir, T.E.; Kiziltay, A.; Hasirci, V.; Hasirci, N. *PCL and PCL-based materials in biomedical applications*; Taylor & Francis, 2018; Vol. 29; ISBN 9031221031.

43. Matta, A.K.; Rao, R.U.; Suman, K.N.S.; Rambabu, V. Preparation and Characterization of Biodegradable PLA/PCL Polymeric Blends. *Procedia Mater. Sci.* **2014**, *6*, 1266–1270, doi:10.1016/j.mspro.2014.07.201.

44. Shi, G.; Cooper, D.G.; Maric, M. Poly(ε-caprolactone)-based "green" plasticizers for poly(vinyl choride). *Polym. Degrad. Stab.* **2011**, *96*, 1639–1647, doi:10.1016/j.polymdegradstab.2011.06.007.

45. Zhang, C. Biodegradable Polyesters, First Edition, pp1-24. *Biodegrad. Polyesters Synth. Prop. Appl.* **2005**, 1–24.

46. Tan, G.Y.A.; Chen, C.L.; Li, L.; Ge, L.; Wang, L.; Razaad, I.M.N.; Li, Y.; Zhao, L.; Mo, Y.; Wang, J.Y. Start a research on biopolymer polyhydroxyalkanoate (PHA): A review. *Polymers (Basel).* **2014**, *6*, 706–754, doi:10.3390/polym6030706.

47. Sharma, V.; Sehgal, R.; Gupta, R. Polyhydroxyalkanoate (PHA): Properties and Modifications. *Polymer (Guildf).* **2021**, *212*, 123161, doi:10.1016/j.polymer.2020.123161.

48. Rodriguez-Perez, S.; Serrano, A.; Pantión, A.A.; Alonso-Fariñas, B. Challenges of scaling-up PHA production from waste streams. A review. *J. Environ. Manage.* **2018**, *205*, 215–230, doi:10.1016/j.jenvman.2017.09.083.

49. SN, B.; G, S. Need for Bioplastics and Role of Biopolymer PHB: A Short Review. *J. Pet. Environ. Biotechnol.* **2016**, *07*, doi:10.4172/2157-7463.1000272.

50. Markl, E.; Grünbichler, H.; Lackner, M. Cyanobacteria for PHB Bioplastics Production: A Review. *Algae* **2019**, 1–10, doi:10.5772/intechopen.81536.

51. Mohammed, A.S.A.; Naveed, M.; Jost, N. Polysaccharides; Classification, Chemical Properties, and Future Perspective Applications in Fields of Pharmacology and Biological Medicine (A Review of Current Applications and Upcoming Potentialities). *J. Polym. Environ.* **2021**, *29*, 2359–2371, doi:10.1007/s10924-021-02052-2.

52. SANDFORD, P.A.; BAIRD, J. *Industrial Utilization of Polysaccharides*; ACADEMIC PRESS, INC., 1983; ISBN 0120656027.

53. Yang, X.; Li, A.; Li, X.; Sun, L.; Guo, Y. An overview of classifications, properties of food polysaccharides and their links to applications in improving food textures. *Trends Food Sci. Technol.* **2020**, *102*, 1–15, doi:10.1016/j.tifs.2020.05.020.

54. Zobel, H.F. Molecules to Granules: A Comprehensive Starch Review. *Starch - Stärke* **1988**, *40*, 44–50, doi:10.1002/star.19880400203.

55. Miles, M.J.; Morris, V.J.; Orford, P.D.; Ring, S.G. The roles of amylose and amylopectin in the gelation and retrogradation of starch. *Carbohydr. Res.* **1985**, *135*, 271–281, doi:10.1016/S0008-6215(00)90778-X.

56. Wang, S.; Li, C.; Copeland, L.; Niu, Q.; Wang, S. Starch Retrogradation: A Comprehensive Review. *Compr. Rev. Food Sci. Food Saf.* **2015**, *14*, 568–585, doi:10.1111/1541-4337.12143.

57. Li, J.H.; Vasanthan, T.; Hoover, R.; Rossnagel, B.G. Starch from hull-less barley: Ultrastructure and distribution of granule-bound proteins. *Cereal Chem.* **2003**, *80*, 524–532, doi:10.1094/CCHEM.2003.80.5.524.

58. Hari, P.K.; Garg, S.; Garg, S.K. Gelatinization of Starch and Modified Starch. *Starch - Stärke* **1989**, *41*, 88–91, doi:10.1002/star.19890410304.

59. Tharanathan, R.N. Starch - Value addition by modification. *Crit. Rev. Food Sci. Nutr.* **2005**, *45*, 371–384, doi:10.1080/10408390590967702.

60. Duvernay, W.H.; Chinn, M.S.; Yencho, G.C. Hydrolysis and fermentation of sweetpotatoes for production of fermentable sugars and ethanol. *Ind. Crops Prod.* **2013**, *42*, 527–537, doi:10.1016/j.indcrop.2012.06.028.

61. Saha, D.; Bhattacharya, S. Hydrocolloids as thickening and gelling agents in food: A critical review. *J. Food Sci. Technol.* **2010**, *47*, 587–597, doi:10.1007/s13197-010-0162-6.

62. ROHWER, R.G.; KLEM, R.E. *Acid-Modified Starch: Production and Uses*; Second Edi.; ACADEMIC PRESS, 1984; ISBN 0127462708.

63. Kraak, A. Industrial applications of potato starch products. *Ind. Crops Prod.* **1992**, *1*, 107–112, doi:10.1016/0926-6690(92)90007-I.

64. Wang, Z.; Li, Z.; Gu, Z.; Hong, Y.; Cheng, L. Preparation, characterization and properties of starch-based wood adhesive. *Carbohydr. Polym.* **2012**, *88*, 699–706, doi:10.1016/j.carbpol.2012.01.023.

65. Li, H.; Qi, Y.; Zhao, Y.; Chi, J.; Cheng, S. Starch and its derivatives for paper coatings: A review. *Prog. Org. Coatings* **2019**, *135*, 213–227, doi:10.1016/j.porgcoat.2019.05.015.

66. Yin, H.; Zheng, P.; Zhang, E.; Rao, J.; Lin, Q.; Fan, M.; Zhu, Z.; Zeng, Q.; Chen, N. Improved wet shear strength in eco-friendly starch-cellulosic adhesives for woody composites. *Carbohydr. Polym.* **2020**, *250*, 116884, doi:10.1016/j.carbpol.2020.116884.

67. Builders, P.F.; Arhewoh, M.I. Pharmaceutical applications of native starch in conventional drug delivery. *Starch/Staerke* **2016**, *68*, 864–873, doi:10.1002/star.201500337.

68. Zhang, Y.; Rempel, C.; Liu, Q. Thermoplastic Starch Processing and Characteristics-A Review. *Crit. Rev. Food Sci. Nutr.* **2014**, *54*, 1353–1370, doi:10.1080/10408398.2011.636156.

69. Bastioli, C. Properties and applications of Mater-Bi starch-based materials. **1998**, *59*.

70. García-Ochoa, F.; Santos, V.E.; Casas, J.A.; Gómez, E. Xanthan gum: Production, recovery, and properties. *Biotechnol. Adv.* **2000**, *18*, 549–579, doi:10.1016/S0734-9750(00)00050-1.

71. Siddiqui, I.R. An extracellular polysaccharide from Xanthomonas campestris. *Carbohydr. Res.* **1967**, *4*, 284–291, doi:10.1016/S0008-6215(00)80181-0.

72. Song, K.W.; Kuk, H.Y.; Chang, G.S. Rheology of concentrated xanthan gum solutions: Oscillatory shear flow behavior. *Korea Aust. Rheol. J.* **2006**, *18*, 67–81.

73. Lee, H.; Yoo, B. Agglomerated xanthan gum powder used as a food thickener: Effect of sugar binders on physical, microstructural, and rheological properties. *Powder Technol.* **2020**, *362*, 301–306, doi:10.1016/j.powtec.2019.11.124.

74. Zhang, R.; Tao, Y.; Xu, Q.; Liu, N.; Chen, P.; Zhou, Y.; Bai, Z. Rheological and ion-conductive properties of injectable and self-healing hydrogels based on xanthan gum and silk fibroin. *Int. J. Biol. Macromol.* **2020**, *144*, 473–482, doi:10.1016/j.ijbiomac.2019.12.132.

75. Petri, D.F.S. Xanthan gum: A versatile biopolymer for biomedical and technological applications. *J. Appl. Polym. Sci.* **2015**, *132*, doi:10.1002/app.42035.

76. Bhat, I.M.; Wani, S.M.; Mir, S.A.; Masoodi, F.A. Advances in xanthan gum production, modifications and its applications. *Biocatal. Agric. Biotechnol.* **2022**, *42*, 102328, doi:10.1016/j.bcab.2022.102328.

77. Kohajdová, Z.; Karovičová, J.; Schmidt, Š. Significance of Emulsifiers and Hydrocolloids in Bakery Industry. *Acta Chim. Slovaca* **2009**, *2*, 46–61.

78. Akkarachaneeyakorn, S.; Tinrat, S. Effects of types and amounts of stabilizers on physical and sensory characteristics of cloudy ready-to-drink mulberry fruit juice.

Food Sci. Nutr. **2015**, *3*, 213–220, doi:10.1002/fsn3.206.

79. Hecht, H.; Srebnik, S. Structural Characterization of Sodium Alginate and Calcium Alginate. *Biomacromolecules* **2016**, *17*, 2160–2167, doi:10.1021/acs.biomac.6b00378.

80. Shsh, H.N.; Rao, a V Rheological Properties of Sodium Alginate. *Indian J. Technol.* **1969**, *7*, 261.

81. Sachan, N.K.; Pushkar, S.; Jha, A.; Bhattcharya, A. Sodium alginate: the wonder polymer for controlled drug delivery. *J Pharm Res* **2009**, *2*, 1191–1199.

82. Lacoste, C.; El Hage, R.; Bergeret, A.; Corn, S.; Lacroix, P. Sodium alginate adhesives as binders in wood fibers/textile waste fibers biocomposites for building insulation. *Carbohydr. Polym.* **2018**, *184*, 1–8, doi:10.1016/j.carbpol.2017.12.019.

83. Ishikawa, K.; Miyamoto, Y.; Kon, M.; Nagayama, M.; Asaoka, K. Non-decay type fast-setting calcium phosphate cement: composite with sodium alginate. *Biomaterials* **1995**, *16*, 527–532, doi:10.1016/0142-9612(95)91125-I.

84. Gaggero, G.; Delucchi, M.; Allegretta, G.; Vicini, S.; Botter, R. Interaction of sodium alginate thickener with components of architectural water-based coatings. *Prog. Org. Coatings* **2021**, *151*, 106016, doi:10.1016/j.porgcoat.2020.106016.

85. Lee, K.Y.; Mooney, D.J. Alginate: Properties and biomedical applications. *Prog. Polym. Sci.* **2012**, *37*, 106–126, doi:10.1016/j.progpolymsci.2011.06.003.

86. Eiselt, P.; Yeh, J.; Latvala, R.K.; Shea, L.D.; Mooney, D.J. Porous carriers for biomedical applications based on alginate hydrogels. *Biomaterials* **2000**, *21*, 1921–1927, doi:10.1016/S0142-9612(00)00033-8.

87. García-García, P.; Reyes, R.; Pérez-Herrero, E.; Arnau, M.R.; Évora, C.; Delgado, A. Alginate-hydrogel versus alginate-solid system. Efficacy in bone regeneration in osteoporosis. *Mater. Sci. Eng. C* **2020**, *115*, 111009, doi:10.1016/j.msec.2020.111009.

88. Melchiorre Di Crescenzo, M.; Zendri, E.; Sánchez-Pons, M.; Fuster-López, L.; Yusá-Marco, D.J. The use of waterborne paints in contemporary murals: Comparing the stability of vinyl, acrylic and styrene-acrylic formulations to outdoor weathering conditions. *Polym. Degrad. Stab.* **2014**, *107*, 285–293, doi:10.1016/j.polymdegradstab.2013.12.034.

89. Grøstad, K.; Pedersen, A. Emulsion polymer isocyanates as wood adhesive: A review. *J. Adhes. Sci. Technol.* **2010**, *24*, 1357–1381, doi:10.1163/016942410X500981.

90. Zhou, X.; Li, Y.; Fang, C.; Li, S.; Cheng, Y.; Lei, W.; Meng, X. Recent Advances in Synthesis of Waterborne Polyurethane and Their Application in Water-based Ink: A Review. *J. Mater. Sci. Technol.* **2015**, *31*, 708–722, doi:10.1016/j.jmst.2015.03.002.

91. Lei, L.; Zhong, L.; Lin, X.; Li, Y.; Xia, Z. Synthesis and characterization of waterborne polyurethane dispersions with different chain extenders for potential application in waterborne ink. *Chem. Eng. J.* **2014**, *253*, 518–525, doi:10.1016/j.cej.2014.05.044.

92. Bandera, D.; Meyer, V.R.; Prevost, D.; Zimmermann, T.; Boesel, L.F. Polylactide/montmorillonite hybrid latex as a barrier coating for paper applications. *Polymers (Basel).* **2016**, *8*, 1–9, doi:10.3390/polym8030075.

93. Nestorson, A.; Neon, K.G.; Kang, E.T.; Järnström, L.; Leufvén, A. Enzyme

immobilization in latex dispersion coatings for active food packaging. *Packag. Technol. Sci.* **2008**, *21*, 193–205, doi:10.1002/pts.796.

94. Chapman, R.A. *Chemical bonding*; Woodhead Publishing Limited, 2006; ISBN 9781845691998.

95. Belletti, G.; Buoso, S.; Ricci, L.; Guillem-Ortiz, A.; Aragón-Gutiérrez, A.; Bortolini, O.; Bertoldo, M. Preparations of poly(Lactic acid) dispersions in water for coating applications. *Polymers (Basel).* **2021**, *13*, 1–19, doi:10.3390/polym13162767.

96. McClements, D.J. Critical review of techniques and methodologies for characterization of emulsion stability. *Crit. Rev. Food Sci. Nutr.* **2007**, *47*, 611–649, doi:10.1080/10408390701289292.

97. Pal, R. Suspensions and Pickering Emulsions. *Fluids* **2019**, *4*, 1–22.

98. Aben, S.; Holtze, C.; Tadros, T.; Schurtenberger, P. Rheological Investigations on the Creaming of Depletion-Flocculated Emulsions. **2012**, doi:10.1021/la300221m.

99. Nor Bainun, I.; Alias, N.H.; Syed-Hassan, S.S.A. Nanoemulsion: Formation, Characterization, Properties and Applications - A Review. *Adv. Mater. Res.* **2015**, *1113*, 147–152, doi:10.4028/www.scientific.net/amr.1113.147.

100. Napper, D.H. Flocculation studies of sterically stabilized dispersions. *J. Colloid Interface Sci.* **1970**, *32*, 106–114, doi:10.1016/0021-9797(70)90107-4.

101. Sober, D.L.; Walz, J.Y. Measurement of Long Range Depletion Energies between a Colloidal Particle and a Flat Surface in Micellar Solutions. *Langmuir* **1995**, *11*, 2352–2356, doi:10.1021/la00007a006.

102. Dickinson, E.; Eriksson, L. Particle flocculation by adsorbing polymers. *Adv. Colloid Interface Sci.* **1991**, *34*, 1–29, doi:10.1016/0001-8686(91)80045-L.

103. Jenkins, P.; Snowden, M. Depletion flocculation in colloidal dispersions. *Adv. Colloid Interface Sci.* **1996**, *68*, 57–96, doi:10.1016/s0001-8686(96)90046-9.

104. McClements, D.J. Comments on viscosity enhancement and depletion flocculation by polysaccharides. *Food Hydrocoll.* **2000**, *14*, 173–177, doi:10.1016/S0268-005X(99)00065-X.

105. Dickinson, E. Strategies to control and inhibit the flocculation of protein-stabilized oil-in-water emulsions. *Food Hydrocoll.* **2019**, *96*, 209–223, doi:10.1016/j.foodhyd.2019.05.021.

106. Dreher, T.M.; Glass, J.; O'Connor, A.J.; Stevens, G.W. Effect of rheology on coalescence rates and emulsion stability. *AIChE J.* **1999**, *45*, 1182–1190, doi:10.1002/aic.690450604.

107. Ho, T.M.; Razzaghi, A.; Ramachandran, A.; Mikkonen, K.S. Emulsion characterization via microfluidic devices: A review on interfacial tension and stability to coalescence. *Adv. Colloid Interface Sci.* **2022**, *299*, 102541, doi:10.1016/j.cis.2021.102541.

108. Pilpel, N.; Rabbani, M.E. Formation of liquid crystals in sunflower oil in water emulsions. *J. Colloid Interface Sci.* **1987**, *119*, 550–558, doi:10.1016/0021-9797(87)90302-X.

109. Taylor, P. Ostwald ripening in emulsions. *Adv. Colloid Interface Sci.* **1998**, *75*, 107–163, doi:10.1016/S0001-8686(98)00035-9.

110. Izquierdo, P.; Esquena, J.; Tadros, T.F.; Dederen, C.; Garcia, M.J.; Azemar, N.; Solans, C. Formation and stability of nano-emulsions prepared using the phase inversion temperature method. *Langmuir* **2002**, *18*, 26–30, doi:10.1021/la010808c.

111. Pham, B.T.T.; Zondanos, H.; Such, C.H.; Warr, G.G.; Hawkett, B.S. Miniemulsion polymerization with arrested ostwald ripening stabilized by amphiphilic RAFT copolymers. *Macromolecules* **2010**, *43*, 7950–7957, doi:10.1021/ma101087t.

112. Park, D.W.; Roe, R.J. Effect of Added Block Copolymer on the Phase-Separation Kinetics of a Polymer Blend. 2. Optical Microscopic Observations. *Macromolecules* **1991**, *24*, 5324–5329, doi:10.1021/ma00019a018.

113. Ogawa, T.; Shinoda, K. The Solubilization of Water in Nonaqueous Solutions of Polyoxyethylene Nonylphenyl Ethers. *Nippon kagaku zassi* **1967**, *88*, 940–943, doi:10.1246/nikkashi1948.88.9_940.

114. Shinoda, K.; Saito, H. The Stability of O/W type emulsions as functions of temperature and the HLB of emulsifiers: The emulsification by PIT-method. *J. Colloid Interface Sci.* **1969**, *30*, 258–263, doi:10.1016/S0021-9797(69)80012-3.

115. Novales, B.; Papineau, P.; Sire, A.; Axelos, M.A.V. Characterization of emulsions and suspensions by video image analysis. *Colloids Surfaces A Physicochem. Eng. Asp.* **2003**, *221*, 81–89, doi:10.1016/S0927-7757(03)00102-X.

116. Horozov, T.S.; Binks, B.P. Stability of suspensions, emulsions, and foams studied by a novel automated analyzer. *Langmuir* **2004**, *20*, 9007–9013, doi:10.1021/la0489155.

117. Pal, R. Techniques for measuring the composition (oil and water content) of emulsions - a state of the art review. *Colloids Surfaces A Physicochem. Eng. Asp.* **1994**, *84*, 141–193, doi:10.1016/0927-7757(93)02711-M.

118. Clementi, L.A.; Vega, J.R.; Gugliotta, L.M. Particle size distribution of multimodal polymer dispersions by multiangle dynamic light scattering. Solution of the inverse problem on the basis of a genetic algorithm. *Part. Part. Syst. Charact.* **2010**, *27*, 146–157, doi:10.1002/ppsc.201000011.

119. Chanamai, R.; McClements, D.J. Creaming stability of flocculated monodisperse oil-in-water emulsions. *J. Colloid Interface Sci.* **2000**, *225*, 214–218, doi:10.1006/jcis.2000.6766.

120. Mengual, O.; Meunier, G.; Cayre, I.; Puech, K.; Snabre, P. Talanta 50 (1999) 445–456.pdf. *Talanta* **1999**, *50*, 445–456.

121. Buron, H.; Mengual, O.; Meunier, G.; Cayré, I.; Snabre, P. Optical characterization of concentrated dispersions: Applications to laboratory analyses and on-line process monitoring and control. *Polym. Int.* **2004**, *53*, 1205–1209, doi:10.1002/pi.1231.

122. LATREILLE, B.; PAQUIN, P. Evaluation of Emulsion Stability by Centrifugation with Conductivity Measurements. *J. Food Sci.* **1990**, *55*, 1666–1668, doi:10.1111/j.1365-2621.1990.tb03595.x.

123. Yow, H.N.; Biggs, S. Probing the stability of sterically stabilized polystyrene particles by centrifugal sedimentation. *Soft Matter* **2013**, *9*, 10031–10041, doi:10.1039/c3sm51534f.

124. Bury, M.; Gerhards, J.; Erni, W.; Stamm, A. Application of a new method based on conductivity measurements to determine the creaming stability of o/w emulsions. *Int. J. Pharm.* **1995**, *124*, 183–194, doi:10.1016/0378-5173(95)00075-T.

125. Howe, A.M.; Mackie, A.R.; Robins, M.M. Technique to measure emulsion creaming by velocity of ultrasound. *J. Dispers. Sci. Technol.* **1986**, *7*, 231–243, doi:10.1080/01932698608943457.

126. Newling, B.; Glover, P.M.; Keddie, J.L.; Lane, D.M.; McDonald, P.J. Concentration profiles in creaming oil-in-water emulsion layers determined with stray field magnetic resonance imaging. *Langmuir* **1997**, *13*, 3621–3626, doi:10.1021/la9610056.

127. Moschakis, T.; Murray, B.S.; Dickinson, E. Microstructural evolution of viscoelastic emulsions stabilised by sodium caseinate and xanthan gum. *J. Colloid Interface Sci.* **2005**, *284*, 714–728, doi:10.1016/j.jcis.2004.10.036.

128. Quemada, D.; Berli, C. *Energy of interaction in colloids and its implications in rheological modeling*; 2002; Vol. 98; ISBN 3314427433.

129. Krebs, T.; Ershov, D.; Schroen, C.G.P.H.; Boom, R.M. Coalescence and compression in centrifuged emulsions studied with in situ optical microscopy. *Soft Matter* **2013**, *9*, 4026–4035, doi:10.1039/c3sm27850f.

130. Dickinson, E.; Murray, B.S.; Stainsby, G. Coalescence stability of emulsion-sized droplets at a planar oil-water interface and the relationship to protein film surface rheology. *J. Chem. Soc. Faraday Trans. 1 Phys. Chem. Condens. Phases* **1988**, *84*, 871–883, doi:10.1039/F19888400871.

131. Tcholakova, S.; Denkov, N.D.; Ivanov, I.B.; Campbell, B. Coalescence in β-lactoglobulin-stabilized emulsions: Effects of protein adsorption and drop size. *Langmuir* **2002**, *18*, 8960–8971, doi:10.1021/la0258188.

132. Rehfeld, S.J. Stability of hydrocarbon-in-water emulsions during centrifugation. Influence of dispersed phase composition. *J. Colloid Interface Sci.* **1974**, *46*, 448–459, doi:10.1016/0021-9797(74)90055-1.

133. Julian McClements, D.; Henson, L.; Popplewell, L.M.; Decker, E.A.; Jun Choi, S. Inhibition of Ostwald ripening in model beverage emulsions by addition of poorly water soluble triglyceride oils. *J. Food Sci.* **2012**, *77*, 33–38, doi:10.1111/j.1750-3841.2011.02484.x.

134. De Smet, Y.; Deriemaeker, L.; Parloo, E.; Finsy, R. On the determination of Ostwald ripening rates from dynamic light scattering measurements. *Langmuir* **1999**, *15*, 2327–2332, doi:10.1021/la9807513.

135. Rondón-González, M.; Sadtler, V.; Marchal, P.; Choplin, L.; Salager, J.L. Emulsion catastrophic inversion from abnormal to normal morphology. 7. Emulsion evolution produced by continuous stirring to generate a very high internal phase ratio emulsion. *Ind. Eng. Chem. Res.* **2008**, *47*, 2314–2319, doi:10.1021/ie071482r.

136. Allouche, J.; Tyrode, E.; Sadtler, V.; Choplin, L.; Salager, J.L. Simultaneous Conductivity and Viscosity Measurements as a Technique To Track Emulsion Inversion by the Phase-Inversion-Temperature Method. *Langmuir* **2004**, *20*, 2134–2140, doi:10.1021/la035334r.

137. Steward, P.A.; Hearn, J.; Wilkinson, M.C. Stewart2000_an overview of polymer latex film formation and prop.pdf. **2000**, 195–267.

138. Felton, L.A. Mechanisms of polymeric film formation. *Int. J. Pharm.* **2013**, *457*, 423–427, doi:10.1016/j.ijpharm.2012.12.027.

139. Keddie, J.L. Reports : A Review Journal Film formation of latex. *Mater. Sci. Eng.* **1997**, *21*, 101–170.

140. Steward, P.A.; Hearn, J.; Wilkinson, M.C. Overview of polymer latex film formation and properties. *Adv. Colloid Interface Sci.* **2000**, *86*, 195–267, doi:10.1016/S0001-8686(99)00037-8.

141. Ristić, M.M.; Milosević, S.D. Frenkel's Theory of Sintering. *Sci. Sinter.* **2006**, *38*, 7–11, doi:10.2298/SOS0601007R.

142. Brown, G.L. Formation of films from polymer dispersions. *J. Polym. Sci.* **1956**, *22*, 423–434, doi:10.1002/pol.1956.1202210208.

143. Paulsson, M.; Singh, S.K. Colloidal and thermal characteristics of concentrated dispersions of polymethacrylate-based latices for aqueous enteric coating. *J. Pharm. Sci.* **1999**, *88*, 406–411, doi:10.1021/js9803555.

144. Haley, J.C.; Liu, Y.; Winnik, M.A.; Lau, W. The onset of polymer diffusion in a drying acrylate latex: How water initially retards coalescence but ultimately enhances diffusion. *J. Coatings Technol. Res.* **2008**, *5*, 157–168, doi:10.1007/s11998-007-9061-9.

145. Protzman, T.F.; Brown, G.L. An apparatus for the determination of the minimum film temperature of polymer emulsions. *J. Appl. Polym. Sci.* **1960**, *4*, 81–85, doi:10.1002/app.1960.070041012.

146. Jensen, D.P.; Morgan, L.W. Particle size as it relates to the minimum film formation temperature of latices. *J. Appl. Polym. Sci.* **1991**, *42*, 2845–2849, doi:10.1002/app.1991.070421024.

147. Okor, R.S. Influence of hydrophilic character of plasticizer and polymer on certain film properties. *Int. J. Pharm.* **1982**, *11*, 1–9, doi:10.1016/0378-5173(82)90172-7.

148. Berce, P.; Skale, S.; Razboršek, T.; Slemnik, M. Influence of coalescing aids on the latex properties and film formation of waterborne coatings. *J. Appl. Polym. Sci.* **2017**, *134*, 1–9, doi:10.1002/app.45142.

149. Sawyer, L.C.; Bone, T. Effect of surfactants on film formation of Poly (Vinyl Acetate) and Poly (Vinyl Acetate-Butyl Acrylate) latexes. *J. Dispers. Sci. Technol.* **1982**, *3*, 81–97, doi:10.1080/01932698208943627.

150. Bradford, E.B.; Vanderhoff, J.W. Additional Studies of Morphological Changes in Latex Films. *J. Macromol. Sci. Part B* **1972**, *6*, 671–693, doi:10.1080/00222347208212565.

151. Bindschaedler, C.; Gurny, R.; Doelker, E. Influence of emulsifiers on film formation from cellulose acetate latexes. Modeling approach to the fate of emulsifiers in highly plasticized films. II. *J. Appl. Polym. Sci.* **1989**, *37*, 173–182, doi:10.1002/app.1989.070370113.

152. Roulstone, B.J.; Wilkinson, M.C.; Hearn, J. Studies on polymer latex films: IV. Comparison of the permeability of latex and solvent-cast films. *Polym. Int.* **1992**, *27*, 305–308, doi:10.1002/pi.4990270404.

153. Hong, J.S.; Srivastava, D.; Lee, I. Fabrication of poly(lactic acid) nano- and microparticles using a nanomixer via nanoprecipitation or emulsion diffusion. *J. Appl. Polym. Sci.* **2018**, *135*, 1–8, doi:10.1002/app.46199.

154. Legrand, P.; Lesieur, S.; Bochot, A.; Gref, R.; Raatjes, W.; Barratt, G.; Vauthier, C. Influence of polymer behaviour in organic solution on the production of polylactide nanoparticles by nanoprecipitation. *Int. J. Pharm.* **2007**, *344*, 33–43, doi:10.1016/j.ijpharm.2007.05.054.

155. Pandey, S.K.; Patel, D.K.; Thakur, R.; Mishra, D.P.; Maiti, P.; Haldar, C. Anti-cancer evaluation of quercetin embedded PLA nanoparticles synthesized by emulsified nanoprecipitation. *Int. J. Biol. Macromol.* **2015**, *75*, 521–529, doi:10.1016/j.ijbiomac.2015.02.011.

156. Gavory, C.; Durand, A.; Six, J.L.; Nouvel, C.; Marie, E.; Leonard, M. Polysaccharide-covered nanoparticles prepared by nanoprecipitation. *Carbohydr. Polym.* **2011**, *84*, 133–140, doi:10.1016/j.carbpol.2010.11.012.

157. Allémann, E.; Leroux, J.C.; Gurny, R.; Doelker, E. In Vitro Extended-Release Properties of Drug-Loaded Poly(DL-Lactic Acid) Nanoparticles Produced by a Salting-Out Procedure. *Pharm. Res. An Off. J. Am. Assoc. Pharm. Sci.* 1993, *10*, 1732–1737.

158. Mendoza-Munoz, N.; Quintanar-Guerrero, D.; Allemann, E. The Impact of the Salting-Out Technique on the Preparation of Colloidal Particulate Systems for Pharmaceutical Applications. *Recent Pat. Drug Deliv. Formul.* **2012**, *6*, 236–249, doi:10.2174/187221112802652688.

159. Balakrishanan, M.H.; Rajan, M. Size-controlled synthesis of biodegradable nanocarriers for targeted and controlled cancer drug delivery using salting out cation. *Bull. Mater. Sci.* **2016**, *39*, 69–77, doi:10.1007/s12034-015-0946-4.

160. Samuli Hirsjärvi *Preparation and characterization of poly (lactic acid) Nanoparticles for pharmaceutical use*; 2008; ISBN 9789521044557.

161. Quintanar-Guerrero, D.; Fessi, H.; Allémann, E.; Doelker, E. Influence of stabilizing agents and preparative variables on the formation of poly(D,L-lactic acid) nanoparticles by an emulsification-diffusion technique. *Int. J. Pharm.* **1996**, *143*, 133–141, doi:10.1016/S0378-5173(96)04697-2.

162. Coffin, M.D.; McGinity, J.W. Biodegradable Pseudolatexes: The Chemical Stability of Poly(D,L-Lactide) and Poly (ε-Caprolactone) Nanoparticles in Aqueous Media. *Pharm. Res. An Off. J. Am. Assoc. Pharm. Sci.* 1992, *9*, 200–205.

163. Zhang, H.; Xiang, S.; Luan, Q.; Bao, Y.; Deng, Q.; Zheng, M.; Liu, S.; Song, J.; Tang, H.; Huang, F. Development of poly (lactic acid) microspheres and their potential application in Pickering emulsions stabilization. *Int. J. Biol. Macromol.* **2018**, *108*, 105–111, doi:10.1016/j.ijbiomac.2017.11.079.

164. Xu, W.; Shen, R.; Yan, Y.; Gao, J. Preparation and characterization of electrospun alginate/PLA nanofibers as tissue engineering material by emulsion eletrospinning. *J. Mech. Behav. Biomed. Mater.* **2017**, *65*, 428–438, doi:10.1016/j.jmbbm.2016.09.012.

165. polyester based nano e micro particles.

166. Byun, Y.; Hwang, J.B.; Bang, S.H.; Darby, D.; Cooksey, K.; Dawson, P.L.; Park, H.J.; Whiteside, S. Formulation and characterization of α-tocopherol loaded poly e{open}-caprolactone (PCL) nanoparticles. *LWT - Food Sci. Technol.* **2011**, *44*, 24–28, doi:10.1016/j.lwt.2010.06.032.

167. Lee, J.; Jung, S.G.; Park, C.S.; Kim, H.Y.; Batt, C.A.; Kim, Y.R. Tumor-specific hybrid polyhydroxybutyrate nanoparticle: Surface modification of nanoparticle by enzymatically synthesized functional block copolymer. *Bioorganic Med. Chem. Lett.* **2011**, *21*, 2941–2944, doi:10.1016/J.BMCL.2011.03.058.

168. Sébastien, F.; Stéphane, G.; Copinet, A.; Coma, V. Novel biodegradable films made from chitosan and poly(lactic acid) with antifungal properties against mycotoxinogen

strains. *Carbohydr. Polym.* **2006**, *65*, 185–193, doi:10.1016/j.carbpol.2006.01.006.

169. Grande, R.; Carvalho, A.J.F. Compatible ternary blends of chitosan/poly(vinyl alcohol)/poly(lactic acid) produced by oil-in-water emulsion processing. *Biomacromolecules* **2011**, *12*, 907–914, doi:10.1021/bm101227q.

170. Li, X.; Hegyesi, N.; Zhang, Y.; Mao, Z.; Feng, X.; Wang, B.; Pukánszky, B.; Sui, X. Poly(lactic acid)/lignin blends prepared with the Pickering emulsion template method. *Eur. Polym. J.* **2019**, *110*, 378–384, doi:10.1016/j.eurpolymj.2018.12.001.

171. Zhang, Y.; Wu, J.; Wang, B.; Sui, X.; Zhong, Y.; Zhang, L.; Mao, Z.; Xu, H. Cellulose nanofibril-reinforced biodegradable polymer composites obtained via a Pickering emulsion approach. *Cellulose* **2017**, *24*, 3313–3322, doi:10.1007/s10570-017-1324-8.

172. Zhang, Y.; Jiang, Y.; Han, L.; Wang, B.; Xu, H.; Zhong, Y.; Zhang, L.; Mao, Z.; Sui, X. Biodegradable regenerated cellulose-dispersed composites with improved properties via a pickering emulsion process. *Carbohydr. Polym.* **2018**, *179*, 86–92, doi:10.1016/j.carbpol.2017.09.065.

173. Bertoldo, M.; Coltelli, M.B.; Messina, T.; Bronco, S.; Castelvetro, V. Emulsion Blending Approach for the Preparation of Gelatin/Poly(butylene succinate-co-adipate) Films. *ACS Biomater. Sci. Eng.* **2016**, *2*, 677–686, doi:10.1021/acsbiomaterials.6b00050.

174. Liu, R.; Ma, G.H.; Wan, Y.H.; Su, Z.G. Influence of process parameters on the size distribution of PLA microcapsules prepared by combining membrane emulsification technique and double emulsion-solvent evaporation method. *Colloids Surfaces B Biointerfaces* **2005**, *45*, 144–153, doi:10.1016/j.colsurfb.2005.08.004.

175. Torrado, J.J.; Pavic, A.; Stojanovic, Z.; Pekmezovic, M.; De Veljovi´cveljovi´c, Đ.¯; O'connor, K.; Malagurski, I.; Nikodinovic-Runic, J. Polyenes in Medium Chain Length Polyhydroxyalkanoate (mcl-PHA) Biopolymer Microspheres with Reduced Toxicity and Improved Therapeutic Effect against Candida Infection in Zebrafish Model. *Pharmaceutics* **2022**, *2022*, 696, doi:10.3390/pharmaceutics14040696.

176. Koller, M. molecules Biodegradable and Biocompatible Polyhydroxy-alkanoates (PHA): Auspicious Microbial Macromolecules for Pharmaceutical and Therapeutic Applications. **2018**, doi:10.3390/molecules23020362.

177. Iqbal, M.; Valour, J.-P.; Fessi, H.; Elaissari, A. Preparation of biodegradable PCL particles via double emulsion evaporation method using ultrasound technique., doi:10.1007/s00396-014-3464-9.

178. Alex, A.T.; Joseph, A.; Shavi, G.; Rao, J.V.; Udupa, N. Development and evaluation of carboplatin-loaded PCL nanoparticles for intranasal delivery. *Drug Deliv.* **2016**, *23*, 2144–2153, doi:10.3109/10717544.2014.948643.

179. Rodríguez-Contreras, A.; Guillem-Marti, J.; Lopez, O.; Manero, J.M.; Ruperez, E. Antimicrobial PHAs coatings for solid and porous tantalum implants. *Colloids Surfaces B Biointerfaces* **2019**, *182*, 110317, doi:10.1016/j.colsurfb.2019.06.047.

180. Rodríguez-Contreras, A.; García, Y.; Manero, J.M.; Rupérez, E. Antibacterial PHAs coating for titanium implants. *Eur. Polym. J.* **2017**, *90*, 66–78, doi:10.1016/j.eurpolymj.2017.03.004.

181. Mentink, Leon; Bouvier, Frederic; Clabaux, Pierre-Philippe; Bernaerts, J. Use of an aqueous dispersion of at least one biodegradable polymer containing at least one

stabilizing agent for the preparation of an aqueous filmogenic composition, U.S. Patent 0197807A1 2007.

182. Serpelloni, Michel; Mentink, Léon; Bernaerts, J. Aqueous dispersions of at least one biodegradable polymer, U.S. Patent 0237710 A1 2011.

183. Whitehouse, R.. Process for latex production by melt emulsification,U.S. Patent 20130225761A1 2015.

184. Sobotka, Gwenaelle; Nenov, N. Method for producing an aqueous dispersion of poly(hydroxyalkanoates), U.S. Patent 0009914A1 2016.

185. Kimura, Y. Method of Manufacturing Polyactic Acid, U.S. Patent 0161505A1 2008.

186. Rhim, J.W.; Lee, J.H.; Hong, S.I. Increase in water resistance of paperboard by coating with poly(lactide). *Packag. Technol. Sci.* **2007**, *20*, 393–402, doi:10.1002/pts.767.

187. Habel, C.; Schöttle, M.; Daab, M.; Eichstaedt, N.J.; Wagner, D.; Bakhshi, H.; Agarwal, S.; Horn, M.A.; Breu, J. High-Barrier, Biodegradable Food Packaging. *Macromol. Mater. Eng.* **2018**, *303*, 1–5, doi:10.1002/mame.201800333.

188. Forgiarini, A.; Esquena, J.; González, C.; Solans, C. Formation of nano-emulsions by low-energy emulsification methods at constant temperature. *Langmuir* **2001**, *17*, 2076–2083, doi:10.1021/la001362n.

189. Schultz, S.; Wagner, G.; Urban, K.; Ulrich, J. High-pressure homogenization as a process for emulsion formation. *Chem. Eng. Technol.* **2004**, *27*, 361–368, doi:10.1002/ceat.200406111.

190. Urban, K.; Wagner, G.; Schaffner, D.; Röglin, D.; Ulrich, J. Rotor-stator and disc systems for emulsification processes. *Chem. Eng. Technol.* **2006**, *29*, 24–31, doi:10.1002/ceat.200500304.

191. Canselier, J.P.; Delmas, H.; Wilhelm, A.M.; Abismaïl, B. Ultrasound emulsification - An overview. *J. Dispers. Sci. Technol.* **2002**, *23*, 333–349, doi:10.1080/01932690208984209.

192. Joscelyne, S.M.; Trägårdh, G. Membrane emulsification - A literature review. *J. Memb. Sci.* **2000**, *169*, 107–117, doi:10.1016/S0376-7388(99)00334-8.

193. Kubo, M.T.K.; Augusto, P.E.D.; Cristianini, M. Effect of high pressure homogenization (HPH) on the physical stability of tomato juice. *Food Res. Int.* **2013**, *51*, 170–179, doi:10.1016/j.foodres.2012.12.004.

194. Chern, C.S. Emulsion polymerization mechanisms and kinetics. *Prog. Polym. Sci.* **2006**, *31*, 443–486, doi:10.1016/j.progpolymsci.2006.02.001.

195. Lovell, P.A.; Schork, F.J. Fundamentals of Emulsion Polymerization. *Biomacromolecules* **2020**, *21*, 4396–4441, doi:10.1021/acs.biomac.0c00769.

196. Molina-Gutiérrez, S.; Ladmiral, V.; Bongiovanni, R.; Caillol, S.; Lacroix-Desmazes, P. Radical polymerization of biobased monomers in aqueous dispersed media. *Green Chem.* **2019**, *21*, 36–53, doi:10.1039/c8gc02277a.

197. Spekreijse, J.; Le Nôtre, J.; Van Haveren, J.; Scott, E.L.; Sanders, J.P.M. Simultaneous production of biobased styrene and acrylates using ethenolysis. *Green Chem.* **2012**, *14*, 2747–2751, doi:10.1039/c2gc35498e.

198. Mohsenzadeh, A.; Zamani, A.; Taherzadeh, M.J. Bioethylene Production from

Ethanol: A Review and Techno-economical Evaluation. *ChemBioEng Rev.* **2017**, *4*, 75–91, doi:10.1002/cben.201600025.

199. Allémann, E.; Gurny, R.; Doelker, E. Preparation of aqueous polymeric nanodispersions by a reversible salting-out process: influence of process parameters on particle size. *Int. J. Pharm.* **1992**, *87*, 247–253, doi:10.1016/0378-5173(92)90249-2.

200. Grunlan, M.A.; Xing, L.L.; Glass, J.E. Waterborne Coatings with an Emphasis on Synthetic Aspects: An Overview. *ACS Symp. Ser.* **1997**, *663*, doi:10.1021/bk-1997-0663.ch001.

201. Noble, K.L. Waterborne polyurethanes. *Prog. Org. Coatings* **1997**, *32*, 131–136, doi:10.1016/S0300-9440(97)00071-4.

202. Galindo-Rodriguez, S.; Allémann, E.; Fessi, H.; Doelker, E. Physicochemical parameters associated with nanoparticle formation in the salting-out, emulsification-diffusion, and nanoprecipitation methods. *Pharm. Res.* **2004**, *21*, 1428–1439, doi:10.1023/B:PHAM.0000036917.75634.be.

203. Jenjob, R.; Phakkeeree, T.; Seidi, F.; Theerasilp, M.; Crespy, D. Emulsion Techniques for the Production of Pharmacological Nanoparticles. *Macromol. Biosci.* **2019**, *19*, 1–13, doi:10.1002/mabi.201900063.

204. Bibette, J.; Leal-Calderon, F. Surfactant-stabilized emulsions. *Curr. Opin. Colloid Interface Sci.* **1996**, *1*, 746–751, doi:10.1016/s1359-0294(96)80076-8.

205. Zembyla, M.; Murray, B.S.; Sarkar, A. Water-in-oil emulsions stabilized by surfactants, biopolymers and/or particles: a review. *Trends Food Sci. Technol.* **2020**, *104*, 49–59, doi:10.1016/j.tifs.2020.07.028.

206. Kume, G.; Gallotti, M.; Nunes, G. Review on anionic/cationic surfactant mixtures. *J. Surfactants Deterg.* **2008**, *11*, 1–11, doi:10.1007/s11743-007-1047-1.

207. Rebello, S.; Asok, A.K.; Mundayoor, S.; Jisha, M.S. Surfactants: Toxicity, remediation and green surfactants. *Environ. Chem. Lett.* **2014**, *12*, 275–287, doi:10.1007/s10311-014-0466-2.

208. Mohamed, A.I.A.; Sultan, A.S.; Hussein, I.A.; Al-Muntasheri, G.A. Influence of Surfactant Structure on the Stability of Water-in-Oil Emulsions under High-Temperature High-Salinity Conditions. *J. Chem.* **2017**, *2017*, doi:10.1155/2017/5471376.

209. Pasquali, R.C.; Sacco, N.; Bregni, C. The studies on Hydrophilic-Lipophilic Balance (HLB): Sixty years after William C. Griffin's Pioneer Work (1949-2009). *Lat. Am. J. Pharm.* **2009**, *28*, 313–317.

210. Davies, J.T. Reprinted from : Gas/Liquid and Liquid/Liquid Interfaces. Proceedings of 2nd International Congress Surface Activity,. *Aquantitive Kinet. Theory Emuls. Type. I Phys. Chem. Emuls. Agent* **1957**, 426–438.

211. Dickinson, E. Mixed biopolymers at interfaces: Competitive adsorption and multilayer structures. *Food Hydrocoll.* **2011**, *25*, 1966–1983, doi:10.1016/j.foodhyd.2010.12.001.

212. Dickinson, E. Hydrocolloids as emulsifiers and emulsion stabilizers. *Food Hydrocoll.* **2009**, *23*, 1473–1482, doi:10.1016/j.foodhyd.2008.08.005.

213. Garti, N.; Reichman, D. Food Structure Hydrocolloids as Food Emulsifiers and

Stabilizers. *Food Struct.* **1993**, *12*, 411–426.

214. Nilsson, L.; Bergenståhl, B. Adsorption of hydrophobically modified starch at oil/water interfaces during emulsification. *Langmuir* **2006**, *22*, 8770–8776, doi:10.1021/la060870f.

215. Karlberg, M.; Thuresson, K.; Lindman, B. Hydrophobically modified ethyl(hydroxyethyl)cellulose as stabilizer and emulsifying agent in macroemulsions. *Colloids Surfaces A Physicochem. Eng. Asp.* **2005**, *262*, 158–167, doi:10.1016/j.colsurfa.2005.04.026.

216. Cao, Y.; Dickinson, E.; Wedlock, D.J. Creaming and flocculation in emulsions containing polysaccharide. *Top. Catal.* **1990**, *4*, 185–195, doi:10.1016/S0268-005X(09)80151-3.

217. Dickinson, E.; Ma, J.; Povey, M.J.W. *Creaming of concentrated oil-in-water emulsions containing xanthan*; 1994; Vol. 8;.

218. Gunning, P.A.; Hibberd, D.J.; Howe, A.M.; Robins, M.M. Gravitational destabilization of emulsions flocculated by non-adsorbed xanthan. *Top. Catal.* **1988**, *2*, 119–129, doi:10.1016/S0268-005X(88)80010-9.

219. Hemar, Y.; Tamehana, M.; Munro, P.A.; Singh, H. Influence of xanthan gum on the formation and stability of sodium caseinate oil-in-water emulsions. *Food Hydrocoll.* **2001**, *15*, 513–519, doi:10.1016/S0268-005X(01)00075-3.

220. Krstonošić, V.; Dokić, L.; Nikolić, I.; Milanović, M. Influence of xanthan gum on oil-in-water emulsion characteristics stabilized by OSA starch. *Food Hydrocoll.* **2015**, *45*, 9–17, doi:10.1016/j.foodhyd.2014.10.024.

221. Krstonošickrstonošicá, V.; Dokic´b, L.; Dokic´b, D.; Dokic´c, P.; Dokic´c, D.; Dapčevic, T.; Dapčevic´c, D. Effects of xanthan gum on physicochemical properties and stability of corn oil-in-water emulsions stabilized by polyoxyethylene (20) sorbitan monooleate. *Food Hydrocoll. 23*, 2212–2218, doi:10.1016/j.foodhyd.2009.05.003.

222. Siró, I.; Plackett, D. Microfibrillated cellulose and new nanocomposite materials: A review. *Cellulose* **2010**, *17*, 459–494, doi:10.1007/s10570-010-9405-y.

223. Andresen, M.; Stenius, P. Water-in-oil emulsions stabilized by hydrophobized microfibrillated cellulose. *J. Dispers. Sci. Technol.* **2007**, *28*, 837–844, doi:10.1080/01932690701341827.

224. Winuprasith, T.; Suphantharika, M. Properties and stability of oil-in-water emulsions stabilized by microfibrillated cellulose from mangosteen rind. *Food Hydrocoll.* **2015**, *43*, 690–699, doi:10.1016/j.foodhyd.2014.07.027.

225. Winuprasith, T.; Suphantharika, M. Microfibrillated cellulose from mangosteen (Garcinia mangostana L.) rind: Preparation, characterization, and evaluation as an emulsion stabilizer. *Food Hydrocoll.* **2013**, *32*, 383–394, doi:10.1016/j.foodhyd.2013.01.023.

226. Villamonte, G.; Jury, V.; de Lamballerie, M. Stabilizing emulsions using high-pressure-treated corn starch. *Food Hydrocoll.* **2016**, *52*, 581–589, doi:10.1016/j.foodhyd.2015.07.031.

227. Zhao, Y.; Khalid, N.; Shu, G.; Neves, M.A.; Kobayashi, I.; Nakajima, M. Formulation and characterization of oil-in-water emulsions stabilized by gelatinized kudzu starch. *Int. J. Food Prop.* **2017**, *20*, 1329–1341, doi:10.1080/10942912.2017.1347675.

228. Li, C.; Li, Y.; Sun, P.; Yang, C. Pickering emulsions stabilized by native starch granules. *Physicochem. Eng. Asp.* **2013**, *431*, 142–149, doi:10.1016/j.colsurfa.2013.04.025.

229. Tesch, S.; Gerhards, C.; Schubert, H. Stabilization of emulsions by OSA starches. *J. Food Eng.* **2002**, *54*, 167–174, doi:10.1016/S0260-8774(01)00206-0.

230. Hwa, J.C.H. Mechanism of film formation from latices. Phenomenon of flocculation. *J. Polym. Sci. Part A Gen. Pap.* **1964**, *2*, 785–796, doi:10.1002/pol.1964.100020216.

231. Raso, J.; Mañas, P.; Pagán, R.; Sala, F.J. Influence of different factors on the output power transferred into medium by ultrasound. *Ultrason. Sonochem.* **1999**, *5*, 157–162, doi:10.1016/S1350-4177(98)00042-X.

232. Agama-Acevedo, E.; Bello-Perez, L.A. Starch as an emulsions stability: the case of octenyl succinic anhydride (OSA) starch. *Curr. Opin. Food Sci.* **2017**, *13*, 78–83, doi:10.1016/j.cofs.2017.02.014.

233. Zembyla, M.; Murray, B.S.; Sarkar, A. Water-in-oil emulsions stabilized by surfactants, biopolymers and/or particles: a review. *Trends Food Sci. Technol.* **2020**, *104*, 49–59, doi:10.1016/j.tifs.2020.07.028.

234. Cai, B.; Mazahreh, J.; Ma, Q.; Wang, F.; Hu, X. Ultrasound-assisted fabrication of biopolymer materials: A review. *Int. J. Biol. Macromol.* **2022**, *209*, 1613–1628, doi:10.1016/j.ijbiomac.2022.04.055.

235. Eom, Y.; Choi, B.; Park, S. il A Study on Mechanical and Thermal Properties of PLA/PEO Blends. *J. Polym. Environ.* **2019**, *27*, 256–262, doi:10.1007/s10924-018-1344-y.

236. Erukhimovich, I.; de la Cruz, M.O. Phase equilibria and charge fractionation in polydisperse polyelectrolyte solutions. **2004**, 11–17, doi:10.1002/polb.

237. Zhao, J.H.; Wang, X.Q.; Zeng, J.; Yang, G.; Shi, F.H.; Yan, Q. Biodegradation of poly(butylene succinate-co-butylene adipate) by Aspergillus versicolor. *Polym. Degrad. Stab.* **2005**, *90*, 173–179, doi:10.1016/j.polymdegradstab.2005.03.006.

238. Siracusa, V.; Lotti, N.; Munari, A.; Dalla Rosa, M. Poly(butylene succinate) and poly(butylene succinate-co-adipate) for food packaging applications: Gas barrier properties after stressed treatments. *Polym. Degrad. Stab.* **2015**, *119*, 35–45, doi:10.1016/j.polymdegradstab.2015.04.026.

239. Ahn, B.D.; Kim, S.H.; Kim, Y.H.; Yang, J.S. Synthesis and characterization of the biodegradable copolymers from succinic acid and adipic acid with 1,4-butanediol. *J. Appl. Polym. Sci.* **2001**, *82*, 2808–2826, doi:10.1002/app.2135.

240. Rastogi, V.K.; Samyn, P. Bio-based coatings for paper applications. *Coatings* **2015**, *5*, 887–930, doi:10.3390/coatings5040887.

241. Khwaldia, K.; Arab-Tehrany, E.; Desobry, S. Biopolymer Coatings on Paper Packaging Materials. *Compr. Rev. Food Sci. Food Saf.* **2010**, *9*, 82–91, doi:10.1111/j.1541-4337.2009.00095.x.

242. Zhang, Z.; Britt, I.J.; Tung, M.A. Water Absorption in EVOH Films and Its Influence on Glass Transition Temperature. *J. Polym. Sci. Part B Polym. Phys.* **1999**, *37*, 691–699, doi:10.1002/(sici)1099-0488(19990401)37:7<691::aid-polb20>3.0.co;2-v.

243. Shorten, D.W. Polyolefins for food packaging. *Food Chem.* **1982**, *8*, 109–119, doi:10.1016/0308-8146(82)90006-1.

244. Adibi, A.; Valdesueiro, D.; Mok, J.; Behabtu, N.; Lenges, C.; Simon, L.; Mekonnen, T.H. Sustainable barrier paper coating based on alpha-1,3 glucan and natural rubber latex. *Carbohydr. Polym.* **2022**, *282*, 119121, doi:10.1016/j.carbpol.2022.119121.

245. Vaswani, S.; Koskinen, J.; Hess, D.W. Surface modification of paper and cellulose by plasma-assisted deposition of fluorocarbon films. *Surf. Coatings Technol.* **2005**, *195*, 121–129, doi:10.1016/j.surfcoat.2004.10.013.

246. Derksen, J.T.P.; Cuperus, F.P.; Kolster, P. Renewable resources in coatings technology: A review. *Prog. Org. Coatings* **1996**, *27*, 45–53, doi:10.1016/0300-9440(95)00518-8.

247. Han, J.H.; Krochta, J.M. WETTING PROPERTIES AND WATER VAPOR PERMEABILITY OF WHEY-PROTEIN-COATED PAPER. **1999**, *42*, 1375–1382.

248. Despond, S.; Espuche, E.; Cartier, N.; Domard, A. Barrier properties of paper-chitosan and paper-chitosan-carnauba wax films. *J. Appl. Polym. Sci.* **2005**, *98*, 704–710, doi:10.1002/app.21754.

249. Rhim, J.W.; Lee, J.H.; Kwak, H.S. Mechanical and water barrier properties of soy protein and clay mineral composite films. *Food Sci. Biotechnol.* 2005, *14*, 112–116.

250. Thurber, H.; Curtzwiler, G.W. Suitability of poly(butylene succinate) as a coating for paperboard convenience food packaging. *Int. J. Biobased Plast.* **2020**, *2*, 1–12, doi:10.1080/24759651.2020.1785094.

251. Cheng, H.Y.; Yang, Y.J.; Li, S.C.; Hong, J.Y.; Jang, G.W. Modification and extrusion coating of polylactic acid films. *J. Appl. Polym. Sci.* **2015**, *132*, 1–8, doi:10.1002/app.42472.

252. Mekonnen, T.; Mussone, P.; Khalil, H.; Bressler, D. Progress in bio-based plastics and plasticizing modifications. *J. Mater. Chem. A* **2013**, *1*, 13379–13398, doi:10.1039/c3ta12555f.

253. Bierwagen, G.P. Film coating technologies and adhesion. *Electrochim. Acta* **1992**, *37*, 1471–1478, doi:10.1016/0013-4686(92)80092-Z.

254. Athawale, V.D.; Nimbalkar, R. V. Waterborne coatings based on renewable oil resources: An overview. *JAOCS, J. Am. Oil Chem. Soc.* **2011**, *88*, 159–185, doi:10.1007/s11746-010-1668-9.

255. Duan, H.; Zhao, C.; Wu, Y.; Zhang, Q.; Wang, S. Performance in paper coating of styren/acrylate copolymer latex. *Polym. Adv. Technol.* **1999**, *10*, 78–81, doi:10.1002/(SICI)1099-1581(199901/02)10:1/2<78::AID-PAT771>3.0.CO;2-J.

256. Ahammad, S. Z.; Gomes, J.; Sreekrishnan, T.R. Wastewater treatment forproductionofH2S-free biogas. *J. Chem. Technol. Biotechnol.* **2008**, *83*, 1163–1169, doi:10.1002/jctb.

257. Naser, A.Z.; Deiab, I.; Darras, B.M. Poly(lactic acid) (PLA) and polyhydroxyalkanoates (PHAs), green alternatives to petroleum-based plastics: a review. *RSC Adv.* **2021**, *11*, 17151–17196, doi:10.1039/d1ra02390j.

258. Rhim, J.W. Effect of coating methods on the properties of Poly(lactide)-coated paperboard: Solution coating vs. Thermo-compression coating. *Food Sci. Biotechnol.* **2009**, *18*, 1155–1160.

259. Rhim, J.W.; Kim, J.H. Properties of poly(lactide)-coated paperboard for the use of 1-way paper cup. *J. Food Sci.* **2009**, *74*, 105–111, doi:10.1111/j.1750-

3841.2009.01073.x.

260. Aldana, D.S.; Villa, E.D.; Hernández, M.D.D.; Sánchez, G.G.; Cruz, Q.R.; Gallardo, S.F.; Castillo, H.P.; Casarrubias, L.B. Barrier properties of polylactic acid in cellulose based packages using montmorillonite as filler. *Polymers (Basel).* **2014**, *6*, 2386–2403, doi:10.3390/polym6092386.

261. Zhang, H.; Hortal, M.; Jordá-Beneyto, M.; Rosa, E.; Lara-Lledo, M.; Lorente, I. ZnO-PLA nanocomposite coated paper for antimicrobial packaging application. *LWT - Food Sci. Technol.* **2017**, *78*, 250–257, doi:10.1016/j.lwt.2016.12.024.

262. Song, Z.; Xiao, H.; Zhao, Y. Hydrophobic-modified nano-cellulose fiber/PLA biodegradable composites for lowering water vapor transmission rate (WVTR) of paper. *Carbohydr. Polym.* **2014**, *111*, 442–448, doi:10.1016/j.carbpol.2014.04.049.

263. N, S.; S, A.K.; A, P.; S, G. Studies on Semi-crystalline Poly Lactic Acid (PLA) as a Hydrophobic Coating Material on Kraft Paper for Imparting Barrier Properties in Coated Abrasive Applications. *Prog. Org. Coatings* **2020**, *145*, doi:10.1016/j.porgcoat.2020.105682.

264. Tabilo-Munizaga, G.; Barbosa-Cánovas, G. V. Rheology for the food industry. *J. Food Eng.* **2005**, *67*, 147–156, doi:10.1016/j.jfoodeng.2004.05.062.

265. Eley, R.R. Applied rheology and architectural coating performance. *J. Coatings Technol. Res.* **2019**, *16*, 263–305, doi:10.1007/s11998-019-00187-5.

266. Bhavsar, R.A.; Nehete, K.M. Rheological approach to select most suitable associative thickener for water-based polymer dispersions and paints. *J. Coatings Technol. Res.* **2019**, *16*, 1089–1098, doi:10.1007/s11998-019-00194-6.

267. Kästner, U. The impact of rheological modifiers on water-borne coatings. *Colloids Surfaces A Physicochem. Eng. Asp.* **2001**, *183–185*, 805–821, doi:10.1016/S0927-7757(01)00507-6.

268. Worldwide, M.I. Malvern Instruments Worldwide Sales and service centres in over 65 countries Optimizing Rheology for Paint and Coating Applications RHEOLOGY AND VISCOSITY. 1–14.

269. Reiffers-Magnani, C.K.; Cuq, J.L.; Watzke, H.J. Composite structure formation in whey protein stabilized O/W emulsions. I. Influence of the dispersed phase on viscoelastic properties. *Food Hydrocoll.* **1999**, *13*, 303–316, doi:10.1016/S0268-005X(99)00013-2.

270. Lorenzo, G.; Checmarev, G.; Zaritzky, N.; Califano, A. Linear viscoelastic assessment of cold gel-like emulsions stabilized with bovine gelatin. *LWT - Food Sci. Technol.* **2011**, *44*, 457–464, doi:10.1016/j.lwt.2010.08.023.

271. P. N. Pusey; Megen, W. van Phase behaviour of concentrated suspensions of nearly colloidal spheres. *Nature* **1986**, 2–4.

272. Al-Itry, R.; Lamnawar, K.; Maazouz, A. Biopolymer blends based on poly (lactic acid): Shear and elongation rheology/structure/blowing process relationships. *Polymers (Basel).* **2015**, *7*, 939–962, doi:10.3390/polym7050939.

273. Glass, J.E.; Schulz, D.N.; Zukoski, C.F. Polymers as Rheology Modifiers. **1991**, 2–17, doi:10.1021/bk-1991-0462.ch001.

274. Zheng, Y.J.; Loh, X.J. Natural rheological modifiers for personal care. *Polym. Adv. Technol.* **2016**, *27*, 1664–1679, doi:10.1002/pat.3822.

275. Gibiński, M.; Kowalski, S.; Sady, M.; Krawontka, J.; Tomasik, P.; Sikora, M. Thickening of sweet and sour sauces with various polysaccharide combinations. *J. Food Eng.* **2006**, *75*, 407–414, doi:10.1016/j.jfoodeng.2005.04.054.

276. Cai, X.; Du, X.; Zhu, G.; Cai, Z.; Cao, C. The use of potato starch/xanthan gum combinations as a thickening agent in the formulation of tomato ketchup. *CYTA - J. Food* **2020**, *18*, 401–408, doi:10.1080/19476337.2020.1760943.

277. Fijan, R.; Šostar-Turk, S.; Lapasin, R. Rheological study of interactions between non-ionic surfactants and polysaccharide thickeners used in textile printing. *Carbohydr. Polym.* **2007**, *68*, 708–717, doi:10.1016/j.carbpol.2006.08.006.

278. Zhang, L.M. Cellulosic associative thickeners. *Carbohydr. Polym.* **2001**, *45*, 1–10, doi:10.1016/S0144-8617(00)00276-9.

279. Tothill, I.E.; Seal, K.J. Biodeterioration of waterborne paint cellulose thickeners. *Int. Biodeterior. Biodegrad.* **1993**, *31*, 241–254, doi:10.1016/0964-8305(93)90020-3.

280. Arancibia, C.; Navarro-Lisboa, R.; Zúñiga, R.N.; Matiacevich, S. Application of CMC as thickener on nanoemulsions based on olive oil: Physical properties and stability. *Int. J. Polym. Sci.* **2016**, *2016*, doi:10.1155/2016/6280581.

281. Obele, C.M.; Ibenta, M.E.; Chukwuneke, J.L.; Nwanonenyi, S.C. Carboxymethyl cellulose and cellulose nanocrystals from cassava stem as thickeners in reactive printing of cotton. *Cellulose* **2021**, *28*, 2615–2633, doi:10.1007/s10570-021-03694-0.

282. Lehmann, A.; Volkert, B.; Fischer, S.; Schrader, A.; Nerenz, H. Starch based thickening agents for personal care and surfactant systems. *Colloids Surfaces A Physicochem. Eng. Asp.* **2008**, *331*, 150–154, doi:10.1016/j.colsurfa.2008.09.055.

283. Fonnum, G.; Bakke, J.; Hansen, F.K. Associative thickeners. Part I: Synthesis, rheology and aggregation behavior. *Colloid Polym. Sci.* **1993**, *271*, 380–389, doi:10.1007/BF00657419.

284. Quienne, B.; Pinaud, J.; Robin, J.J.; Caillol, S. From Architectures to Cutting-Edge Properties, the Blooming World of Hydrophobically Modified Ethoxylated Urethanes (HEURs). *Macromolecules* **2020**, *53*, 6754–6766, doi:10.1021/acs.macromol.0c01353.

285. Larson, R.G.; Van Dyk, A.K.; Chatterjee, T.; Ginzburg, V. V. Associative thickeners for waterborne paints: Structure, characterization, rheology, and modeling. *Prog. Polym. Sci.* **2022**, *129*, 101546, doi:10.1016/j.progpolymsci.2022.101546.

286. Lochhead, R.Y. The role of polymers in cosmetics: Recent trends. *ACS Symp. Ser.* **2007**, *961*, 3–56, doi:10.1021/bk-2007-0961.ch001.

287. Shay, G.D. Alkali-Swellable and Alkali-Soluble Thickener Technology. **1989**, 457–494, doi:10.1021/ba-1989-0223.ch025.

288. Candau, F.; Selb, J. Hydrophobically-modified polyacrylamides prepared by micellar polymerization. *Adv. Colloid Interface Sci.* **1999**, *79*, 149–172, doi:10.1016/S0001-8686(98)00077-3.

289. Galván, Z.R.N.; Soares, L. de S.; Medeiros, E.A.A.; Soares, N. de F.F.; Ramos, A.M.; Coimbra, J.S. dos R.; de Oliveira, E.B. Rheological Properties of Aqueous Dispersions of Xanthan Gum Containing Different Chloride Salts Are Impacted by both Sizes and Net Electric Charges of the Cations. *Food Biophys.* **2018**, *13*, 186–197, doi:10.1007/s11483-018-9524-9.

290. Rochefort, W.E.; Middleman, S. Rheology of Xanthan Gum: Salt, Temperature, and Strain Effects in Oscillatory and Steady Shear Experiments. *J. Rheol. (N. Y. N. Y).* **1987**, *31*, 337–369, doi:10.1122/1.549953.

291. Muller, G.; Aurhourrache, M.; Lecourtier, J.; Chauveteau, G. Salt dependence of the conformation of a single-stranded xanthan. *Int. J. Biol. Macromol.* **1986**, *8*, 167–172, doi:10.1016/0141-8130(86)90021-8.

292. Wang, L.; Xiang, D.; Li, C.; Zhang, W.; Bai, X. Effects of lyophilization and low-temperature treatment on the properties and conformation of xanthan gum. *Food Hydrocoll.* **2021**, *112*, 106352, doi:10.1016/j.foodhyd.2020.106352.

293. Yadav, K.; Yadav, B.S.; Yadav, R.B.; Dangi, N. Physicochemical, pasting and rheological properties of colocasia starch as influenced by the addition of guar gum and xanthan gum. *J. Food Meas. Charact.* **2018**, *12*, 2666–2676, doi:10.1007/s11694-018-9884-3.

294. Barbara Katzbauer Properties and applications of xanthan gum. *Polym. Degrad. Stab.* **1998**, *59*, 81–84.

295. Sharma, S.; Rao, T.V.R. Xanthan gum based edible coating enriched with cinnamic acid prevents browning and extends the shelf-life of fresh-cut pears. *Lwt* **2015**, *62*, 791–800, doi:10.1016/j.lwt.2014.11.050.

296. Hans Martin Laun Rheological properties of aqueous polymer dispersion. *Angewante Makromol. Chemie* **1984**, *123*, 335–359.

297. Kennedy, J.R.M.; Kent, K.E.; Brown, J.R. Rheology of dispersions of xanthan gum, locust bean gum and mixed biopolymer gel with silicon dioxide nanoparticles. *Mater. Sci. Eng. C* **2015**, *48*, 347–353, doi:10.1016/j.msec.2014.12.040.

298. Ferry, J.D. *Viscoelastic Properties of Polymers*; 1980, Ed.; 3rd editio.; New York;

299. Miyazaki, K.; Wyss, H.M.; Weitz, D.A.; Reichman, D.R. Nonlinear viscoelasticity of metastable complex fluids. *Europhys. Lett.* **2006**, *75*, 915–921, doi:10.1209/epl/i2006-10203-9.

300. Hyun, K.; Kim, S.H.; Ahn, K.H.; Lee, S.J. Large amplitude oscillatory shear as a way to classify the complex fluids. *J. Nonnewton. Fluid Mech.* **2002**, *107*, 51–65, doi:10.1016/S0377-0257(02)00141-6.

301. Barnes, H.A. a Review of the Rheology of Filled Viscoelastic Systems. *Rheol. Rev.* **2003**, *2003*, 1–36.

302. Genovese, D.B. Shear rheology of hard-sphere, dispersed, and aggregated suspensions, and filler-matrix composites. *Adv. Colloid Interface Sci.* **2012**, *171–172*, 1–16, doi:10.1016/j.cis.2011.12.005.

303. Gerth, M.; Bohdan, M.; Fokkink, R.; Voets, I.K.; Van Der Gucht, J.; Sprakel, J. Supramolecular assembly of self-healing nanocomposite hydrogels. *Macromol. Rapid Commun.* **2014**, *35*, 2065–2070, doi:10.1002/marc.201400543.

304. Łojewski, T.; Miśkowiec, P.; Molenda, M.; Lubańska, A.; Łojewska, J. Artificial versus natural ageing of paper. Water role in degradation mechanisms. *Appl. Phys. A Mater. Sci. Process.* **2010**, *100*, 625–633, doi:10.1007/s00339-010-5645-9.

305. Paul, D.R.; Barlow, J.W. Polymer Blends (or Alloys). *J. Macromol. Sci. Part C* **1980**, *18*, 109–168, doi:10.1080/00222358008080917.

306. Koning, C.; Van Duin, M.; Pagnoulle, C.; Jerome, R. Strategies for compatibilization

of polymer blends. *Prog. Polym. Sci.* **1998**, *23*, 707–757, doi:10.1016/S0079-6700(97)00054-3.

307. Kim, S.H.; Kim, D.; Lee, D.S. Gas permeation behavior of PS/PPO blends. *J. Memb. Sci.* **1997**, *127*, 9–15, doi:10.1016/S0376-7388(96)00291-8.

308. Shinoda, H.; Asou, Y.; Kashima, T.; Kato, T.; Tseng, Y.; Yagi, T. Amphiphilic biodegradable copolymer, poly(aspartic acid-co-lactide): Acceleration of degradation rate and improvement of thermal stability for poly(lactic acid), poly(butylene succinate) and poly(-caprolactone). *Polym. Degrad. Stab.* **2003**, *80*, 241–250, doi:10.1016/S0141-3910(02)00404-4.

309. Pötschke, P.; Paul, D.R. Formation of co-continuous structures in melt-mixed immiscible polymer blends. *J. Macromol. Sci. - Polym. Rev.* **2003**, *43*, 87–141, doi:10.1081/MC-120018022.

310. Utracki, L.A.; Wilkie, C.A. *Polymer blends handbook*; 2014; ISBN 9789400760646.

311. Utracki, L.A. Compatibilization of polymer blends. *Can. J. Chem. Eng.* **2002**, *80*, 1008–1016, doi:10.1002/cjce.5450800601.

312. Navas, I.O.; Kamkar, M.; Arjmand, M.; Sundararaj, U. Morphology evolution, molecular simulation, electrical properties, and rheology of carbon nanotube/polypropylene/polystyrene blend nanocomposites: Effect of molecular interaction between styrene-butadiene block copolymer and carbon nanotube. *Polymers (Basel).* **2021**, *13*, 1–25, doi:10.3390/polym13020230.

313. Yu, L.; Dean, K.; Li, L. Polymer blends and composites from renewable resources. *Prog. Polym. Sci.* **2006**, *31*, 576–602, doi:10.1016/j.progpolymsci.2006.03.002.

314. Spiegel, S. Biodegradable compatibilized polymer blends for packaging applications: A literature review. *J. Appl. Polym. Sci.* **2018**, *135*, doi:10.1002/app.46279.

315. Ke, T.; Sun, X.S. Starch , Poly (lactic acid), and Poly (vinyl alcohol) Blends. **2003**, *11*.

316. Supthanyakul, R.; Kaabbuathong, N.; Chirachanchai, S. Poly(L-lactide-b-butylene succinate-b-L-lactide) triblock copolymer: A multi-functional additive for PLA/PBS blend with a key performance on film clarity. *Polym. Degrad. Stab.* **2017**, *142*, 160–168, doi:10.1016/j.polymdegradstab.2017.05.029.

317. Na, Y.H.; He, Y.; Shuai, X.; Kikkawa, Y.; Doi, Y.; Inoue, Y. Compatibilization effect of poly (ε-caprolactone)-b-poly(ethylene glycol) block copolymers and phase morphology analysis in immiscible poly(lactide)/poly(ε-caprolactone) blends. *Biomacromolecules* **2002**, *3*, 1179–1186, doi:10.1021/bm020050r.

318. Zhang, H.C.; Kang, B. hao; Chen, L.S.; Lu, X. Enhancing toughness of poly (lactic acid)/Thermoplastic polyurethane blends via increasing interface compatibility by polyurethane elastomer prepolymer and its toughening mechanism. *Polym. Test.* **2020**, *87*, 106521, doi:10.1016/j.polymertesting.2020.106521.

319. Sheth, M.; Kumar, R.A.; Dave, V. Biodegradable Polymer Blends of Poly (lactic acid) and Poly (ethylene glycol). **2008**, 1495–1505.

320. Kiatiporntipthak, K.; Thajai, N.; Kanthiya, T.; Rachtanapun, P.; Leksawasdi, N.; Phimolsiripol, Y.; Rohindra, D.; Ruksiriwanich, W.; Sommano, S.R.; Jantanasakulwong, K. Reaction mechanism and mechanical property improvement of poly(lactic acid) reactive blending with epoxy resin. *Polymers (Basel).* **2021**, *13*, doi:10.3390/polym13152429.

321. García Cruz, D.M.; Gomez Ribelles, J.L.; Salmerón Sánchez, M. Blending polysaccharides with biodegradable polymers. I. Properties of chitosan/polycaprolactone blends. *J. Biomed. Mater. Res. - Part B Appl. Biomater.* **2008**, *85*, 303–313, doi:10.1002/jbm.b.30947.

322. Feng, J.; Winnik, M.A. Latex blends as an approach to zero VOC coatings. *Polym. Mater. Sci. Eng. Proc. ACS Div. Polym. Mater. Sci. Eng.* **1997**, *76*, 176.

323. Rippel, M.M.; Galembeck, F. Latex Blends : Overcoming Compatibility Limitations By Electrostatic Adhesion. **1805**, *5*, 1805–1808, doi:10.13140/RG.2.1.5061.1040.

324. Chowdhury, R. Electron-Beam-Induced Crosslinking of Natural Rubber/Acrylonitrile–Butadiene Rubber Latex Blends in the Presence of Ethoxylated Pentaerythritol Tetraacrylate Used as a Crosslinking Promoter. *J. Appl. Polym. Sci.* **2007**, *103*, 1206–1214, doi:10.1002/app.

325. Lu, G.; Li, Z.F.; Li, S.D.; Xie, J. Blends of natural rubber latex and methyl methacrylate-grafted rubber latex. *J. Appl. Polym. Sci.* **2002**, *85*, 1736–1741, doi:10.1002/app.10718.

326. Varkey, J.T.; Augustine, S.; Groeninckx, G.; Bhagawan, S.S.; Rao, S.S.; Thomas, S. Morphology and mechanical and viscoelastic properties of natural rubber and styrene butadiene rubber latex blends. *J. Polym. Sci. Part B Polym. Phys.* **2000**, *38*, 2189–2211, doi:10.1002/1099-0488(20000815)38:16<2189::AID-POLB120>3.0.CO;2-E.

327. Li, X.; Hegyesi, N.; Zhang, Y.; Mao, Z.; Feng, X.; Wang, B.; Pukánszky, B.; Sui, X. Poly(lactic acid)/lignin blends prepared with the Pickering emulsion template method. *Eur. Polym. J.* **2019**, *110*, 378–384, doi:10.1016/j.eurpolymj.2018.12.001.

328. Zhang, Y.; Jiang, Y.; Han, L.; Wang, B.; Xu, H.; Zhong, Y.; Zhang, L.; Mao, Z.; Sui, X. Biodegradable regenerated cellulose-dispersed composites with improved properties via a pickering emulsion process. *Carbohydr. Polym.* **2018**, *179*, 86–92, doi:10.1016/j.carbpol.2017.09.065.

329. Cheong, K.S.; Balasubramaniam, J.R.; Hung, Y.P.; Chuong, W.S.; Amartalingam, R. Development of Biodegradable Plastic Composite Blends Based on Sago Derived Starch and Natural Rubber. *Pertanika J. Sci. Technol.* **2010**, *18*, 411–420.

330. Rouilly, A.; Rigal, L.; Gilbert, R.G. Synthesis and properties of composites of starch and chemically modified natural rubber. *Polymer (Guildf).* **2004**, *45*, 7813–7820, doi:10.1016/j.polymer.2004.09.043.

331. Zhang, N.; Cao, H. Enhancement of the antibacterial activity of natural rubber latex foam by blending it with chitin. *Materials (Basel).* **2020**, *13*, 1–15, doi:10.3390/ma13051039.

332. Pichayakorn, W.; Suksaeree, J.; Boonme, P.; Amnuaikit, T.; Taweepreda, W.; Ritthidej, G.C. Deproteinized natural rubber latex/hydroxypropylmethyl cellulose blending polymers for nicotine matrix films. *Ind. Eng. Chem. Res.* **2012**, *51*, 8442–8452, doi:10.1021/ie300608j.

333. Tsuji, H.; Ikada, Y. Stereocomplex formation between enantiomeric poly(lactic acid)s. XI. Mechanical properties and morphology of solution-cast films. *Polymer (Guildf).* **1999**, *40*, 6699–6708, doi:10.1016/S0032-3861(99)00004-X.

334. Tsuji, H. Autocatalytic hydrolysis of amorphous-made polylactides: Effects of L-lactide content, tacticity, and enantiomeric polymer blending. *Polymer (Guildf).* **2002**, *43*, 1789–1796, doi:10.1016/S0032-3861(01)00752-2.

335. Al-Itry, R.; Lamnawar, K.; Maazouz, A. Improvement of thermal stability, rheological and mechanical properties of PLA, PBAT and their blends by reactive extrusion with functionalized epoxy. *Polym. Degrad. Stab.* **2012**, *97*, 1898–1914, doi:10.1016/j.polymdegradstab.2012.06.028.

336. Restrepo, I.; Medina, C.; Meruane, V.; Akbari-Fakhrabadi, A.; Flores, P.; Rodríguez-Llamazares, S. The effect of molecular weight and hydrolysis degree of poly(vinyl alcohol)(PVA) on the thermal and mechanical properties of poly(lactic acid)/PVA blends. *Polimeros* **2018**, *28*, 169–177, doi:10.1590/0104-1428.03117.

337. Jain, N.; Singh, V.K.; Chauhan, S. A review on mechanical and water absorption properties of polyvinyl alcohol based composites/films. *J. Mech. Behav. Mater.* **2017**, *26*, 213–222, doi:10.1515/jmbm-2017-0027.

338. Yeh, J.T.; Yang, M.C.; Wu, C.J.; Wu, X.; Wu, C.S. Study on the Crystallization Kinetic and Characterization of Poly(lactic acid) and Poly(vinyl alcohol) Blends. *Polym. - Plast. Technol. Eng.* **2008**, *47*, 1289–1296, doi:10.1080/03602550802497958.

339. An Tran, N.H.; Brünig, H.; Hinüber, C.; Heinrich, G. Melt spinning of biodegradable nanofibrillary structures from poly(lactic acid) and poly(vinyl alcohol) blends. *Macromol. Mater. Eng.* **2014**, *299*, 219–227, doi:10.1002/mame.201300125.

340. Gajria, A.M.; Davé, V.; Gross, R.A.; McCarthy, S.P. Miscibility and biodegradability of blends of poly(lactic acid) and poly(vinyl acetate). *Polymer (Guildf).* **1996**, *37*, 437–444, doi:10.1016/0032-3861(96)82913-2.

341. Chuaponpat, N.; Ueda, T.; Ishigami, A.; Kurose, T.; Ito, H. Morphology, thermal and mechanical properties of co-continuous porous structure of PLA/PVA blends by phase separation. *Polymers (Basel).* **2020**, *12*, doi:10.3390/POLYM12051083.

342. Li, H.Z.; Chen, S.C.; Wang, Y.Z. Thermoplastic PVA/PLA blends with improved processability and hydrophobicity. *Ind. Eng. Chem. Res.* **2014**, *53*, 17355–17361, doi:10.1021/ie502531w.

343. Jiang, B.; Hao, J.; Wang, W.; Jiang, L.; Cai, X. Miscibility and phase structure of binary blends of poly(L-lactide) and poly(vinyl alcohol). *J. Appl. Polym. Sci.* **2001**, *81*, 762–772, doi:10.1002/app.1493.

344. Tsuji, H.; Muramatsu, H. Blends of aliphatic polyesters. IV. Morphology, swelling behavior, and surface and bulk properties of blends from hydrophobic poly(L-lactide) and hydrophilic poly(vinyl alcohol). *J. Appl. Polym. Sci.* **2001**, *81*, 2151–2160, doi:10.1002/app.1651.

345. Lipsa, R.; Tudorachi, N.; Vasile, C. Poly(vinyl alcohol)/Poly(lactic acid) blends biodegradable films doped with colloidal silver. *Rev. Roum. Chim.* **2008**, *53*, 405–413.

346. Mansur, H.S.; Sadahira, C.M.; Souza, A.N.; Mansur, A.A.P. FTIR spectroscopy characterization of poly (vinyl alcohol) hydrogel with different hydrolysis degree and chemically crosslinked with glutaraldehyde. *Mater. Sci. Eng. C* **2008**, *28*, 539–548, doi:10.1016/j.msec.2007.10.088.

347. Congdon, T.; Shaw, P.; Gibson, M.I. Thermoresponsive, well-defined, poly(vinyl alcohol) co-polymers. *Polym. Chem.* **2015**, *6*, 4749–4757, doi:10.1039/c5py00775e.

348. Betti, N.A. Thermogravimetric analysis on PVA/PVP blend under air atmosphere. *Eng. Tech. J.* **2016**, *34*, 2433–2441.

349. Schindler, A.; Harper, D. Polylactide - 2. Viscosity-Molecular Weight Relationships and Unperturbed Chain Dimensions. *J Polym Sci Polym Chem Ed* **1979**, *17*, 2593–2599, doi:10.1002/pol.1979.170170831.

350. Geoghegan, M.; Krausch, G. Wetting at polymer surfaces and interfaces. *Prog. Polym. Sci.* **2003**, *28*, 261–302, doi:10.1016/S0079-6700(02)00080-1.

351. Lipatov, Y.S. Phase separation in filled polymer blends. *J. Macromol. Sci. Part B Phys.* **2006**, *45 B*, 871–888, doi:10.1080/15583720600824615.

352. Scheffold, F.; Budkowski, A.; Steiner, U.; Eiser, E.; Klein, J.; Fetters, L.J. Surface phase behavior in binary polymer mixtures. II. Surface enrichment from polyolefin blends. *J. Chem. Phys.* **1996**, *104*, 8795–8806, doi:10.1063/1.471569.

353. Composto, R.J.; Chung, H.J. Surface-induced structure formation of polymer blends. *Nanolithography Patterning Tech. Microelectron.* **2005**, *391*, 39–75, doi:10.1533/9781845690908.39.

354. Bertoldo, M.; Coltelli, M.B.; Miraglia, L.; Narducci, P.; Bronco, S. Surface energy inducing asymmetric phase distribution in films of a bynary polymeric blend. *Polymer (Guildf).* **2005**, *46*, 11311–11321, doi:10.1016/j.polymer.2005.10.040.

355. Xiang, S.; Feng, L.; Bian, X.; Li, G.; Chen, X. Evaluation of PLA content in PLA/PBAT blends using TGA. *Polym. Test.* **2020**, *81*, 106211, doi:10.1016/j.polymertesting.2019.106211.

356. Avella, M.; Martuscelli, E. Poly-d-(-)(3-hydroxybutyrate)/poly(ethylene oxide) blends: phase diagram, thermal and crystallization behaviour. *Polymer (Guildf).* **1988**, *29*, 1731–1737, doi:10.1016/0032-3861(88)90384-9.

357. Zhang, L.; Goh, S.H.; Lee, S.Y. Miscibility and crystallization behaviour of poly(L-lactide)/poly(p-vinylphenol) blends. *Polymer (Guildf).* **1998**, *39*, 4841–4847, doi:10.1016/S0032-3861(97)10167-7.

358. Irimia-Vladu, M. “Green” electronics: Biodegradable and biocompatible materials and devices for sustainable future. *Chem. Soc. Rev.* **2014**, *43*, 588–610, doi:10.1039/c3cs60235d.

359. Zoeteman, B.C.J.; Krikke, H.R.; Venselaar, J. Handling WEEE waste Hows: On the effectiveness of producer responsibility in a globalizing world. *Int. J. Adv. Manuf. Technol.* **2010**, *47*, 415–436, doi:10.1007/s00170-009-2358-3.

360. Hainault, T.; Smith, D.S.; Cauchi, D.J.; Thompson, D.A.; Fisher, M.M.; Hetzel, C. Minnesota’s multi-stakeholder approach to managing electronic products at end-of-life. *IEEE Int. Symp. Electron. Environ.* **2000**, 310–317, doi:10.1109/isee.2000.857667.

361. Tanskanen, P. Management and recycling of electronic waste. *Acta Mater.* **2013**, *61*, 1001–1011, doi:10.1016/j.actamat.2012.11.005.

362. Sahajwalla, V.; Gaikwad, V. The present and future of e-waste plastics recycling. *Curr. Opin. Green Sustain. Chem.* **2018**, *13*, 102–107, doi:10.1016/j.cogsc.2018.06.006.

363. Tue, N.M.; Takahashi, S.; Subramanian, A.; Sakai, S.; Tanabe, S. Environmental contamination and human exposure to dioxin-related compounds in e-waste recycling sites of developing countries. *Environ. Sci. Process. Impacts* **2013**, *15*, 1326–1331, doi:10.1039/c3em00086a.

364. Kumar, A.; Holuszko, M.; Espinosa, D.C.R. E-waste: An overview on generation, collection, legislation and recycling practices. *Resour. Conserv. Recycl.* **2017**, *122*, 32–42, doi:10.1016/j.resconrec.2017.01.018.

365. Li, W.; Liu, Q.; Zhang, Y.; Li, C.; He, Z.; Choy, W.C.H.; Low, P.J.; Sonar, P.; Kyaw, A.K.K. Biodegradable Materials and Green Processing for Green Electronics. *Adv. Mater.* **2020**, *32*, 1–40, doi:10.1002/adma.202001591.

366. Owens, R.M.; Malliaras, G.G. Organic electronics at the interface with biology. *MRS Bull.* **2010**, *35*, 449–456, doi:10.1557/mrs2010.583.

367. Sun, H.S.; Chiu, Y.C.; Chen, W.C. Renewable polymeric materials for electronic applications. *Polym. J.* **2017**, *49*, 61–73, doi:10.1038/pj.2016.95.

368. Li, R.; Wang, L.; Yin, L. Materials and devices for biodegradable and soft biomedical electronics. *Materials (Basel).* **2018**, *11*, doi:10.3390/ma11112108.

369. Cocchi, M.; Bertoldo, M.; Seri, M.; Maccagnani, P.; Summonte, C.; Buoso, S.; Belletti, G.; Dinelli, F.; Capelli, R. Fully Recyclable OLEDs Built on a Flexible Biopolymer Substrate. *ACS Sustain. Chem. Eng.* **2021**, *9*, 12733–12737, doi:10.1021/acssuschemeng.1c03374.

370. Tobjörk, D.; Österbacka, R. Paper electronics. *Adv. Mater.* **2011**, *23*, 1935–1961, doi:10.1002/adma.201004692.

371. Nandy, S.; Goswami, S.; Marques, A.; Gaspar, D.; Grey, P.; Cunha, I.; Nunes, D.; Pimentel, A.; Igreja, R.; Barquinha, P.; et al. Cellulose: A Contribution for the Zero e-Waste Challenge. *Adv. Mater. Technol.* **2021**, *6*, 1–59, doi:10.1002/admt.202000994.

372. Zhu, M.; Jia, C.; Wang, Y.; Fang, Z.; Dai, J.; Xu, L.; Huang, D.; Wu, J.; Li, Y.; Song, J.; et al. Isotropic Paper Directly from Anisotropic Wood: Top-Down Green Transparent Substrate Toward Biodegradable Electronics. *ACS Appl. Mater. Interfaces* **2018**, *10*, 28566–28571, doi:10.1021/acsami.8b08055.

373. Rinaudo, M. Chitin and chitosan: Properties and applications. *Prog. Polym. Sci.* **2006**, *31*, 603–632, doi:10.1016/j.progpolymsci.2006.06.001.

374. Chen, Y.; Liu, Z.; Li, M.; Wu, X.; You, J.; Li, C. Guiding growth orientation of two-dimensional Au nanocrystals with marine chitin nanofibrils for ultrasensitive and ultrafast sensing hybrids. *J. Mater. Chem. B* **2017**, *5*, 9502–9506, doi:10.1039/c7tb02792c.

375. Díaz, F.; Engel, F.; Altman, G.H.; Diaz, F.; Jakuba, C.; Calabro, T.; Horan, R.L.; Chen, J.; Lu, H.; Richmond, J.; et al. Silk-based biomaterials.

376. Wang, C.; Xia, K.; Zhang, Y.; Kaplan, D.L. Silk-Based Advanced Materials for Soft Electronics. *Acc. Chem. Res.* **2019**, *52*, 2916–2927, doi:10.1021/acs.accounts.9b00333.

377. Tao, H.; Brenckle, M.A.; Yang, M.; Zhang, J.; Liu, M.; Siebert, S.M.; Averitt, R.D.; Mannoor, M.S.; McAlpine, M.C.; Rogers, J.A.; et al. Silk-based conformal, adhesive, edible food sensors. *Adv. Mater.* **2012**, *24*, 1067–1072, doi:10.1002/adma.201103814.

378. Ji, X.; Song, L.; Zhong, S.; Jiang, Y.; Lim, K.G.; Wang, C.; Zhao, R. Biodegradable and Flexible Resistive Memory for Transient Electronics. *J. Phys. Chem. C* **2018**, *122*, 16909–16915, doi:10.1021/acs.jpcc.8b03075.

379. Li, W.; Liu, Q.; Zhang, Y.; Li, C.; He, Z.; Choy, W.C.H.; Low, P.J.; Sonar, P.; Kyaw, A.K.K. Biodegradable Materials and Green Processing for Green Electronics. *Adv. Mater.* **2020**, *32*, doi:10.1002/adma.202001591.

380. Zhou, Y.; Fuentes-Hernandez, C.; Khan, T.M.; Liu, J.C.; Hsu, J.; Shim, J.W.; Dindar, A.; Youngblood, J.P.; Moon, R.J.; Kippelen, B. Recyclable organic solar cells on cellulose nanocrystal substrates. *Sci. Rep.* **2013**, *3*, 24–26, doi:10.1038/srep01536.

381. Najafabadi, E.; Zhou, Y.H.; Knauer, K.A.; Fuentes-Hernandez, C.; Kippelen, B. Efficient organic light-emitting diodes fabricated on cellulose nanocrystal substrates. *Appl. Phys. Lett.* **2014**, *105*, doi:10.1063/1.4891046.

382. Zhang, M.; Zhao, X. Alginate hydrogel dressings for advanced wound management. *Int. J. Biol. Macromol.* **2020**, *162*, 1414–1428, doi:10.1016/j.ijbiomac.2020.07.311.

383. Pradhan, S.; Brooks, A.K.; Yadavalli, V.K. Nature-derived materials for the fabrication of functional biodevices. *Mater. Today Bio* **2020**, *7*, 100065, doi:10.1016/j.mtbio.2020.100065.

384. Maccagnani, P.; Bertoldo, M.; Dinelli, F.; Murgia, M.; Summonte, C.; Ortolani, L.; Pizzochero, G.; Verucchi, R.; Collini, C.; Capelli, R. Flexible conductors from brown algae for green electronics. *Adv. Sustain. Syst.* **2019**, *3*, 1–7, doi:10.1002/adsu.201900001.

385. Zhang, R.; Wang, L.; Zhao, J.; Guo, S. Effects of Sodium Alginate on the Composition, Morphology, and Electrochemical Properties of Electrospun Carbon Nanofibers as Electrodes for Supercapacitors. *ACS Sustain. Chem. Eng.* **2019**, *7*, 632–640, doi:10.1021/acssuschemeng.8b04191.

386. Wang, F.; Jiang, J.; Sun, F.; Sun, L.; Wang, T.; Liu, Y.; Li, M. Flexible wearable graphene/alginate composite non-woven fabric temperature sensor with high sensitivity and anti-interference. *Cellulose* **2020**, *27*, 2369–2380, doi:10.1007/s10570-019-02951-7.

387. Lim, C.; Shin, Y.; Jung, J.; Kim, J.H.; Lee, S.; Kim, D.H. Stretchable conductive nanocomposite based on alginate hydrogel and silver nanowires for wearable electronics. *APL Mater.* **2019**, *7*, doi:10.1063/1.5063657.

388. Kim, H.S.; Lee, C.G.; Lee, E.Y. Alginate lyase: Structure, property, and application. *Biotechnol. Bioprocess Eng.* **2011**, *16*, 843–851, doi:10.1007/s12257-011-0352-8.

389. Sutherland, I.W. Polysaccharide lyases. *FEMS Microbiol. Rev.* **1995**, *16*, 323–347, doi:10.1016/0168-6445(95)00020-D.

390. Karaki, N.; Aljawish, A.; Humeau, C.; Muniglia, L.; Jasniewski, J. Enzymatic modification of polysaccharides: Mechanisms, Properties, And potential applications: A review. *Enzyme Microb. Technol.* **2016**, *90*, 1–18, doi:10.1016/j.enzmictec.2016.04.004.

391. Cheng, D.; Jiang, C.; Xu, J.; Liu, Z.; Mao, X. Characteristics and applications of alginate lyases: A review. *Int. J. Biol. Macromol.* **2020**, *164*, 1304–1320, doi:10.1016/j.ijbiomac.2020.07.199.

392. Yang, J.; Cui, D.; Ma, S.; Chen, W.; Chen, D.; Shen, H. Characterization of a novel PL 17 family alginate lyase with exolytic and endolytic cleavage activity from marine bacterium Microbulbifer sp. SH-1. *Int. J. Biol. Macromol.* **2021**, *169*, 551–563, doi:10.1016/j.ijbiomac.2020.12.196.

393. Xu, F.; Wang, P.; Zhang, Y.Z.; Chen, X.L. Diversity of three-dimensional structures

and catalytic mechanisms of alginate lyases. *Appl. Environ. Microbiol.* **2018**, *84*, doi:10.1128/AEM.02040-17.

394. Liu, J.; Yang, S.; Li, X.; Yan, Q.; Reaney, M.J.T.; Jiang, Z. Alginate Oligosaccharides: Production, Biological Activities, and Potential Applications. *Compr. Rev. Food Sci. Food Saf.* **2019**, *18*, 1859–1881, doi:10.1111/1541-4337.12494.

395. Patel, K.K.; Tripathi, M.; Pandey, N.; Agrawal, A.K.; Gade, S.; Anjum, M.M.; Tilak, R.; Singh, S. Alginate lyase immobilized chitosan nanoparticles of ciprofloxacin for the improved antimicrobial activity against the biofilm associated mucoid P. aeruginosa infection in cystic fibrosis. *Int. J. Pharm.* **2019**, *563*, 30–42, doi:10.1016/j.ijpharm.2019.03.051.

396. Lee, O.K.; Lee, E.Y. Sustainable production of bioethanol from renewable brown algae biomass. *Biomass and Bioenergy* **2016**, *92*, 70–75, doi:10.1016/j.biombioe.2016.03.038.

397. Dharani, S.R.; Srinivasan, R.; Sarath, R.Temptemptemp.; Ramya, M. Recent progress on engineering microbial alginate lyases towards their versatile role in biotechnological applications. *Folia Microbiol. (Praha).* **2020**, 937–954, doi:10.1007/s12223-020-00802-8.

398. Shinar, J.; Shinar, R. Organic light-emitting devices (OLEDs) and OLED-based chemical and biological sensors: An overview. *J. Phys. D. Appl. Phys.* **2008**, *41*, doi:10.1088/0022-3727/41/13/133001.

399. Li, Y.; Tan, L.W.; Hao, X.T.; Ong, K.S.; Zhu, F.; Hung, L.S. Flexible top-emitting electroluminescent devices on polyethylene terephthalate substrates. *Appl. Phys. Lett.* **2005**, *86*, 1–3, doi:10.1063/1.1900940.

400. Lei, P.H.; Hsu, C.M.; Fan, Y.S. Flexible organic light-emitting diodes on a polyestersulfone (PES) substrate using Al-doped ZnO anode grown by dual-plasma-enhanced metalorganic deposition system. *Org. Electron.* **2013**, *14*, 236–249, doi:10.1016/j.orgel.2012.10.030.

401. Legnani, C.; Vilani, C.; Calil, V.L.; Barud, H.S.; Quirino, W.G.; Achete, C.A.; Ribeiro, S.J.L.; Cremona, M. Bacterial cellulose membrane as flexible substrate for organic light emitting devices. *Thin Solid Films* **2008**, *517*, 1016–1020, doi:10.1016/j.tsf.2008.06.011.

402. Zhu, H.; Xiao, Z.; Liu, D.; Li, Y.; Weadock, N.J.; Fang, Z.; Huang, J.; Hu, L. Biodegradable transparent substrates for flexible organic-light-emitting diodes. *Energy Environ. Sci.* **2013**, *6*, 2105–2111, doi:10.1039/c3ee40492g.

403. Liu, Y.; Xie, Y.; Liu, Y.; Song, T.; Zhang, K.Q.; Liao, L.; Sun, B. Flexible organic light emitting diodes fabricated on biocompatible silk fibroin substrate. *Semicond. Sci. Technol.* **2015**, *30*, 104004, doi:10.1088/0268-1242/30/10/104004.

404. Liu, Y.F.; An, M.H.; Bi, Y.G.; Yin, D.; Feng, J.; Sun, H.B. Flexible Efficient Top-Emitting Organic Light-Emitting Devices on a Silk Substrate. *IEEE Photonics J.* **2017**, *9*, doi:10.1109/JPHOT.2017.2740618.

405. Jin, J.; Lee, D.; Im, H.G.; Han, Y.C.; Jeong, E.G.; Rolandi, M.; Choi, K.C.; Bae, B.S. Chitin Nanofiber Transparent Paper for Flexible Green Electronics. *Adv. Mater.* **2016**, *28*, 5169–5175, doi:10.1002/adma.201600336.

406. Pagliaro, M.; Ciriminna, R.; Palmisano, G. Flexible solar cells. *ChemSusChem* **2008**,

1, 880–891, doi:10.1002/cssc.200800127.

407. Qiu, W.; Paetzold, U.W.; Gehlhaar, R.; Smirnov, V.; Boyen, H.G.; Tait, J.G.; Conings, B.; Zhang, W.; Nielsen, C.B.; McCulloch, I.; et al. An electron beam evaporated TiO2 layer for high efficiency planar perovskite solar cells on flexible polyethylene terephthalate substrates. *J. Mater. Chem. A* **2015**, *3*, 22824–22829, doi:10.1039/c5ta07515g.

408. Tsang, M.P.; Sonnemann, G.W.; Bassani, D.M. Life-cycle assessment of cradle-to-grave opportunities and environmental impacts of organic photovoltaic solar panels compared to conventional technologies. *Sol. Energy Mater. Sol. Cells* **2016**, *156*, 37–48, doi:10.1016/j.solmat.2016.04.024.

409. Cheng, Q.; Ye, D.; Yang, W.; Zhang, S.; Chen, H.; Chang, C.; Zhang, L. Construction of Transparent Cellulose-Based Nanocomposite Papers and Potential Application in Flexible Solar Cells. *ACS Sustain. Chem. Eng.* **2018**, *6*, 8040–8047, doi:10.1021/acssuschemeng.8b01599.

410. Ma, X.; Deng, Q.; Wang, L.; Zheng, X.; Wang, S.; Wang, Q.; Chen, L.; Huang, L.; Ouyang, X.; Cao, S. Cellulose transparent conductive film and its feasible use in perovskite solar cells. *RSC Adv.* **2019**, *9*, 9348–9353, doi:10.1039/C9RA01301F.

411. Jin, Y.; Sun, Y.; Wang, K.; Chen, Y.; Liang, Z.; Xu, Y.; Xiao, F. Long-term stable silver nanowire transparent composite as bottom electrode for perovskite solar cells. *Nano Res.* **2018**, *11*, 1998–2011, doi:10.1007/s12274-017-1816-8.

412. Jia, C.; Li, T.; Chen, C.; Dai, J.; Kierzewski, I.M.; Song, J.; Li, Y.; Yang, C.; Wang, C.; Hu, L. Scalable, anisotropic transparent paper directly from wood for light management in solar cells. *Nano Energy* **2017**, *36*, 366–373, doi:10.1016/j.nanoen.2017.04.059.

413. Pawar, S.N.; Edgar, K.J. Alginate derivatization: A review of chemistry, properties and applications. *Biomaterials* **2012**, *33*, 3279–3305, doi:10.1016/j.biomaterials.2012.01.007.

414. Kim, K.B.; Tak, Y.H.; Han, Y.S.; Baik, K.H.; Yoon, M.H.; Lee, M.H. Relationship between surface roughness of indium tin oxide and leakage current of organic light-emitting diode. *Japanese J. Appl. Physics, Part 2 Lett.* **2003**, *42*, doi:10.1143/jjap.42.l438.

415. Siegel, J.; Lyutakov, O.; Rybka, V.; Kolská, Z.; Švorčík, V. Properties of gold nanostructures sputtered on glass. *Nanoscale Res. Lett.* **2011**, *6*, 1–9, doi:10.1186/1556-276X-6-96.

416. Zhang, Y.W.; Wu, B.Y.; Chen, K.C.; Wu, C.H.; Lin, S.Y. Highly conductive nanometer-thick gold films grown on molybdenum disulfide surfaces for interconnect applications. *Sci. Rep.* **2020**, *10*, 1–6, doi:10.1038/s41598-020-71520-x.

417. Capelli, R.; Maccagnani, P.; Dinelli, F.; Murgia, M.; Bertoldo, M.; Montecchi, M.; Doyle, B.P.; Carleschi, E.; Pasquali, L. Understanding adhesion of gold conductive films on sodium-alginate by photoelectron spectroscopy. *Thin Solid Films* **2019**, *690*, 137535, doi:10.1016/j.tsf.2019.137535.

418. Marchi, L.; Dinelli, F.; Maccagnani, P.; Costa, V.; Chenet, T.; Belletti, G.; Natali, M.; Cocchi, M.; Bertoldo, M.; Seri, M. Sodium Alginate as a Natural Substrate for Efficient and Sustainable Organic Solar Cells. **2022**, doi:10.1021/acssuschemeng.2c05633.

419. Bolognesi, M.; Prosa, M.; Seri, M. Biocompatible and biodegradable organic electronic materials. In *Sustainable Strategies in Organic Electronics*; Marrocchi, A.B.T.-S.S. in O.E., Ed.; Elsevier, 2022; pp. 297–338 ISBN 978-0-12-823147-0.

420. Elumalai, N.K.; Uddin, A. Open circuit voltage of organic solar cells: an in-depth review. *Energy Environ. Sci.* **2016**, *9*, 391–410, doi:10.1039/C5EE02871J.

421. Zhu, B.; Yin, H. Alginate lyase: Review of major sources and classification, properties, structure-function analysis and applications. *Bioengineered* **2015**, *6*, 125–131, doi:10.1080/21655979.2015.1030543.

422. Yoshimasa Yonemoto, Hirokazu Tanaka, Tetsuo Yamashita, Naofumi Kitabatake; Yuzaburo Ishida, Akira Kimura, k.m. Promotion of Germination and Shoot Elongation of Some Plants by Alginate Oligomers Prepared with Bacterial Alginate Lyase. **1993**, *75*, 68–70.

423. de Meneses, A.C.; Almeida Sá, A.G.; Lerin, L.A.; Corazza, M.L.; de Araújo, P.H.H.; Sayer, C.; de Oliveira, D. Benzyl butyrate esterification mediated by immobilized lipases: Evaluation of batch and fed-batch reactors to overcome lipase-acid deactivation. *Process Biochem.* **2019**, *78*, 50–57, doi:10.1016/j.procbio.2018.12.029.

424. Olivero, R.A.; Nocerino, J.M.; Deming, S.N. Experimental Design and Optimization. *Handb. Environ. Chem.* **1995**, *2*, 73–122, doi:10.1007/978-3-540-49148-4_3.

425. Ernst, F.A.; Reed, F.C.; Edwards, W.L. A Direct Synthetic Ammonia Plant. *Ind. Eng. Chem.* **1925**, *17*, 775–788, doi:10.1021/ie50188a002.

426. Sánchez, A.; Martín, M. Optimal renewable production of ammonia from water and air. *J. Clean. Prod.* **2018**, *178*, 325–342, doi:10.1016/j.jclepro.2017.12.279.

427. Yeom, C.K.; Jegal, J.G.; Lee, K.H. Characterization of relaxation phenomena and permeation behaviors in sodium alginate membrane during pervaporation separation of ethanol-water mixture. *J. Appl. Polym. Sci.* **1996**, *62*, 1561–1576, doi:10.1002/(SICI)1097-4628(19961205)62:10<1561::AID-APP8>3.0.CO;2-M.

428. Synooka, O.; Kretschmer, F.; Hager, M.D.; Himmerlich, M.; Krischok, S.; Gehrig, D.; Laquai, F.; Schubert, U.S.; Gobsch, G.; Hoppe, H. Modification of the active layer/PEDOT:PSS interface by solvent additives resulting in improvement of the performance of organic solar cells. *ACS Appl. Mater. Interfaces* **2014**, *6*, 11068–11081, doi:10.1021/am503284b.

429. Zhao, Z.; Guo, M.; Zhang, M. Extraction of molybdenum and vanadium from the spent diesel exhaust catalyst by ammonia leaching method. *J. Hazard. Mater.* **2015**, *286*, 402–409, doi:10.1016/j.jhazmat.2014.12.063.

430. Guo, S.; Cao, B.; Wang, W.; Moulin, J.F.; Müller-Buschbaum, P. Effect of alcohol treatment on the performance of PTB7:PC71BM bulk heterojunction solar cells. *ACS Appl. Mater. Interfaces* **2015**, *7*, 4641–4649, doi:10.1021/am5079418.

431. Safety assessment of the substance zinc oxide, nanoparticles, for use in food contact materials. *EFSA J.* **2017**, *14*, doi:10.2903/j.efsa.2016.4408.

432. Han, J.H.; Krochta, J.M. Physical properties and oil absorption of whey-protein-coated paper. *J. Food Sci.* **2001**, *66*, 294–299, doi:10.1111/j.1365-2621.2001.tb11335.x.

433. Wanwei Zhanga, Chao Huanga, Olga Kusmartsevab, Noreen L. Thomasa, Elisa Melea Electrospinning of polylactic tree and manuka oil. *React. Funct. Polym.* **2017**, *117*, 106– 111.